Hyperspectral Remote Sensing of Closed Forest Canopies: Estimation of Chlorophyll Fluorescence and Pigment Content

Pablo J. Zarco-Tejada

A thesis submitted to the Faculty of Graduate Studies
in partial fulfilment of the requirements
for the degree of

Doctor of Philosophy

Supervisor: Prof. John R. Miller

Graduate Programme in Earth and Space Science
York University
Toronto, Ontario, Canada

September, 2000

ABSTRACT

Quantitative assessment of vegetation physiological condition from remote sensing requires the development of methodologies to estimate biochemical constituents and physiological measures through the use of radiative transfer models. This dissertation provides a description of the investigations carried out to assess whether two indicators of stress in vegetation at leaf level, chlorophyll content and chlorophyll fluorescence, can be predicted using hyperspectral reflectance data. This study was focussed on twelve sites of *Acer saccharum* M. in the Algoma Region (Canada), where field measurements, laboratory-simulation experiments, and hyperspectral CASI imagery have been carried out in 1997, 1998, 1999 and 2000 campaigns. Radiative transfer theory and modelling assumptions are applied at laboratory and field scales in order to define the link between leaf reflectance and transmittance and canopy hyperspectral data.

Research work related to chlorophyll fluorescence estimation consisted of a series of laboratory and field measurements of spectral reflectance under artificial and natural light conditions which demonstrate that effects of natural chlorophyll fluorescence are observable in the reflectance red edge spectral region. Leaf samples from the study sites were used for reflectance and transmittance measurements with the Li-Cor Model 1800 integrating sphere apparatus coupled to an Ocean Optics Model ST1000 fibre spectrometer with and without fluorescence-exciting radiation. A study of the diurnal change in leaf reflectance spectra, combined with fluorescence measurements with the PAM-2000 Fluorometer show that the difference spectra are consistent with observed diurnal changes in fluorescence. Small canopies of *Acer saccharum* M. were used for measurements in the laboratory and under natural light conditions in diurnal trials, in which the variation of measured reflectance was shown experimentally to be consistent with a fluorescence signature imposed on the inherent leaf reflectance signature. The Fluorescence-Reflectance-Transmittance (FRT) leaf radiative transfer model was developed to theoretically simulate the effects of fluorescence emission on the apparent reflectance. Optical indices were identified to track fluorescence emission effects on the observations of apparent reflectance at the leaf and canopy level.

Infinite reflectance and canopy reflectance models were used to link leaf to canopy levels through radiative transfer simulation. Optically thick simulation formulae and SAILH and MCRM canopy reflectance models were used for chlorophyll content estimation by scaling-up and by numerical model inversion approaches through coupling to PROSPECT leaf radiative transfer model. Study of the merit function showed that red edge optical indices perform better than single spectral reflectance channels from hyperspectral airborne CASI data, and effects of shadows and LAI variation were minimized. Estimates of leaf pigment by hyperspectral remote sensing of closed forest canopies were shown to be feasible with root mean square errors ranging from 3 to 5.5 $\mu g/cm^2$. MERIS sensor onboard ENVISAT (to be launched in 2001) is shown to be a satellite sensor with the potential to provide global mapping of foliar pigment content.

Deciduous forest area in the Algoma Region, Northern Ontario, Canada where field and airborne campaigns were carried out, in collaborative research between York University (Toronto), Ontario Forest Research Institute (OFRI, Sault. Ste. Marie) - Ontario Ministry of Natural Resources (OMNR), and the Centre for Research in Earth and Space Technology (CRESTech).

ACKNOWLEDGEMENTS

I would like to extend my sincere gratitude to everyone who made this research work possible. A very special word of appreciation to Prof. John R. Miller for his guidance and challenging discussions that enabled continuous progress. His encouragement and optimism resulted in a stimulating working environment that I will forever value.

I am indebted to Gina Mohammed, Thomas Noland and Paul Sampson, from the *Ontario Forest Research Institute*, for their considerable work in this genuine research collaboration. Valuable insights and guidance is acknowledged from my committee members Dr. Treitz and Dr. Cheng. Particular mention is also due to colleagues who have contributed at different stages, such as John Harron (ISL/CRESTech); Lawrence Gray, Jim Freemantle, and Paul Shepherd (EOL/CRESTech), Phil Brasher, and Heidi Beck whose dedication and skill made the airborne CASI field campaigns work; Denzil Irving, Brian Brown, Nick Symour, Maara Packalen and Desmond Hickie, who planned and executed complex site sampling campaigns; and M. Bahlai, who helped with the maple seedlings. N. Goel, A. Kuusk, W. Verhoef and S. Jacquemoud are also gratefully acknowledged for the provision of computer code for leaf and canopy reflectance models.

Financial support provided for this research through the *Centre for Research in Earth and Space Technology* (CRESTech), the *Ontario Ministry of Natural Resources*, the *Canadian Forestry Service*, the *Ministry of Environment and Energy* and GEOIDE (Geomatics for Informed Decisions) part of the Canadian Networks of Centres of Excellence programme, and York University is gratefully acknowledged.

Thanks also goes out to all the members of the *Remote Sensing Group* at *York University*, especially to Peter White, Kris Innanen, Jeff Czapla-Myers and Sebastian Martin, who facilitated my cultural integration throughout my term in Canada.

Finally I wish to thank my parents and family, Jose, Alicia, Jose-chico and Alvaro; Marián and Antonio, without whose constant support this wonderful experience in Canada would not have been possible. To V.D.L.A for her guidance.

And deeply thoughtful to Esperanza, for her inexhaustible faith and support displayed through understanding, enthusiasm and sacrifice at a distance.

To Esperanza

"Ná máh que'so"

Spanish Proverb, La Yea

TABLE OF CONTENTS

LIST OF FIGURES

LIST OF TABLES

GLOSSARY OF ACRONYMS

AIS	Airborne Imaging Spectrometer
AVHRR	Advance Very High Resolution Radiometer
AVIRIS	Airborne Visible InfraRed Imaging Spectrometer
BRF	Bidirectional Reflectance Factor
CASI	Compact Airborne Spectrographic Imager
CF	Chlorophyll Fluorescence
CR	Canopy Reflectance
ESA	European Space Agency
FCR	Forest Condition Rating system
FRT	Fluorescence-Reflectance-Transmittance
Fv/Fm	Maximal efficiency of photon capture by open PSII reaction centres
ΔF/Fm'	Effective quantum yield, efficiency of PSII photon capture in the light by closed PSII reaction centres
G	Greenness Index
GORT	Geometric Optical & Radiative Transfer
K-M	Kubelka-Munk
LAD	Leaf Angle Distribution Function
LAI	Leaf Area Index
LIDF	Leaf Inclination Distribution Function
LUT	Look Up Tables
MERIS	Medium Resolution Imaging Spectrometer
MSR	Modified Simple Ratio
NDPI	Normalized Difference Pigment Index
NDVI	Normalized Difference Vegetation Index
NNT	Neural NeTworks
NPCI	Normalized Pigment Chlorophyll ratio Index
NPQI	Normalized Phaeophytinization Index
OFRI	Ontario Forest Research Institute
OMNR	Ontario Ministry of Natural Resources
OPT	Iterative Optimization
PAR	Photosynthetically Active Radiation
PPFD	Photosynthetic Photon Flux Density
PRI	Photochemical Reflectance Index
PS-I/II	Photosystem I/II
REIP	Red Edge Inflection Point
RTE	Radiative Transfer Equation
SAIL	Scattering by Arbitrarily Inclined Leaves
SIPI	Structure Intensive Pigment Index
SNR	Signal-to-Noise Ratio
SR	Simple Ratio
SRPI	Simple Ratio Pigment Index

CHAPTER 1.

INTRODUCTION

The development of methodologies for quantitative assessment of forest physiological condition at different spatial scales is a key element to the successful application of satellite and airborne sensors in vegetation monitoring. Research is focussed at different levels of detail to develop techniques based on physical principles that connect leaf physiological condition to the measurement of interaction processes between solar radiation and the vegetation canopy under observation.

Extensive research has been carried out at the leaf level in order to assess physiological condition based on the study of the light interaction with the foliar medium. The successful application of such extensive research to Earth observing instruments at a much broader scales in order to predict condition, requires the development of links between the leaf and the canopy, where photon-vegetation interactions are affected by the two different media.

This dissertation provides a description of the investigations carried out in order to assess whether two indicators of stress in vegetation at leaf level, chlorophyll content (chl_{a+b})

and Chlorophyll Fluorescence (CF[1]) can be predicted using airborne hyperspectral reflectance data. Radiative transfer theory and modelling assumptions are applied at laboratory and field scales in order to define the link between leaf reflectance and transmittance and canopy airborne hyperspectral data acquired with different spectral and spatial characteristics.

In the remainder of this introductory chapter, a description of leaf biochemical constituents shown to be of importance for characterization of physiological condition is provided. The measurement of the light interaction in the visible and near infrared with the leaf medium is shown to be a method for pigment content and fluorescence quantification linked to stress condition. This is followed by the description of traditional and new leaf-level optical indices used for a quantification of pigment content and chlorophyll fluorescence using spectral data at leaf and canopy levels. The last part of this chapter explains the context of this research, as part of the multi-disciplinary, multi-agency *Bioindicators of Forest Sustainability Project*.

The *Theoretical Background*, in Chapter 2, describes the radiative transfer equation through a medium under assumptions which apply to vegetation media, such as leaf and vegetation canopies. The need for a leaf model accounting for the effects of chlorophyll fluorescence in leaf apparent reflectance motivated the development of the Fluorescence-Reflectance-Transmittance (FRT) model. The link between leaf and canopy levels

[1] All acronyms throughout this dissertation are summarized in the Glossary found on page xxvi.

through canopy reflectance models is described here, with simplification through simulation formulae such as infinite reflectance models. The chapter ends with the description of methodologies for quantitative estimation and prediction of pigment content in vegetation canopies.

Chapter 3 describes the *Experimental Methods and Materials* used for investigations of both chlorophyll content and chlorophyll fluorescence at the different levels of study. Leaf-level measurements, with fibre spectrometer, integrating sphere, leaf fluorometer, and different experiments under artificial light in the laboratory and under natural light for a diurnal temporal pattern are described. Experiments were needed to simulate the effects of canopy structure for seedlings using the Compact Airborne Spectrographic Imager (CASI) hyperspectral airborne sensor and a Bidirectional Reflectance Factor (BRF) facility in a laboratory setting. Finally, field airborne campaigns were carried out with different spatial and spectral resolutions in order to assess the developed methodologies with reflectance data acquired over forest study sites under different stress conditions.

The *Experimental Results* are reported in Chapter 4, starting with the results obtained at leaf level with optical indices for the two campaigns where leaf samples were collected. All the findings from the investigations of chlorophyll fluorescence, at all different scales of study, are presented here. This is followed by airborne canopy-level results where the findings are presented for the application of different methodologies for pigment

estimation. Operational issues are discussed and presented with respect to the Medium Resolution Imaging Spectrometer (MERIS) sensor from the European Space Agency (ESA) to be launched in 2001, whose spectral resolution is simulated with CASI hyperspectral data.

This dissertation ends with final conclusions and recommendations for further research.

1.1.- LEAF BIOCHEMICAL CONSTITUENTS AND CHLOROPHYLL FLUORESCENCE FOR FOREST CONDITION

Assessment of forest physiological condition may provide diagnostic indication of the healthy or stress state of stand populations. Stress can be due to a range of factors that can be grouped into natural and anthropogenic causes. Natural causes are, amongst others, the action of insects, disease, drought, heat and freezing. Anthropogenic causes include erosion, soil compaction, nutrient loss, air pollution, increased UV radiation and climate change.

The large number of variables involved in determining the functioning of a forest ecosystem can produce complex physiological responses. A forest ecosystem is a complex multivariate system exposed to a multitude of stresses, with mechanisms and cumulative effects that are poorly understood. The number of controlling variables involved suggests that several diagnostic bioindicators might be used to establish the presence of conditions of stress in forest stands.

Temperature, precipitation and soil moisture, insolation, wind, soil structure and fertility, stand structure and density, competing vegetation, air pollution and acid rain are primary variables playing a role in the multivariate forest ecosystem that may cause stress and bring about forest decline. As a result of action by one or more of these factors, a visual or non-visual response may occur in the plant that might be detectable. These response manifestations, called diagnostic bioindicators, are the key to the early detection of stress and are likely to be related to leaf pigment and biochemical content, as they are critical to plant photosynthetic functioning.

1.1.1.- Leaf Biochemical Constituents

The chlorophyll content in leaves is potentially one of the most important indicators of vegetation strain. The most active photosynthetic tissue in higher plants is the mesophyll leaf tissue in which chloroplasts contain specialized light-absorbing pigments. In the chloroplast, light energy is harvested by two functional units called photosystems used to power the transfer of electrons through a series of compounds connecting Photosystem II (called P680 because the centre of the maximum absorption is at 680nm, PS-II) with Photosystem I (P700, PS-I) in a series of reduction-oxidation reactions. Chlorophylls and carotenoids are molecules suited for light absorption, energy transfer, and electron transfer functions between the two photoreaction centres, with PS-I preferentially absorbing far-red light of wavelength greater than 680nm, and PS II absorbing red light of about 680 nm and driven inefficiently by far-red light (Taiz and Zeiger, 1998). The light-absorbing pigments transfer their energy to the reaction centres by a sequence of

pigments with absorption maxima that are progressively shifted toward longer red wavelengths: carotenoids transfer the photons to chlorophyll *b*, with absorption maximum at 650 nm, and then the photon is transferred to chlorophyll *a*, with absorption maximum at 670 nm, losing energy as heat in the process. The photon is therefore transported from pigments with lower to higher wavelength absorption maximum, thus from higher to lower energy status. This energy-trapping process ensures that the energy transfer is always in a direction towards longer wavelengths while the photosystems receive the energy for photochemical reactions (Taiz and Zeiger, 1998).

Stressed vegetation losses regulation in the electron transfer needed after the molecule has absorbed a photon, therefore resulting in self-damage because light-absorbing processes continue without efficient pathways for disposing energy through electron transfer, with toxic oxygen being formed as a result. Therefore, the total chlorophyll content in leaves decreases in stressed vegetation, changing the proportion of light-absorbing pigments and leading to less overall absorption (Figure 1.1). Chlorophyll *a* and *b* are the most important plant pigments, absorbing blue and red light in the 430-660 nm region (Taiz and Zeiger, 1998; Curran, 1983; Farabee, 1997). The absorption of electromagnetic radiation by this pigment varies with the wavelength, with strong absorption in the blue (400-500 nm) and red (600-700 nm) portions of the visible spectrum and relatively less absorption in the green (500-600 nm) portion (Figure 1.2). The other pigments present in the leaf are usually masked by the chlorophyll *a* and *b* absorption; examples include the *carotenes* and *xanthophyll*, absorbing primarily in the

blue region. In advanced senescence stages and under stress status, chlorophyll content in leaves decreases, allowing the other pigments to become dominant, therefore allowing *carotenes* (yellow) and *xanthophyll* (pale yellow) to be more dominant. Differences in reflectance between healthy and stressed vegetation due to changes in pigment levels have been detected in the *green peak* and along the *red edge* (690 to 750 nm) (e.g. Rock *et al.*,1988; Vogelmann *et al.*, 1993; Carter, 1994; Gitelson and Merzlyak, 1996), allowing remote detection methods to identify vegetation stress through the influence of chlorophyll content variation. Variations in leaf biochemical constituents, such as lignins, proteins and nitrogen may be used as indicators of stress (Fourty *et al.*, 1996; Zagolski *et al.*, 1996; Wessman *et al.*, 1989), although leaf lignin concentration is unlikely to change rapidly due to stress. Nevertheless, this approach may be useful for

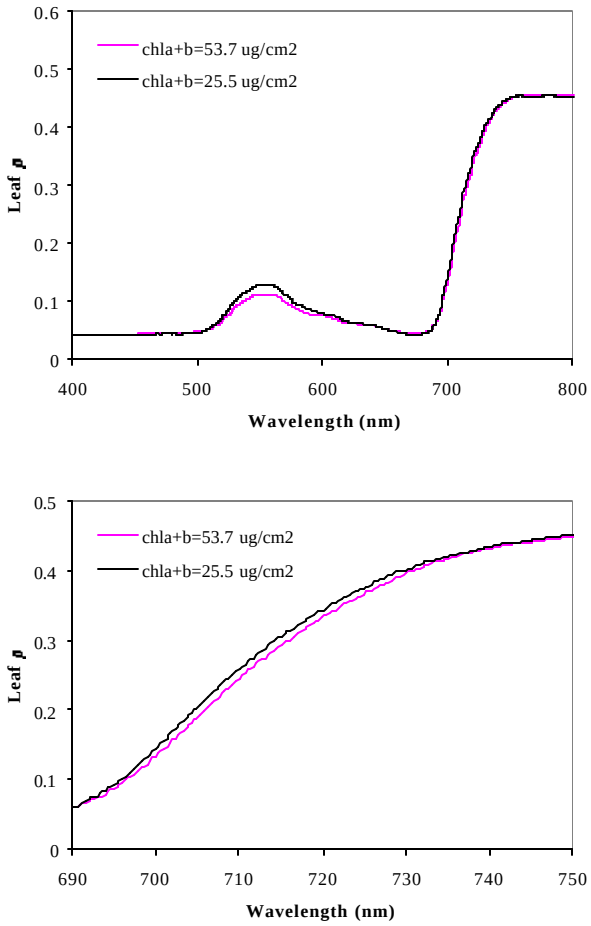

Figure 1.1. *Acer Saccharum* M. leaf reflectance from two foliar samples with high (chl_{a+b}=53.7 µg/cm^2) and low (chl_{a+b}=25.5 µg/cm^2) chlorohpyll content in the 400-800nm range (top) and in the red edge (bottom). Reflectance difference in the visible at 550nm (1.56%) is comparable to changes in the red edge at 710nm (1.41%) due to the effect of pigment absorption.

measuring long-term stress. Measurement of nitrogen and lignin contents of forest canopies could allow predictions of biogeochemical processes such as productivity, decomposition and nutrition turnover rates (Peterson *et al*., 1988). Other indicators could be those that can be detected in gaseous emissions of vegetation, such as the volatile constituents isoprenes, monoterpenes and ethanol (Guenther *et al*., 1993).

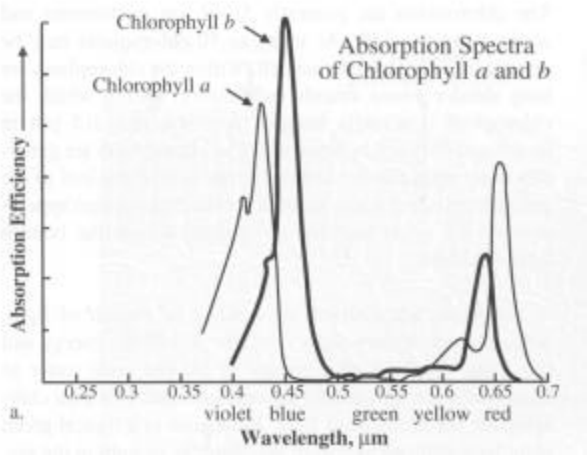

Figure 1.2. Absorption spectra of chlorophyll *a* and *b* pigments, absorbing primarily in blue and red. Source: Jensen, 2000.

1.1.2.- Leaf Chlorophyll Fluorescence

Chlorophyll Fluorescence has been shown to be a useful tool in identifying previsual strain (Mohammed *et al.*, 1995). Specifically, changes in chlorophyll function frequently precede changes in chlorophyll content, hence changes in CF can be observed long before leaves become chlorotic. CF is red and far-red light that is produced in plant photosynthetic tissues upon excitation with natural or artificial light in the visible spectrum. When the chlorophyll molecule absorbs a photon, it makes a transition from the ground state to an excited state, becoming extremely unstable, giving up some of its energy very rapidly as heat, entering a lower excited state. In this state of excitation, the chlorophyll molecule can re-emit a photon to return to its ground state, a process called

fluorescence (Figure 1.3). In this process, the wavelength of fluorescence is always longer than the wavelength of absorption of the same electron, because a portion of the excitation energy is converted into heat before the fluorescence photon is emitted. Therefore, according to conservation of energy, the energy of the fluorescence photon is lower than energy of the absorbed photon. A second process that may occur is that all the energy of the excited chlorophyll can be converted into heat, with no emission of a photon. A third process is energy transfer, in which all the energy is transferred to other molecules. The last process is referred to as photochemistry (Vidaver *et al*., 1991), in which the energy of the excited state causes the chemical reactions needed in the photosynthesis (Figure 1.4).

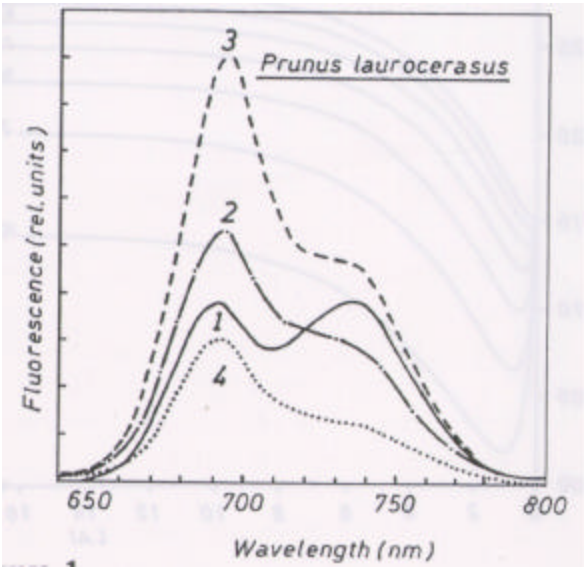

Figure 1.3. Chlorophyll fluorescence emission of *Prunus laurocerasus* leaves with decreasing chlorophyll content from leaf 1 (52 μg/cm^2) to 4 (1.1 μg/cm^2). Source: Lichtenthaler (1988).

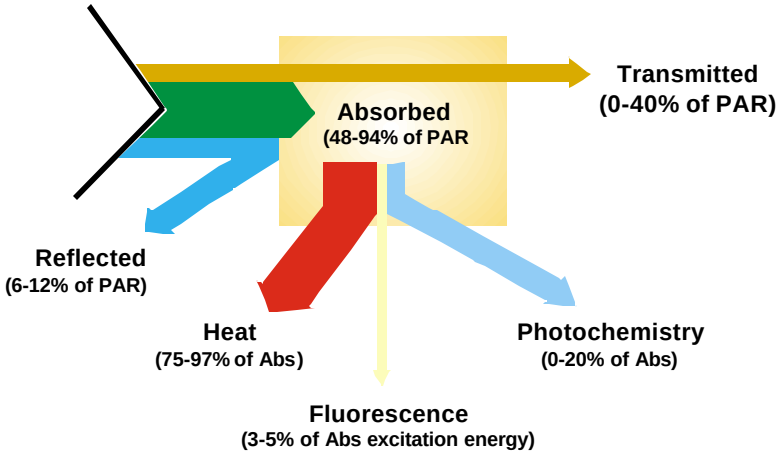

Figure 1.4. Schematic view of the different processes occurring to the energy reaching photosynthetic tissue: reflectance, absorption and transmission. Fluorescence, heat transfer, and photochemistry are processes in which the absorbed energy is transformed. Source: Vidaver *et al*., 1991

CF emanates primarily from chlorophyll *a* in Photosystem II at room temperature. Production of CF is, therefore, one of the ways in which plant chloroplasts harmlessly dissipate light energy that is in excess of the needs of photosynthesis, thereby, protecting the chloroplast from oxidative damage. Several reviews of CF theory, measurement methods and interpretation are available (e.g., Schreiber *et al.*, 1994; Larcher, 1994; Lichtenthaler, 1992; Lichtenthaler and Rinderle, 1988; Schreiber and Bilger, 1987; Krause and Weis, 1984; Papageorgiou, 1975).

In a general way, steady-state CF and photosynthetic rate are inversely related, such that CF is low when photosynthesis is high. However, CF can also decrease when photosynthesis is low, because of an intensified protective quenching action on CF production, from heat dissipation. The interdependence of photosynthesis and CF, and the various mechanisms of CF quenching have been the subject of much research into the

photobiology of a wide range of plant species (Govindjee, 1995; Mohammed *et al.*, 1995; Larcher, 1994; Schreiber and Bilger, 1993; Lichtenthaler, 1992).

CF techniques possess the advantage of being rapid, non-destructive, and non-invasive (Mohammed *et al.*, 1995). In particular, CF has often been used to investigate stress effects and recovery in plant tissues, and in comparing the stress resistance of different populations. In the last 15-20 years, it has been used increasingly with forest tree species in studies of dormancy induction, cold hardiness, light acclimation, heat damage, water stress, disease effects, nutrient deficiencies, and forest decline (Mohammed *et al.*, 1995). Significantly, leaf photosynthetic status as indicated by chlorophyll pigment content is a primary factor in determining leaf reflectance and transmittance spectra (e.g. Yamada and Fujimura, 1991; Jacquemoud *et al.*, 1996) and hence is amenable to optical remote sensing methods. On the other hand, the leaf photosynthetic functioning as indicated by fluorescence emission is controlled by a wide range of factors in addition to leaf chlorophyll content, thereby underscoring the value in developing methods to estimate pigment levels in addition to measuring leaf fluorescence for effective stress detection methods. The effects of CF emission on measured vegetation leaf and canopy reflectance at both photosystem spectral regions of 700 (PSII) and 685 nm (PSI) will be the focus of part of this research work.

Leaf water content is another indicator of plant response to stress, although it is a less sensitive indicator than leaf chlorophyll content, appearing consistently only at advanced

stages of leaf dehydration (Hunt and Rock, 1987; Carter, 1993). Sensitivity is high at 480 and 680 nm although this effect tends to be masked by that of leaf chlorophyll content (Carter, 1991). Leaf water content will not therefore be part of this study since pre-visual and early-stress bioindicators are the focus of this dissertation.

A traditional way of non-destructive estimation of chlorophyll content in vegetation is performed through the use of optical indices calculated from measured reflectance. Ratios calculated at specific wavelengths allow the development of relationships with chlorophylls, other light-absorbing pigments, and CF that may be used afterward for prediction. The next section reviews this traditional remote sensing methodology summarizing a variety of optical indices calculated across the spectrum in the visible and near infrared that have reported utility.

1.2.- OPTICAL INDICES FOR BIOINDICATORS OF VEGETATION STATUS AND FUNCTION: CHLOROPHYLL CONTENT AND CHLOROPHYLL FLUORESCENCE

The objective of developing links between physiologically-based bio-indicators (e.g. pigment concentrations, chlorophyll fluorescence) measured from field and laboratory data with vegetation reflectance is traditionally made through optical indices. Optical indices are based on observed relationships between reflectance at a specific wavelength and leaf pigments or photosynthetic functioning measures that are related directly or indirectly to conditions of stress.

Most studies related to optical indices for vegetation functioning are based on measurements made at the leaf level, rather than at the canopy level, where correlation between chlorophyll fluorescence and spectral reflectance can be readily observed (Peñuelas *et al.*, 1998; Gamon *et al.*, 1997; Peñuelas *et al.*, 1997; Gitelson *et al.*, 1999; Gamon and Surfus, 1999). For example, the effective quantum yield of PSII under illumination is a quantitative measure of the rate at which pigment molecules give up their excitation energy or decay, denoted $\Delta F/Fm'$, shown to be related linearly to the Photochemical Reflectance Index, defined as PRI = $(R_{531}-R_{570})/(R_{531}+R_{570})$, in top-canopy leaves of a wide range of species. Gamon *et al.* (1997) suggested that PRI could be used as an interspecific index of photosynthetic radiation-use efficiency for leaves and canopies in full sun, but not across wide ranges of illumination from deep shade to full sun. Further, they suggested that relative photosynthetic rates could be derived remotely

if issues of canopy and stand structure could be resolved. Gitelson *et al.* (1999) showed that the inverse reflectance $(R_{700})^{-1}$ was an excellent predictor of leaf chlorophyll content at a leaf level but that the apparent reflectance value was also significantly affected by fluorescence emission, and would also be affected by canopy structure in remote observation of canopies.

Changes in the slope and position of the red edge (0.70-0.74 μm) with leaf chlorophyll concentrations have been discussed by Horler (1980; 1983), as well as in some other recent studies at leaf and canopy levels. The position and slope of the red edge will change as healthy leaves progress from active photosynthesis through various stages of senescence due to loss of chlorophyll and the addition of tannins (Knipling, 1969). A shift in the position of the red edge to shorter wavelengths is known as the *blue shift* and is associated with heavy metal-induced stress in several vegetation types (Chang and Collins, 1983; Horler *et al*., 1980; 1983). The *blue shift* has been attributed to reductions of chlorophyll-b and a relative decrease of chlorophylls for needles of high-damaged sites, as compared with those from low-damage sites (Rock *et al*., 1988). Promising results were obtained by Vogelmann *et al*. (1993) correlating red edge spectral parameters and chlorophyll content in sugar maple leaves affected by intensive insect damage. The indices used were the red edge inflection point (REIP), the ratio R_{740}/R_{720}, and the ratio of first derivative values at 715-705 nm (D_{715}/D_{705}). The three indices demonstrated a high correlation with chlorophyll-a, chlorophyll-b and total chlorophyll content at a leaf level. However, neither the Normalized Difference Vegetation Index

(NDVI), calculated as $(R_{NIR}-R_{RED})/(R_{NIR}+R_{RED})$, or vegetation indices commonly used in vegetation mapping using satellite optical remote sensing, correlated well. The red edge position has also been studied as estimator of leaf area index (LAI) and hydric status at the canopy level (Filella and Peñuelas, 1994). Red edge position, amplitude of red edge peak and area of red edge peak were studied in the field at canopy level with hand-held radiometers and correlated with chlorophyll content, LAI and water content. The area of the red edge peak ($\Sigma dr_{680\text{-}780nm}$) was the best estimator of LAI, and the red edge position was highly correlated with chlorophyll content. When water stress is well developed, a correlation with the amplitude of the derivative reflectance peak in the red edge was found. These results suggest that red edge spectral parameters may be used to detect and map areas of damage due to the effects of the canopy structure, it can also be used as an early indicator of forest damage and thus could be of considerable value in monitoring forest condition and state of health. Zarco-Tejada and Miller (1999) demonstrated the use of red edge spectral parameters for forest land cover classification based on systematic species (cover) characteristics of pigment content and canopy structure and their effects on red edge spectral parameters, calculated by an inverted Gaussian least-square fit from airborne CASI reflectance data in a 13x13 km grid.

Recent studies by Peñuelas *et al*. (1995) showed that the Simple Ratio Pigment Index (SRPI) (R_{430}/R_{680}), based on carotenoid/chlorophyll-a content, correlates well at leaf level with different levels of mite attacks in apple trees. Carotenoid/chlorophyll-a ratio increases with increasing level of attack. Classical reflectance indices such as NDVI or

even the red edge position were unable to distinguish among treatments. The wavelength for the red edge was not sensitive to stress caused by mite attack apparently due to the saturation of signal when chlorophyll concentration is high (Filella and Peñuelas, 1994). SRPI demonstrated its sensitivity at a phenologically later state, i.e. when chlorophyll concentration is lower.

Normalized Phaeophytinization Index (NPQI) calculated as $(R_{415}-R_{435})/(R_{415}+R_{435})$ is considered responsive to chlorophyll degradation (Barnes *et al*., 1992) in studies at a leaf level. The same study by Peñuelas *et al*. (1995) shows that NPQI was the most sensitive index to the stress caused by mite attacks at leaf level. This is in agreement with Lorenzen and Jensen (1989) and Ahern (1988) for leaves of bark beetle-attacked lodgepole pine. NPQI could be used for detection of stress at early stages. Photochemical Reflectance Index (PRI) is a physiological reflectance index that correlates with the epoxidation state of the xanthophyll cycle pigments and with the efficiency of photosynthesis in control and nitrogen stress canopies (Gamon *et al*., 1992). PRI is calculated as $(R_{REF}-R_{531})/(R_{REF}+R_{531})$ with R_{REF} at a wavelength to minimize complications associated with diurnal sun angle changes and the corresponding effects on canopy reflectance. R_{REF} has been selected as R_{550} and R_{570} (Gamon *et al*., 1992; Filella *et al*., 1996) and in other studies R_{531} has been shifted to R_{530} (Peñuelas *et al*., 1994) and to R_{539} (Filella *et al*., 1996). The xanthophyll cycle may be associated with diurnal reductions in photosynthetic efficiency: under conditions of excess light the xanthophyll cycle pigment violaxanthin is de-epoxidized since this reaction is readily reversed under

limiting light (Gamon *et al*., 1992). Thus, the epoxidation state, or in other words, the concentration of the three xanthophyll cycle pigments, may be a useful indicator of short-term changes in photosynthetic activity. PRI revealed its utility in the assessment of radiation-use efficiency at canopy level; Filella *et al*. (1996) showed that PRI was significantly correlated with epoxidation state and zeaxanthin and with photosynthetic radiation-use efficiency, working on a cereal canopy and measuring reflectance, fluorescence, gas exchange and xanthophyll cycle pigments. Recent research undertaken by Peñuelas *et al*. (1997) presents new results validating PRI to assess photosynthetic-radiation-use efficiency at a leaf level in Mediterranean trees *Quercus ilex* and *Phillyrea latifolia*. However, a consistent relation between PRI and radiation-use efficiency at the canopy level has not always been found. In fact, its application at larger scales would present additional complications due to heterogeneous landscape composition, atmospheric interference and calibration errors (Guyot, 1990).

Normalized Pigment Chlorophyll ratio Index (NPCI) and derivative analysis indices were tested by Peñuelas *et al*. (1994) at a leaf level. NPCI, calculated as $(R_{680}-R_{430})/(R_{680}+R_{430})$ was found to vary with total pigments/chlorophyll. The maximum (dG) and minimum (dg) of the first derivatives of reflectance in the green, at approximately 525 nm and 570 nm respectively, were correlated with diurnal photosynthetic rate, and with seasonal chlorophyll and N changes. The normalized ratio between the maxima of the first derivatives of reflectance at the red edge and green regions (EGFN) was correlated with chlorophyll and N contents at a leaf level. Other derivative analysis indices tested at a

leaf level were the normalized difference between *d*G and *d*g (GGFN) calculated as (*d*G-*d*g)/(*d*G+*d*g); the maximum of the first derivative of reflectance in the red edge, at approximately 700-710 nm (*d*RE); the normalized difference between *d*RE and *d*G, calculated as (*d*RE-*d*G)/(*d*RE+*d*G); the minimum of the second derivative of reflectance in the green, at approximately 530 nm (*dd*g); and the maximum of the second derivative of reflectance in the red edge, at approximately 690 nm (*dd*RE). Results at a leaf level showed that *d*G followed diurnal photosynthetic rates and seasonal chlorophyll and nitrogen changes, and NPCI varied with the total pigments/chlorophyll ratio, indicative of plant phenology and physiological status.

Other canopy-level ratios have been studied as indicators of plant stress, such as R_{695}/R_{670}, R_{695}/R_{420}, R_{605}/R_{760}, R_{695}/R_{760} and R_{710}/R_{760} (Carter, 1994). The ratios that most strongly indicated plant stress were R_{695}/R_{420} and R_{695}/R_{760} when 6 different plant species were affected by 8 stress agents. The results obtained, coupled with the observation at near-infrared (760 nm) reflectance to stress, indicated that reflectance in any waveband throughout the 760 nm - 800 nm range could be divided into reflectance at 605 nm, 695 nm or 710 nm to produce a stress-sensitive ratio. As in other indices related to situations of stress, these indicators could be particularly useful for detection of plant stress in forests. For the Normalized Difference Pigment Index (NDPI) calculated as $(R_{\lambda 1} - R_{\lambda 2})/ (R_{\lambda 1} + R_{\lambda 2})$ and the Structure Intensive Pigment Index (SIPI) calculated as $(R_{800} - R_{\lambda 1})/ (R_{800} - R_{\lambda 2})$, the best results at a leaf level were obtained for the domains [400 nm$<\lambda_1<$530 nm, 600 nm$<\lambda_2<$700 nm].

The inverse reflectance $(R_{550})^{-1}$ and $(R_{700})^{-1}$ are proportional to chlorophyll *a* concentration (Gitelson and Merzlyak, 1996) and therefore the tested indices R_{750}/R_{550} and R_{750}/R_{700} were directly proportional to chlorophyll concentration in a wide range of chlorophyll *a* concentrations at a leaf level. This relationship has been confirmed in a more recent study (Gitelson and Merzlyak, 1997) where high correlations where found between R_{550} and R_{700} and the leaf chlorophyll content through a relationship of the form $Chl = a + b\ R_{750} / R_x$, where R_x is R_{550}, and R_{700}, and *a*, and *b* coefficients for different plant species. Work at leaf level by Curran *et al*. (1992) proposed selected wavelengths by stepwise regression on derivative reflectance for leaf chemical concentration estimation, such as chlorophyll, amaranthin, starch, sugar, protein and water.

Classical vegetation indices such as NDVI (Rouse, 1974), Simple Ratio (SR), Modified Simple Ratio (MSR) (Chen, 1996) and Greenness Index (G) may also serve as indicators of prolonged vegetation stress due to changes in canopy structure. A near-linear relationship has been reported by Sellers (1989) between the canopy photosynthetic rate, canopy stomatal resistance and the absorbed photosynthetically active radiation, with LAI as biophysical property linking those variables. Nevertheless, a lower correlation of these classical indices is expected with leaf pigment contents and, therefore, a correspondingly lower sensitivity to plant stress. Peñuelas *et al.* (1992) demonstrated a lower sensitivity of NDVI than SRPI or NPQI in his experiment on plant stress caused by mites attack in leaves. Nevertheless, classical indices may be useful in distinguishing stress (Peñuelas *et al.*, 1994) although better physiological information is provided by

narrow-band indices. Gamon *et al*. (1990; 1992) reports that NDVI is a sensitive indicator of canopy structure and chemical content (green biomass, green leaf area index, chlorophyll content, and foliar nitrogen content) when LAI ε (0-2), but insensitive when LAI > 2. Both NDVI and SR exhibit near-linear correlations with fractional photosynthetically active radiation (PAR) intercepted by green leaves over a wide range of canopy densities. Their results support the use of NDVI and SR as indicators of PAR absorption, and thus potential photosynthetic activity, even in heterogeneous landscapes. These results are in accordance with Goward *et al*. (1985) and Sellers (1987) where SR and NDVI are described as indices that can detect the quantity and spatial arrangement of green vegetation and can be used to estimate canopy photosynthetic capacity and net primary productivity. Insensitivity of these indices is observed for daily to weekly variation in photosynthetic rates under certain stress conditions (Running and Nemani, 1988) and therefore fails to capture dynamic physiological processes that may occur on fine temporal and spectral scales.

The investigation of fluorescence contributions to the observed signature requires attention to optical indices related specifically to fluorescence emission in the 680-740 nm spectral region. Furthermore, indices related to fluorescence maxima at 685 and 740 nm are considered potentially useful, such as the spectral curvature index (Zarco-Tejada *et al.*, 2000a; 2000b) to study the relationship of canopy reflectance with chlorophyll fluorescence: i.e. R_{685}/R_{655}, $R_{683}^2/(R_{675} \cdot R_{691})$, D_{730}/D_{706}, where D represents

derivative spectra; these fluorescence-sensitive indices will be discussed fully later in this manuscript.

These potentially valuable optical indices, derived from extensive recent research, from reflectance and derivative spectra, have been summarized below and grouped into 4 categories, based on the spectral region and the type of parameter used (Zarco-Tejada *et al.*, 1999a; 1999b).

(a) Visible Ratios: SRPI (R_{430}/R_{680}); NPQI ($R_{415}-R_{435}$)/($R_{415}+R_{435}$); PRI calculated as ($R_{531}-R_{570}$)/($R_{531}+R_{570}$), ($R_{550}-R_{531}$)/($R_{550}+R_{531}$) and ($R_{570}-R_{539}$)/($R_{570}+R_{539}$); NPCI ($R_{680}-R_{430}$)/($R_{680}+R_{430}$); Carter (R_{695}/R_{420}), G (R_{554}/R_{677}) and Lichtenthaler (R_{440}/R_{690}).

(b) Visible/NIR Ratios: NDVI ($R_{774}-R_{677}$)/($R_{774}+R_{677}$); SR (R_{774}/R_{677}); Lichtenthaler ($R_{800}-R_{680}$)/($R_{800}+R_{680}$), (R_{440}/R_{740}); and SIPI ($R_{800}-R_{450}$)/($R_{800}+R_{650}$).

(c) Red Edge Reflectance-Ratio Indices: Vogelmann (R_{740}/R_{720}), ($R_{734}-R_{747}$)/($R_{715}+R_{726}$), ($R_{734}-R_{747}$)/($R_{715}+R_{720}$); Gitelson & Merzylak (R_{750}/R_{700}), (R_{750}/R_{550}); Carter (R_{695}/R_{760}); curvature index ($R_{675}\cdot R_{690}$)/(R_{683}^2), and the area of the derivative under the red edge $\int_{680}^{760} D$.

(d) Spectral and Derivative Red Edge Indices: λ_p, λ_o, R_o, R_s and σ from red edge *inverted-gaussian* curve fitting, as well as spectral indices calculated from derivative

analysis: (D_{715}/D_{705}); DPR1 ($D_{\lambda p}/D_{\lambda p+12}$), DPR2 ($D_{\lambda p}/D_{\lambda p+22}$), DP21 ($D_{\lambda p}/D_{703}$) and DP22 ($D_{\lambda p}/D_{720}$).

Development of methodologies for chlorophyll content and fluorescence estimation in vegetation canopies is the main objective of this research work, as part of the multi-disciplinary *Bioindicators of Forest Sustainability Project*, whose goal was to develop a *Forest Condition Rating System*. Extensive modelling research efforts have been undertaken over the past 10 years to simulate the effect of pigment on leaf reflectance and in turn the arrangement of leaves on the canopy reflectance. Such developments have the potential to replace the statistically-based approaches for estimation of leaf bioindicators with quantitative model-based methods. Progress in this approach is reviewed in Chapter 2 along with the development of the theoretical framework of the approach developed in this research.

The nature of the *Bioindicators of Forest Sustainability Project*, its rationale, and the context of the research described in this dissertation in the overall project are described in the next section.

1.3. THE BIOINDICATORS OF FOREST SUSTAINABILITY PROJECT

It is generally accepted that measures of forest ecosystem health are needed in order to assess the effects of natural phenomena and management activities on sustainability. Forest health and management practices sustainability assessment has been called for by different sources in recent years: the *Canadian Council of Forest Ministers* produced a report on sustainable forest management that indicates the need for providing a measure of ecosystem health, vitality and rates of biological production in forest ecosystems (*Canadian Council of Forest Ministers,* 1995). On the other hand, from the operational perspective, forest managers dealing with forest activities such as renewal, tending, harvesting and productivity of forested lands require tools to evaluate the effects of management practices *(Terms and Conditions of the Environmental Assessment for Ontario, OMNR* 1994). Legislative requirements by the *Crown Forest Sustainability Act*, international standards, and global market pressures have generated an agreement between government and industry for the need to develop a *Forest Condition Rating* (FCR) *system* as a means to monitor forest sustainability. Such a rating system would help to demonstrate that the government is managing its forests sustainably and that the management practices of the forest industry seek sustainability. For example, the position of the Government of Ontario, *Ontario Ministry of Natural Resources,* is presented in reports such as *the Provincial Annual Report on Forest Management, State of the Forest Report*, and *An Assessment of Ontario's Forest Resources,* in which a requirement is stated for a homogeneous and accepted forest health rating system to help demonstrate

that Ontario is managing its forests sustainably (Mohammed *et al.,* 1997b). Knowing whether forests are healthy or stressed could assist in planning and management, particularly if advance warning can be provided to allow measures to be taken to conserve health and productivity.

A research project was undertaken in response to these policy demands in a joint effort between *the Ontario Ministry of Natural Resources* (OMNR) – *Ontario Forest Research Institute* (OFRI), York University (Toronto, Canada), and CRESTech (*Centre for Research in Earth and Space Technology*) with the goal to develop a *Forest Condition Rating* system. The *Bioindicators of Forest Sustainability Project* (Mohammed *et al.,* 1997a; Sampson, *et al.*, 1998) adopted as its research strategy to develop links between physiologically-based bio-indicators, such as pigment concentrations and chlorophyll fluorescence, from field and laboratory data and passive or active remote sensing methods for assessing forest condition. Hyperspectral optical remote sensing was identified as one promising approach, which led to the research carried out in the present work. Previous work by Mohammed *et al*. (1995), Templeton and Colombo (1995), Mohammed (1997), Mohammed *et al*. (1997a), Sampson *et al*. (1997), among others, demonstrates that physiological analysis is effective in early identification of strain and forecasting of stress on survival and growth in tree species. The challenge was to develop suitable optical remote sensing methodologies. Traditional methods of forest health assessment are based on in-situ measurements and visual assessment that require direct contact between the measuring instrument and the tree. Therefore these techniques are

labour-intensive and expensive, making them unsuitable for routine physiological monitoring of large extensions of forest stands. This advocates investigations to identify the optical expression of vegetation stress at the canopy level using the imaging spectrometry remote sensing methods, investigating whether pigment estimation and CF can be quantitatively retrieved through hyperspectral remote sensing.

Twelve study sites of *Acer saccharum* M. (sugar maple) were selected in 1997 from existing provincial plot networks in the Algoma Region (Ontario, Canada) situated at the junction of Lake Superior and Lake Huron, entirely within Sault Ste. Marie District (Figure 1.5). The sites were selected to represent a range of productivity and decline. In particular, six permanent sample plots from the provincial Growth & Yield Program (Anon, 1993; Hayden *et al.,* 1995) were chosen to investigate the effects of stand productivity in maple. Another six plots were selected from the provincial Hardwood Forest Health network (McLaughlin *et al.,* 1992; 1999) to represent a gradient in maple forest decline. Detailed stand records exist and these sites are considered representative of tolerant hardwood forests in the Algoma Region (McLaughlin *et al.,* 1999), and are therefore suitable for research in which canopy hyperspectral remote sensing is used to investigate the effects of bioindicators on measured canopy reflectance.

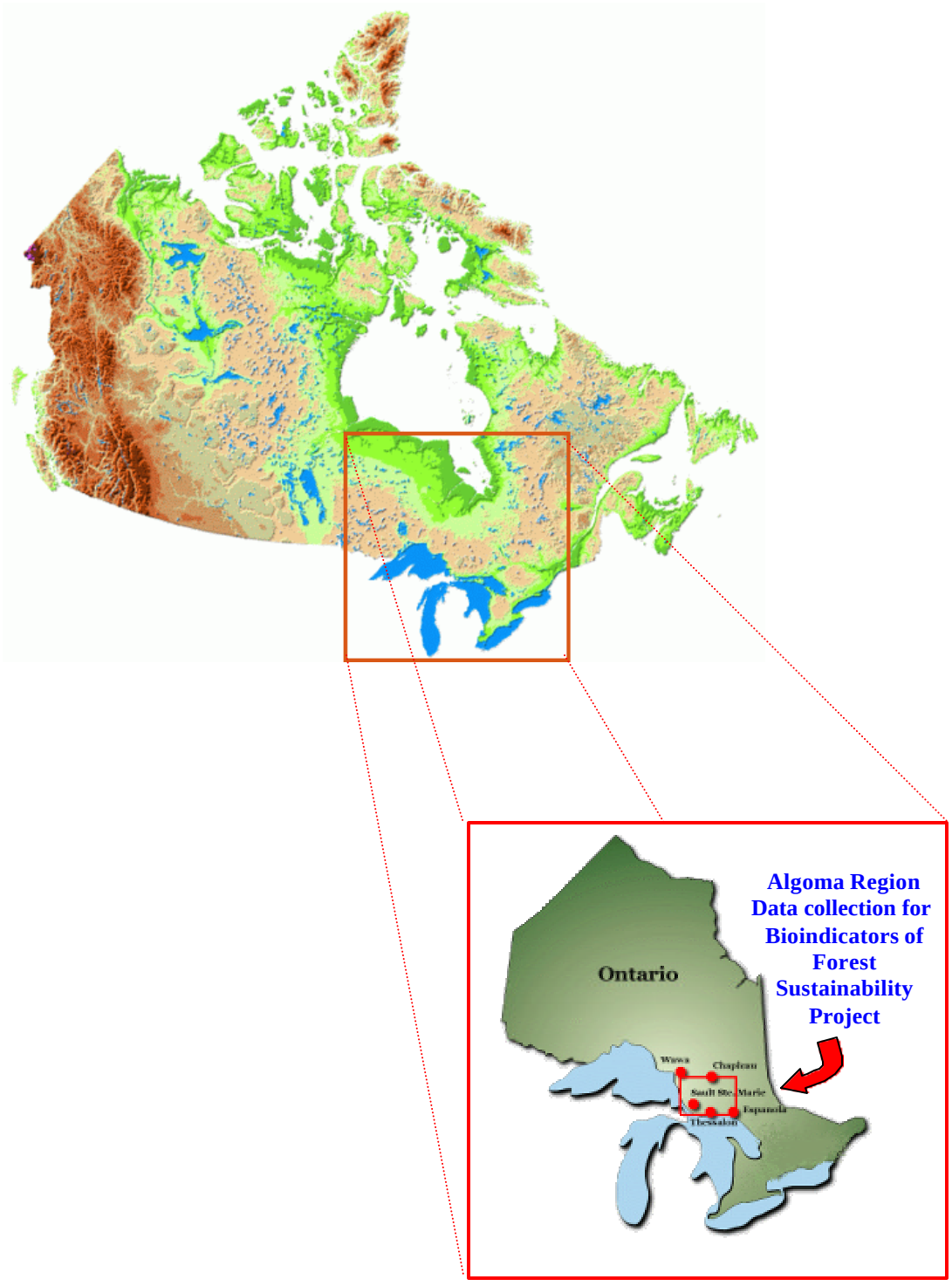

Figure 1.5. Location of the study sites of *Acer saccharum* M. used in this research work, selected from existing provincial plot networks in the Algoma Region (Ontario, Canada), Sault Ste. Marie District, representing a range of productivity and decline.

This research is focussed on the theoretical basis for quantitative estimation of pigments and CF from canopy reflectance using hyperspectral remote sensing. The framework for the link between leaf and canopy levels through radiative transfer models is presented in the next Chapter, in order to quantitatively relate pigment content and CF measured at leaf level with canopy reflectance obtained from the airborne CASI imaging spectrometer. Airborne hyperspectral sensors allow data collection at optimum times with flexibility in the spatial resolution and spectral mode of operation, therefore enabling important issues in the application of remote sensing such the effects of spatial resolution and radiometric canopy texture to be addressed in detail. In addition, the performance of existing and proposed satellite sensors can be readily simulated, enabling the value of these research results to be assessed for future forest monitoring.

CHAPTER 2.

THEORETICAL BACKGROUND

Most of the optical indices noted in the Introduction, which were used to relate pigment content with measured reflectance, have been developed at a leaf level, where the effects of canopy structure and viewing geometry on reflectance are not considered. When leaf reflectance and transmittance are measured for a leaf sample, generally good relationships are found with chl_{a+b}, CF and other pigments. Remote sensing of forest canopies, however requires the understanding of photon-vegetation interactions under different structural and illumination conditions: optical indices derived at leaf level do not necessarily work at canopy level, where canopy structural characteristics and viewing geometry affect the relationships between optical indices and biochemical constituents. Canopy Reflectance (CR) models described in the next section help in understanding the photon-vegetation interactions and will be used as a link between leaf and canopy reflectance. Moreover, leaf-level apparent reflectance due to the absorption of chl_{a+b} and CF emissions can be modelled with the same framework as those applied to the leaf medium, to simulate the effect of such leaf constituents and processes in different spectral regions.

2.1.- THE RADIATIVE TRANSFER EQUATION FOR LEAF AND CANOPY MODELLING

Reflectance and transmittance modelling at leaf and canopy levels provides a framework to address fundamental research issues in remote sensing. Leaf level relationships between leaf reflectance and biochemical constituents is not only a function of constituents, but also depends on leaf structure, which varies with growth stages. Changes in cell size and leaf thickness affect the scattering properties. Therefore relationships based solely on leaf-level optical indices should be considered season and species specific. Application of estimation algorithms to sensor-measured above-canopy reflectance needs a link between leaf and canopy levels that includes the effect of canopy structure and viewing geometry: aggregation of leaves in a tree, leaf inclination, tree shape, leaf size, leaf area index, among others, affect differently the above-canopy reflectance measured by an airborne or satellite sensor. This section introduces leaf and canopy radiative transfer models that have been used in the estimation of chl_{a+b} and CF at leaf and canopy levels, which are all based on the radiative transfer equation.

The Radiative Transfer theory has been extensively studied (Chandrasekhar, 1950; Ishimaru, 1978) and is the basis for leaf and canopy radiative transfer models. The theory is based on the radiance loss due to extinction processes, absorption and scattering, and the radiance gain to the system, source radiance or intensification. The variation of

radiance L_λ along a path s depends on a proportionality factor $\aleph_\lambda$ and density of the medium ρ. The variation of L_l due to extinction processes is therefore:

$$\frac{dL_l}{ds} = -\aleph_l \cdot \rho \cdot L_l \quad \Rightarrow \quad dL_l = -\aleph_l \cdot \rho \cdot L_l \cdot ds \qquad [2.1]$$

Integrating the previous equation, results in the law of extinction,

$$\int_{L_{0l}}^{L_l} \frac{dL_l}{L_l} = -\int_0^s \aleph_l \cdot \rho \cdot ds \quad \Rightarrow \quad \left[\ln L_l\right]_{L_{0l}}^{L_l} = -\left[s \cdot \aleph_l \cdot \rho\right]_0^s \quad \Rightarrow$$

$$\Rightarrow \quad \ln L_l - \ln L_{0l} = -s \cdot \aleph_l \cdot \rho \quad \Rightarrow \quad \frac{L_l}{L_{0l}} = e^{-s \cdot \aleph_l \cdot \rho} \quad \Rightarrow$$

$$\Rightarrow L_l = L_{0l} \cdot e^{-s \cdot \aleph_l \cdot \rho} \qquad [2.2]$$

Considerations are that the optical density $\aleph_l \cdot \rho$ is the extinction or attenuation coefficient k_{ext}; the optical depth for an atmospheric column s is $s \cdot \aleph_l \cdot \rho$; and transmission $T_l = e^{-s \cdot \aleph_l \cdot \rho}$.

The radiance gain, source radiance or intensification describes the radiance gain in a volume, $dL_{scl} = j_{scl} \cdot ds$, with dL_{scl} as the gain by in-scattering and self emission radiation, and j_{scl} as the volume scattering coefficient.

The radiance loss $dL_l = -\aleph_l \cdot \rho \cdot L_l \cdot ds \Rightarrow dL_l = -k_{ext} \cdot L_l \cdot ds$, and gain $dL_{scl} = j_{scl} \cdot ds$ to the system forms the integro-differential equation for unpolarized radiation,

$$dL_l = -k_{ext} \cdot L_l \cdot ds + j_{scl} \cdot ds \qquad [2.3]$$

which can be transformed from path length s to zenith direction z for radiation flowing at a θ angle to the vertical, by

$$dz = \cos\theta \cdot ds = \mu \cdot ds \qquad [2.4]$$

where $\mu = \cos\theta$, yielding the optical depth,

$$\tau = \int -\aleph_l \cdot \rho \cdot dz = \int -k_{ext} \cdot dz \Rightarrow d\tau = -k_{ext} \cdot dz \qquad [2.5]$$

and from [2.3] and [2.4],

$$d\tau = -k_{ext} \cdot \mu \cdot ds \Rightarrow k_{ext} = -\frac{d\tau}{\mu \cdot ds} \qquad [2.6]$$

From [2.4, 2.5, 2.6] and [2.3] we get the following transformation:

$$dL_l = -k_{ext} \cdot L_l \cdot ds + j_{scl} \cdot ds = \frac{d\tau}{\mu} \cdot L_l + j_{scl} \cdot \frac{-d\tau}{k_{ext} \cdot \mu} \Rightarrow$$

$$\mu \cdot dL_l = d\tau \cdot L_l - \frac{j_{scl}}{k_{ext}} \cdot d\tau \qquad [2.7]$$

and considering that $J_{scl} = \frac{j_{scl}}{k_{ext}}$ is the scattering source function, the final form of the Radiative Transfer Equation (RTE), is

$$\frac{\mu \cdot dL_l}{d\tau} = -L_l + J_{scl} \qquad [2.8]$$

The scattering source function J_{scl} is defined as the sum of in-scattered radiation due to diffuse radiation and in-scattered radiation due to collimated downwelling radiation,

$$J_{scl} = \frac{\omega_o}{4\pi}\int_{4\pi} P(\gamma)\cdot L_l \cdot d\Omega' + \frac{\omega_o}{4\pi}\cdot P(\gamma_o)\cdot\pi\cdot E_o \cdot e^{\frac{-(t-t_o)}{\mu}} \qquad [2.9]$$

with $P(\gamma)=\frac{\beta(\gamma)}{k_{sc}/4\pi}$ as scattering phase function; $\beta(\gamma)$ as volume scattering function; $k_{sc}=\int_{4\pi}\beta(\gamma)\cdot d\Omega$ as volume scattering coefficient; γ as scattering angle $\cos\gamma=\mu\cdot\mu'+\sqrt{1-\mu^2}\cdot\sqrt{1-\mu'^2}\cdot\cos\phi$; and $\omega_o=\frac{k_{sc}}{k_{ext}}$ as single scattering albedo.

The solution of the RTE for the radiance at a distance *s* from an extended source, or at an optical depth τ^o is the sum of extinction of source radiance and in-scattered path radiance,

$$L_l(\tau^o,\mu) = L_l(0)\cdot e^{-\tau^o/\mu} + \int_0^{2\pi} J_{scl}(t)\cdot e^{\frac{-(\tau^o-t)}{\mu}}\frac{dt}{\mu} \qquad [2.10]$$

With zenith θ and azimuth ϕ angles, the RTE solution is then:

$$L_l(\tau^o;\pm\mu,\phi) = L_l(0;\pm\mu,\phi)\cdot e^{-\tau^o/\mu} + \frac{1}{\mu}\cdot\int_0^{2\pi} J_{scl}(\tau;\pm\mu,\phi)\cdot e^{\frac{-(\tau^o-\tau)}{\mu}}d\tau \qquad [2.11]$$

The variables required to solve the RTE equation are $\tau^o(l)$, total optical depth of the medium; $\omega_o(l)$, single scattering albedo; and $P(\gamma)$, scattering phase function.

Solution of the RTE requires the specification of the scattering phase function in terms of the properties of the medium (Goel, 1988) and solving the equation for given boundary conditions. Properties of the medium considered, such as leaf tissue in the case of a single leaf radiative transfer model, or an assembly of individual leaves in a canopy model, may define the solution to the RTE by considering an approximation based on the distribution randomness of the medium particles. The complexity of the numerical solution for the RTE has been traditionally overcome by different alternatives based on approximations, such as the Kubelka-Munk (1931) approximation theory (K-M) for a plane-parallel medium. It is based on the assumption of an horizontally-homogeneous parallel medium, with diffuse absorption a_d and hemisphere scattering b_{dh} coefficients, downwelling irradiance E_- and upwelling irradiance E_+, and isotropic scattering (Figure 2.1) where bi-hemispheric reflectance is $E_+(0)/E_-(0)$ and transmittance $E_+(Z_o)/E_-(0)$.

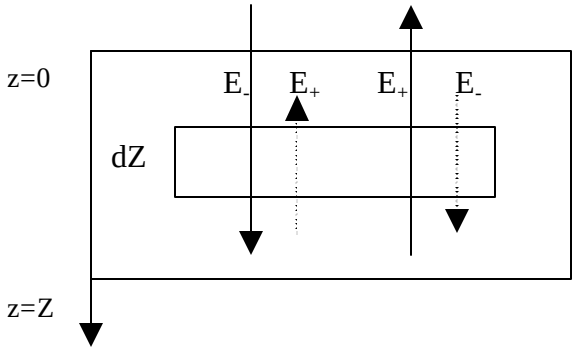

Figure 2.1. Kubelka-Munk approximation theory for a plane-parallel medium based on the assumption of an horizontally-homogeneous parallel medium, with downwelling E_- and upwelling E_+ irradiance, and isotropic scattering, where reflectance is $E_+(0)/E_-(0)$ and transmittance $E_+(Z_o)/E_-(0)$.

The flux approximation by Kubelka-Munk can be implemented in different ways, according to the consideration of diffuse light only (two-flux), diffuse and downwelling collimated light (three-flux), and diffuse and collimated light (four-flux): two-flux approximation (2 parameters) considers only diffuse light, E_-, E_+ a_d, b_{dh}; three-flux

approximation (5 parameters) by Duntley (1942) considers diffuse irradiances E_-, E_+ and collimated incident flux F_- (assuming $F_+=0$) with a_d, b_{dh} as before, and s_1 as scattering coefficient for collimated light in the forward direction, s_2 as scattering coefficient for collimated light in the backscattering direction, and m absorption coefficient for collimated light. Four-flux approximation (5 parameters) assumes both diffuse E_-, E_+ and collimated light F_+, F_-, with coefficients defined as above [2.12].

Downwelling diffuse: $$\frac{dE_-}{dZ} = -(a_d + b_{dh}) \cdot E_- + b_{dh} \cdot E_+ + s_1 \cdot F_- + s_2 \cdot F_+ \qquad [2.12a]$$

Upwelling diffuse: $$-\frac{dE_+}{dZ} = -(a_d + b_{dh}) \cdot E_+ + b_{dh} \cdot E_- + s_1 \cdot F_+ + s_2 \cdot F_- \qquad [2.12b]$$

Downwelling collimated: $$\frac{dF_-}{dZ} = -(m + s_1 + s_2) \cdot F_- \qquad [2.12c]$$

Upwelling collimated: $$-\frac{dF_+}{dZ} = -(m + s_1 + s_2) \cdot F_+ \qquad [2.12d]$$

where fluxes E_+ and E_- are related to L_l [see eq. 2.11] by the equations,

$$E_+ = \int_0^{2p} dy_s \cdot \int_0^{p/2} L_l(t^o; +m, y_s) \cdot m \cdot \sin q_s \cdot dq_s \qquad [2.13a]$$

$$E_- = \int_0^{2p} dy_s \cdot \int_0^{p/2} L_l(t^o; -m, y_s) \cdot m \cdot \sin q_s \cdot dq_s \qquad [2.13b]$$

where E_- and E_+ at the top of the plane parallel medium are known as irradiance and radiant emittance (or radiant excitance), respectively. Kubelka-Munk theory assumes isotropic scattering, applicable to bi-hemispherical reflectance considering an horizontally-homogeneous parallel medium. This theory has been extensively applied in leaf and canopy modelling when the characteristics of the medium are considered as a horizontally-homogeneous plane parallel, although inherently it does not consider mutual

shadowing in discrete targets forming the medium. The solution for the original two-flux approximation by K-M (2 parameters) is given by Equations [2.14].

$$E_{-}(z) = \frac{m+w}{b_{dh}} \cdot C_1 \cdot e^{wz} + \frac{m-w}{b_{dh}} \cdot C_2 \cdot e^{-wz} \qquad [2.14a]$$

$$E_{+}(z) = C_1 \cdot e^{wz} + C_2 \cdot e^{-wz} \qquad [2.14b]$$

where,

$m = (a_d + b_{dh})$

$w = \sqrt{m^2 - b_{dh}^2}$

$C_1, C_2 \equiv$ constant for boundary conditons

The RTE fundamentals explained above can be applied to both leaf (e.g. FRT model in Section 2.2) and canopy media (e.g. SAIL model in Section 2.3) for modelling purposes under specific assumptions. The K-M solution, for plane-parallel turbid media is therefore applied in those cases in which foliar and canopy media can be assumed to meet those conditions. The next sections describe the application of the RTE for both leaf and canopy modelling.

2.1.1.- Leaf Radiative Transfer Models

Willstätter and Stoll (1913) presented the earliest description of a theory to explain leaf reflectance, with subsequent improvements and development of new leaf models: Allen and Richardson, 1968; Breece and Holmes, 1971; Woolley 1971; Allen *et al.*, 1969; 1970. Allen and Richardson (1968) applied K-M theory to study the interaction of light with stacked plant leaves, relating leaf reflectance and transmittance to leaf scattering and

extinction properties of a single compact leaf layer. Improvements to the Allen and Richardson theory were introduced by Yamada and Fujimura (1988) with their matrix calculation to account for four inhomogeneous leaf layers: two cuticles, one palisade mesophyll, and one spongy mesophyll, each one defined in a matrix form by the reflectance and transmittance of the single layer.

The *plate model* by Allen *et al.* (1969) described diffuse reflectance and transmittance of a compact leaf by two parameters: *n,* refractive index, and *k,* absorption coefficient, showing improvements upon the K-M formulation (Allen *et al.,* 1969). The model, originally developed for a single compact leaf layer, was later extended to N layers (Allen *et al.,* 1970 and Gausman *et al.,* 1970) by introducing the VAI index (Void Area Index) where VAI = N – 1, where N refers to the number of layers or "plates". Monocotyledoneous leaves are a compact "plate", with N = 1, and VAI = 0. Dicotyledoneous leaves have a variable VAI depending on species and leaf development. This *plate model,* on which PROSPECT (Jacquemoud and Baret, 1990) leaf model is based, is a discrete approach to the problem of radiative transfer within a leaf, as opposite to the continuous medium approach of Allen and Richardson (1968) based on K-M theory. LIBERTY (Dawson *et al.,*1998) and LEAFMOD (Ganapol *et al.,* 1998) are the latest leaf models in the literature but they lack the extensive validation of PROSPECT. LEAFMOD uses radiative transfer characterization of photon scattering within a homogeneous leaf, rather than the commonly used two-stream or plate approximations

(Ganapol *et al.,* 1999) and using the leaf thickness as input parameter rather than the non-physically measurable structural parameter N in the PROSPECT leaf model.

All these models account for the effect of leaf biochemical constituents such as chl_{a+b}, lignin, and leaf water thickness on reflectance and transmittance, with a structural measure such as leaf thickness or internal structural parameters. Nevertheless, these single leaf models do not include the effects of chlorophyll fluorescence in the measured leaf apparent reflectance. The Fluorescence-Reflectance-Transmittance (FRT) model (Zarco-Tejada *et al.,* 2000a; 2000b) described in the next section was developed with the objective of modelling the effect of fluorescence emission spectra on leaf reflectance and transmittance, since such effects have been postulated as a small but perturbing effect on measurements of radiance or irradiance emerging from a leaf under broadband illumination.

2.2.- MODELLING CF AT LEAF LEVEL: THE FLUORESCENCE-REFLECTANCE-TRANSMITTANCE (FRT) MODEL

Leaf radiative transfer models previously described, based on K-M theory, plate model, or other assumptions for solving the RTE, account for the effect of leaf biochemical constituents such as chl_{a+b}, lignin or leaf water thickness in leaf reflectance and transmittance. Nevertheless, no leaf radiative transfer models are available for CF modelling and simulation of its effect on leaf apparent reflectance. Thus, a model had to be developed for such purposes (Zarco-Tejada *et al.*, 2000a) in order to evaluate theoretically the experimental results obtained at leaf and canopy levels in which the effects of CF could be a component of the apparent reflectance. The Fluorescence-Reflectance-Transmittance (FRT) model (Zarco-Tejada *et al.*, 2000a; 2000b) is developed based on Kubelka-Munk theory, modified following Fukshansky and Kazarinova (1980) to include the addition of fluorescence flux F, in which the K-M differential equations are solved following the doubling method as in Rosema *et al.* (1991), and considering the spectral character of fluorescence emission as the sum of two Gaussian emissions (Subhash and Mohanan, 1997). The matrix formulation from Yamada and Fujimura (1991) permits an individual leaf to be represented as a stack of 3 layers: a top epidermal layer, a compact inner layer containing the chloroplasts and cellular material, and a lower epidermal layer. This model is described in detail below.

The FRT model is presented in four steps and is described in the following sections, i) Kubelka-Munk theory and its modification to include fluorescence flux; ii) solution of the differential equations using the doubling method; iii) matrix calculation of the single leaf as a stack of layers, and iv) definition of extinction and scattering coefficients.

2.2.1.- Modification of the Kubelka-Munk theory to include Fluorescence flux

The work by Fukshansky and Kazarinova modifies the initial 2-flux theory of Kubelka and Munk, in which radiation within an object consists of two diffuse fluxes propagating in opposite directions, and includes fluorescence flux. The flow of total diffuse flux transmittance across a horizontal slab of thickness *dz* at any wavelength λ can be written in differential form as:

$$-dT^{-}(z) = -(a_d + b_{dh})(E^{-}(z) + F^{-}(z))dz + b_{dh}(E^{+}(z) + F^{+}(z))dz + 0.5P(z)dz \qquad [2.15a]$$

$$dT^{+}(z) = -(a_d + b_{dh})(E^{+}(z) + F^{+}(z))dz + b_{dh}(E^{-}(z) + F^{-}(z))dz + 0.5P(z)dz \qquad [2.15b]$$

where

b_{dh} is the linear back-scattering coefficient (mm^{-1}) for diffuse light,
a_d is the linear absorption coefficient (mm^{-1}) for diffuse light,
$E^{-}(z)$ is the downward flowing illuminating irradiance at depth z,
$E^{+}(z)$ is the upward flowing, back-scattered, illuminating irradiance at depth z,
$F^{-}(z)$ is the downward fluorescence flux at depth z,
$F^{+}(z)$ is the upward fluorescence flux at depth z,
$T^{-}(z) = E^{-}(z) + F^{-}(z)$, is the total downward irradiance at depth z,
$T^{+}(z) = E^{+}(z) + F^{+}(z)$, is the total upward irradiance at depth z,
$P(z)$ is the fluorescence emission flux at depth z, assumed to be isotropic.

P(z) is defined as:

$$P(z) = f\varsigma_{\ddot{e}} \int_{400}^{700} a_d \{E^{+}(z) + E^{-}(z)\} \{\ddot{e} / \ddot{e}_{670}\} \cdot d\ddot{e} \qquad [2.16]$$

where the integration is over the PAR spectral region and,

f is the fraction of absorbed upward and downward illuminating PAR energy flux that contributes to fluorescence excitation;

h_l is the fluorescence emission spectral distribution function.

The term *P(z)* [Equation 2.16] assumes that, i) all absorbed photons of E^{+} and E^{-} in the wavelength range λ_1-λ_2 contribute to the excitation of the photosystems; ii) f is the photon fluorescence efficiency; and iii) the fluorescence emission has a spectral distribution h_l. The spectral character of h_l of fluorescence emission has been shown by Subhash and Mohanan (1997) to be effectively described as the sum of two Gaussian emissions with spectral peaks l_L and l_H at approximately 685-690 and 725-730 nm, respectively, with varying relative amplitudes (Figure 2.2). In vivo laser-induced chlorophyll fluorescence spectra of sunflower leaves were measured on a monochromator with a He-Ne laser excitation. The fluorescence spectra were fitted to different spectral functions (Gaussian, Lorentzian, Pearson, Voigt, and exponential Gaussian), showing that best fits were found using a function with two Gaussians centered at 690 and 730 nm. Centre peaks showed to

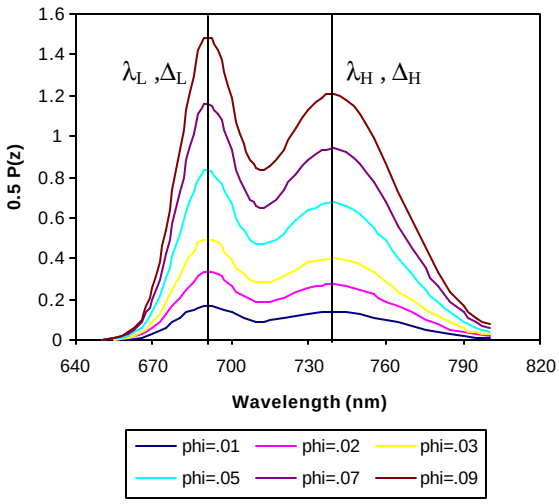

Figure 2.2. P(z) as a function of different values of f (0.01 - 0.09) for λ_L=690, λ_H=735, Δ_L=25, Δ_H=80, f_R=1, a=0.3607.

be dependent on stress conditions, shifting towards the blue region with nutrient stress. Therefore peaks in the 685-690 and 725-730 nm ranges for the low (PSII) and high (PSI) fluorescence maxima should adequately characterize the spectral distribution of fluorescence for the modelling simulation study.

The equation for *P(z)* was originally introduced by Fukshansky and Kazarinova (1980), but without the conversion factor λ/λ_{670}: in that case ϕ is defined as quantum yield. In Rosema *et al.* (1991) the λ/λ_{670} factor is included in order to make the conversion so that ϕ is defined as photon fluorescence efficiency. The spectral distribution of fluorescence can be expressed as:

$$\eta_\lambda = f_R \exp\left(\frac{-(\lambda - \lambda_L)^2}{a\Delta_L^2}\right) + \exp\left(\frac{-(\lambda - \lambda_H)^2}{a\Delta_H^2}\right) \qquad [2.17]$$

where,

f_R	is the ratio of the fluorescence peak at λ_L relative to that at λ_H;
a	is a Gaussian distribution constant equal to 0.3607;
Δ_L and Δ_H	are the full-width at half maximum of the fluorescence emissions centered at λ_L and λ_H , respectively, with typical values of 25 nm and 80 nm (Subhash and Mohanan, 1997).

2.2.2.- Solving the K-M Differential Equations using the Doubling Method

The method selected for solving the differential equations [Equation 2.15] is the doubling method as in Rosema *et al.* (1991) that is extended to allow a description of expected fluorescence emission over the red edge region (650 to 800nm region), resulting from

stimulation by incident radiant flux over the entire PAR region, shown schematically in Figure 2.3. The inherent reflectance r_l, transmittance t_l, and fluorescence f_l of the elementary leaf layer are defined as:

$$r_l = b_{dh\,l}\,dz \qquad [2.18]$$

$$t_l = 1 - (a_{d\,l} + b_{dh\,l})\,dz \qquad [2.19]$$

$$f_l = \phi h_l a_{dp}(l_p/l)dz/2 \qquad [2.20]$$

where the subscript p denotes the average spectral value for the PAR light absorbing region.

Following Rosema *et al.* (1991), we consider 3 important fluxes through the leaf layers: i) excitation fluxes in the PAR region, E_p^+, E_p^-; ii) incident irradiance fluxes at any wavelength, E^+, E^-; and iii) fluorescence fluxes at λ>660.

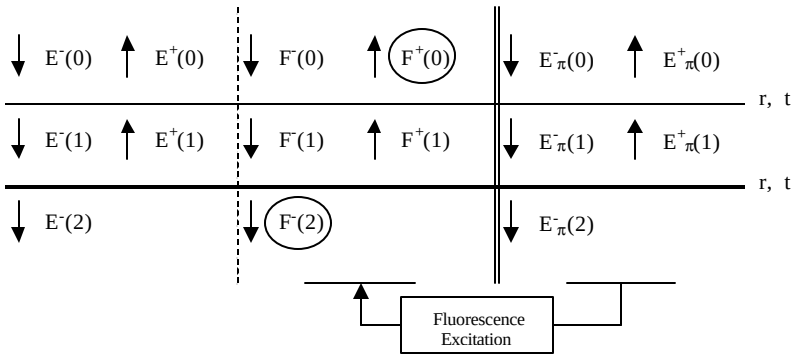

Figure 2.3. Schematic representation of the flow of irradiance for two elemental leaf layers. *F*, *E* and E_π refer to fluorescence irradiance flux, irradiance and irradiance in the PAR region, respectively. The superscripts + and - refer to up- and down-ward flowing flux. The reflectance and transmittance of the elemental layer within the leaf are *r* and *t*, respectively.

If we consider two identical layers placed in close proximity (Figure 2.4), the reflectance and transmittance of the double layer $R(2)$ and $T(2)$ is calculated as follows:

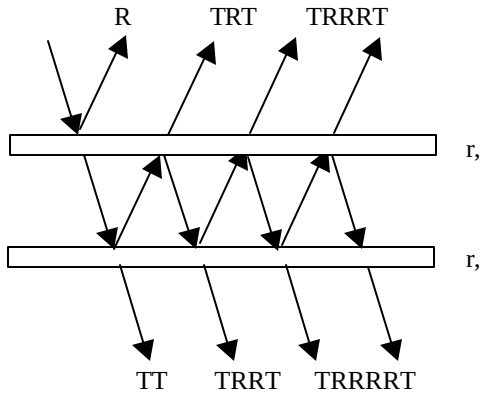

Figure 2.4. Schematic representation of light interaction in two identical layers placed in close proximity.

$$R(2) = R + TRT + TRRRT + TRRRRRT + \ldots = R + TRT\,(1 + R^2 + R^4 + \ldots) \Rightarrow$$

$$R(2) = R(1) + T(1)R(1)T(1) \cdot \left\{ \frac{1}{1 - R(1) \cdot R(1)} \right\} \qquad [2.21]$$

$$T(2) = TT + TRRT + TRRRRT + TRRRRRRT + \ldots = TT\,(1 + R^2 + R^4 + R^6 + \ldots) \Rightarrow$$

$$T(2) = T(1)T(1) \cdot \left\{ \frac{1}{1 - R(1) \cdot R(1)} \right\} \qquad [2.22]$$

where,

$R(1)$, $T(1)$	are r and t of a single layer;
$R(2)$, $T(2)$	are r and t of the double layer.

The application of this methodology to the 3 important fluxes through the leaf layers is given below.

A. Excitation fluxes in the PAR region: E_p^+, E_p^-

$$E_{\lambda}^{-}(2) = t_{D\lambda}\, E_{\lambda}^{-}(0) \qquad [2.23a]$$

$$E_{\lambda}^{+}(0) = r_{D\lambda}\, E_{\lambda}^{-}(0) \qquad [2.23b]$$

where,

t_{Dp}	double layer transmittance;
r_{Dp}	double layer reflectance;

Using the Doubling Method, as demonstrated before, t_{Dp} and r_{Dp} are calculated as:

$$t_{Dp} = T(2) = T(1)T(1) \cdot \left\{ \frac{1}{1 - R(1) \cdot R(1)} \right\} = t_p \cdot t_p \cdot \left\{ \frac{1}{1 - r_p \cdot r_p} \right\} \qquad [2.24]$$

$$r_{Dp} = R(2) = R(1) + T(1)R(1)T(1) \cdot \left\{ \frac{1}{1 - R(1) \cdot R(1)} \right\} =$$

$$= r_p + t_p \cdot r_p \cdot t_p \cdot \left\{ \frac{1}{1 - r_p \cdot r_p} \right\} \qquad [2.25]$$

Considering that,

$$x_{\lambda} = \frac{t_{\lambda}}{(1 - r_{\lambda} \cdot r_{\lambda})} \qquad [2.26]$$

then,

$$t_{D\lambda} = x_{\lambda}\, t_{\lambda} \qquad [2.27a]$$

$$r_{D\lambda} = r_{\lambda}\,(1 + x_{\lambda}\, t_{\lambda}) \qquad [2.27b]$$

Therefore,

$$E_{\delta}^{-}(2) = t_{D\delta}\, E_{\delta}^{-}(0) = x_{\delta}\, t_{\delta}\, E_{\delta}^{-}(0) \quad [2.28a]$$

$$E_{\delta}^{+}(0) = r_{D\delta}\, E_{\delta}^{-}(0) = r_{\delta}(1+x_{\delta}\, t_{\delta})E_{\delta}^{-}(0) \quad [2.28b]$$

where r_p and t_p are the equivalent reflectance and transmittance of the elementary layer in the PAR region and r_{Dp} and t_{Dp}, are the equivalent reflectance and transmittance in the PAR region of the doubled elementary layer. These fluxes contribute to the fluorescence at longer wavelengths (660 to 800 nm).

B. Incident irradiance fluxes at any wavelength: E^{+}, E^{-}

This is analogous to the previous demonstration for excitation fluxes in the PAR region, but without the π subscript:

$$E^{-}(2) = t_D E^{-}(0) \quad [2.29a]$$

$$E^{+}(0) = r_D E^{-}(0) \quad [2.29b]$$

Considering that,

$$x = \frac{t}{(1-r \cdot r)} \quad [2.30]$$

then,

$$t_D = xt \quad [2.31a]$$

$$r_D = r(1+xt) \quad [2.31b]$$

Therefore,

$$E^{-}(2) = t_D E^{-}(0) = xtE^{-}(0) \quad [2.32a]$$

$$E^{+}(0) = r_D E^{-}(0) = r(1+xt)E^{-}(0) \quad [2.32b]$$

C. Fluorescence fluxes at l >660

The fluorescence flux at wavelength λ>660 is function of the downward fluorescence flux F^{-} and irradiance E^{-} in the PAR region according to:

$$F^{-}(2) = t_D F^{-}(0) + f_D E^{-}_{\partial}(0) \quad [2.33a]$$

$$F^{+}(0) = r_D F^{-}(0) + g_D E^{-}_{\partial}(0) \quad [2.33b]$$

where g_D and f_D are the front side and backside fluorescence response of the double-layer to the flow of incident excitation flux in PAR region given by:

$$g_D = f(1 + x_{\partial}\, t + x_{\partial}\, r_{\partial} + xr) + xrx_{\partial}\, f(r + r_{\partial}) \quad [2.34a]$$

$$f_D = f(x + x_{\partial}) + xx_{\partial}\, f(r + r_{\partial}) \quad [2.34b]$$

with

$$x_{\partial} = \frac{t_{\partial}}{(1 - r_{\partial}.r_{\partial})} \quad [2.35]$$

The recursion relations described above allow the optical properties of the double-layer to be expressed in terms of the single layer. The irradiance and fluorescence fluxes can be simulated through an entire leaf layer by successive doublings, in which r_D, t_D, g_D and f_D are substituted into the recursion equations for r, t, g and f, and the new double-layer E_p, E and F fluxes are calculated.

The number of doublings required depends on the layer thickness D_L, and the relationship:

$$\frac{D_L}{dZ} = 2^n \qquad [2.36]$$

where,

D_L is the thickness of the leaf;
dZ is the thickness of the initial thin layer;
n is the number of doubling steps;

If we consider that:

$dZ = 10^{-7}$ m order of the size of a photosystem or the wavelength;

$D_L = 10^{-3}$ m thickness of the leaf;

$$\frac{10^{-3}}{10^{-7}} = 2^n \Rightarrow n = 13.28 \cong 14 \; doublings$$

Implementation of the Doubling Method for a Single Leaf

The doubling method, performed as suggested by 14 doublings, results in a calculation of r_{Dl}, t_{Dl}, r_{Dp}, t_{Dp}, g_{Dl} and f_{Dl}.

1. Excitation fluxes in the PAR region: E_p^+, E_p^-

$$t_{D\delta} = x_\delta t_\delta \qquad r_{D\delta} = r_\delta (1+x_\delta t_\delta) \qquad x_\delta = \frac{t_\delta}{(1-r_\delta \cdot r_\delta)}$$

These are not wavelength dependent (because we are calculating in the PAR region), and initial values of r_π and t_π are:

$r_p = b_{dhp} \cdot dz$

$t_p = 1-(a_{dp} \cdot b_{dhp}) \cdot dz$

$$b_{dhp} = \frac{\sum_{PAR} b_{dh}}{n}; \qquad a_{dp} = \frac{\sum_{PAR} a_d}{n}$$

where PAR [400:700]; n=60 (5nm); $\frac{Z}{dZ} = 2^n \Rightarrow dZ = \frac{Z}{2^n} = \frac{L_{Thickness}}{2^{14}}$

2. Incident irradiance fluxes at any wavelength: E^+, E^-

$$t_D = xt \qquad r_D = r(1+xt) \qquad x = \frac{t}{(1-r \cdot r)}$$

$r_l = b_{dhl} \cdot dz$

$t_l = 1-(a_{dl} \cdot b_{dhl}) \cdot dz$

3. Fluorescence fluxes at l >660

$$g_D = f(1+ x_{\delta}\, t+x_{\delta}\, r_{\delta} + xr)+xrx_{\delta}\, f(r+r_{\delta})$$
$$f_D = f(x + x_{\delta})+xx_{\delta}\, f(r+r_{\delta})$$

$$x_{\delta} = \frac{t_{\delta}}{(1-r_{\delta}.r_{\delta})}$$

where $f_l = fh_l a_{dp}(l_p/l)dz/2$, with λ_{π}=690

Example:

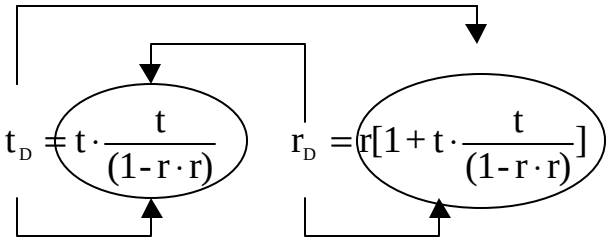

The final calculation of *r* and *t* with the effect of fluorescence (r^*, f^*) is:

$$r_l^* = r_{Dl} + g_{Dl}$$
$$t_l^* = t_{Dl} + f_{Dl}$$

2.2.3. Matrix Calculation: Single Leaf as a Stack of Layers

The flux flow across a leaf layer calculated using the Doubling Method described in Section 2.2.2 does not consider the epidermal layers. Estimates of *r** and *t** need now to be modified by considering the two epidermal layers. Yamada and Fujimura (1991) provided a convenient framework for the description of the flow of radiant fluxes across a leaf considered as a stack of layers.

The matrix formulation from Yamada and Fujimura permits an individual leaf to be represented as a stack of 3 layers (Figure 2.5): a top epidermal layer, a compact inner layer containing the chloroplasts and cellular leaf material, and a lower epidermal layer. In the FRT model, the leaf was considered for simplicity as a stack of 3 layers, the upper epidermis, an active compact layer containing the chloroplasts and cells which give rise to the absorption, scattering and fluorescence, and the lower epidermal layer.

The two epidermal layers are assumed to contain no chlorophyll and may be defined solely in terms of their scattering properties as determined by the index of refraction. The corresponding reflectance and transmittance of the cuticular layer is then used to define the radiative transfer matrix G_e, and the radiative transfer matrix of the leaf inner compact layer G_I. The corresponding inner leaf layer reflectance and transmittance is then calculated.

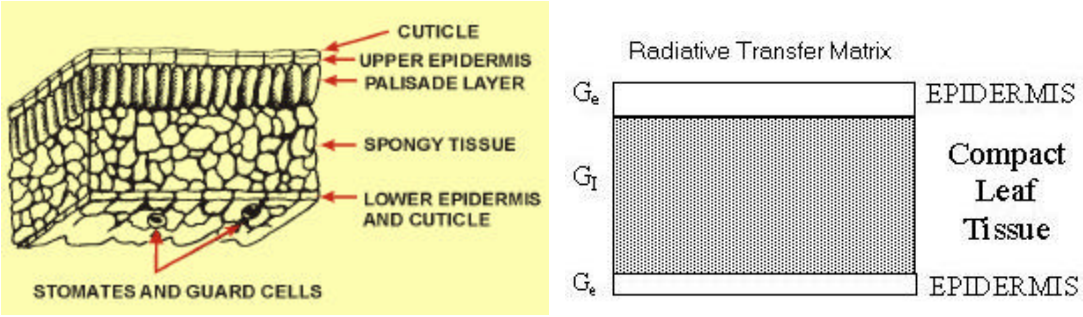

Figure 2.5. Schematic view of a leaf (left) and the matrix formulation from Yamada and Fujimura (right) allowing an individual leaf to be represented as a stack of 3 layers: a top epidermal layer, a compact inner layer containing the chloroplasts and cellular material, and a lower epidermal layer.

The total downward irradiance entering and the total upward irradiance emerging from above any layer or group of layers (Figure 2.6) are designated T^-_a and T^+_a, respectively, and below this layer the total emerging downward irradiance and the total incident upward irradiance are designated T^-_b and T^+_b, respectively.

Accordingly one can write the recursion relations for the flux across any layer k:

$$T_a^+ = r_a^* T_a^- + t_b^* T_b^+ \qquad [2.37a]$$

$$T_b^- = t_a^* T_a^- + r_b^* T_b^+ \qquad [2.37b]$$

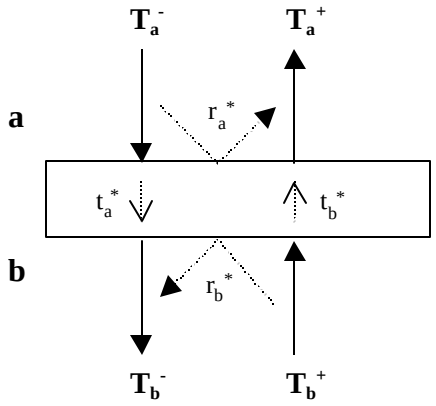

Figure 2.6. Total downward irradiance entering (T_a^-) and upward emerging (T_a^+) from above a layer, with T_b^- and T_b^+ from below the layer.

where the layer (or group of layers) is defined by the apparent reflectance and transmittance coefficients, r^*_a, r^*_b, t^*_a, and t^*_b, with '*a*' denoting a view from the top and '*b*' denoting the view from the bottom.

The upward and backward coefficients are, in general, not equal for an inhomogeneous layer or for a stack of different homogeneous layers, and is a well-known property for a dicotyledoneous leaf.

For the i^{th} layer in a leaf, or an arbitrary number of layers, the equation can be written in matrix form as (Yamada and Fujimura, 1991):

$$\begin{bmatrix} T_{bi}^{-} \\ T_{bi}^{+} \end{bmatrix} = G_i \begin{bmatrix} T_{ai}^{-} \\ T_{ai}^{+} \end{bmatrix} \quad [2.38]$$

where $$G_i = \frac{1}{t_{bi}^{*}} \begin{bmatrix} (t_{ai}^{*} t_{bi}^{*} - r_{ai}^{*} r_{bi}^{*}) & r_{bi}^{*} \\ -r_{ai}^{*} & 1 \end{bmatrix} \quad [2.39]$$

which for a homogeneous layer reduces to,

$$G_i = \frac{1}{t_i^{*}} \begin{bmatrix} (t_i^{*2} - r_i^{*2}) & r_i^{*} \\ -r_i^{*} & 1 \end{bmatrix} \quad [2.40]$$

The demonstration is given below:

$$\begin{bmatrix} T_b^{-} \\ T_b^{+} \end{bmatrix} = G \cdot \begin{bmatrix} T_a^{-} \\ T_a^{+} \end{bmatrix} \text{ with } G = \frac{1}{t_b^{*}} \begin{bmatrix} (t_a^{*} t_b^{*} - r_a^{*} r_b^{*}) & r_b^{*} \\ -r_a^{*} & 1 \end{bmatrix} \quad [2.41]$$

Therefore,

$$\begin{bmatrix} T_b^{-} \\ T_b^{+} \end{bmatrix} = \frac{1}{t_b^{*}} \begin{bmatrix} (t_a^{*} t_b^{*} - r_a^{*} r_b^{*}) & r_b^{*} \\ -r_a^{*} & 1 \end{bmatrix} \cdot \begin{bmatrix} T_a^{-} \\ T_a^{+} \end{bmatrix} \quad [2.42]$$

Expanding the previous Equation [2.42],

$$T_b^- = (t_a^* - \frac{r_a^* \cdot r_b^*}{t_b^*}) \cdot T_a^- + \frac{r_b^*}{t_b^*} \cdot T_a^+$$

$$T_b^+ = \frac{-r_a^*}{t_b^*} \cdot T_a^- + \frac{T_a^+}{t_b^*} \Rightarrow t_b^* \cdot T_b^+ = -T_a^- \cdot r_a^* + T_a^+ \Rightarrow \boxed{T_a^+ = T_b^+ \cdot t_b^* + T_a^- \cdot r_a^*} \qquad [2.43]$$

$$T_b^- = t_a^* \cdot T_a^- - \frac{r_a^* \cdot r_b^*}{t_b^*} \cdot T_a^- + \frac{r_b^*}{t_b^*} \cdot T_a^+ = t_a^* \cdot T_a^- - \frac{r_a^* \cdot r_b^*}{t_b^*} \cdot T_a^- + \frac{r_b^*}{t_b^*} (T_b^+ \cdot t_b^* + T_a^- \cdot r_a^*) =$$

$$= t_a^* \cdot T_a^- - \frac{r_a^* \cdot r_b^*}{t_b^*} \cdot T_a^- + r_b^* \cdot T_b^+ + \frac{r_a^* \cdot r_b^*}{t_b^*} \cdot T_a^-) \Rightarrow \boxed{T_b^- = t_a^* \cdot T_a^- + r_b^* \cdot T_b^+} \qquad [2.44]$$

Therefore, for a 3 layer model (Figure 2.7) for a leaf the matrix radiative transfer equation becomes:

$$\begin{bmatrix} T_3^- \\ T_3^+ \end{bmatrix} = G \begin{bmatrix} T_1^- \\ T_1^+ \end{bmatrix} \qquad \text{where,} \qquad \boldsymbol{G = G_3 G_2 G_1} \qquad [2.45]$$

The upper and lower cuticular layers (G_3 and G_1) were calculated as in the Section 2: $r_e = r_1 = r_3 = 1 - t_1 = 1 - t_3$; and the reflectance of the epidermis r_e is defined only by its refractive index:

$$r_e = \frac{(n-1)^2}{(n+1)^2}; \text{ with } n \text{ refractive index;}$$

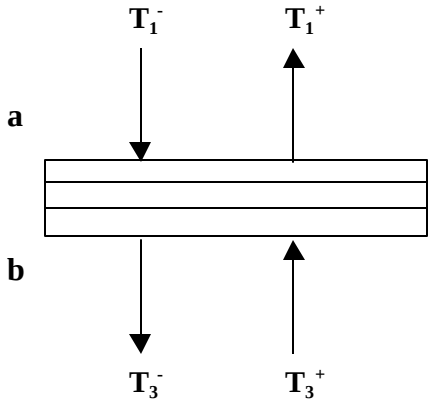

Figure 2.7. Schematic view of a three-layer model for a leaf used for the matrix radiative transfer equation. Leaf reflectance from above is calculated as T_1^+/T_1^-, and leaf transmittance is as T_3^-/T_1^-.

Therefore G_1 and G_3 are calculated as:

$$G_e = G_3 = G_1 = \frac{1}{(1-r_e)}\begin{bmatrix}(1-2r_e) & r_e\\ -r_e & 1\end{bmatrix} \quad [2.46]$$

And G_2 is calculated as:

$$G_2 = \frac{1}{t^*}\begin{bmatrix}(t^{*2}-r^{*2}) & r^*\\ -r^* & 1\end{bmatrix} \quad [2.47]$$

Alternately, writing

$$G = \begin{bmatrix}g_{11} & g_{12}\\ g_{21} & g_{22}\end{bmatrix} \quad [2.48]$$

Therefore,

$$\begin{bmatrix}T_3^-\\ T_3^+\end{bmatrix} = G\begin{bmatrix}T_1^-\\ T_1^+\end{bmatrix} \Rightarrow \begin{bmatrix}T_3^-\\ T_3^+\end{bmatrix} = \begin{bmatrix}g_{11} & g_{12}\\ g_{21} & g_{22}\end{bmatrix}\cdot\begin{bmatrix}T_1^-\\ T_1^+\end{bmatrix} \quad [2.49]$$

and,

$$T_3^- = g_{11}T_1^- + g_{12}T_1^+ \quad [2.50a]$$

$$T_3^+ = g_{21}T_1^- + g_{22}T_1^+ \quad [2.50b]$$

The above equations allow the definition of the apparent front and back leaf reflectance, r^*_a and r^*_b, respectively, and the apparent leaf transmittances t^*_a and t^*_b (considering *a* from above, and *b* from below) (Figure 2.7):

From above:

$$r_1 = \frac{T_1^+}{T_1^-} \quad considering \quad T_3^+ = 0 \quad \Rightarrow \quad g_{21} \cdot T_1^- + g_{22} \cdot T_1^+ = 0 \quad \Rightarrow$$

$$r_1 = \frac{T_1^+}{T_1^-} = -g_{21}/g_{22} \qquad [2.51]$$

$$t_1 = \frac{T_3^-}{T_1^-}; \quad T_3^- = g_{11}T_1^- + g_{12}T_1^+ \quad \Rightarrow \quad \frac{T_3^-}{T_1^-} = g_{11} + g_{12} \cdot \frac{T_1^+}{T_1^-} \Rightarrow \frac{T_3^-}{T_1^-} = g_{11} + g_{12} \cdot (-g_{21}/g_{22}) \Rightarrow$$

$$\Rightarrow \frac{T_3^-}{T_1^-} = g_{11} - \frac{g_{12} \cdot g_{21}}{g_{22}} = \frac{g_{11} \cdot g_{22} - g_{12} \cdot g_{21}}{g_{22}} \quad \Rightarrow$$

$$t_1 = \frac{T_3^-}{T_1^-} = \frac{g_{11} \cdot g_{22} - g_{12} \cdot g_{21}}{g_{22}} \qquad [2.52]$$

From below:

$$r_3 = \frac{T_3^-}{T_3^+} \quad considering \; T_1^- = 0 \quad \Rightarrow \quad r_3 = \frac{T_3^-}{T_3^+} = g_{12}/g_{22} \qquad [2.53]$$

$$t_3 = \frac{T_1^+}{T_3^+} \quad considering \; T_1^- = 0 \quad \Rightarrow \quad t_3 = \frac{T_1^+}{T_3^+} = 1/g_{22} \qquad [2.54]$$

2.2.4. Extinction and Scattering coefficients

The linear absorption and scattering coefficients (a_d and b_{dh}) of the leaf layers need to be specified in the Kubelka-Munk differential equations, or more precisely, in the elemental equations [2.18-2.20] used in the Doubling Method Solution. A specific linear extinction coefficient that takes into account the effects of pigment concentration is required. The a_d

coefficient from the PROSPECT model (Jacquemoud and Baret, 1990; Jacquemoud *et al.*, 1996) is used with the thickness of the leaf.

The selection of a specific linear scattering coefficient is more difficult due to large differences in the spectral behaviour of b_{dh} reported in the literature: Fukshansky *et al.* (1991), Yamada and Fujimura (1991), Rosema *et al.* (1991). Therefore, the equations in Allen and Richardson (1968) were used to derive the Stokes parameters from measured leaf layer reflectance and transmittance, which are used with the measured leaf thickness, to compute the leaf layer Kubelka-Munk linear scattering and extinction parameters a_d and b_{dh}. Therefore, a_d was taken from PROSPECT and b_{dh} was calculated through the K-M model from leaf sample reflectance and transmittance.

Extinction Coefficient a_d

To simulate and to solve the radiation flux through the leaf using the Kubelka-Munk differential equations we need to calculate a_d and b_{dh} coefficients of the leaf layers. A specific linear extinction coefficient that takes into account the effects of pigment concentration is required. The a_d coefficient from the PROSPECT model (Jacquemoud and Baret, 1990; Jacquemoud *et al.*, 1996) is used with the thickness of the leaf (*K* from PROSPECT is used to calculate a_d dividing by the leaf thickness). PROSPECT radiative transfer model, based on the Allen's *plate model* (1969), models leaf optical properties from 400 to 2500 nm. Scattering is defined by a refractive index (*n*) and by a parameter that is function of the leaf mesophyll structure (*N*). For a leaf layer with total thickness

D_L, the specific linear absorption coefficient (mm^{-1}) at any wavelength can be expressed by:

$$a_d = g(SC_j K_j)/N \cdot D_L + k_e/D_L \quad [2.55]$$

where,

C_j is the content of layer constituent j per unit area;
K_i the corresponding specific absorption coefficient;
N the structure parameter from the PROSPECT model;
k_e the residual absorption term attributed to the albino leaf;
g is a factor which accounts for the variation in the coefficients with the diffuseness of the irradiance flow in the layer, with $\gamma = 1$ for perfectly diffuse light and $\gamma = 1/2$ for collimated light;

This formulation allows the PROSPECT tabulations of K_j to be used for pigment, cellulose, lignin, protein and water, although only pigments are relevant to the spectral region in this study.

Scattering Coefficient b_{dh}

The specific linear scattering coefficient was calculated from *Acer saccharum* M. leaf reflectance and transmittance measurements following Allen and Richardson (1968) to derive the Stokes parameters, along with leaf thickness. The theory of Yamada and Fujimura was again used now because it provides a convenient framework for the description of the flow of radiant fluxes across a leaf considered as a stack of layers. This theory was used specifically to define the upper and lower cuticular layers and to calculate the scattering coefficient from the inner layer by matrix inversion:

- the upper and lower cuticular layers are considered equal with no pigment content, so that $r_e=r_1=r_3=1-t_1=1-t_3$;
- the reflectance of the epidermis r_e is considered defined only by its refractive index, $r_e = \frac{(n-1)^2}{(n+1)^2}$, with n refractive index.

From Equations [2.46-2.49], the radiation transfer matrices for the cuticular layers are then (Figure 2.7):

$$G_e=G_3=G_1=\frac{1}{(1-r_e)}\begin{bmatrix}(1-2r_e) & r_e\\ -r_e & 1\end{bmatrix} \quad [2.56]$$

The optical properties of the active layer of the leaf, can be derived from measurements of the reflectance and transmittances of the entire leaf by noting that the radiation transfer matrix of the inside of the leaf is given by:

$$G = G_3G_2G_1 \Rightarrow G = G_eG_IG_e \Rightarrow G_I = G_e^{-1}G\,G_e^{-1} \quad [2.57]$$

where G_e^{-1} denotes the inverse of the matrix G_e. The apparent reflectance and transmittances of the inside active layer of the leaf is:

$$r^*_{Ia} = -\,g_{21}/g_{22} \quad [2.58]$$

$$t^*_{Ia} = (g_{11}g_{22} - g_{12}g_{21})/g_{22} \quad [2.59]$$

These values of r^*_{Ia} and t^*_{Ia} are used to calculate s. Leaf r^*_{Ia} and t^*_{Ia} can be related to leaf scattering and extinction properties of a compact leaf inner layer using Kubelka-

Munk radiative transfer theory. Allen and Richardson (1968) shows the corresponding Stokes (1862) parameters a and b to leaf r and t, with the Kubelka-Munk scattering and extinction parameters for the layer, as:

$$a = (1 + r^2 - t^2 + \Delta)/2r \quad [2.60a]$$

$$b = (1 - r^2 + t^2 + \Delta)/2t \quad [2.60b]$$

where,

$$\Delta = \{(1+r+t)(1+r-t)(1-r+t)(1-r-t)\}^{1/2} \quad [2.60c]$$

and the Kubelka-Munk scattering and extinction parameters for the layer (Allen and Richardson, 1968) are:

$$S = [\frac{2a}{(a^2-1)}]\log b \quad [2.61a]$$

$$K = [\frac{(a-1)}{(a+1)}]\log b \quad [2.61b]$$

where division by the leaf layer thickness yields the linear scattering and extinction coefficients b_{dh} ($S/D_L=b_{dh}$) and a_d ($K/D_L= a_d$). Figure 2.8 shows a_d from PROSPECT and that from Allen and Richardson, using the approach discussed above, demonstrating good correspondence. Figures 2.9 and 2.10 show an overview of the FRT model implementation with input parameters. The above theoretical development and discussion provides the framework for the simulation of expected radiance,

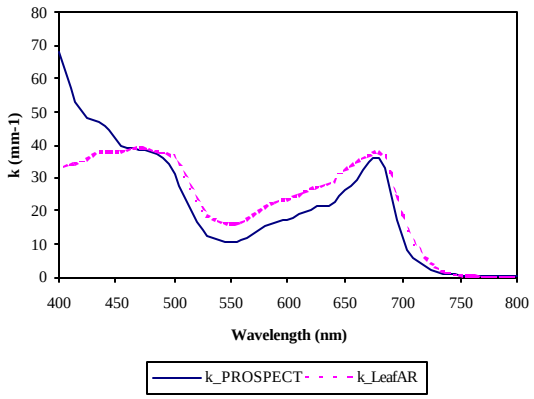

Figure 2.8. a_d from PROSPECT (k_PROSPECT) and calculated from Allen & Richardson (k_LeafAR) using *Acer saccharum* M. leaf material from one of the study sites used in this research.

backscattering and fluorescence, emerging from a single leaf as a function of the pigment content and the scattering properties of the leaf.

General overview of the FRT model implementation

1. **Kubelka-Munk theory and its modification to include Fluorescence flux**

   Fukshansky and Kazarinova $\Rightarrow$ $P(z)$=f(f, h_l, E^+, E^-)
   Subhash and Mohanan (2 gaussians) $\Rightarrow$ h_l

2. **Calculation of Extinction and Scattering coefficients**

   a_d from PROSPECT
   b_{dh} from K-M $\Rightarrow$ Allen and Richardson (experiment leaf samples)
   Yamada and Fujimura $G_l=G^{-1}GG^{-1}$

3. **Solving the Differential Equations using the Doubling Method**

   Rosema

4. **Matrix Calculation: Single Leaf as a Stack of Layers**

   Yamada and Fujimura $G=G_1G_2G_3$

Simulation of leaf *r, t*

Figure 2.9. General overview of the FRT model implementation, showing the theories and assumptions in each different step.

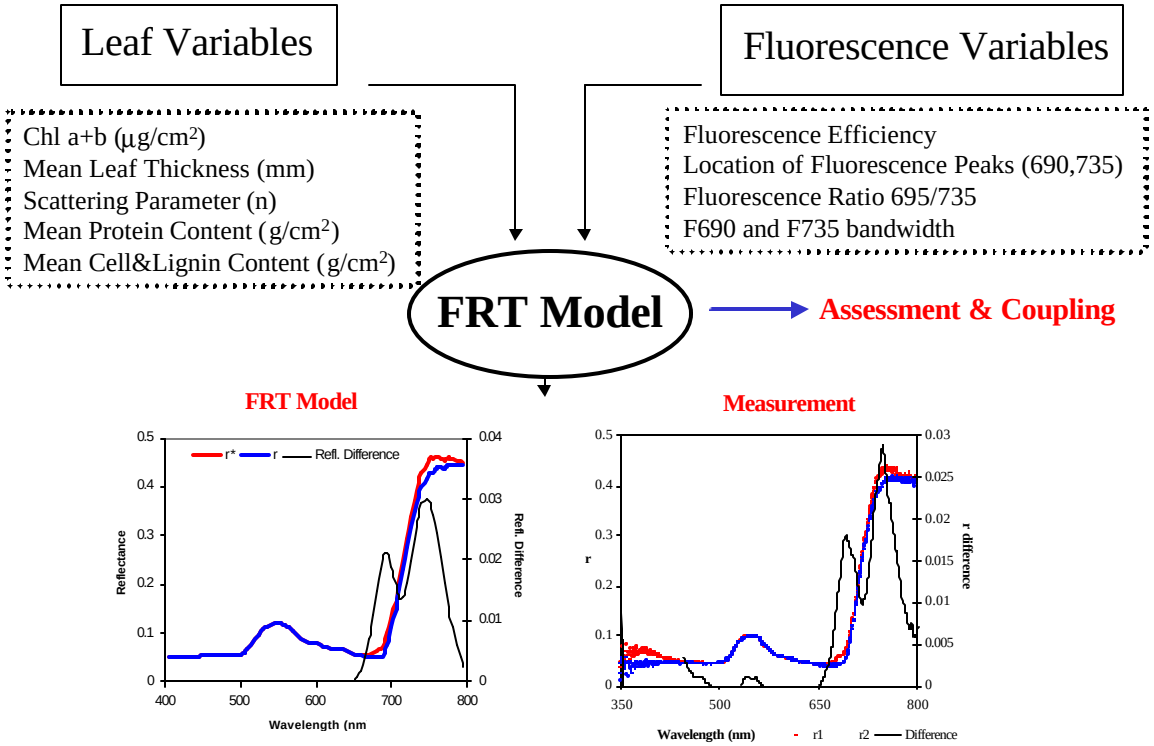

Figure 2.10. Schematic view of the input parameters to the FRT model.

2.3.- CANOPY AND INFINITE REFLECTANCE MODELS: CLASSIFICATION AND APPLICATION OF K-M THEORY TO HORIZONTALLY-HOMOGENEOUS PARALLEL MEDIUM CANOPIES

Simulation of the tree crown reflectance spectral content for comparison to the measured canopy reflectance and retrieved optical indices may be done through infinite reflectance (R_∞) and canopy reflectance models (CR), depending upon the complexity and assumptions made with respect to the type of vegetation canopy and viewing geometry. Infinite reflectance formulations model reflectance without canopy structure or viewing geometry considerations, based solely on leaf reflectance and transmittance. These formulations are derived from optically-thick leaf material, and making different assumptions for the multiple scattering between leaf layers. This thick leaf or leaf stack concept may have applicability to closed deciduous canopies characterized generally by high LAI, therefore with little effect of soil background and understorey. CR models, on the other hand, take into account viewing geometry and canopy structure, therefore modelling those effects in the canopy reflectance by different approximations generally based on the RTE and geometrical optical considerations. This section describes 3 infinite reflectance models explored in this research, a classification of CR models, and a brief description of the SAIL turbid medium CR model, which is based on K-M theory.

2.3.1.- Infinite Reflectance Models

Different infinite reflectance formulations have been derived based on assumptions related to the scattering between layered leaves forming the optically-thick canopy. In

each case, the reflectance for an optically thick medium, known as Infinite Reflectance R_∞, is expressed in terms of the inherent single leaf reflectance and transmittance. Lillestaeter (1982) derived a simple formulation (referred here as $R_{\infty 1}$) from measurements of leaf-stack apparent reflectance over known dark and bright backgrounds, ignoring multiple scattering, and considering equal reflectance for both sides of the leaf [Equation 2.62a]. This simple formulation was found inadequate by Miller *et al.* (1992) to simulate the measured reflectance of leaf stacks. A matrix formulation (Yamada and Fujimura, 1991) was used in a simulation which included multiple reflectance between leaves and considering different adaxial and abaxial reflectance for the leaf ($R_{\infty 2}$, Equation 2.62b). The Hapke (1993) infinite reflectance formulae ($R_{\infty 3}$) corresponds to a medium with a single scattering albedo w_o assumed approximately equal to reflectance (r) + transmittance (t) for a pile of leaves, [Equation 2.62c]. The corresponding formulae approximating thick leaf canopies are:

$R_{\infty 1}$ *approx. leaf stack* → $$R_\infty = \frac{r}{1-t^2} \qquad [2.62a]$$

$R_{\infty 2}$ *leaf stack* → $$R_\infty = \frac{r}{1-\dfrac{2t^2}{1+(1-4t^2)^{1/2}}} \qquad [2.62b]$$

$R_{\infty 3}$ *thick leaf* → $$R_\infty = \frac{1-\alpha^{1/2}}{1+\alpha^{1/2}}; \qquad [2.62c]$$

where, $\alpha = 1 - r - t$

2.3.2.- Canopy Reflectance Models

Canopy reflectance models can be classified in four different categories depending upon the assumptions and theory used in its formulation. Different canopy types present structural characteristics that allow for specific assumptions and therefore for the correct use of particular CR models: agricultural canopies can easily be assumed to be horizontally-homogeneous plane-parallel turbid mediums, and therefore the K-M theory can be applied with success. On the other hand, open forest canopies, showing heterogeneous structure with different shapes, need the development of models with a specific treatment of the effects of openings, shadows, and canopy geometry on the modelled reflectance. A classification of models into the four categories is discussed here, with special emphasis on the application of K-M theory. A more detailed discussion of CR models can be found in Goel (1988).

2.3.2.1.- Turbid Medium Models for Homogeneous Canopies

In turbid medium models, the canopy is approximated by a parallel-planar infinitely-extended medium, in which non-random dimensions, distances or distributions of elements are ignored. The elements of the canopy are considered to be randomly distributed, similar to particles in a turbid medium. The architecture of the canopy is defined by the LAI and the leaf angle distribution function (LAD), and therefore no geometrical effects other than the leaf inclinations are considered. In each layer, the elements of vegetation are treated as small absorbing and scattering particles, with given

geometrical and optical properties. Thus, its usefulness is primarily for dense-canopy simulations, such as corn, soybean, and wheat crop canopies.

Turbid medium canopy models can be divided into 3 different types, i) single-layer K-M *Theory Based Models*, that use the Kubelka-Munk approximation to the radiative transfer equation; ii) Multi-layer *Discrete Models*, in which the *z*-coordinate is discretized: the canopy is discretized into a finite number of layers (15 to 40) and algebraic equations are solved to obtain upward and downward fluxes on top of each of the layers, with the incident and view direction hemispheres being also discretized into a finite number of zenith angle contiguous zones; and iii) *Radiative Transfer Equation Model*, in which assumptions are made about the relationship between the optical length and scattering phase function and the canopy's architectural parameters (LAI and LAD).

K-M Theory Based Models have been extensively applied due to the less demanding approximation made to the radiative transfer equation. With variation of the number and specific parameters used in the approximation, K-M theory based models have seen significant development in the last 30 years. The Allen-Richardson model (Allen and Richardson, 1968) used the two-flux K-M theory (collimated fluxes $F_{-}=F_{+}=0$). Equations are solved to derive a relationship between canopy height (h), canopy reflectance (R), and soil reflectance (R_s). Allen-Gayle-Richardson model (1970) used the three-flux (5-parameters) Duntley theory: specular (collimated) incident radiation is reflected as diffused light. Park-Deering model (Park and Deering, 1982) modified the Allen-

Richardson model by allowing unequal absorption and scattering coefficients for diffuse fluxes in the upward and downward directions. They introduce a_{d-} and a_{d+} as the absorption coefficients associated with E and E_+ respectively; and b_{dh-} and b_{dh+} as the respective scattering coefficients. The Suits model (Suits 1972 a, b, c; Suits and Safir, 1972) brought significant improvement compared to previous models that do not take into account solar and viewing angles, nor architectural parameters of the canopy. Their 3-flux (5-parameter) K-M theory model (extended later to 4-flux, 9 parameters) expressed the K-M parameters in terms of field-measurable parameters defining the canopy and viewing geometry. Verhoef-Bunnik SAIL model (Verhoef, 1984; Verhoef and Bunnik, 1981) and Youkhana-Suits prime model (Youkhana, 1983) developed SAIL (Scattering by Arbitrarily Inclined Leaves) as an extension of the *Suits* model. SAIL was a refinement of *Suits*, in which the absorption and scattering coefficients can be computed for any leaf inclination, with random leaf azimuth distribution assumed [Equations 2.63a-2.63d].

$$\frac{dE_-}{dz} = k \cdot E_- \qquad [2.63a]$$

$$\frac{dE_-}{dz} = a \cdot E_- - b \cdot E_+ - c' \cdot F_- \qquad [2.63b]$$

$$\frac{dE_+}{dz} = b \cdot E_- - a \cdot E_+ + c \cdot F_- \qquad [2.63c]$$

$$\frac{dE_0}{dz} = u \cdot E_+ + v \cdot E_- + w' \cdot F_- - K \cdot E_0 \qquad [2.63d]$$

Suits		SAIL
a	→	$a(\theta_L)$
b	→	$\sigma(\theta_L)$
c	→	$s'(\theta_L)$
c'	→	$s(\theta_L)$
k	→	$k(\theta_L)$
K	→	$K(\theta_L)$
u	→	$u(\theta_L)$
v	→	$v(\theta_L)$
w'	→	$w(\theta_L)$

where,

E_-, E_+, downwelling and upwelling irradiance for diffuse flux;
a, attenuation (extinction+scattering) coefficient for diffuse flux;
b, scattering coefficient for diffuse flux;
c, backscatter coefficient for specular flux;
c', forward scatter coefficient for specular flux;
F_-, E_o, downwelling and upwelling specular flux;
u, scattering coefficient for specular flux into a diffuse flux in the same dir.;
v, scattering coeff.for specular flux into a diffuse flux in the opposite dir.;
w', bidirectional scattering coefficient for specular flux;
k, extinction coefficient for specular flux;
K, extinction coefficient in the viewing direction;

The refinement by Verhoef (1984) improved the modelled bidirectional reflectance as a function of viewing angle considering leaves of arbitrary inclination under the assumption that the leaf azimuth distribution is uniform (Verhoef, 1998). The extinction and scattering coefficients in SAIL [Equations 2.63] are expressed in the leaf inclination angle (θ_L), and the leaf inclination distribution function (LIDF) applied in order to form a weighted sum of such absorption and scattering coefficients. LIDF is discretized into an array of inclination frequencies for 13 distinct inclination angles θ_L located at the centre of intervals 0°-10°, 10°-20°, … , 70°-80° and 80°-82°, 82°-84°, … , 88°-90°. The refinement of the interval 80°-90° is used because the extinction and scattering coefficients are very sensitive to LIDF variations in this region of θ_L if the view zenith angle θ_v is close to the nadir. Different equations are used for the leaf angle distribution functions (Figure 2.11), with Suits being a special case of SAIL where LADF is considered exclusively as fractions of horizontal and vertical leaf area. The total radiance L_l is the sum of the four fields in the differential equations, and the absorption and scattering coefficients are expressed in terms of the canopy parameters, the viewing

zenith angle θ_v, and the relative azimuth angle ψ between solar and viewing direction (Goel, 1988). The dependency of extinction and scattering coefficients are, therefore, a function of morphological properties (LAI, LIDF), optical properties (r, t), and observational variables (θ_s, θ_v, ψ). Full description of the relationships between coefficients and such properties can be found in Verhoef (1998).

Leaf Angle Distribution Function (LADF)

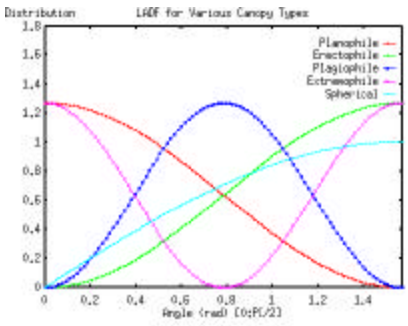

Canopy Type	LADF $f(\theta_L)$	ALA
Planophile	$2/\pi\ (1+\cos 2\theta_L)$	26.76°
Erectophile	$2/\pi\ (1-\cos 2\theta_L)$	63.24°
Plagiophile	$2/\pi\ (1-\cos 4\theta_L)$	45.00°
Extremophile	$2/\pi\ (1+\cos 4\theta_L)$	45.00°
Spherical	$\sin \theta_L$	57.30°

Figure 2.11. LADFs implemented in the SAILH canopy reflectance model.

The incorporation of the hotspot effect (*Kuusk*, 1985) resulted in a variant called SAILH, used in all calculations reported in this research. The size of the leaves and the associated shadowing effects are taken into account for the calculation of the single scattering contribution to the bidirectional reflectance. Figure 2.12 shows the simulation obtained from SAIL and SAILH for different solar zenith angles (θ_s) and view angles (θ_v) for the red region with LAI=2, spherical LADF, r=0.135, t=0.055, soil reflectance r_s=0.126, and hotspot s/l (leaf size/tree length) parameter 0.116 for SAILH.

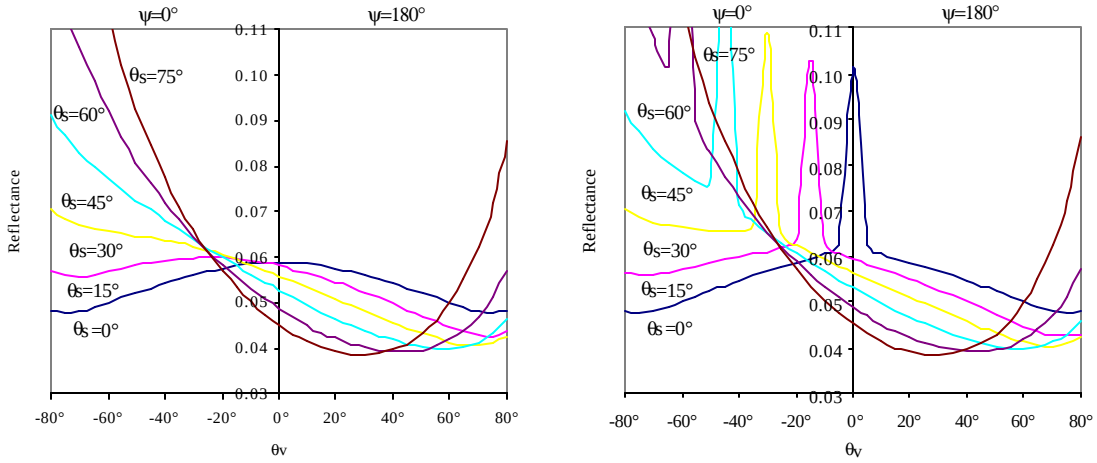

Figure 2.12. Modelled Canopy Reflectance using SAIL (left) and SAILH (right) for different solar zenith angles (θ_s) and view angles (θ_v) for the red region with LAI=2, spherical LADF, r=0.135, t=0.055, r_s=0.126 (soil). Hotspot s/l = 0.116 for SAILH.

2.3.2.2.- Geometric Models

In a geometric model, the canopy is designed with elements with known dimensions and shape, placed and distributed in different configurations. There are basically two different ways of dealing with the geometrical effects of shapes in vegetation canopies, i) using geometrical optics theory to calculate the effects of shadows within the canopy for different viewing angles and solar zenith and azimuth angles, and then applying empirical relationships to determine the radiation regime to simulate canopy reflectance; and ii) using a simplified form of the RTE and making assumptions about the canopy geometry, shapes and distribution of leaves. Geometric models are used primarily in non-dense canopies, where canopy gaps and openings, and individual tree shapes are modelled geometrically: modelled crop canopies assume cylindrical shapes to individual vegetative elements; trees are modelled with shapes such as cones for conifers, and cylinders with

spheres or spheroids for deciduous trees. The earliest geometrical model (Jahnke and Lawrence, 1965) used cones and flat discs for the geometrical objects to represent vegetation. Several developments were carried out since then, generalizing the work to other shapes (Terjung and Louie, 1972). Canopy reflectance was assumed to be a linear sum of different terms (Jackson *et al.*,1979): reflectance from sunlit plants, from sunlit soil, from shadowed soil, and from shadowed plants, and considering fractions of the ground covered by each of them. Li and Strahler (1986, 1992) and Strahler and Jupp (1990) developed a model using optical principles and parallel-ray geometry, and are well regarded in the field and commonly employed for simulation.

2.3.2.3.- Hybrid Models

When the vegetation canopy does not totally fall into any of the previous categories and therefore turbid-medium and geometric models are not adequate, hybrid CR models better represent the canopy by combination of elements of both. Geometric shapes are taken into account, therefore the canopy is designed by elements with known size, relative positions and distances. The interaction of the radiation with the canopy is solved by a turbid-medium model, considering that the foliage is distributed into subcanopies, each of them with different shape and size. These models can represent homogeneous and inhomogeneous canopies but are the most complex and computer-time intensive. A recent example is the GORT (Geometric Optical & Radiative Transfer) hybrid models (Li *et al.*, 1995), that combine the geometric optics of canopy structure with principles of radiative transfer within individual crowns, assuming uniform multiple scattering from

the sunlit and shaded surfaces of crowns; Ni *et al.* (1999) have developed an analytical solution as alternative to the more complicated numerical solution of Li *et al.* (1995).

2.3.2.4.- Monte Carlo Models

These models simulate the positions and orientation of the elements forming the vegetation canopy in a very realistic way, using the Monte-Carlo method to follow the trajectory of the photon. The trajectory is followed from its origin to its absorption or reflection and detection by the sensor. Generation of random numbers determine the direction and point of interception of an incident ray with the canopy, and the location, type, and orientation of the nearest vegetative element. If the photon hits the nearest element, appropriate statistics are used to determine the direction in which it is scattered, according to the scattering phase function or the LAD. Application of this method to realistic canopies is computer-intensive and limit the application of these models in estimating canopy parameters. Goel and Thompson (2000) presented SPRINT as an efficient computer simulation model based on the Monte Carlo method.

The description given here regarding the application of the RTE to leaf and canopy media, with leaf and canopy radiative transfer models, is used in the next section. Methodologies for estimation of pigment content in forest canopies are described with the different approaches and implications discussed.

2.4.- METHODOLOGIES FOR ESTIMATION OF PIGMENT CONTENT IN FOREST CANOPIES

Predictions of chlorophyll content or any other canopy biophysical parameter from airborne or satellite canopy reflectance have been carried out through four different methodologies: i) directly studying the statistical relationships between ground-measured biochemical data and canopy-measured reflectance (Johnson *et al.,* 1994; Matson *et al.,* 1994); ii) applying the leaf-level relationships derived between optical indices and the pigment content directly to canopy-measured reflectance (Peterson *et al.,* 1988; Yoder and Pettigrew-Crosby, 1995; Zagolski *et al.,* 1996); iii) scaling up the leaf-level relationships based on optical indices related to pigment content through models of canopy reflectance or infinite reflectance (Zarco-Tejada *et al.,* 1999a, 2000a, 2000b); and iv) inverting the observed canopy reflectance through a canopy reflectance or infinite reflectance model coupled with a leaf model to estimate the optimum pigment content (Jacquemoud, 1993; Jacquemoud *et al.,* 1995; Kuusk, 1998; Demarez and Gastellu-Etchegorry, 2000; Weiss *et al.,* 2000; Jacquemoud *et al.,* 2000).

The four proposed methodologies have advantages and disadvantages that are related to the complexity of the modelling approach selected, and the degree of general or local applicability of the methodology in remote sensing. The first method studies the correlations between canopy-measured reflectance by a field, airborne or satellite sensor with ground-measured pigment or any other biophysical constituent. In this case no leaf reflectance is measured, therefore the link between canopy reflectance and biochemical

content is found through statistical relationships. Multivariate analysis between Airborne Visible InfraRed Imaging Spectrometer (AVIRIS) reflectance and total nitrogen, lignin, starch, chlorophyll content and LAI (Johnson *et al.,* 1994) and with nitrogen and chlorophyll (Matson *et al.,* 1994) applied by stepwise multiple-regression procedure using the AVIRIS spectral bands showed good statistical relationships derived at specific wavebands. Although significant correlations were found, no prediction capabilities could be inferred from either one of the mentioned research results since the locally-derived relationships are affected by species and canopy structure.

The second method, that uses statistical leaf-level relationships applied to canopy reflectance for pigment estimation is site and species specific (Chappelle *et al.,* 1992; Gitelson and Merzylak, 1997) and therefore require relationship calibration that is a function of the canopy structure and viewing geometry at the time of remote sensing data collection. Therefore, the statistical relationships derived at leaf level need to be calibrated in order to be useful for estimation at the canopy level, due to the differences between the two media: one where the relationship is derived (leaf) and the other where it is applied for estimations (forest canopy). This methodology allows the derivation of relationships based on optical indices calculated at wavelengths where subtle changes in leaf reflectance are due to specific biophysical processes that are targeted for measurement at the canopy level. Stepwise multiple-regression is often used to develop predictive algorithms from leaf reflectance which are then applied to airborne data: AVIRIS (Zagolsky *et al.,* 1996) and Airborne Imaging Spectrometer (AIS) spectra

(Peterson *et al.*, 1988). Laboratory canopy studies (Yoder and Pettigrew-Crosby, 1995) and those using AVIRIS spectra (Kupiec and Curran, 1995) were directed to the identification of spectral bands at both leaf and canopy levels which are less sensitive to changes between levels, therefore minimizing effects due to the canopy, thus selecting spectral bands that could be used directly for prediction at canopy level. Application of leaf-level relationships to canopy reflectance through optical indices has been the traditional method used in the past, and a full review of the optical indices derived at the leaf level using this approach was described in Chapter 1.

In the third methodology, the same relationships between leaf constituent content and canopy reflectance are derived by scaling up the optical indices through infinite or canopy reflectance models; this is a new approach introduced during the course of the present research (Zarco-Tejada, *et al.*, 1999a, 1999b). A primary advantage is that the use of infinite or canopy reflectance models as part of the calculation of relationships avoids the post-calibration step to compensate for canopy structure or viewing geometry. Therefore, scaled-up leaf-level relationships can be used directly for bioindicator predictions on measured canopy reflectance data by considering canopy structure and viewing geometry information in the model scaling up step. The objective of this method is the derivation of predictive algorithms to be used under certain canopy assumptions, not simply the evaluation of statistical correlations between sensor reflectance and ground measurements. In closed dense vegetation canopies, the reflectance canopy model can sometimes be replaced by different infinite reflectance formulations, as explained in

previous section, therefore simplifying the need for input parameters defining structure and geometry. As in the first methodology, this approach enables a search for subtle changes in leaf reflectance due to specific biophysical processes, and the reflectance model permits direct prediction of the canopy biochemical parameter. The main disadvantage is the requirement for leaf sample collection for the derivation of leaf-level relationships.

The fourth methodology, inversion of a canopy reflectance model coupled with a leaf model, attempts to avoid the development of leaf-level relationships through the use of a leaf model. In this approach (Jaquemoud, 1993; Jacquemoud *et al.*, 1995; Kuusk, 1998; Demarez and Gastellu-Etchegorry, 2000; Jacquemoud *et al.*, 2000), the leaf radiative transfer simulation uses leaf biochemical constituents as input to model leaf reflectance and transmittance that is in turn used as input for the canopy reflectance model. The main advantage of this approach is that no leaf sample collection is needed to derive relationships, but suffers from the constraint that only biophysical parameters considered in the leaf model can be estimated from measured canopy reflectance. No subtle changes due to specific functioning effects can be sought, and therefore no changes at specific absorption wavelengths due to chlorophyll degradation at different senescence stages can be studied. That is, it is implicitly assumed that the leaf model captures all actual radiative processes accurately. The method is computational-intensive, and no validation has been found in the literature reporting results from airborne or satellite-measured reflectance with ground truth, with most of the work carried out with synthetic data

(Jacquemod, 1993; Weiss *et al.,* 2000), field spectrometer (Jacquemoud *et al.,* 1995), estimation of results with no validation due to the lack of ground truth (Kuusk, 1998), comparison of different model inversion techniques using simulated data (Pragnère *et al.,* 1999), and simulation studies modelling 3D canopies used for applying inversion techniques (Demarez and Gastellu-Etchegorry, 2000; Weiss *et al.,* 2000). Other studies with lower spatial and spectral resolution data by Braswell *et al.* (1996) and Weiss and Baret (1999) use canopy model inversion for extracting canopy biophysical information from large swath satellite data at global scales, using the Advanced Very High Resolution Radiometer (AVHRR), and VEGETATION/SPOT4 respectively, and therefore its applicability and portability to narrow-band hyperspectral high-spatial airborne data cannot be evaluated.

It is important to note that the findings reported in this research related to red-edge optical indices and CF estimation were found during the detailed study of leaf reflectance and transmittance collected from the study sites, and in the process of calculation of leaf-level optical indices. If the fourth approach (direct use of leaf models) had been adopted as an analysis strategy at the outset, it would have precluded the derivation of very important conclusions reported later.

The next sections specify and describe the methodology for the two types of approaches used in this research for pigment estimation: scaling up leaf-level relationships through

infinite and canopy reflectance models, and model inversion techniques using a coupled leaf and canopy reflectance model.

2.4.1.- Methodology for Scaling-up Optical Indices

The schematic view of the approach used for estimation of leaf bioindicators through the scaling-up of leaf-level optical indices is shown in Figure 2.13. Single leaf reflectance and transmittance measurements (r_i, t_i) from the field data sampling are used for the simulation of above-canopy reflectance through infinite reflectance and canopy reflectance models, constrained by a Canopy Model Parameter Assumption Set (j). Such an assumption of input parameters to the CR model defines the canopy structure, by a more or less complex set of canopy parameters, and viewing geometry, such as solar zenith and azimuth, and viewing angles, needed for simulating canopy reflectance from single leaf reflectance and transmittance measurements. Canopy Spectral Reflectances (CR_{ij}) simulated through the Canopy Simulation Model are used to calculate specific Optical Indices k (OI_k). For a given optical index, a set of n values are calculated from the leaf-level spectral measurements used for CR simulation. Leaf Bioindicators (B_{mi}) measured in each leaf sample (chl_{a+b}, carotenoids, Fv/Fm, etc) are used to derive relationships with the optical indices OI_{ijk} calculated from the above-canopy simulated spectra. Therefore, the relationship between a given bioindicator (e.g. $\mu g\ chl_{a+b}/cm^2$) and a given optical index (e.g. R_{750}/R_{710}) is calculated from simulated canopy reflectance rather than from leaf-level measured reflectance. This relationship is therefore affected by

canopy structural parameters and viewing geometry, which enables its application to above-canopy measured reflectance. Thus, the relationships between the set of optical indices OI_{ijk} and the set of bioindicators B_{mi} are then applied to hyperspectral CASI reflectance data to obtain bioindicator estimations. To do so, above-canopy measured CASI reflectance is used to calculate the CASI-optical indices input of such relationships of the form $B_{mi} = f(OI_{ijk})$, e.g. $\mu g\ chl_{a+b}/cm^2 = a \cdot R_{750}/R_{710} + b$, with a,b constant parameters for above-canopy simulation, and R_{750}/R_{710} an optical index derived from the above-canopy reflectance. This methodology enables the direct application of sensor-derived optical indices in scaled-up algorithms that are therefore a function of the canopy structure and viewing geometry, precluding the need for calibration of prediction relationships. Assessment of optical indices as estimators of bioindicators is then made comparing *in-field* measured bioindicators (measured B_m) with CASI-derived estimations (estimated B_m).

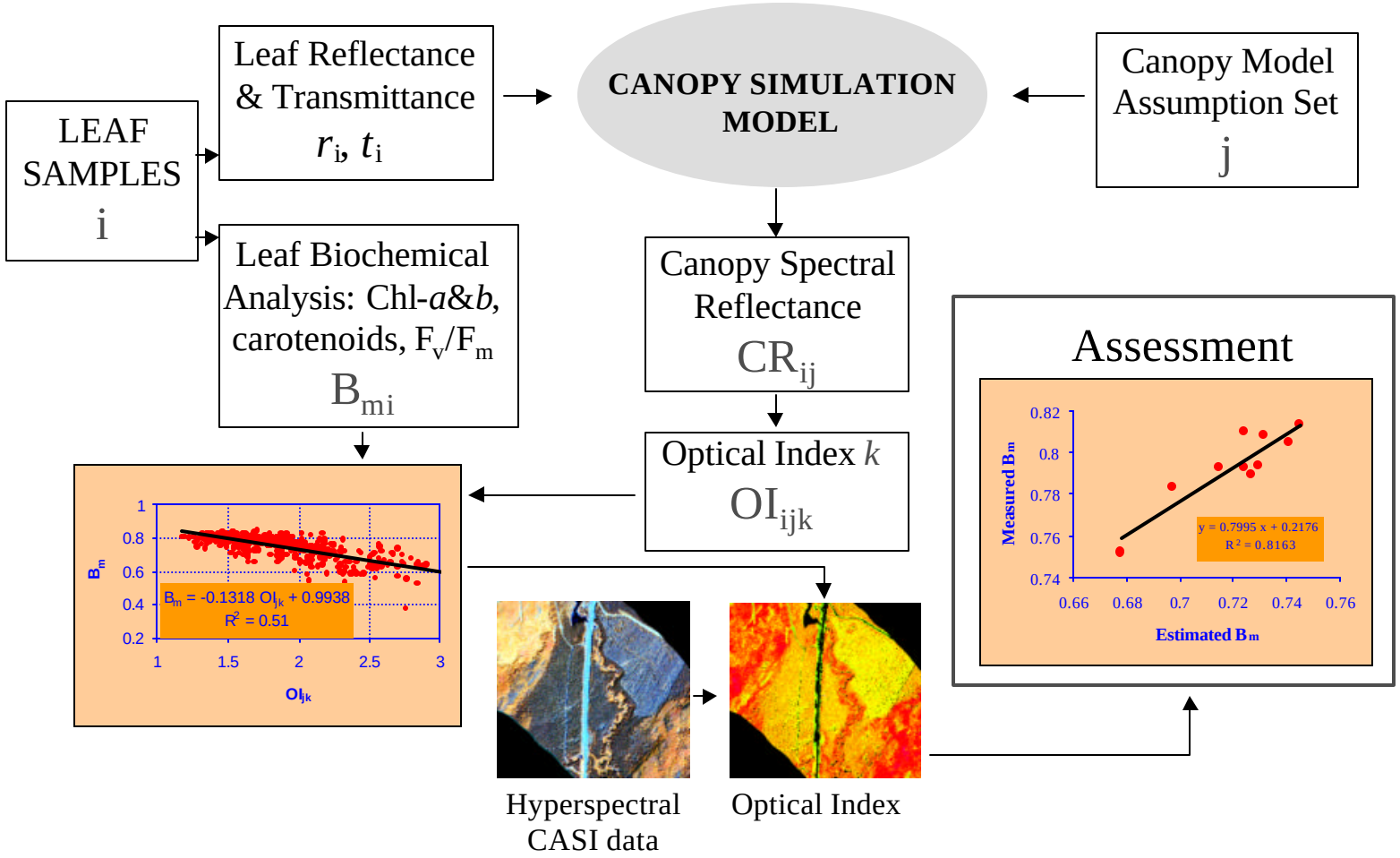

Figure 2.13. Schematic view of the overall analysis methodology followed for the scaling up method. Leaf-level reflectance and transmittance measurements are scaled-up to canopy level through infinite and CR models and input parameters related to the canopy structure and viewing geometry. Relationships between optical indices calculated from above-canopy simulated reflectance and ground-truth bioindicators are applied to above-canopy hyperspectral CASI reflectance to obtain bioindicator estimation. Assessment is made comparing ground-truth measured with estimated bioindicators.

2.4.2.- Estimation of chl_{a+b} by Model Inversion

The estimation of a biophysical canopy parameter by numerical model inversion can generally be carried out by different methodologies: i) Look-Up Tables (LUT); ii) Iterative Optimization (OPT); and iii) Neural NeTworks (NNT). The Look-Up Table technique is conceptually the simplest (Pragnère *et al.*, 1999) and consists of the generation of an output table for a discrete set of input parameters covering the expected range of the parameters. The table is used to find the measured value that is directly related to a given set of input parameters. This method requires the generation of large amount of cases that are afterwards used to compare with measured data. Iterative Optimization is the classical technique for inverting radiative transfer models in remote sensing (Bicheron *et al.*, 1998; Jacquemoud *et al.*, 1995; Kuusk, 1998, Goel, 1988) and consists in minimizing a function that calculates the root mean square error between the measured and estimated quantities by successive input parameter iteration. Neural Networks are non-physical methods that relate a set of input variables to a set of output variables by a learning process, and have been shown to be efficient in inversion of canopy models (Abuelgasim *et al.*, 1998; Smith, 1993). This third technique is not considered here because the objective is to develop methods for canopy modelling based in physically-based radiative transfer models. Iterative-optimization numerical model-inversion techniques to estimate chlorophyll content by using a coupled leaf model and a canopy model requires three consecutive steps (Figure 2.14):

i) estimation of leaf reflectance and transmittance (*r*, *t*) from a set of leaf model input parameters, such as the parameter to be estimated, chl_{a+b}, and other leaf structural parameters; ii) estimation of canopy reflectance from leaf-level model-estimated *r*, *t* and set of canopy model parameters that define canopy structure and viewing geometry; and iii) error calculation by comparison of estimated canopy reflectance r^* to the at-sensor measured reflectance r_m. Figure 2.15 shows the input parameters and iteration procedure for chl_{a+b} and LAI estimation with the coupled SAIL canopy reflectance and PROSPECT leaf radiative transfer models. Error calculation consists in determining the set of parameters $P=(N,Chl_{a+b},C_w,LAI,\boldsymbol{q}_s\ldots)$ which minimizes a merit function Δ^2 over the whole spectrum,

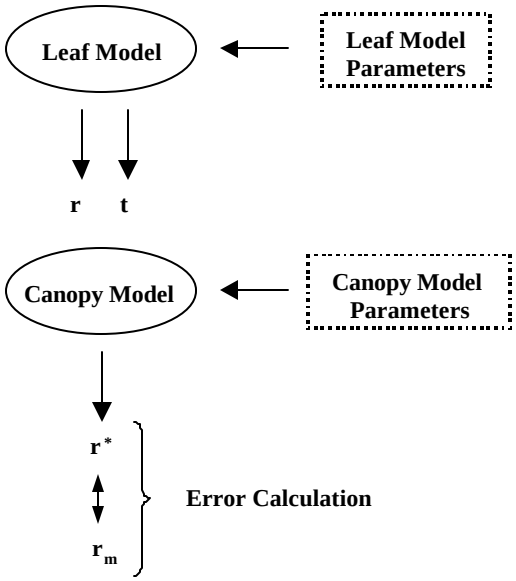

Figure 2.14. Iterative-optimization numerical model-inversion technique to estimate leaf and canopy biophysical parameters coupling leaf and canopy models with input set of leaf and canopy parameters. Error calculation between modelled and measured canopy reflectance allows for estimation of the optimum set of input parameters by iterative optimization.

$$\Delta^2 = \sum_n [r_m(\boldsymbol{l}_i) - r^*(\boldsymbol{l}_i, P)]^2 \qquad [2.64]$$

where,

$r_m(\boldsymbol{l}_i)$ is the measured canopy spectral reflectance;

$r^*(\boldsymbol{l}_i, P)$ is the modelled canopy spectral reflectance with a set of *P* parameters;

Different merit functions have been defined by researchers, each based on different assumptions. The minimizing function for numerical model inversion using reflectance data in several spectral bands can be calculated i) from single reflectance channels, comparing the estimated with the measured reflectance in all spectral bands [Equation 2.64] (Jacquemoud 1993; Jacquemoud *et al.*, 1995); ii) using w_i weighting factors that represent the weight given to the *i*th wavelength. The usual protocol is to choose weighting coefficients w_i to be proportional to the inverse of the measured canopy reflectance, $w_i = 1/r_{m,i}$, thereby placing more weight to wavelengths in the visible part of the spectrum where pigment absorption is maximum, and minimizing the impact of errors between measured and estimated reflectance in the NIR, where chlorophyll absorption decreases and reflectance is driven by canopy structure; iii) by a more sophisticated construction of merit functions as in Kuusk (1998), where penalization to the merit function (Kuusk, 1991) is introduced if the best fit is found when a parameter being inverted falls outside the prior-

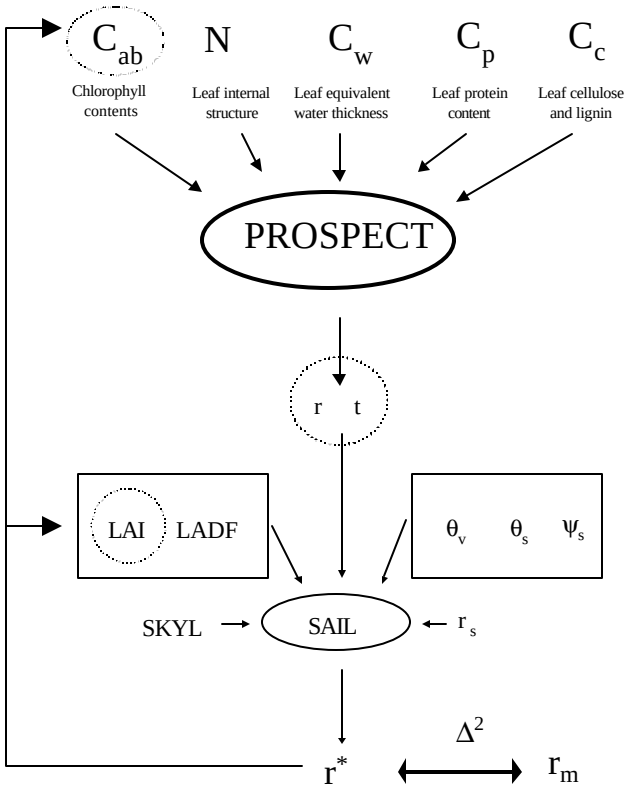

Figure 2.15. Schematic view of the methodology for PROSPECT and SAIL numerical inversion by iteration, allowing LAI and chl_{a+b} to vary. LAI varied from 4 to 7, and chl_{a+b} from 10-70 μg/cm^2.

established range of allowed values; and iv) building merit functions based on spectral transforms or vegetation indices (Goel, 1988), in which the merit function generated is based on the optical index that is supposed to be related with the parameter subject to estimation, such as chl_{a+b}. Equation [2.65] presents a merit function when the red-edge spectral parameter R_{750}/R_{710} is used for pigment estimation, which could easily be modified if a combination of optical indices is used:

$$\Delta^2 = \left[\left(\frac{R750}{R710} \right)_m - \left(\frac{R750}{R710}, P \right)_* \right]^2 \qquad [2.65]$$

where,

$\left(\frac{R750}{R710} \right)_m$ is the optical index calculated from measured canopy reflectance;

$\left(\frac{R750}{R710}, P \right)_*$ is the optical index calculated from modelled canopy reflectance, for a given set of input parameters P;

The use of optical indices in the merit function has not been reported in any of the validation work found in the literature, although there is significant inherent potential of this approach in remote sensing application. Reflectance values measured from airborne or satellite sensors are a function of illumination, canopy structure, and atmospheric condition at the time of data collection. On the other hand, estimation of biophysical parameters through optical indices enable to maximize sensitivity to such biophysical parameters, normalizing external effects due to atmosphere, illumination conditions, and viewing geometry (Running *et al.*, 1994; Huete and Justice, 1999). Therefore in this research, leaf-level optical indices and ratios that showed good correlation with pigment

content are proposed here to be used as a basis for the merit function for model inversion, especially those calculated from the red edge as discussed later.

These different approaches have been tested in this research, in order to compare the pigment estimation by different techniques using hyperspectral airborne data collected in 1998, 1999 and 2000; this dataset is considered a rare, if not unique, validation database for model inversion with hyperspectral data in closed dense maple canopies. The experimental methods and materials used to carry out the fluorescence and pigment investigations at all the different levels of study are described in Chapter 3 that follows.

CHAPTER 3.

EXPERIMENTAL METHODS AND MATERIALS

Experiments were carried out in 1997, 1998, 1999 and 2000 at different levels of scale to test the hypothesis of this research: the study of whether canopy chlorophyll fluorescence and chlorophyll content can be measured in closed forest canopies using hyperspectral remote sensing reflectance data and predicted through radiative transfer models. The objectives can be described as follows: i) study methodologies for linking leaf to canopy-level reflectance through radiative transfer modelling; ii) model the effects of CF on multi-level vegetation reflectance in laboratory and under natural illumination conditions through radiative transfer simulation; and iii) study RT numerical model inversion techniques to estimate pigment content in closed canopies through coupling leaf and canopy reflectance models.

For the estimation of CF, four levels of study were carried out: i) at the leaf level, with leaf samples collected from study sites, to develop relationships between leaf reflectance and CF and pigment content; diurnal studies were also carried out at leaf level to study the effects of diurnal changes in leaf apparent reflectance due to changes in CF; ii) at a canopy simulation level in the laboratory using the CASI hyperspectral sensor and maple seedlings; iii) at a canopy simulation level under natural illumination conditions in a

diurnal trial using maple seedlings; and iv) at an above-canopy level over selected forest maple stands at specific study sites.

3.1.- LEAF-LEVEL EXPERIMENTAL METHODS AND MATERIALS

Leaves from three-year old potted trees of *Acer saccharum* M. (sugar maple) were used in the laboratory-greenhouse experiments of this study. Two experiments were designed to examine leaves with fixed pigment levels but under conditions in which fluorescence signals were expected to vary, in order to test whether experimental measurement methods presented were able to track such variations. Below we first describe the measurement methodologies employed in these experiments, and then the experimental procedures for the two leaf-level experiments: diurnal fluorescence variations and time decay of fluorescence amplitude following light exposure.

3.1.1.- Laboratory Measurement Methodologies

3.1.1.1.- Chlorophyll fluorescence

Chlorophyll fluorescence was analyzed with a Pulse Amplitude Modulation (PAM-2000) Fluorometer (Heinz Walz GmbH, Effeltrich, Germany), an instrument that has been used widely in basic and applied fluorescence research (Mohammed *et al.*, 1995). Procedures used for measuring Fv/Fm and ΔF/Fm' were based on standard methodologies as documented in the PAM-2000 manual (Heinz-Walz-GmbH, 1993). The leaf was positioned in the PAM-2000 leaf clip holder, which exposes a sample area approximately 1-cm in diameter to the fibreoptic light emitter and detector array. Steady-state

fluorescence features were measured at 110 (Ft110) and 2820 (Ft2820) µmol quanta m^{-2} s^{-1} (supplied by a halogen light attachment, excitation wavelength < 710 nm), to correspond to photosynthetic photon flux densities (PPFD) used in the reflectance and transmittance assessments (PPFD was monitored by a quantum sensor built into the leaf clip holder). Effective quantum yield, which denotes the actual efficiency of PSII photon capture in the light by closed PSII reaction centers, was determined as $\Delta F/Fm' = (Fm'-Ft)/Fm'$, where Fm' is the maximal fluorescence of a pre-illuminated sample with PSII centers closed, and Ft is the fluorescence at steady-state (Genty *et al.*, 1989; Van Kooten and Snel; 1990). The leaf was exposed to the PPFD for 2 to 3 sec, then Ft was measured followed by Fm' upon application of a saturating pulse. For measurement of maximal fluorescence induction, leaves were dark-adapted in the bags at room temperature for at least 30 min. Dark adaptation is necessary to oxidize electron carriers in the photosynthetic tissues, so that when the tissues are subsequently exposed to bright light, maximal fluorescence may be observed (Walker, 1985). The ratio of variable to maximal fluorescence Fv/Fm was determined for the adaxial (upper) leaf surface. Fv/Fm quantifies the maximal efficiency of photon capture by open PSII reaction centers (Butler and Kitajima, 1975), and is one of the most widely used chlorophyll fluorescence features (Mohammed *et al.*, 1995). It is calculated from the equation $Fv/Fm = (F_{max}-F_o)/F_{max}$, where F_{max} is the maximal fluorescence yield of a dark-adapted sample, with all PSII reaction centers fully closed, and F_o is the minimum fluorescence yield of a dark-adapted sample, with all PSII reaction centers fully open (Van Kooten and Snel, 1990). F_o is measured first, using a red measuring light with a maximum emission of 655 nm, at a

very low PPFD of about 0.1 µmol quanta m^{-2} s^{-1}, and a modulation frequency of 600 Hz. F_{max} was determined by exposing the sample to a saturating pulse of light (> 6000 µmol quanta m^{-2} s^{-1}, < 710 nm wavelength) of 0.8 s duration and 20 kHz modulation frequency. Fluorescence from the plant is detected at wavelengths > 700 nm. The instrument runs this test using an automated procedure and calculates the Fv/Fm ratio. Most of the measurements of leaf fluorescence with the PAM-2000 instrument were made at OFRI, at the study sites, and some at York University, but all under the direction and supervision of Dr. Gina Mohammed.

3.1.1.2.- Apparent leaf reflectance and transmittance spectra

Single leaf reflectance and transmittance measurements were acquired on all leaf samples using a Li-Cor 1800-12 Integrating Sphere apparatus coupled by a 200 µm diameter single mode fibre to an Ocean Optics model ST 1000 spectrometer, with a 1024 element detector array, yielding a 0.5 nm sampling interval and ~7.3 nm spectral resolution in the 340-860 nm range. The spectrometer is controlled and read out by a National Instruments multi-purpose Data Acquisition Card (DAC-550). Software was designed to allow detailed control of signal verification, adjustment of integration time, and data acquisition (Harron and Miller, 1995). Spectral bandpass characterization performed using a mercury spectral line lamp source yielded full-width at half maximum (FWHM) bandwidth estimates of 7.37 nm, 7.15 nm, and 7.25 nm, at 438.5 nm, 546.1 nm and 576.9 nm respectively. Fibre spectrometer wavelength calibration was performed using the Ocean Optics HG-1 Mercury-Argon Calibration Source, that produces Hg and Ar emission lines

between 253 and 922 nm. Single leaf reflectance and transmittance measurements were acquired following the methodology described in the manual for the Li-Cor 1800-12 system (Li-Cor-Inc., 1983) in which six signal measurements are required: transmittance signal (TSP), reflectance signal (RSS), reflectance internal standard (RTS), reflectance external reference (RST), and dark measurements (TDP, RSD). Reflectance (Rfl) and transmittance (Tns) are calculated assuming a constant center wavelength and spectral bandpass (Equations [3.1] and [3.2]). An integration time of 609.3 msec was used for all sample measurements.

$$Rfl = \frac{(RSS - RSD) \cdot Rfl_{BaSO_4}}{RTS - RSD} \qquad [3.1]$$

$$Tns = \frac{(TSP - TDP) \cdot Rfl_{BaSO_4}}{RST - RSD} \qquad [3.2]$$

with Rfl_{BaSO4} the reflectance of Barium Sulfate.

3.1.1.2.1.- Pre-processing for reflectance and transmittance spectral data

A signal-to-noise study was carried out to choose the optimum function and bandwidth for the smoothing and derivative processing to be applied to the single leaf spectral reflectance and transmittance data prior to subsequent analysis and extraction of diagnostic indices. Perhaps the most common and popular method for smoothing and derivatives calculations is described by Savitzky and Golay (1964), evidenced by frequent reference in the literature (Enke and Nieman, 1976; Madden, 1978; Marchand and Marmet, 1983; Kawata and Minami, 1984; Demetriades-Shah *et al.*, 1990; Tsai and Philpot, 1998). The method is based on a simplified polynomial least squares procedure

for smoothing and differentiating data considering that the noise is not wavelength dependent and therefore having similar characteristics throughout the spectrum. Other methods cited in the literature for smoothing purposes are (i) the moving-average filter, that uses a squared window as a filter; (ii) a triangular function, that uses a function with triangular shape that gives more weight to the point being smoothed; and (iii) an adaptive smoothing function based on a linear mean-square estimation of the noise, that it is considered as wavelength dependent (Kawata and Minami, 1984). The amount of distortion suffered by the signal depends on the smoothing process and the properties of the data (Enke and Nieman, 1976); studies to estimate the optimum smoothing bandwidth to be used show that the optimum smoothing bandwidth depends on three factors: (i) type of smoothing function used for smoothing; (ii) shape and characteristics of the spectral features being analyzed; and (iii) the radiometric and spectral response characteristics of the measuring instrument leading to differences in the noise generated (Demetriades-Shah *et al.*, 1990).

Methods for differentiation of spectra have been reported in the literature as (i) finite approximation difference, (ii) linear regression derivative function; and (iii) Savitzky-Golay derivative computation based on the simplified polynomial least square procedure mentioned before. The finite difference method keeps the spectral features depending on the band separation and allows the computation at various band separations, causing scaling effects (Tsai and Philpot, 1998). The optimum differentiating function and

bandwidth depends on the level of noise in the data and the spectral bandwidth of the spectral measuring device (Demetriades-Shah *et al.,* 1990).

An experiment was carried out to test different smoothing and derivative functions suited to the data set generated by the experimental apparatus to obtain reflectance and transmittance spectra for the broad leaves under study. The analysis was focused on the signal-to-noise ratio (SNR) and the noise spectra in the data collected by the optic fibre spectrometer attached to the LI-COR integrating sphere for the three measurement targets.

The analysis of the SNR for data sets being generated is a method widely used to calculate the optimum smoothing bandwidth (Enke and Nieman, 1976; Demetriades-Shah *et al.,* 1990). This approach involves the selection of the optimum spectral bandwidth by smoothing the data using a range of bandwidths. The "signal" is defined as the average of a number of measurements made from the same target under the same conditions; the "noise" is defined as the sum of the absolute values of the deviations between the smoothed measurement spectra and the "signal".

The following smoothing functions were tested from 3 to 50 nm bandwidth at 5 nm intervals in order to study the optimum noise and SNR performance: rectangular (moving-average), triangular and Savitzky-Golay smoothing functions. The Savitzky-Golay function was tested using polynomials of second, third and fourth order. The

results of the SNR study (Figure 3.1), the very high sampling rate (small spacing) of the instrument, the very high frequency of the noise, and the relatively broad spectral features of leaf samples suggest the selection of Savitzky-Golay approach with a third-order polynomial function with 25 nm bandwidth is optimum for our spectral data set.

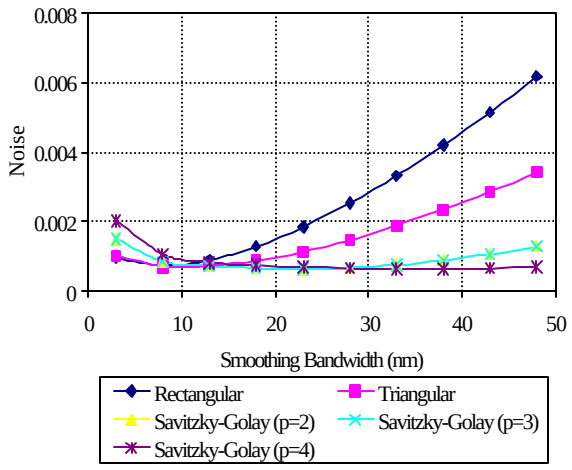

Figure 3.1. Noise calculated from reflectance measurements of Sugar Maple leaf samples using rectangular, triangular and Savitzky-Golay (order 2, 3 and 4) smoothing functions at 5 nm intervals from 3 to 50 nm bandwidth.

3.1.1.3.- Measurement apparatus and protocol for distinguishing fluorescence in measurements of apparent spectral reflectance

The apparatus and methodology employed to measure the reflectance and transmittance spectra is based on the commercial Li-Cor Model 1800 integrating sphere system as shown schematically in Figure 3.2. A simple modification was made to the standard apparatus involving the purchase of a second Li-Cor Lamp/Collimator housing and the insertion of a Schott RG 695 colored long-pass glass filter at the exit aperture of one of the illuminator units. As described below, with a suitable measurement protocol these two light sources enable reflectance and transmittance measurements of a given sample without fluorescence and including the effect of fluorescence.

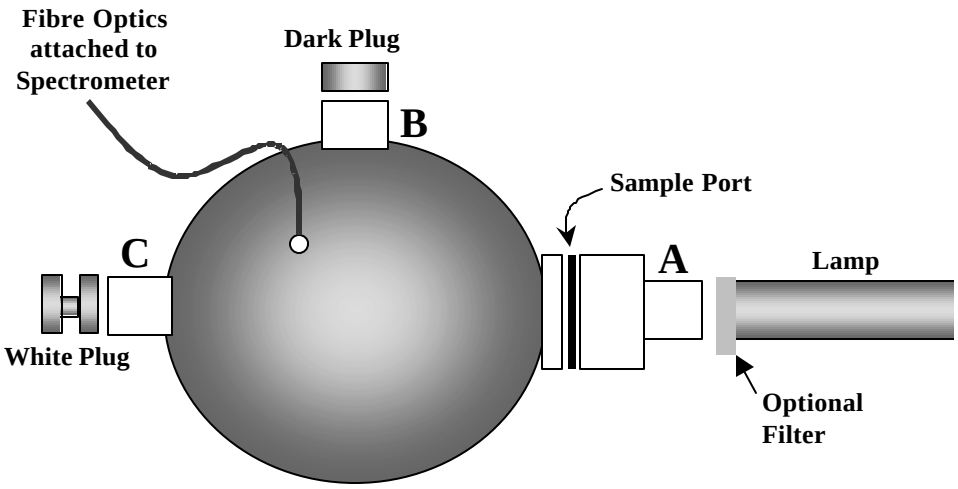

Figure 3.2. Schematic view of the Li-Cor 1800 integrating sphere coated internally with $BaSO_4$, coupled to the Ocean Optics spectrometer. Ports A, B, and C enable the exchange of white and dark plugs as well as the light source. The optional long-pass filter placed at the exit aperture of the light source enables measurements of reflectance and transmittance at $\lambda > 700$ nm while suppressing the fluorescence signal.

Table 3.1. Sequence of measurements with the Li-Cor 1800 and fibre spectrometer to enable the calculation of reflectance and transmittance with Equations [3.1] and [3.2]. Measurements start with the filter IN in order to substantially reduce the activation of PSII with visible light, with no change in the position of the leaf sample needed to proceed with the second set of measurements without the filter.

Step	Setup	Lamp	Filter	White Plug	Dark Plug	Sample	$BaSO_4$
1	TSP	ON	IN	C	B	IN →	OUT
2	RSS	ON	IN	B	A	IN ←	OUT
3	RTS	ON	IN	C	A	IN ←	OUT
4	RSS	ON	OUT	B	A	IN ←	OUT
5	RTS	ON	OUT	C	A	IN ←	OUT
6	TSP	ON	OUT	C	B	IN →	OUT
7	RST	ON	OUT	B	A	OUT	IN
8	RST	ON	IN	B	A	OUT	IN
9	RSD	OFF	IN	B	A	OUT	OUT
10	TDP	OFF	IN	C	B	IN	OUT

IN →: adaxial leaf surface facing sample port A
IN ←: adaxial leaf surface facing sphere

The Schott RG 695 colored glass filter, with 3 mm thickness, blocks radiant flux at $\lambda <$ 695 nm as shown by the measured transmittance spectrum in Figure 3.3. Using the "filtered illuminator" and standard illuminator in turn, reflectance and transmittance measurements were carried out on non-fluorescent (assured by the PAM-2000 Fluorometer) diffusing targets. Measurements showed that relative differences in reflectance and transmittance spectra for $\lambda > 700$ nm, with and without the filter in the illuminator, were less than 2%. Photosynthetic photon flux density (PPFD) illumination values (measured with a Li-Cor quantum sensor) were 110 ± 2 μmol m^{-2} s^{-1} for the illuminator with the filter in and 2820 ± 5 μmol m^{-2} s^{-1} with no filter.

A set of 10 measurements per leaf sample were needed using the Li-Cor 1800 protocol to calculate leaf reflectance and transmittance with fluorescence signal embedded (no filter between target and light source) and without fluorescence signal (filter between target and light source). Leaf samples were dark-adapted before the measurements were carried out. The specific sequence of measurements with the Li-Cor 1800 apparatus and fibre spectrometer and the two illuminators is provided in Table 3.1, and calculation of spectral reflectance and transmittance was determined from Equations [3.1] and [3.2]. Measurements start with the filter between the leaf sample and the light source in order to substantially reduce the activation of PSII with visible light. No change in the position of the leaf sample was needed to proceed with the set of measurements without the filter. The measured leaf reflectance and transmittance with and without the filter can therefore

be accurately compared in order to detect potentially-small differences due to a fluorescence signal.

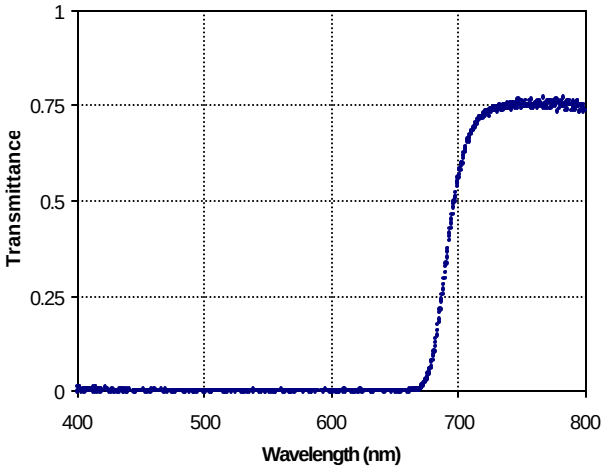

Figure 3.3. Transmittance of the Schott RG 695 high pass filter measured with the Li-Cor 1800 integrating sphere and 7.5nm Ocean Optics fibre spectrometer. The filter blocks out the excitation light at $\lambda < 695$ nm and enables the measurements of leaf reflectance and transmittance without the influence of chlorophyll fluorescence.

A typical pair of reflectance spectra obtained with this measurement protocol is shown in Figure 3.4 illustrating the additive effect of the broad 740 nm fluorescence signal superimposed on the reflectance spectrum due only to the scattering and absorption effects within the leaf. Comparisons were considered valid for $\lambda > 705$ nm due to the rapidly increasing noise level in the signal below that wavelength with the low Schott 695 filter transmission.

3.1.1.4.- Chlorophyll a & b and total carotenoids content of sugar maple leaves

Leaves were stored at –23°C until analysis. Two 2.3 cm circles were cut out of the leaf. One circle was ground in liquid N_2, weighed, and placed in a 15 ml centrifuge tube. The second circle was weighed, oven dried at 80°C for 24 hours, and re-weighed. Ten ml of N, N-dimethylformamide (Spectralanalyzed grade, Fisher) was added to the tube. Tubes were placed horizontally in a darkened 4°C orbital shaker set to 100 rpm for two hours to

extract pigments. Tubes were centrifuged at 5°C and 5,000 g for 20 minutes. Tubes were placed in a dark, 4°C refrigerator for 20 minutes. Tubes were removed from the refrigerator and 3 ml of supernatant removed and placed in a cuvette and the absorbance measured at 663.8 nm, 646.8 nm, and 480 nm with a Cary 1 spectrophotometer. Chlorophyll *a*, chlorophyll *b*, and total carotenoid concentrations were calculated using the extinction coefficients derived by (Wellburn, 1994). Pigment content measurements were made at the OFRI, under the direction of Dr. Thomas N. Noland.

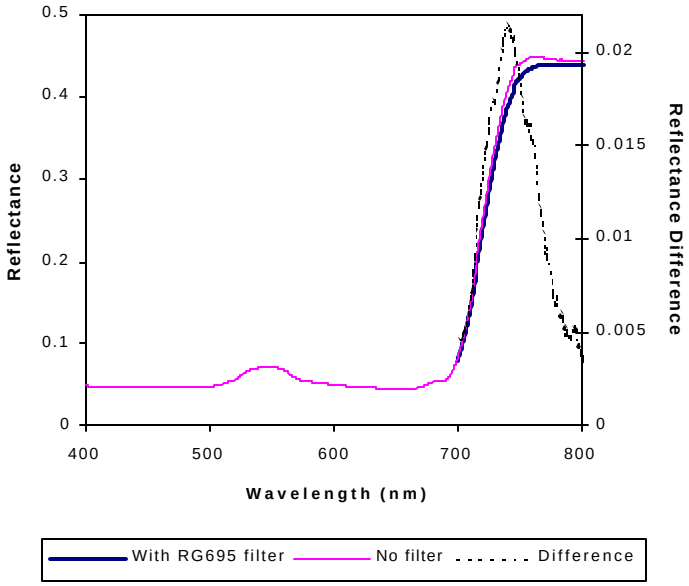

Figure 3.4. Single leaf reflectance measurements obtained with the Li-Cor 1800 apparatus and fibre spectrometer using the measurement protocol with the RG695 filter (thick line) and with no filter (thin line) from a dark-adapted *Acer saccharum* M. leaf sample. The additive effect of the broad 740 nm fluorescence signal superimposed on the reflectance spectrum is shown.

3.1.2.- Diurnal variation of fluorescence

This study sampled 30 leaves which had similar chlorophyll content (49 to 53 units according to SPAD-502 (Minolta Camera Co., Ltd., Japan) chlorophyll meter readings, and from subsequent pigment analysis, $\bar{x}$ =58.08 µg/cm^2, s=5.26, n=30). Leaf samples were selected with similar chlorophyll content in order to study possible variations in the

apparent leaf reflectance and transmittance due to normal diurnal changes of chlorophyll fluorescence. The day before the experiment, leaves were selected and a circular area was marked on each leaf for subsequent sampling. On the morning of the study, trees were transferred from a shaded (50%) greenhouse environment to unshaded outdoor conditions at 0800 h, and returned to the greenhouse at 1430 h. This was done to induce a strong diurnal chlorophyll fluorescence response. Plants were sampled for chlorophyll fluorescence and spectral analysis at 07.00 h, 10.00 h, 13.00 h, 17.00 h, and 20.00 h.

At each sampling time, leaves (with petioles attached) were removed from the plants and immediately placed into plastic bags, sealed, and kept in a cooler on ice until one leaf had been sampled from each of 6 plants, typically < 5 min collection time. They were taken into the laboratory, warmed briefly to room temperature, then sampled for effective quantum yield, then dark adapted for 30 min and re-sampled for Fv/Fm (as described below).

Measurements of reflectance and transmittance were made using the Li-Cor 1800 integrating sphere coupled to the 7.5 nm spectral resolution Ocean Optics ST1000 fibre spectrometer, and applying the methodology explained below which uses a long-pass optical filter to suppress excitation of Photosystem II (PSII) fluorescence signal from the apparent reflectance signal. These spectral readings were taken following the fluorescence measurement, allowing the calculation of the reflectance difference between the measurement with and without the long-pass filter (as described below). Immediately

after optical measurements were completed on each leaf, it was placed in a plastic bag, sealed and stored in the freezer for subsequent analysis of pigments.

3.1.3.- Time decay studies on same leaf

This experiment was designed to study the effects of fluorescence time-decay on the measurements of apparent spectral reflectance. The leaf was inserted into the leaf holder in the Li-Cor apparatus and exposed to light for five minutes. Subsequently, leaf reflectance measurements were taken at 2 second intervals for five minutes, again with and then without the long-pass filter.

3.2.- LABORATORY CANOPY-LEVEL EXPERIMENTAL METHODS AND MATERIALS

3.2.1.- Laboratory BRF facility

CASI hyperspectral canopy reflectance measurements (Figure 3.5) in the laboratory were made using a Bi-Directional Reflectance Factor (BRF) facility (Soffer, 1996) which is comprised of 4 subsystems (Figure 3.6): the CASI sensor, the illumination system, the canopy created by maple seedlings, and the mechanical system. The CASI sensor head unit was installed in the system sensor support arms at the altitude of 2.5 m from the canopy of plant material. The CASI was operated in a hyperspectral mode at maximum spectral resolution with 288 channels, spectral spacing of 1.8 nm and nominal bandwidth of 2.5 nm, with f/2.0 aperture. Collimated illumination at 45° inclination was provided by a regulated 1000W halogen light source and a collimating lens. The raw 12 bit CASI

data were calibrated to spectral radiance using radiance sensitivity factors (Gray *et al.*, 1997) derived from the calibration methodology designed at York University and CRESTech (Miller *et al.*, 1995). A translation table under the plant canopy attached to an electric motor with user-controlled speed enabled the collection of above-canopy spatial imagery with the CASI viewing a line oriented perpendicular to platform motion. A Spectralon reflectance panel placed on the moveable platform with the plant material so as to be viewed at the end of each CASI scene permitted non-uniformities between across-track pixels to be normalized by scaling each canopy pixel by the relative response of the Spectralon panel in the same position. Thus pixel responses were scaled to reflectance values by applying the known reference panel bi-directional reflectance factor values.

Figure 3.5.- Canopy reflectance imagery collected in laboratory from *Acer saccharum* M. seedlings using the CASI hyperspectral imager at 2.5 m above the canopy, at a nominal bandwidth of 2.5 nm between 405 and 940 nm. Collimated illumination by a stabilized 1000W light source at 45° inclination and a Spectralon reflectance panel enabled normalization to scene above-canopy apparent reflectance.

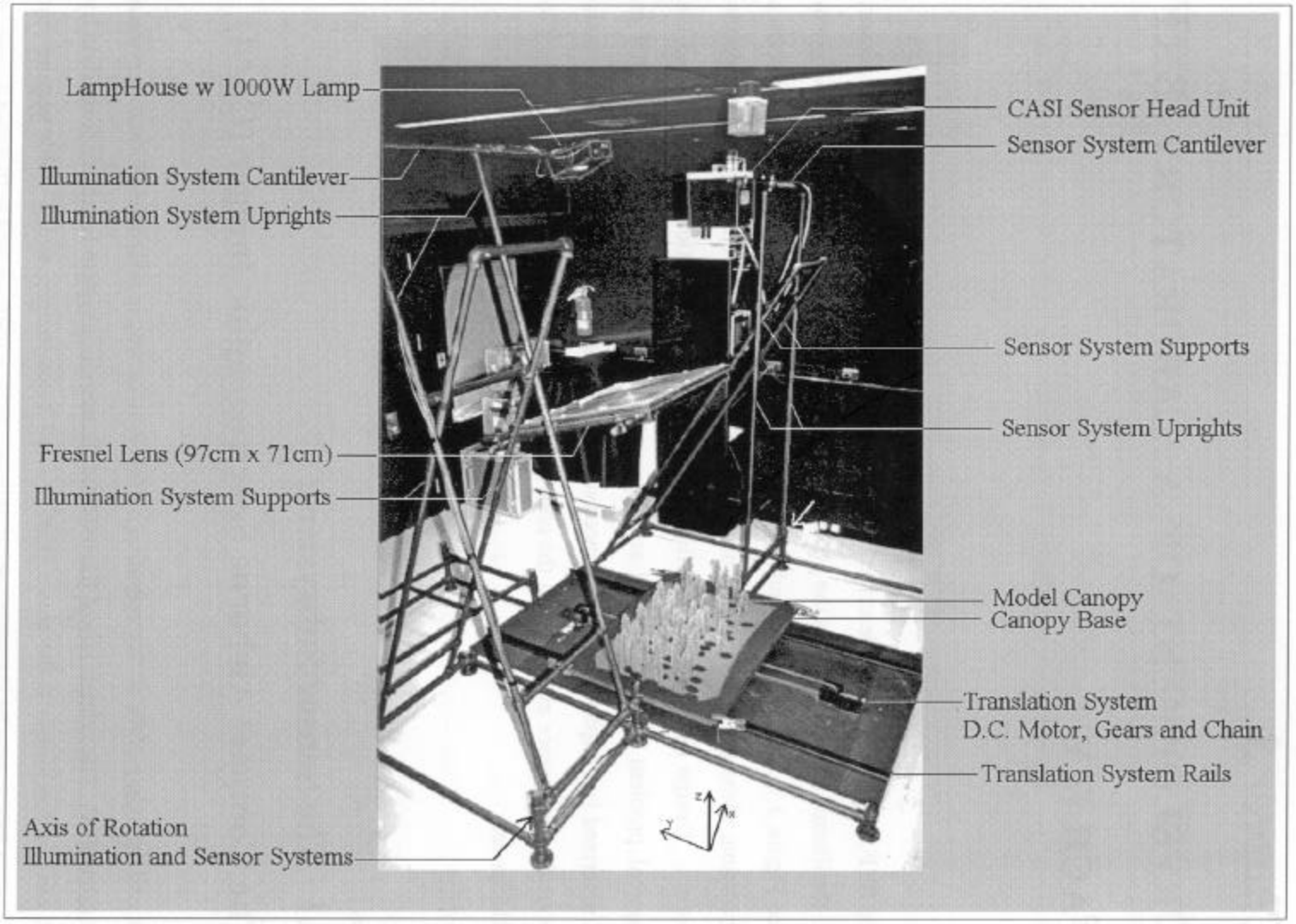

Figure 3.6. Schematic view of the Laboratory BRF Facility (*Source:* Soffer, 1996).

3.2.2.- Measurement Protocols

A filter holder was custom-designed to permit a Schott RG695 high pass filter to be placed in front of the 1000W halogen light source in order to restrict incident radiant energy on the scene to $\lambda > 705$ nm. This facilitated the collection of canopy reflectance measurements with CASI in the absence of fluorescence generating radiation, similar to measurement protocols at the leaf level, as described in Section 3.1.1.3. Canopy scene reflectance measurements were collected using the CASI first with the blocking filter and then without the filter in order to study canopy apparent reflectance signatures as the plant material made a transition from dark-adapted to steady-state illumination conditions.

3.2.3.- Plant Material

Acer saccharum M. seed was collected from a single tree in Sault Ste. Marie, ON, in September, 1998. In November 1998, at the Ontario Forest Research Institute, the seed was soaked in aerated deionized water for 24 hours and placed in stratification (at 2°C) for 60 days. On January 15, 1999 the seeds were sown in seven multipot 6-45 containers with 2:1 (peat:vermiculite) soil mix and placed in +2°C cooler and kept moist. The containers were placed in an outdoor shade house (50% of full sun) on April 6th and germination was complete in about 5 weeks. Seedlings were grown in the shade house at the Ontario Forest Research Institute until July 30th. The containerized seedlings formed a vegetation canopy of 100cmx50cm used for the CASI-laboratory hyperspectral data collection carried out in the BRF facility.

3.2.4.- Experiment Description

3.2.4.1.- Fluorometer Fluorescence measurements

Chlorophyll fluorescence measurements were carried out with a Pulse Amplitude Modulation (PAM-2000) Fluorometer as described before.

3.2.4.2.- Canopy measurements of apparent reflectance

Hyperspectral CASI data were collected from the plant material using the Schott RG695 filter with dark-adapted plant material. The scene reflectance was re-acquired without the blocking filter, therefore allowing red light to reach the plant material, generating steady-state fluorescence.

3.2.4.3.- Time-decay fluorescence in apparent canopy reflectance

A time-decay fluorescence experiment was carried out in order to study the canopy reflectance change with time. Dark-adapted plant material was fixed motionless under the CASI sensor and consecutive hyperspectral data frames were collected over the same image line cross-section plant canopy for a full 3 minutes. A study of the variation in apparent reflectance during the 3-minute experiment was designed to track changes in fluorescence from the same plant material during this time period.

3.2.4.4.- Diurnal variation of apparent reflectance and fluorescence

Fv/Fm measurements were collected with the PAM-2000 Fluorometer during a one-day period in order to study relationships between changes in Fv/Fm and CASI optical

indices. Maple seedlings were moved outside the laboratory to get direct solar illumination and then moved inside the laboratory to make measurements of Fv/Fm, execute a CASI scene data collection, and then moved back outside again. Eight CASI hyperspectral measurements were carried out during the day, between 8.30am and 9.30pm. Plants were dark adapted for 15 minutes before each set of Fv/Fm readings.

3.2.4.5.- Reflectance measurements of steady-state fluorescence in healthy and stressed plant material

The last laboratory experiment was intended to study differences in steady-state fluorescence between two trays of maple seedlings, one healthy and the other one in severe drought stress. CASI images and steady-state readings were collected for 3 hours, and optical indices from CASI data were studied for consistency with PAM-2000 steady-state readings and with the FRT leaf simulation model (Zarco-Tejada *et al.*, 2000a). Canopy reflectance from the plant material was determined by selecting pixels with the 30% highest values in the NIR (850 nm), therefore minimizing effects of shadows and canopy openings, as performed in field CASI canopy reflectance extraction from *Acer saccharum* M. study sites (Zarco-Tejada *et al.*, 1999a; 1999b).

3.3.- EXPERIMENTAL METHODS AND MATERIALS FOR DIURNAL CANOPY DATA COLLECTION UNDER NATURAL ILLUMINATION CONDITIONS

Acer saccharum M. seed was collected from a single tree in Sault Ste. Marie, ON, in September, 1999, and a similar process was carried out as explained before in seedlings for canopy laboratory experiments. Seedlings were grown in the greenhouse at the Ontario Forest Research Institute until April 27th, then transferred to York University before leaf-out. The containerized seedlings formed a vegetation canopy of 70cmx50cm used for the data collection carried out under natural illumination conditions on May 27th, 2000.

Chlorophyll fluorescence was analyzed with a PAM-2000 Fluorometer as explained before for measuring Fv/Fm and Ft in dark-adapted material in a diurnal pattern at 9.09 h, 11.22 h, and 13.23 h. Leaf samples needed 30 minutes for dark adaptation and 3 minutes run for CF measurements.

A 45° full-angle FOV lens apparatus for upwelling radiance and downwelling irradiance measurements was coupled by two 200μm diameter fibre to the same Ocean Optics model ST 1000 triple spectrometer described previously, with 0.5 nm sampling interval, 7.3 nm spectral resolution, and 340-860 nm range.

The spectrometer is controlled and read out by a National Instruments multi-purpose Data Acquisition Card (DAC-750), and data collected at 48.75 msec integration time. Lens apparatus with fibre spectrometers were placed at nadir view over the seedling canopy using a 1.5m tripod (Figure 3.7), and measurements were made at 8.20h, 8.42h, 9.02h, 10.47h, 11.34h, 12.52h, and 13.37h to capture variations in apparent reflectance due to the effect of diurnal changes in CF. Collected spectra were smoothed using third order Savitzky-Golay method with 15 nm bandwidth. A Spectralon reflectance panel was used to calculate canopy reflectance values from the radiance measurements of the canopy.

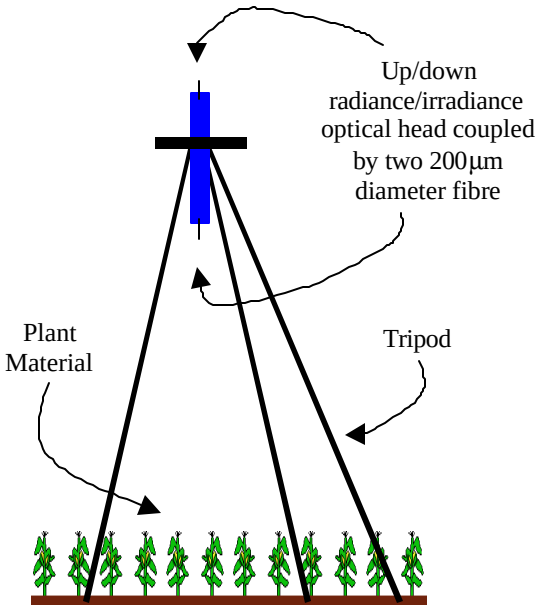

Figure 3.7. Schematic view of the radiometer optics with the fibre spectrometer detector directed at nadir view over the seedling canopy using a 1.5m tripod. Upwelling radiance and downwelling irradiance measurements were made during the day by coupling two 200µm diameter fibres to the Ocean Optics model ST 1000 triple spectrometer.

3.4.- FIELD-CANOPY EXPERIMENTAL METHODS AND MATERIALS

3.4.1.- Study sites description

Twelve study sites of *Acer saccharum* M. were selected in 1997 from existing provincial plot networks in the Algoma Region, Ontario (Sault Ste. Marie and the surrounding area). The sites were selected to represent a range of productivity and decline. In particular, six

permanent sample plots from the provincial Growth & Yield Program (Anon, 1993; Hayden *et al.*, 1995) were chosen to investigate the effects of stand productivity in maple. Another six plots were selected from the provincial Hardwood Forest Health network (McLaughlin *et al.*, 1992; 1999) to represent a gradient in maple forest decline. Detailed stand records exist and these sites are considered representative of tolerant hardwood forests in the Algoma Region.

3.4.2.- Leaf sampling scheme

Two samplings were carried out in June and July 1998 and 1999, collecting from the top of the crowns at each one of the twelve 30x30m *Acer saccharum* M study sites. Trees from each site were sampled collecting four leaves per tree with five trees per study site with a total of 440 leaf samples per year. Samples were used for biochemical analysis and measurement of leaf chlorophyll, carotenoid concentrations, ratio of variable to maximum chlorophyll fluorescence Fv/Fm, and spectral measurements of reflectance and transmittance. Single leaf reflectance and transmittance measurements were acquired on all leaf samples using a Li-Cor 1800-12 Sphere apparatus with an Ocean Optics fibre spectrometer with 0.5 nm spacing and 7.5 nm spectral resolution in the 340-860 nm range. Scaling-up from leaf level to canopy level requires leaf reflectance and transmittance data as input to canopy reflectance models. Reflectance and transmittance measurement techniques are also described in a previous section. LAI measurements were acquired for all the plots using a PCA Li-Cor 2000 instrument by OFRI scientist Mr. Paul Sampson.

3.4.3.- Hyperspectral Remote Sensing data acquisition

CASI data were collected in deployments over the twelve sites selected of *Acer saccharum* M. in the Algoma Region, in 1997, 1998, 1999 and 2000. Mean reflectance values per plot were calculated from the imagery in each *Acer saccharum* M. study site of 20 x 20 m (Figure 3.8).

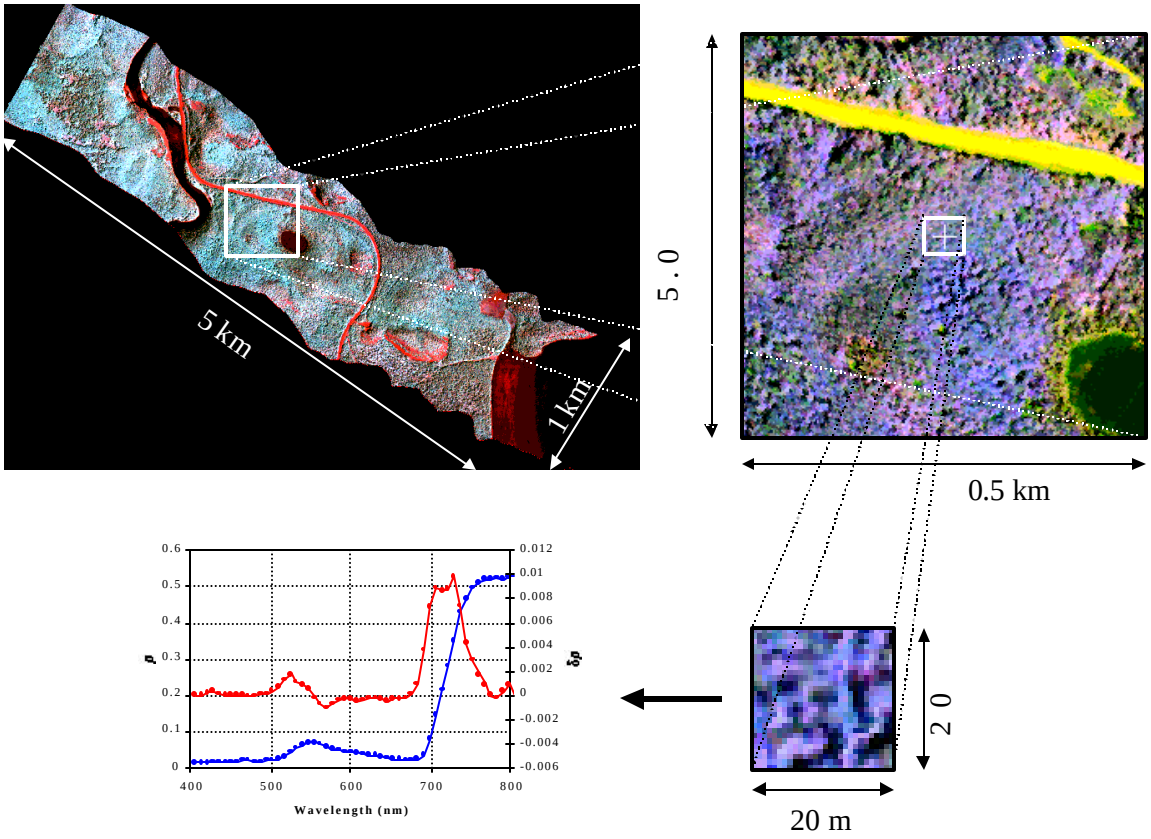

Figure 3.8. CASI image collected over one of the *Acer saccharum* M. study sites where ground truth pigment and CF data were measured in leaf samples. Data were collected in the 72-channel mode of operation, at 2x4 m spatial resolution resampled to 2x2 m. Average reflectance was calculated from the study site of 20 x 20 m for calculation of optical indices and derivative analysis.

The mean reflectance per plot was calculated selecting the 25% of pixels with highest reflectances in the NIR, therefore targeting crowns while minimizing the influence of shadows, canopy openings and the direct understorey reflectance. The above-canopy data acquisition using the CASI sensor was divided into three missions each with a specific sensor mode of operation (see Appendix for CASI spectral modes of operation): the *Mapping Mission*, with 0.5 m spatial resolution and 7 spectral bands (Figures 3.9 and 3.10); the *Hyperspectral Mission*, with 2 m spatial resolution, 72 channels and 7.5 nm spectral resolution (Figures 3.11 and 3.12); and the *Full-spectral Hyperspectral Mission*, with 288 channels, 2.5 nm spectral resolution, and 7 m spatial resolution. In addition, a CASI diurnal mission with the 144-channel mode of operation and 5m spatial resolution was carried out in July 1999 collecting data over two study sites at different times of the day, 8.00h, 9.30h, 12.20, and 16.12h along with ground truth CF measurements with PAM-2000. A second diurnal experiment over two sites was carried out in June 2000 with a specific CASI mode of operation in order to allow for higher spatial resolution data with spectral bands centered at the PSII photosystem. CASI data were collected in 9 spectral bands and 5nm bandwidth at 680.47, 684.26, 688.06, 691.86, 695.66, 699.46, 703.26, 707.06, and 710.87 nm, and 0.56x1.08m spatial resolution re-sampled to 0.5x0.5m. The 12-bit radiometric resolution data collected by CASI was processed to *at-sensor* radiance using calibration coefficients derived in the laboratory by CRESTech. Aerosol optical depth data at 340, 380, 440, 500, 670, 870, and 1020 nm were collected using a Micro-Tops III sunphotometer in the study area at the time of data acquisition in order to derive aerosol optical depth at 550nm to be used to process image data to

ground-reflectance using the CAM5S atmospheric correction model (O'Neill *et al.*, 1997). Reflectance data were geo-referenced using GPS data collected onboard the aircraft. Final registration of the hyperspectral mode imagery was achieved by registration to the CASI mapping-mission imagery using visual identification of ground-referenced 1 m white targets (Figure 3.10), which served to accurately identify the location of the sites.

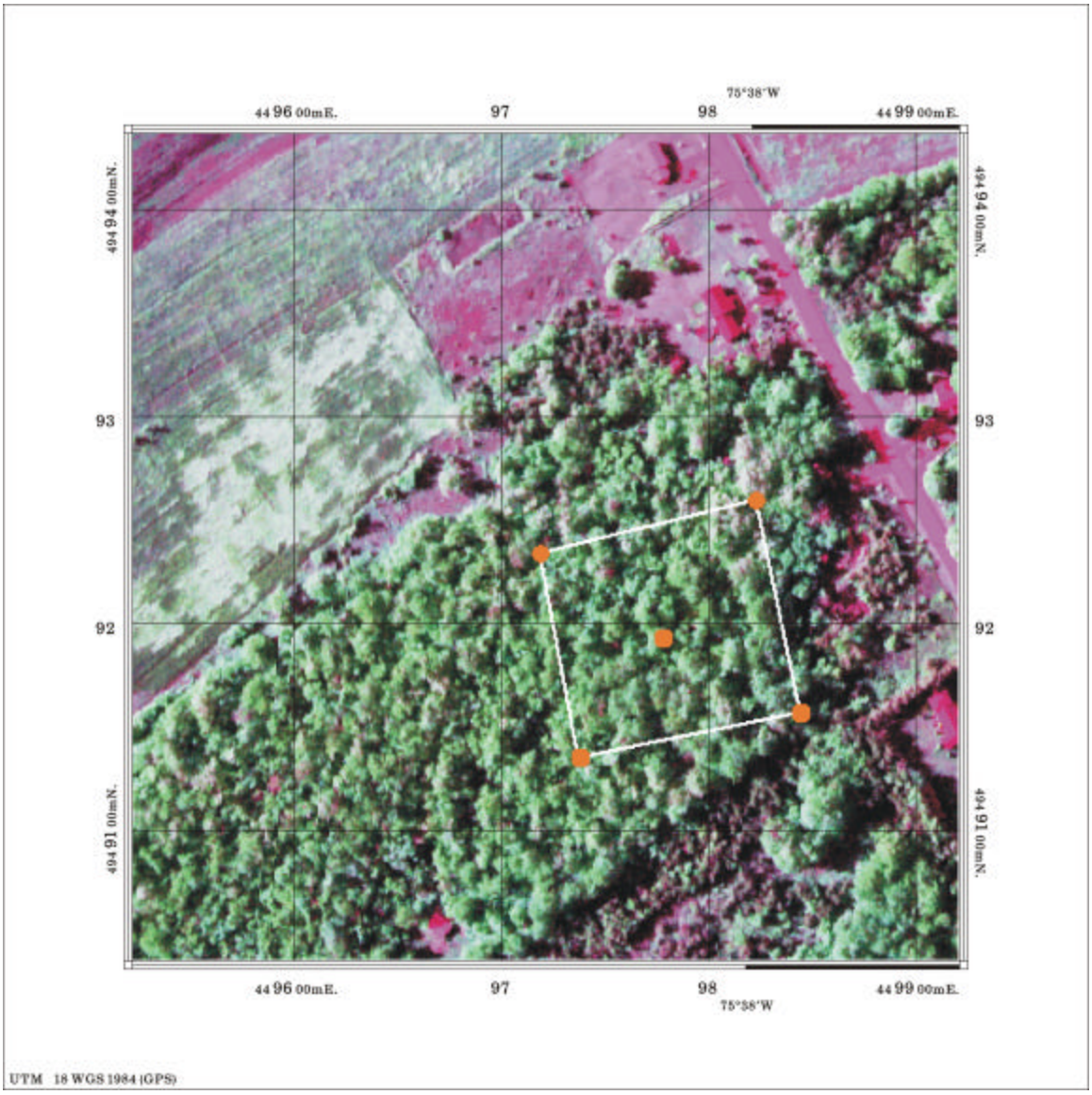

Figure 3.9. CASI image collected over one of the *Acer saccharum* M. study sites in the Mapping Mission mode of operation, with 7 channels and 0.8m spatial resolution. The high spatial resolution facilitated target location needed in the image registration process, therefore locating the study site of 20x20 m (1998 and 1999) and 80x80m blocks (2000 validation campaign, white box in figure). Colour composite of images with 554.9nm (blue), 742.3nm (green), and 489.5nm (red).

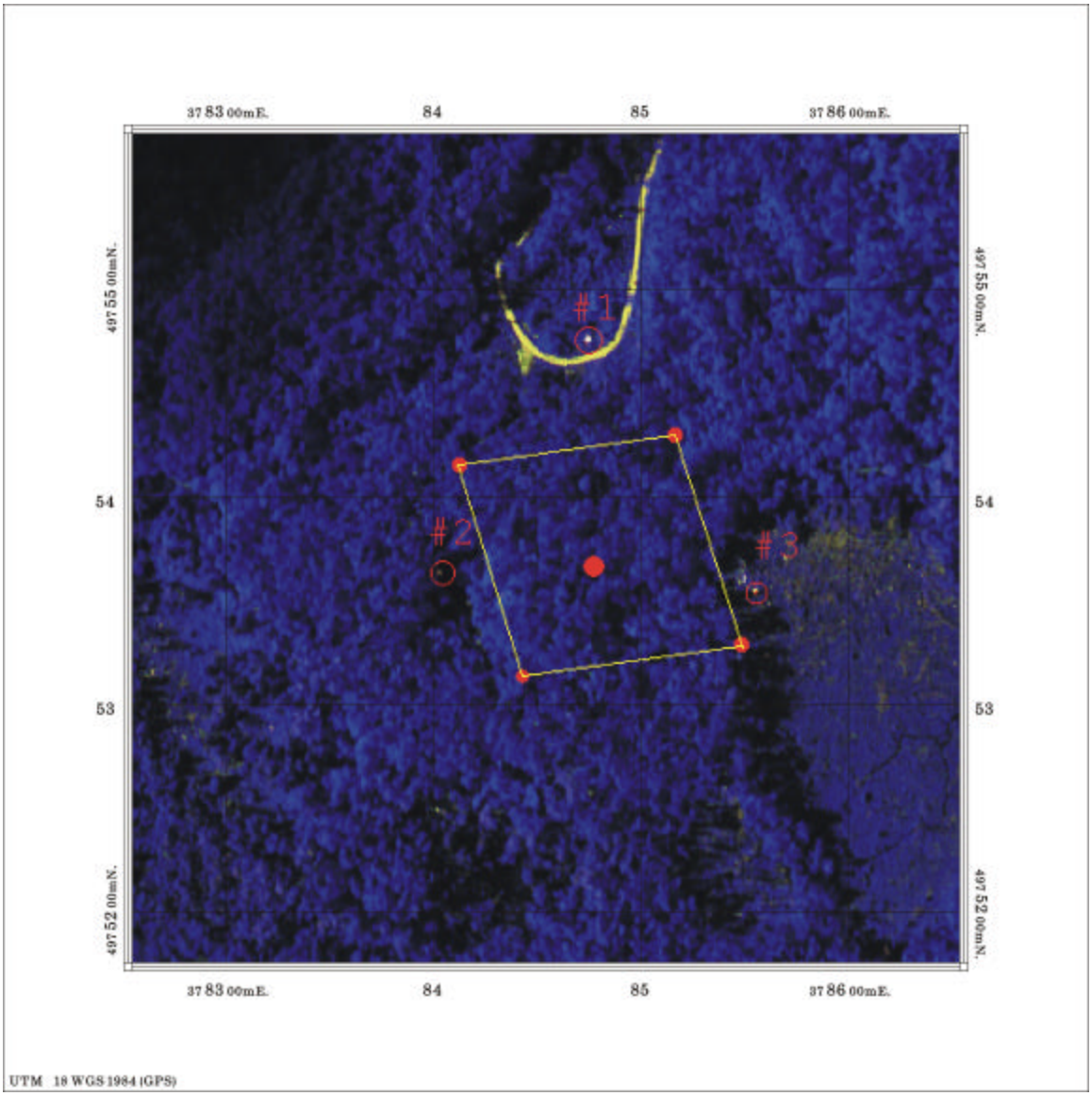

Figure 3.10. Target location from a CASI image collected over one of the *Acer saccharum* M. study sites in the Mapping Mission mode of operation, with 7 channels and 0.8m spatial resolution. Three white targets of 1x1m were placed around the 80x80m study site (labelled as #1, #2 and #3 in image). Colour composite of images with 776.7nm (blue), 681.4nm (green), and 489.5nm (red).

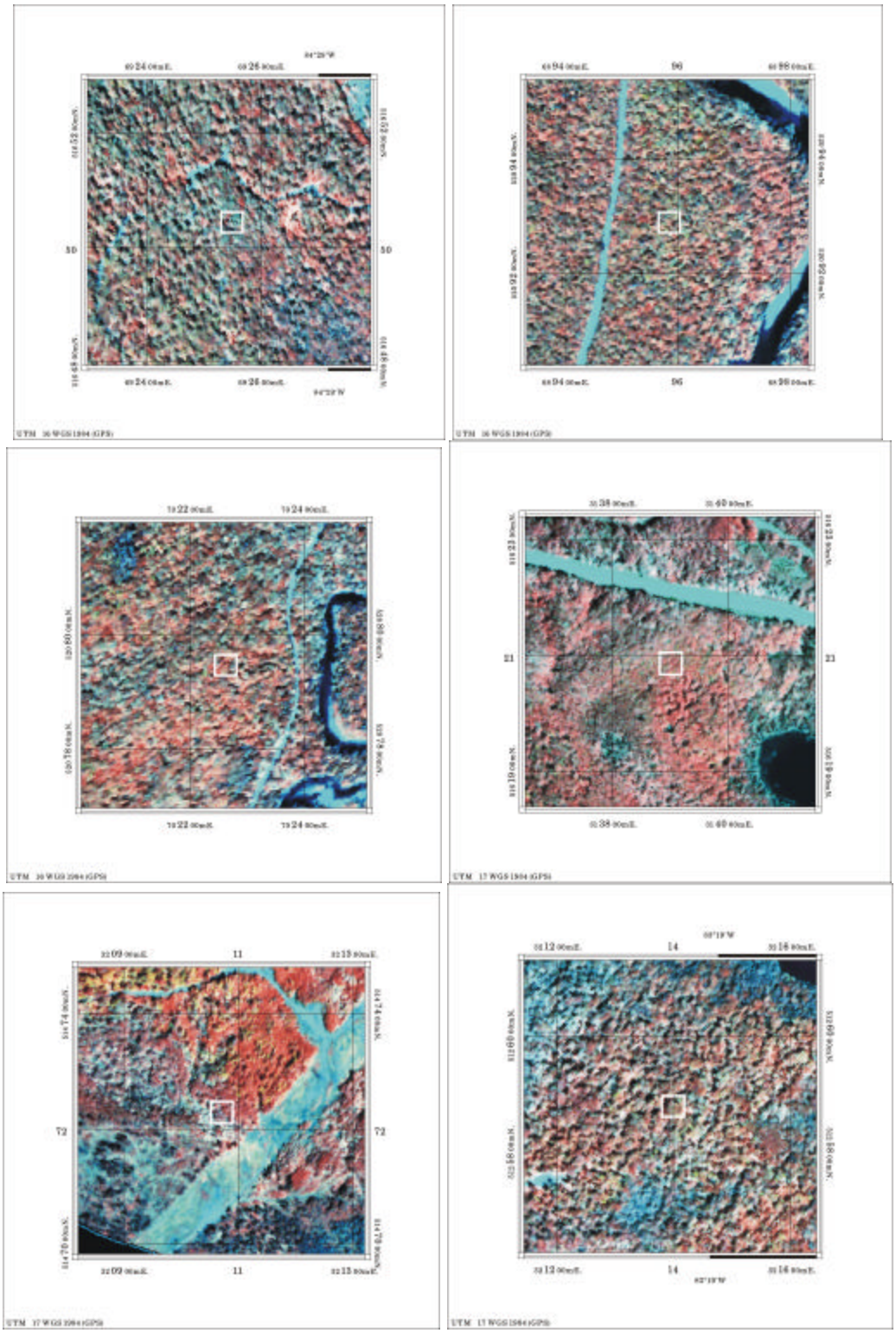

Figure 3.11 Study areas of 500x500m acquired over the *Growth and Yield* plots used for field measurements in 1997, 1998 and 1999. CASI data of 2x4 m (72chnls). Site codes (from upper left): GY1,GY15,GY31,GY41,GY42,GY45. Composite: 555.6nm(blue), 706.8nm(green), 852.1nm (red).

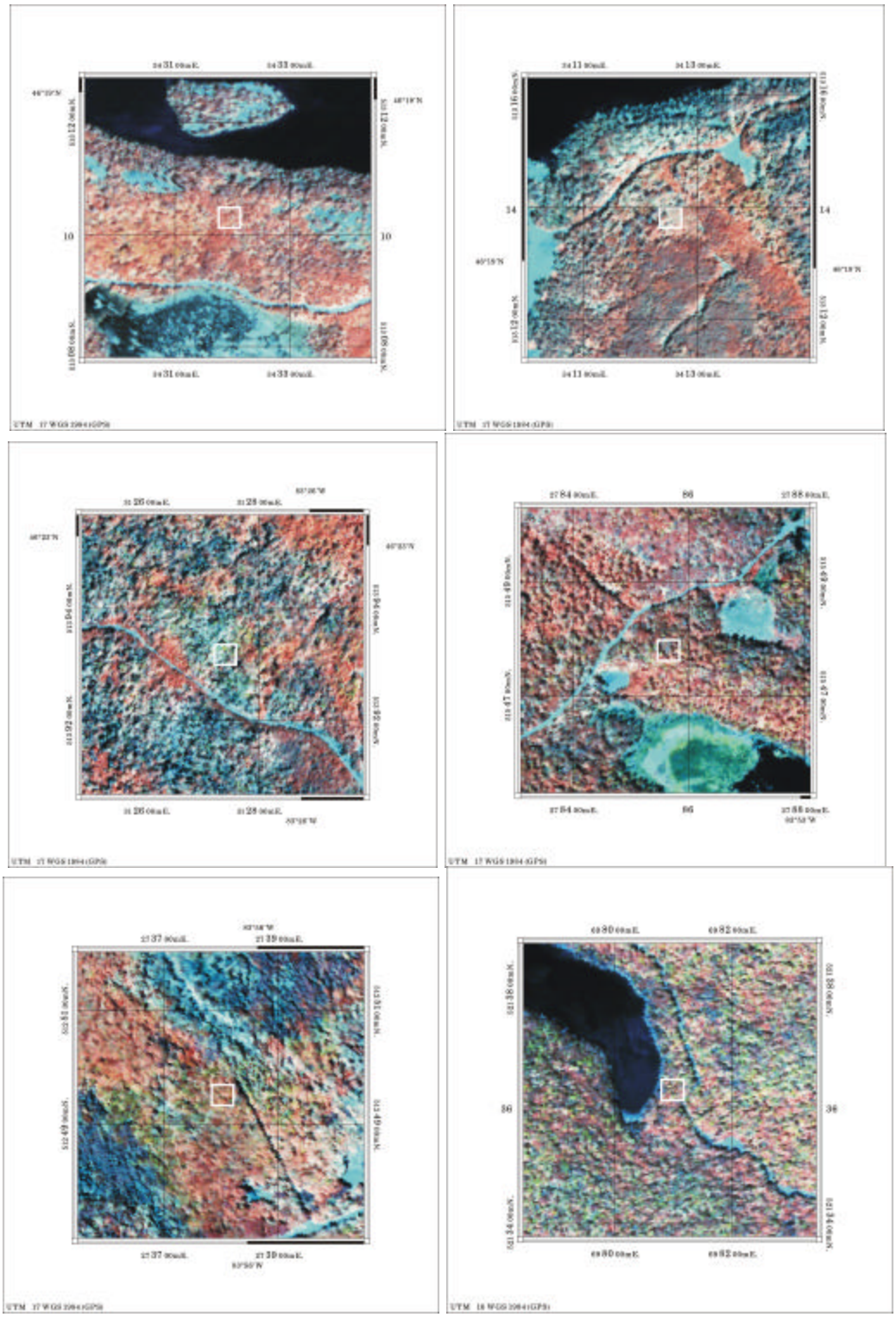

Figure 3.12 Study areas of 500x500m acquired over the *Maple Decline* plots used for field measurements in 1997, 1998 and 1999. CASI data of 2x4 m (72chnls). Site codes (from upper left): MD32,MD33,MD35,MD37,MD38,MD39.Composite:555.6nm(blue),706.8nm(green),852.1nm (red).

CHAPTER 4.

EXPERIMENTAL RESULTS

In this chapter the results obtained at the different levels of study are presented in which retrieval of leaf pigment content and CF have been investigated. The first section shows results obtained at a leaf level with optical indices calculated from leaf reflectance and transmittance data from samples collected in 1998 and 1999. The "good" relationships obtained at leaf level with CF led us to investigate the effects of CF in apparent reflectance, at leaf, canopy-laboratory, and canopy-airborne levels; these results are presented in the second section. Finally, results obtained with the airborne CASI sensor over the study sites in 1998, 1999 and 2000 are presented, showing the effects of the different methodologies for pigment estimation in closed canopies.

4.1.- LEAF-LEVEL RESULTS: OPTICAL INDICES AND BIOINDICATORS, CHLOROPHYLL PIGMENT CONTENT AND FLUORESCENCE MEASURES

Results obtained at a leaf level from leaf samples collected in June and July 1998 and 1999 campaigns demonstrated that a link exists between leaf pigments, chlorophyll-*a*&*b*, carotenoids, leaf fluorescence and certain optical indices derived from the reflectance

spectra. The indices at the individual leaf level are listed in Table 4.1, along with their determination coefficients. As expected from other studies (Matson *et al.*, 1994), better relationships are found with chl_{a+b} per unit area ($\mu g\ chl_{a+b}/cm^2$) rather than per unit weight ($\mu g\ chl_{a+b}/g$) as can be seen with some of the most prominent optical indices: Vog1 (R_{740}/R_{720}) (r^2=0.82 with chl_{a+b} per area; r^2=0.28 with chl_{a+b} per weight); λ_p (r^2=0.81 with chl_{a+b} per area; r^2=0.1 with chl_{a+b} per weight). All the relationships with chl_{a+b} and carotenoids are therefore developed with per area ground truth measurements. Results in Table 4.1, documenting the performance of optical indices summarized in Section 1.2, show improvement in relationships with chl_{a+b} from 1998 to 1999 data collection. This improvement in relationships between optical indices and chl_{a+b} from 1998 to 1999 is considered due to the change in ground truth data collection scheme in 1999. In 1998, two sets of leaves were collected from the tree, one for spectral measurements, the other for biochemical study, whereas in 1999 the same leaf portion was used for both leaf spectral and pigment measurements.

Table 4.1. Correlation coefficients *r* obtained from the statistical analysis between chlorophyll a&*b*, carotenoids and Fv/Fm, and optical indices obtained from *Acer saccharum* M. leaf reflectance and transmittance measurements for 1998 (*n*=113, June+July) and 1999 (*n*=171, June+July), organized by chl_{a+b} in 1999. Colour codes: visible ratios (green), VIS/NIR ratios (yellow), red-edge indices (red), and spectral and derivative indices (blue). Light blue shows relationships with r>0.6.

		chl_{a+b}/cm^2		**$Carot/cm^2$**		**CF (Fv/Fm)**	
		98	**99**	**98**	**99**	**98**	**99**
R_{750}/R_{710}	**750/710**	0.80	0.92	0.81	0.79	0.74	0.48
R_{740}/R_{720}	**Vog1**	0.80	0.91	0.80	0.76	0.69	0.51
R_{750}/R_{700}	**G_M2**	0.80	0.91	0.80	0.79	0.66	0.46
$(R_{734}-R_{747}) / (R_{715}+R_{720})$	**Vog3**	-0.79	-0.91	-0.81	-0.77	-0.66	-0.47
λp	**lpr**	0.79	0.90	0.80	0.80	0.62	0.44
$(R_{734}-R_{747}) / (R_{715}+R_{726})$	**Vog2**	-0.79	-0.90	-0.81	-0.77	-0.67	-0.47
D_{715}/D_{705}	**Vog4**	0.80	0.90	0.79	0.78	0.70	0.52
R_{750}/R_{550}	**G_M1**	0.77	0.83	0.74	0.76	0.53	0.19
R_{695}/R_{760}	**Ctr2**	-0.75	-0.81	-0.74	-0.70	-0.65	-0.50
$D_{\lambda p}/D_{703}$	**DP21**	0.68	0.78	0.72	0.72	0.40	0.21
R_{695}/R_{420}	**Ctr1**	-0.50	-0.77	-0.47	-0.64	-0.35	-0.53
$D_{\lambda p}/D_{720}$	**DP22**	-0.72	-0.76	-0.69	-0.62	-0.73	-0.65
$\int_{450}^{680} R$	**Lic4**	-0.70	-0.73	-0.63	-0.54	-0.51	-0.28
R_{554}/R_{677}	**G**	-0.71	-0.73	-0.67	-0.63	-0.57	-0.23
$(R_{675}\cdot R_{690})/R_{683}^2$	**Cur**	-0.75	-0.73	-0.71	-0.46	-0.75	-0.61
$D_{\lambda p}/D_{\lambda p+12}$	**DPR1**	-0.70	-0.67	-0.67	-0.53	-0.71	-0.61
R_{440}/R_{690}	**Lic2**	0.65	0.65	0.67	0.64	0.52	0.27
$(R_{800}-R_{450}) / (R_{800}+R_{650})$	**SIPI**	0.49	0.44	0.39	0.32	0.30	0.28
$(R_{531}-R_{570}) / (R_{531}+R_{570})$	**PRI1**	0.57	0.36	0.42	0.06	0.72	0.71
$D_{\lambda p}/D_{\lambda p+22}$	**DPR2**	-0.54	-0.35	-0.48	-0.23	-0.62	-0.55
$(R_{550}-R_{531}) / (R_{550}+R_{531})$	**PRI2**	-0.60	-0.32	-0.51	-0.07	-0.68	-0.44
$(R_{570}-R_{539}) / (R_{570}+R_{539})$	**PRI3**	-0.52	-0.30	-0.37	-0.03	-0.68	-0.67
$\int_{680}^{760} D$	**ADR**	0.31	0.28	0.33	0.40	0.23	0.18
$(R_{774}-R_{677}) / (R_{774}+R_{677})$	**NDVI**	-0.04	0.27	-0.01	0.32	-0.12	0.00
R_{774}/R_{677}	**SR**	-0.10	0.27	-0.07	0.33	-0.17	-0.02
$(R_{800}-R_{680}) / (R_{800}+R_{680})$	**Lic1**	-0.10	0.26	-0.06	0.34	-0.18	-0.05
R_s	**Rs**	0.31	0.24	0.33	0.37	0.25	0.18
R_o	**R0**	-0.08	-0.20	0.00	-0.03	0.01	-0.08
$(R_{680}-R_{430}) / (R_{680}+R_{430})$	**NPCI**	0.21	-0.17	0.15	-0.27	0.12	0.05
R_{430}/R_{680}	**SRPI**	-0.25	0.16	-0.18	0.27	-0.18	-0.08
R_{440}/R_{740}	**Lic3**	0.14	0.06	0.19	0.10	0.13	0.05
$(R_{415}-R_{435}) / (R_{415}+R_{435})$	**NPQI**	0.03	0.01	-0.13	-0.17	0.14	0.10

Red edge and spectral and derivative indices consistently show the best relationships in the two-year study, demonstrating that R_{750}/R_{710}, Vog1 (R_{740}/R_{720}), Vog2 (R_{734}-R_{747})/(R_{715}+R_{726}), Vog3 (R_{734}-R_{747})/(R_{715}+R_{720}), Vog4 (D_{715}/D_{705}), GM1 (R_{750}/R_{550}), GM2 (R_{750}/R_{700}) and Ctr2 R_{695}/R_{760} (red-edge indices) and λp, DP21 ($D_{\lambda p}/D_{703}$), and DP22 ($D_{\lambda p}/D_{720}$) (spectral and derivative indices) achieve the best results in both seasons when used for chl_{a+b} estimation. Optical indices calculated from the red edge are consistently well correlated with chl_{a+b}, since this is the spectral region were pigment absorption decreases, therefore exhibiting increasing effects of the medium structure in the measured reflectance, affecting the slope. Thus, results confirm previous work by Horler (1980, 1983), Miller *et al.* (1991), and others that were mentioned previously.

Generally good relationships are also found with carotenoids, primarily due to its correlation with chl_{a+b} (Table 4.2). Measured carotenoids at 480 nm from the leaf samples after extraction into dimethyl foramide happens to be in a spectral region with absorption of both chl_{a+b} and carotenoids, as explained in Chapter 1, therefore with carotenoids being masked by chlorophyll *a* and *b* absorption. The correlation matrix (Table 4.2) shows that carotenoids correlated highly with chl_{a+b} in both 1998 (r=0.7) and 1999 (r=0.82). No further investigation of carotenoid estimation was made due to the difficulties caused by atmospheric effects and the low signal-to-noise ratio in the blue region that do not allow the differentiation of small changes due to carotenoid absorption effects in the presence of dominant masking effects of chl_{a+b}.

Table 4.2. Correlation matrix calculated from pigment (in μg/cm^2) and CF data in 1998 and 1999 leaf sampling collection after averaging single leaf biochemical values per site, with *n*=12 in 1998 and *n*=12 in 1999, in *Acer saccharum* M. study sites. Highlighted values are for r>0.4.

		1998					***1999***				
		chl$_{a+b}$	***carot***	***Fo***	***Fm***	***Fv/Fm***	***chl$_{a+b}$***	***carot***	***Fo***	***Fm***	***Fv/Fm***
1998	**chl$_{a+b}$**	1									
	carot	0.706	1								
	Fo	-0.289	-0.072	1							
	Fm	0.222	0.125	0.529	1						
	Fv/Fm	0.463	0.173	-0.764	0.138	1					
1999	**chl$_{a+b}$**	0.753	0.691	-0.534	-0.131	0.502	1				
	carot	0.398	0.650	-0.272	-0.139	0.212	0.827	1			
	Fo	0.501	0.496	-0.069	-0.101	0.003	0.448	0.391	1		
	Fm	0.500	0.362	-0.143	-0.134	0.058	0.393	0.299	0.936	1	
	Fv/Fm	0.008	-0.127	-0.340	-0.237	0.236	0.173	0.016	0.430	0.510	1

Red edge and spectral and derivative indices also show the best relationships with CF, but joined by other indices such as DP22 ($D_{\lambda p}/D_{720}$), DPR1 ($D_{\lambda p}/D_{\lambda p+12}$) (derivative indices), curvature index ($R_{675}\cdot R_{690})/R_{683}^2$) (red edge) as suggested in Zarco-Tejada *et al.* (2000a, 2000b), and PRI indices, which target changes in the 530-550 nm region responsive to photosynthetic radiation use efficiency changes as described by Gamon *et al.* (1997).

Results indicate a decrease in the significance of the correlation of indices with CF in 1999 compared to 1998 (Table 4.1), where it can be seen that all indices show lower correlation coefficients in 1999 (right column) than with 1998 data (left column). This could be explained by the fact that a narrower range of CF values was measured in 1999 (Fv/Fm ε [0.77, 0.81]) compared to 1998 (Fv/Fm ε [0.74, 0.81]) (Table 4.3), with a range variation=44.15%, therefore showing from ground measurements that the sites were more

stressed in 1998 than in 1999. This is also confirmed by pigment data, which decreased its range by 12.7% from 1998 to 1999, showing a minimum value of chl_{a+b}=19.08 μg/cm^2 in 1998, with a minimum chl_{a+b}=26.5 μg/cm^2 in 1999. Therefore both chl_{a+b} and CF showed a consistent range variation indicative of a lower stress condition in 1999, although CF varied more than chl_{a+b}. Carotenoid range increased from 1998 to 1999, showing lower content in 1999 compared to 1998. A more detailed look at the relationship between pigment and CF shows that, although both chl_{a+b} and Fv/Fm ranges decreased from 1998 to 1999, therefore implying less stress range in 1999, the cross-year variation for all the sites with respect to chl_{a+b} (chl_{a+b} 1998 vs chl_{a+b} 1999) r=0.75 varied more homogeneously than with respect to Fv/Fm (Fv/Fm 1998 vs Fv/Fm 1999) r=0.23. This implies that study sites behaved more similarly from one year to another in their chl_{a+b} content than in their Fv/Fm chlorophyll fluorescence. Moreover, the relationship between chl_{a+b} and Fv/Fm in 1998 was higher (r=0.46) than in 1999 (r=0.17). Therefore a reason why the relationships with optical indices in 1998 were stronger than in 1999, could be due to the fact that red edge spectral indices are affected by both pigment content and CF.

Table 4.3. Percentage variation and ranges obtained in 1998 and 1999 data collection for pigment (in μg/cm^2) and CF measurements from *Acer saccharum* M. leaf samples.

	chl_{a+b}		**carot**		**Fo**		**Fm**		**Fv/Fm**	
	98	**99**	**98**	**99**	**98**	**99**	**98**	**99**	**98**	**99**
Min	19.08	26.58	7.53	5.58	0.24	0.08	1.15	0.37	0.75	0.77
Max	41.09	45.79	9.67	8.75	0.33	0.16	1.48	0.76	0.81	0.81
Range	22.02	19.21	2.14	3.18	0.09	0.08	0.33	0.39	0.07	0.04
% variation	**-12.704**		**48.3903**		**-16.055**		**17.807**		**-44.159**	

Figure 4.1 shows leaf level relationships obtained in 1999 for chl_{a+b} with λp and R_{750}/R_{710} optical indices, and between Fv/Fm and curvature index $(R_{675} \cdot R_{690})/R_{683}^2$ and derivative index DP22 $(D_{\lambda p}/D_{720})$ for 1998.

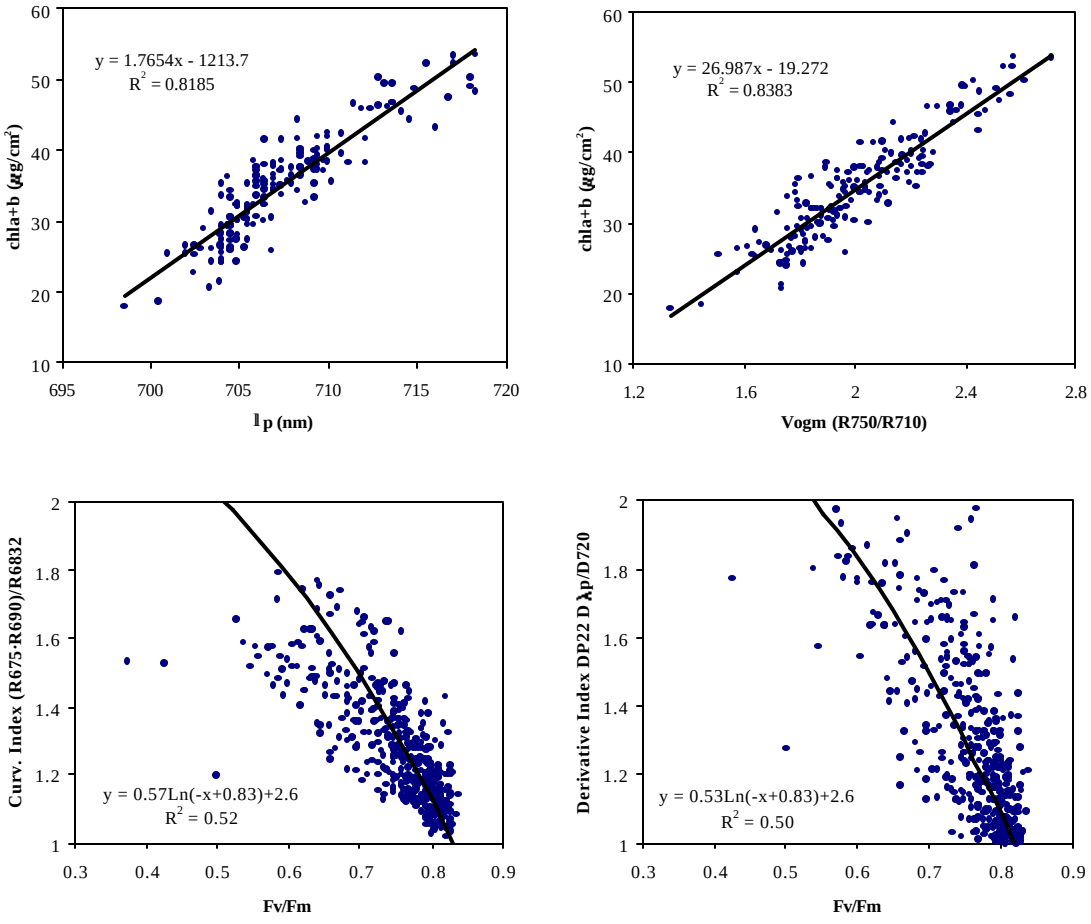

Figure 4.1. Relationships found between chl_{a+b} and λp (upper left) and R_{750}/R_{710} (upper right) for 1999 (*n*=171, June+July), and between CF Fv/Fm and curvature index $R_{675} \cdot R_{690}/R_{683}^2$ (lower left) and derivative index DP22 (Dλp/D720) (lower right) for 1998 (*n*=444, June+July), obtained from *Acer saccharum* M. leaf reflectance measurements .

4.2.- EXPERIMENTAL RESULTS FOR CF INVESTIGATION

The statistical study reported in Section 4.1 clearly demonstrates that both pigment content and CF correlate significantly with specific optical indices in leaf spectra. In this section results for CF investigations will be reported, at all the levels of study: leaf level, laboratory simulation with canopy seedlings, and in the field under natural illumination conditions in order to increase our understanding of the nature of the observed correlations. Simulation results using the FRT model and coupling FRT and PROSPECT for CF and chl_{a+b} estimation at leaf level are also included here.

4.2.1.- Experimental Results from CF studies at leaf level

4.2.1.1.- Time decay studies on same leaf

For this study the experimental protocol described in Section 3.1.3 was followed. Changes in CF amplitude subsequent to exposure were also tracked in apparent reflectance spectra. By exposing a dark-adapted leaf to sudden prolonged illumination, one can expect a classical Kautsky response pattern by which CF initially peaks then gradually decays in the ensuing minutes as a result of photochemical and non-photochemical quenching of CF. This pattern, clearly evident in the CF measurements done with the Fluorometer, should also be discerned in reflectance difference patterns if fluorescence is affecting the apparent reflectance spectra. Measurements were taken every 2 seconds during five minutes of illumination, alternating between *"with"* and then *"without"* the blocking filter. The comparison between the first and last spectral

reflectance measurement made without the filter can be seen in Figure 4.2. The differences in apparent reflectance are easily seen in three spectral regions, with maximal differences at approximately 690 nm and 750 nm corresponding to the two chlorophyll fluorescence emission peaks. The other region, located near 370 nm in the blue is not expected from chlorophyll and needs further study. Figure 4.3 shows the change of the reflectance peak at 755 nm with time when the reflectance measurements made with and without filter are subtracted. The plot shows that the time variation pattern is consistent with the Kautsky curve measured with the fluorometer.

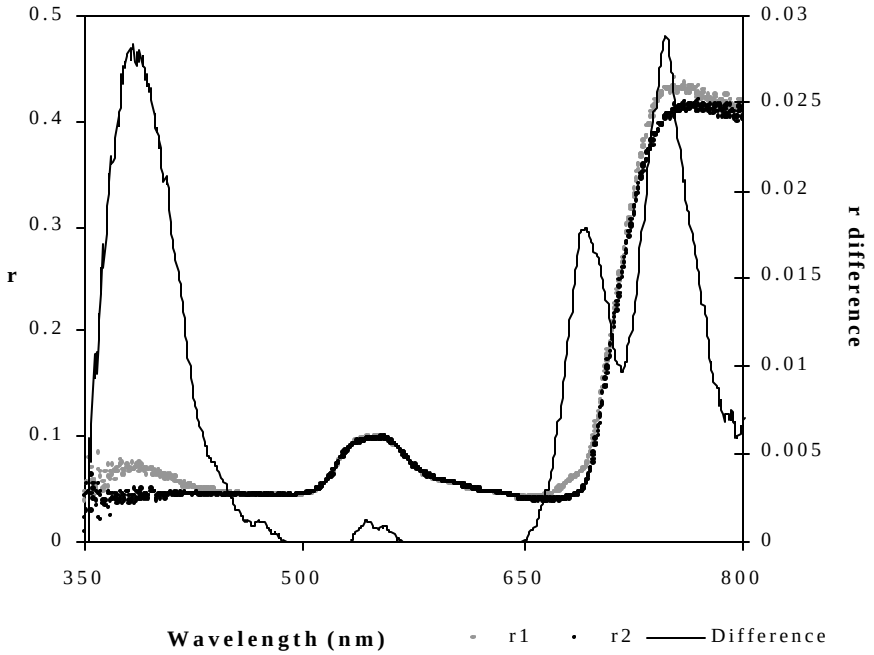

Figure 4.2. Reflectance measurements taken at t_0 (r_1) and t_1(5 min) (r_2) which demonstrates that fluorescence emission bands affect the reflectance measurements.

4.2.1.2.- Diurnal variation in fluorescence

In this experiment the methodology described in Section 3.1.2 was used. Figures 4.4 and 4.5 show the diurnal variation of Fv/Fm and Ft110, respectively, observed during the day compared to the variation of the reflectance difference at 740 nm with and without the filter, therefore tracking the PSII excitation to visible light superimposed on the reflectance when there is no excitation. The changes in the reflectance when there is visible excitation light are consistent and proportional to measurements of fluorescence in the leaf material. Results showed that variations in Fv/Fm during the day are captured in the leaf reflectance measurements even when the pigment concentration is constant.

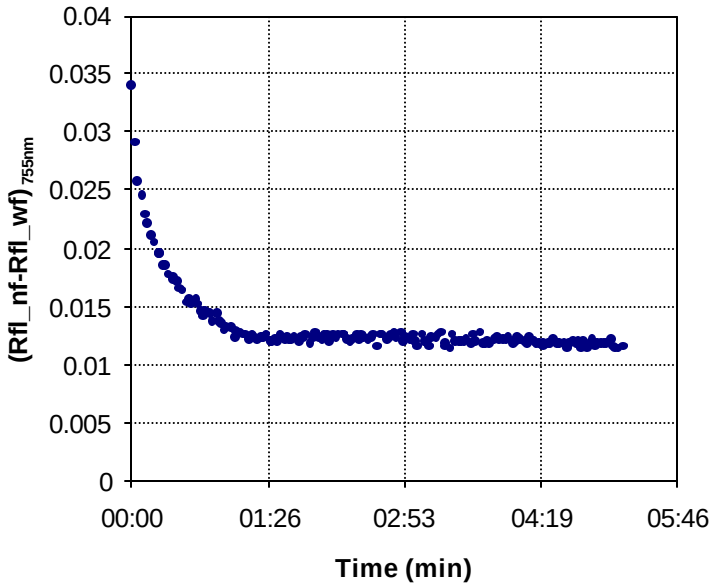

Figure 4.3. Variation of the reflectance difference at 755 nm with (Rfl_wf) and without filter (Rfl_nf) with time. It demonstrates the fluorescence decay at 755 nm with time after the illumination of a dark-adapted leaf.

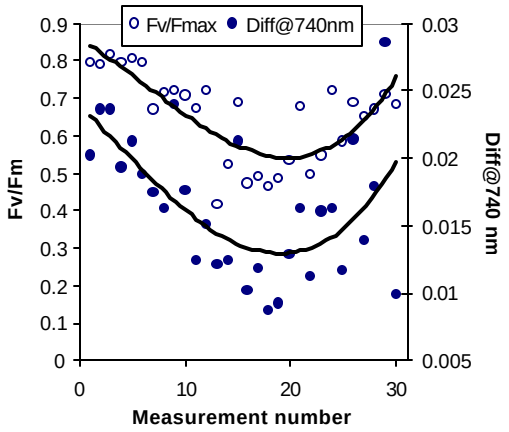

Figure 4.4. Variation of Fv/Fm during the day of the experiment measured in leaf samples, compared to the variation of the reflectance difference at 740 nm (Rdiff@740) with and without the filter. The similar tendencies in solid curves, which are the least-squares best fit through the two sets of data, show that the dark-adapted fluorescence is tracked by reflectance measurements.

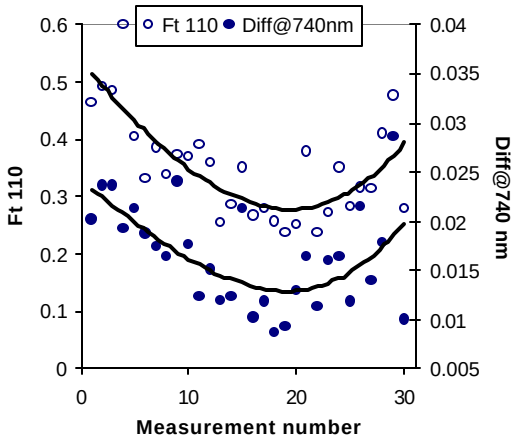

Figure 4.5. Variation of Ft110 during the day of the experiment measured in leaf samples, compared to the variation of the reflectance difference at 740 nm (Rdiff@740) with and without the filter. The similar tendencies in the solid curves, which are the least-squares best fit through the two sets of data, show that the steady-state fluorescence is tracked by reflectance measurements.

Relationships found between the observed reflectance difference at 740 nm (Rdiff@740nm) and Fv/Fm (r^2=0.66, Figure 4.6), F_{MAX} (r^2=0.62), Ft110 (r^2=0.54, Figure 4.7), Ft2820 (r^2=0.51), Fm'2820 (r^2=0.52) demonstrate the consistent relationships between spectral reflectance and CF features. The experiment shows that reflectance difference Rdiff@740nm tracks not only dark-adapted fluorescence (Fv/Fm) but also steady-state fluorescence (Ft and Fm'), and to lesser degree ΔF/Fm' (r^2=0.37). In all cases, changes in CF in this experiment are due to fluorescence mechanisms alone since leaf chlorophyll content was selected to be effectively constant ($\bar{x}$ =58.08 µg/cm^2, *s*=5.26, *n*=30). Changes in R_{690} were not tested with this measurement protocol because of the filter cut-off at 695 nm. Nevertheless, changes in that region are observed and are

reported later using optical indices related to changes in the reflectance curvature in the 680-690 nm region.

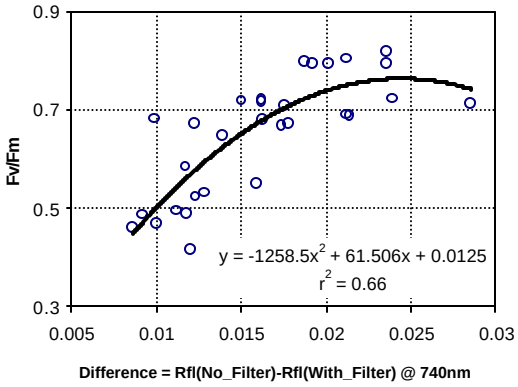

Figure 4.6. Relationship between Fv/Fm and reflectance difference at 740 nm with and without the filter. Reflectance peak at 700-750 nm region is able to track changes in dark-adapted fluorescence Fv/Fm.

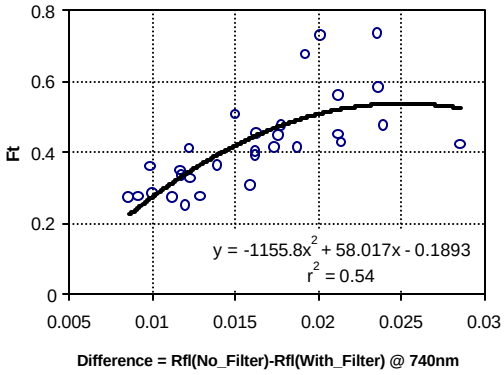

Figure 4.7. Relationship between steady-state fluorescence Ft110 and reflectance difference at 740 nm with and without the filter. Reflectance peak at 700-750 nm region is able to track changes in steady state fluorescence features.

4.2.2.- Leaf Reflectance and CF Simulation Results with the FRT Model

With the Fluorescence, Reflectance and Transmittance simulation model (FRT model) developed as part of this research (as described in Section 2.2), a wide range of experimental results can be simulated. First, with nominal leaf parameters the apparent reflectance with and without fluorescence can be simulated for qualitative comparison with the measurements reported earlier. Here we have used the following leaf parameters: leaf thickness D= 0.075 mm, chl_{a+b} content C=50 $\mu g/cm^2$, protein content (0.0012 $\mu g/cm^2$) and cellulose plus lignin content (0.002 g/cm^2), and PROSPECT structural

parameter N=1.4. For the fluorescence signal we use Equation [2.17] with λ_L = 690 nm, λ_H=735 nm, f_R=1, Δ_L=25nm, Δ_H=60 nm, and a fluorescence yield of 10% or 0% depending on whether the simulation is with, or without, fluorescence stimulation. The FRT model simulation results are shown in the Figure 4.8. It is clear from a comparison with the measurement results reported in Figure 4.8 that the relative magnitudes of the fluorescence signature at 690 and 740 and the deviations from the inherent reflectance signature that the observations at the leaf level are consistent with theory.

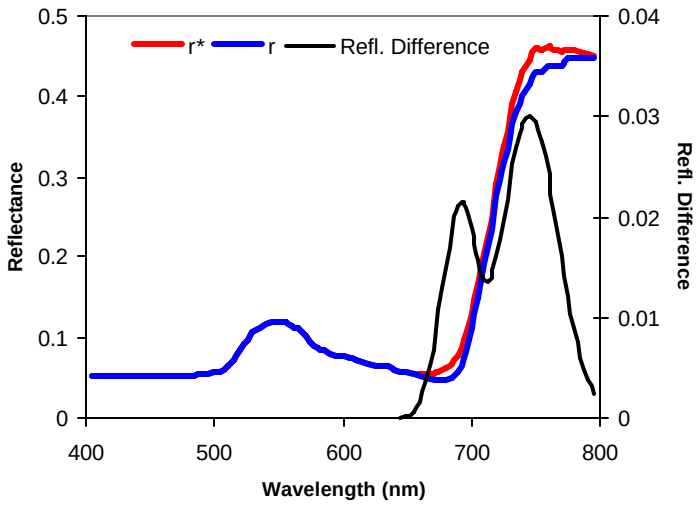

Figure 4.8. FRT Model simulating leaf reflectance with fluorescence (fluorescence efficiency=0.085, chl_{a+b} content = 50 $\mu g.cm^{-2}$, leaf thickness = 0.075 mm, labeled as r*), and without fluorescence (labeled as r).

4.2.2.1.- Model assessment using experimental data

The FRT model simulation was compared to experimental leaf sample data described before. Chlorophyll fluorescence measurements for a constant pigment concentration data

allowed the simulation of reflectance spectra. Comparison with leaf spectral reflectance measurements collected with and without the filter for non-fluorescence disturbance was performed. The test was carried out using the data collected in the experiment where chl_{a+b} contents were constant ($\bar{x}$ =58.08 μg/cm^2, s=5.26, n=30). Input parameters in the model were chl_{a+b}, Fv/Fm as fluorescence efficiency factor (measured with the PAM-2000), and leaf thickness. Results showed that peak at 700-750 nm region due to fluorescence are generally consistent with the model. Figure 4.9 shows that r^2=0.58 was obtained in the comparison between the modeled Rdiff@750 and the real Rdiff@750 calculated from reflectance spectral measurements with the Li-Cor sphere with and without the filter.

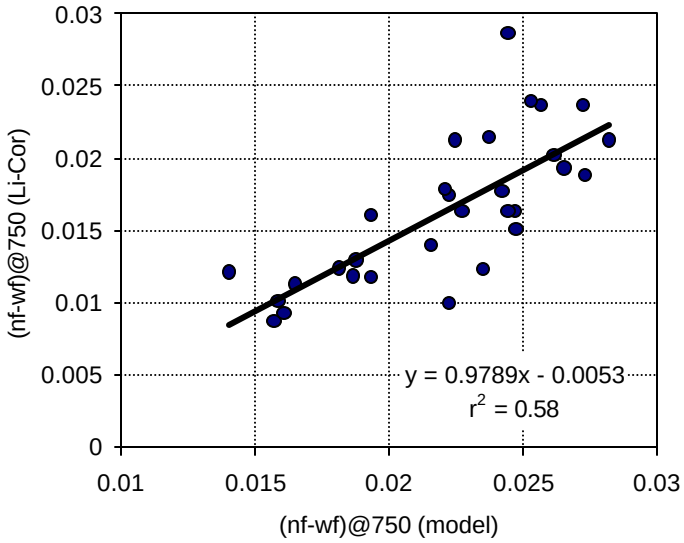

Figure 4.9. Peak at 750 nm due to fluorescence was consistent with the model. Relationship shows that r^2=0.58 was obtained in the comparison between the Rdiff@750 predicted by the model and the real Rdiff@750 calculated from reflectance spectral measurements with the Li-Cor sphere with and without the filter.

The FRT model and the experiment with leaf samples with constant chlorophyll content allow us to investigate optical indices that are able to track changes in reflectance due to chlorophyll fluorescence only, without the influence of chlorophyll content.

R_{750}/R_{800} was calculated from leaf reflectance spectra with and without filter and studied for its relationship with fluorescence measurements: we see that the index tracks changes in CF, producing higher correlations when we use the dataset with a fluorescence signal (r^2=0.62, ΔF/Fm'110; r^2=0.51, Ft110; r^2=0.75, Fv/Fm). When we use the data without fluorescence the reflectance peak at 700-750 region disappears and the relationship with CF is removed (r^2=0.22, ΔF/Fm'110; r^2=0.18, Ft110; r^2=0.23, Fv/Fm). These results are consistent with the expected relationship between the reflectance peak in the region 700-750 nm and fluorescence measurements. For constant chlorophyll content, the index is therefore directly related to chlorophyll fluorescence.

Reflectance changes in the 680-690 nm region can be studied with indices that are able to track the curvature of the reflectance spectrum, such as the curvature index $R_{683}^2/R_{675}\cdot R_{691}$ that tracks changes centered at R_{683}, therefore being affected by variations in reflectance due to CF.

Results show that good relationships are found between the curvature index and CF measurements using data from the same experiment, where chlorophyll content was fixed: r^2=0.53, ΔF/Fm'110; r^2=0.65, Ft110; r^2=0.77, Fv/Fm (Figure 4.10). Other indices also result in high correlation with chlorophyll fluorescence, such as R_{685}/R_{655} (r^2=0.56, ΔF/Fm'110; r^2=0.75, Ft110; r^2=0.85, Fv/Fm), R_{690}/R_{655} (r^2=0.58, ΔF/Fm'110; r^2=0.76, Ft110; r^2=0.86, Fv/Fm).

A comparison between R_{750}/R_{800} and $R_{683}^2/R_{675}\cdot R_{691}$ calculated from leaf reflectance spectra and simulated by the FRT model was made (Figures 4.11 and 4.12, respectively), with agreement between the predicted and measured optical index. Prediction errors are likely due both to the model itself, which needs calibration of input parameters, as well as to experimental errors in the process of leaf reflectance measurements. Reflectance measurement duration time is also a critical factor that affects the reflectance peak at 700-750 nm region, due to rapid temporal changes in chlorophyll fluorescence in dark-adapted leaf samples. Therefore small differences in the time needed for single leaf measurement affects the amplitude of the reflectance peak and the optical index.

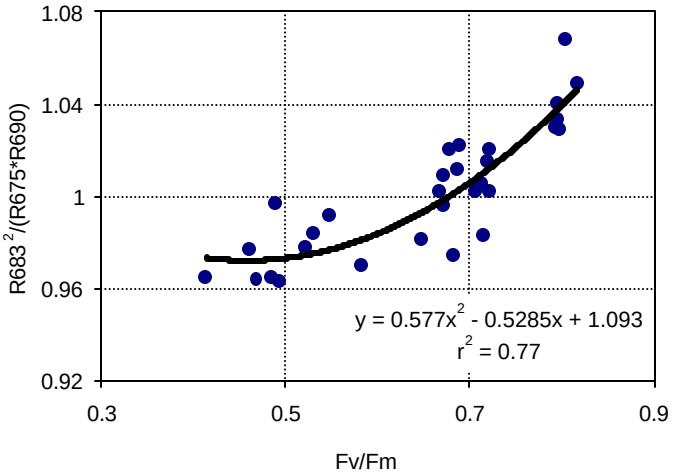

Figure 4.10. Relationship between the optical curvature index $R_{683}^2/R_{675}\cdot R_{690}$ and Fv/Fm, from the experiment with maple leaves with constant chlorophyll content and diurnal variation of chlorophyll fluorescence.

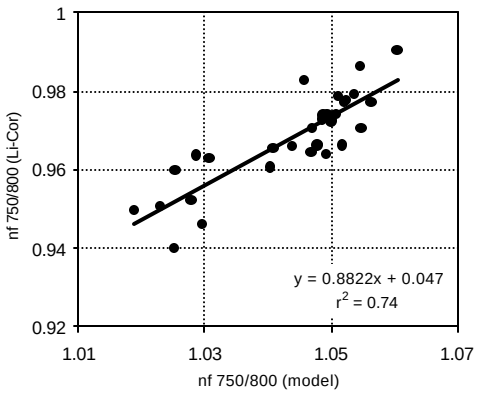

Figure 4.11. Relationship between the optical index R_{750}/R_{800} predicted by the FRT model and calculated from single leaf reflectance spectra.

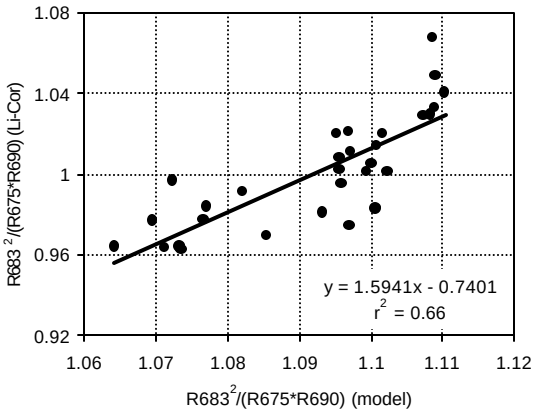

Figure 4.12. Relationship between the curvature optical index $R_{683}^2/R_{675}\cdot R_{690}$ predicted by the FRT model and calculated from single leaf reflectance spectra.

4.2.2.2.- Coupling FRT and PROSPECT models for chl_{a+b} and CF estimations

PROSPECT model has been extensively tested and its use for chl_{a+b} estimation at the leaf level is generally accepted. The results presented previously with the FRT model led us to couple PROSPECT and FRT, so that the combination of the two models would allow leaf reflectance and transmittance to be modelled from chl_{a+b} through PROSPECT and the effect of CF added through FRT. The coupled model allows the estimation of chl_{a+b} and fluorescence efficiency by inversion.

The input parameters for PROSPECT for the VIS-NIR region are the structural parameter N, chl_{a+b}, and for FRT, chl_{a+b}, scattering parameter *n*, D_L (thickness), λ_L and Δ_L (for PS-II peak), λ_H and Δ_H (for PS-I peak), *f* (ratio PS-II/PS-I peaks), and fluorescence efficiency, f. Input parameters N and chl_{a+b} in PROSPECT generate leaf reflectance and

transmittance $r_{PROSPECT}$ and $t_{PROSPECT}$, respectively. Accordingly, the input parameter used in PROSPECT (chl_{a+b}), D_L calculated from an empirical relationship with N using greenhouse sample leaves with variable chl_{a+b}, and the rest of input parameters needed in FRT for fluorescence modelling (λ_L, Δ_L, λ_H, Δ_H , f , and $\boldsymbol{f}$) allowed the calculation of the fluorescence spectra in the 400-800 nm range: Δr_{FRT} and Δt_{FRT} . The final apparent r and t is calculated as $r^* = r_{PROSPECT} + \Delta r_{FRT}$; $t^* = t_{PROSPECT} + \Delta t_{FRT}$.

An assessment of PROSPECT for estimation of leaf chl_{a+b} was performed using the greenhouse experiment that sampled 60 leaves which had variable chlorophyll content ($\bar{x}$ =35.66 µg/cm^2, s=15.87, n=60). Leaf samples were selected with variable chlorophyll content in order to study variations in the apparent leaf reflectance and transmittance due to changes of both pigment content and chlorophyll fluorescence.

The inversion was performed by iteration, varying the structural parameter N from 0.9 to 1.6 as the first step, and the root mean square error (RMSE) function ξ(N) is then minimized looking at both r and t in the NIR (780-800 nm), where structural effects are dominant in reflectance and transmittance [Equation 4.1].

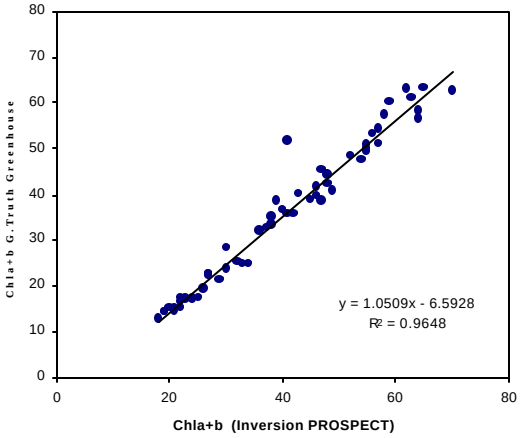

Figure 4.13. Estimation of chl_{a+b} by inversion of the PROSPECT leaf radiative transfer model.

$$RMSE = \chi(N, chl_{a+b}) = \sqrt{\frac{\sum_{l}[(r_{PROSPECT} - r_m)_l^{\,2} + (t_{PROSPECT} - t_m)_l^{\,2}]}{n}} \qquad [4.1]$$

where r_m and t_m are r and t measured from the leaf samples with the Li-Cor and fibre spectrometer. In the second step, with N estimated, chl_{a+b} was varied from 10 to 70 µg/cm^2 and the function $\chi(N, chl_{a+b})$ minimized by calculating the RMSE for the 450-700 nm range, obtaining r^2=0.96 and RMSE=0.02 (Figure 4.13).

An assessment of the coupled PROSPECT and FRT model was performed by looking at the spectral region where CF affects apparent reflectance. Other published work (Jacquemoud *et al.*, 1995; 1996) extensively assessed PROSPECT for the entire VIS and NIR spectral regions.

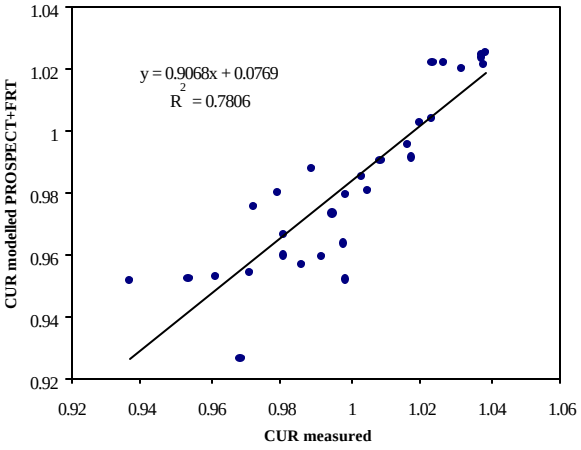

Figure 4.14. Relationship between the curvature index $(R_{675} \cdot R_{690})/R_{683}^2$ (CUR) measured from leaf samples (greenhouse experiment with chl_{a+b} constant) and modelled by PROSPECT+FRT. Fm'110 was used as input for f in PROSPECT+FRT model.

The curvature index $(R_{675} \cdot R_{690})/R_{683}^2$ found to correlate strongly with fluorescence was used for assessment, comparing the curvature index calculated by the coupled PROSPECT+FRT (Figure 4.14) in the forward direction and the curvature index measured from leaf reflectance samples from greenhouse experiments with constant and

variable chl_{a+b} contents, and variable CF. Input parameters used were chl_{a+b} measured from the single leaves; N estimated by inversion of the PROSPECT model; λ_L, Δ_L, λ_H, Δ_H for FRT, in which tests were performed, obtaining best fit for λ_L=685; Δ_L=20 and λ_H=740; Δ_H=50; f (fluorescence efficiency) in which different input values were selected, f = 0, to calculate the curvature index without fluorescence; f = Fv/Fm measured; f = Fm'110 measured; and f = ΔF/Fm'110 and ΔF/Fm'2820.

Results show that when chlorophyll content is fixed, the curvature index tracks changes in chlorophyll fluorescence, and the relationships found between measured and modelled curvature index are: r^2=0.72 (f = Fv/Fm), r^2=0.78 (f = Fm'110), r^2=0.5 (f = ΔF/Fm'@110), r^2=0.34 (f = ΔF/Fm'@2820). No relationship is found between measured and estimated curvature index (r^2=0) when curvature index is modelled using f = 0; the peak centre affects the relationship found between measured and modelled curvature index and demonstrates that λ_L=685 achieves better results than λ_L=690 (in both cases Δ_L=20) obtaining r^2=0.78 (f = Fm'110; λ_L=685) and r^2=0.68 (f = Fm'110; λ_L=690). These results demonstrate that modelled curvature index performs well, and simulation of fluorescence effect in apparent reflectance is well modelled by coupling PROSPECT and FRT. Best results are obtained by Fm'110 and Fv/Fm, and the lack of correlation when f = 0 demonstrates that the curvature index is affected by fluorescence when chl_{a+b} are constant. When both chl_{a+b} and CF are variable, results indicate that the curvature index is also affected by changes in chl_{a+b}: r^2=0.73 is found from the modelled curvature index

with f = 0; r^2=0.85 (f = Fv/Fm) and r^2=0.87 (f = Fm'110). These results indicate that a better fit is found between measured and modelled curvature index when f is considered. But it also indicates that the curvature index is affected by changes in both chl_{a+b} and CF.

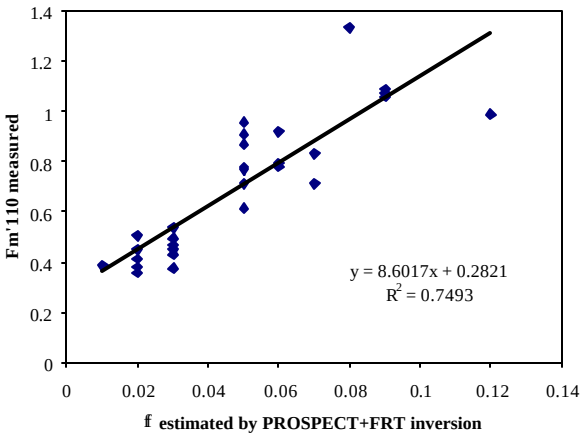

Figure 4.15. Relationship between Fm'110 measured from leaf samples (greenhouse experiment with chl_{a+b} constant) and f estimated by inversion of PROSPECT+FRT.

Inversion of coupled PROSPECT and FRT model was performed using the *r* and *t* spectra from the greenhouse experiments. The function minimized was the RMSE between the measured and modelled curvature index. Results obtained in the experiment with constant chl_{a+b} allowed the comparison between fluorescence efficiency f estimated by inversion with PAM-2000 measured fluorescence features: r^2=0.75 (Fv/Fm); r^2=0.75 (Fm'110, Figure 4.15); r^2=0.79 (Fm'2820); r^2=0.62 (Ft110); r^2=0.77 (Ft2820); r^2=0.55 (ΔF/Fm'@110); r^2=0.39 (ΔF/Fm'@2820). These results, with chl_{a+b} constant, show that inversion of the coupled PROSPECT and FRT models yields good results in the estimation of f. Results obtained in the experiment with variable chl_{a+b} were r^2=0.5 (Fv/Fm); r^2=0.74 (Fm'110); r^2=0.66 (Fm'2820); r^2=0.64 (Ft110); r^2=0.62 (Ft2820); r^2=0.62 (ΔF/Fm'@110); r^2=0.33 (ΔF/Fm'@2820). Figure 4.16 shows PROSPECT and FRT model coupling method.

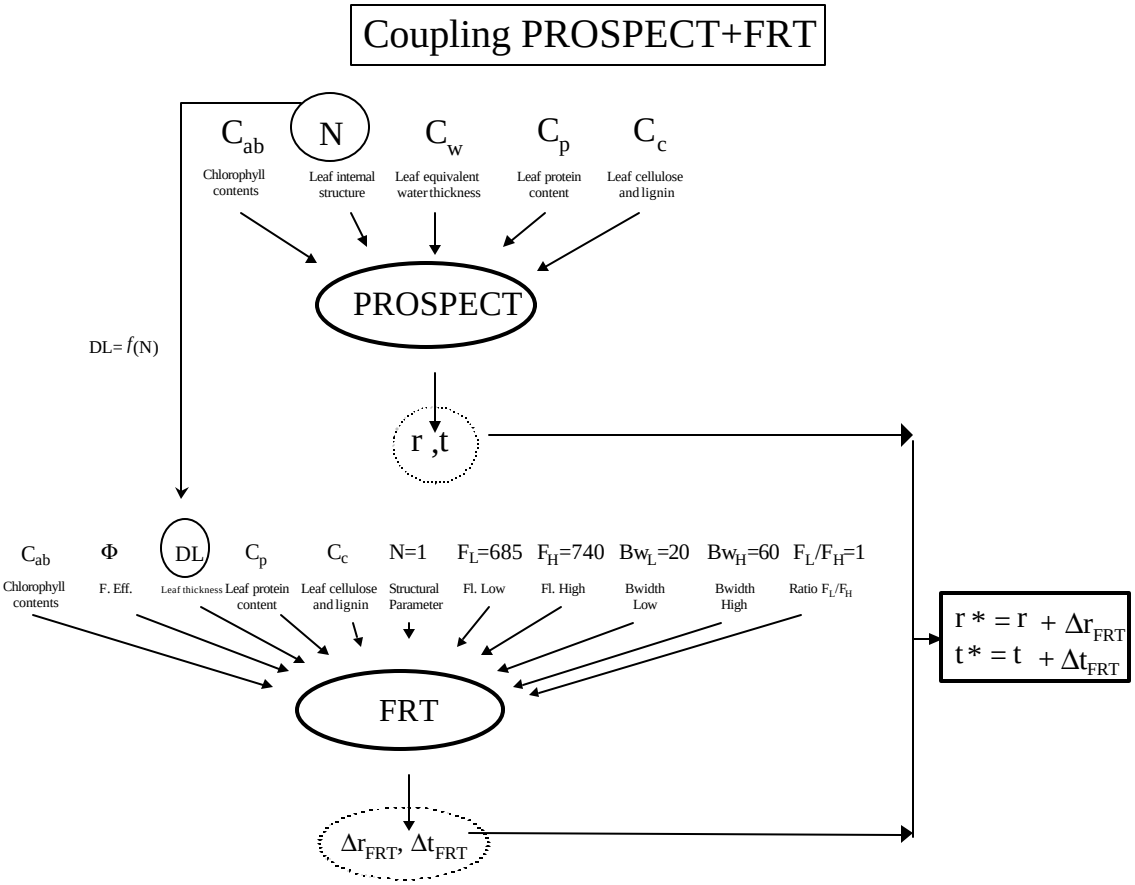

Figure 4.16. Schematic view of FRT and PROSPECT coupling methodology.

4.2.3.- Experimental Results for CF with a Simulated Canopy in Laboratory

Effects of CF on apparent spectral reflectance are quantified at the leaf level in the previous section. Next, the question of the degree to which these results are expressed at the next level (canopy) is examined.

4.2.3.1.- Canopy measurements of apparent reflectance and fluorescence

The experiment described in Section 3.2.4.2 was followed. The results in Figure 4.17 show that changes in canopy apparent reflectance from targeted plant material are observed when Schott 695nm blocking filter is used. This effect is evident at 730-750 nm, and is most pronounced at 742 nm. These findings are generally consistent with results at leaf level, indicating that canopy apparent reflectance is affected by chlorophyll fluorescence. The apparent lack of effect at 690 nm is due to the Schott RG695 cut-off filter, which does not allow a comparison of reflectance at wavelengths less than 695 nm.

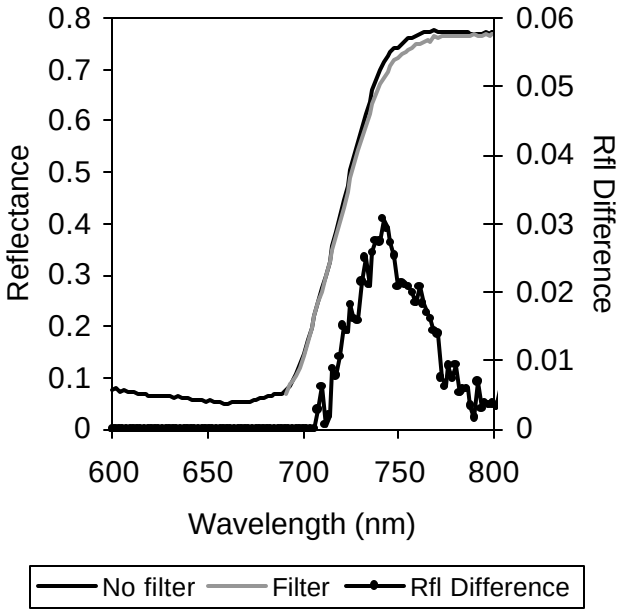

Figure 4.17. CASI canopy-reflectance measurements of *Acer saccharum* M. seedlings in laboratory. Data were collected from the plant material using the Schott RG695 filter with dark-adapted plant material and then without the filter, therefore allowing red light to reach the plant material. A reflectance change in the 730-750 nm can be detected due to the photosystem excitation by red light. The maximum reflectance difference of 3% is observed at 742 nm.

4.2.3.2.- Time-decay fluorescence in apparent canopy reflectance

The maple-seedling canopy was kept in a fixed position during 3 minutes of CASI data acquisition in the 72-channel (7.5 nm bandwidth) mode of operation. Changes in the CASI reflectance bands affected by chlorophyll fluorescence in this time-decay experiment can be seen in Figure 4.18. Changes at 680-690 nm and 730-750 nm spectral regions can be seen clearly (left plot) if we compare the reflectance measurement at the start and at the end of 3 minutes of illumination. Changes of reflectance bands affected by chlorophyll fluorescence can be seen in the right plot ($R_{751.8}$ and R_{689} nm).

The first 30 seconds of reflectance variation show a temporal decay of CASI reflectance at 751.8 nm and 689 nm (left) similar to the behaviour of the Kautsky curve measured

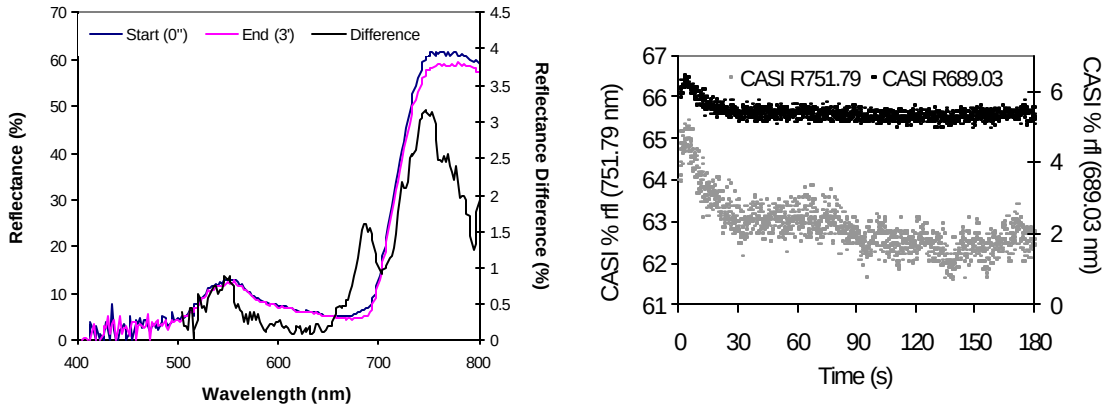

Figure 4.18. Time-decay fluorescence in apparent canopy reflectance. Left plot shows the CASI reflectance measurements from *Acer saccharum* M. seedlings in the laboratory taken after dark adaptation and after 3 minutes of illumination. Differences in reflectances at 680-690 nm and 730-750 nm are observed due to changes in chlorophyll fluorescence. Changes at 530-550 nm region can also be detected, consistent with photosynthetic radiation use efficiency changes as described by Gamon *et al.* (1997). Right plot shows the variation of CASI bands 751.8 nm and 689 nm over the same target during the 3-minute period.

(using the PAM-2000 Fluorometer) from the same leaf (Figure 4.19). No changes in reflectance were found during the 3-minute experiment in bands that are not associated with fluorescence emissions, such as at R_{553} nm.

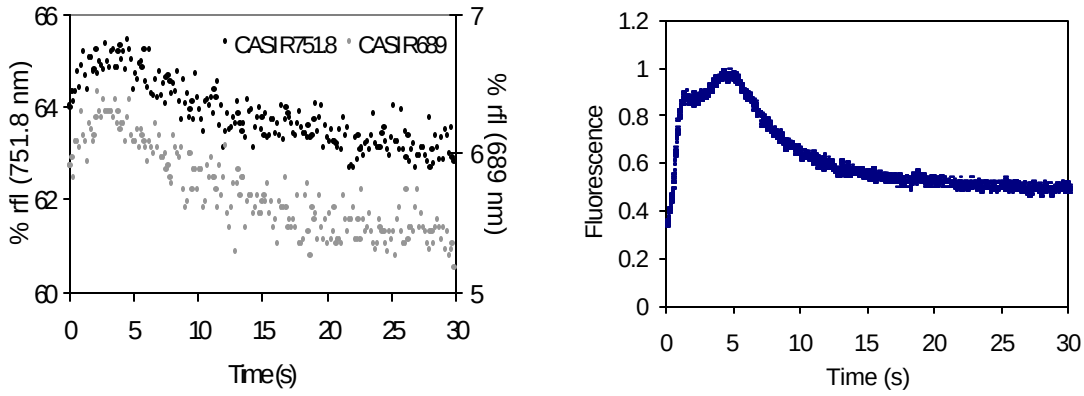

Figure 4.19. Time-decay fluorescence in apparent canopy reflectance during the first 30 seconds of the study. Left plot shows the CASI reflectance bands 751.8 nm and 689 nm from the canopy of *Acer saccharum* M. seedlings in laboratory taken after dark adaptation. Differences in the reflectance bands are associated to changes in chlorophyll fluorescence. Right plot shows the Kautsky curve from one leaf of the canopy measured with PAM-200 Fluorometer. Both CASI apparent reflectance and Kautsky curve show similar behaviour.

The different spectra obtained at leaf (Figure 4.2) and canopy levels (Figure 4.18) with the fibre spectrometer and with the CASI sensor, respectively, allowed for reflectance differences in the red edge to be fitted. A double gaussian function was used, as suggested in Subhash and Mohanan (1997) and as used in the FRT radiative transfer model for CF simulation on apparent reflectance. Parameters showing the centre maxima and bandwidth for both fluorescence emissions from *Acer saccharum* M. leaf samples are shown in Table 4.4 and Figure 4.20. These fits produce high correlation coefficients (R>0.9), generate parameters similar to those of Subhash and Mohanan (1997) and also

show bandwidths at 750 nm that are approximately 2 to 3 times larger than near 690 nm. The centre peaks show shifts from those reported earlier, but these results correspond to natural fluorescence from broadband illumination rather than from laser excitation energy in the earlier results.

Table 4.4. The reflectance difference spectra have been fit with a double gaussian curve defined above. The best fit parameters show spectral peaks and half-widths consistent with fluorescence emissions.

Double Gaussian Fit:

$$R = A1 \cdot \exp\left(\frac{-(\lambda - \lambda_1)^2}{0.36 \cdot \Delta\lambda_{1}^2}\right) + A2 \cdot \exp\left(\frac{-(\lambda - \lambda_2)^2}{0.36 \cdot \Delta\lambda_{2}^2}\right)$$

Parameters	Leaf_Refl.	Canopy_Refl.
A1	1.7	1.1
A2	2.5	2.9
$\lambda 1$	688.3 nm	682.1 nm
$\Delta\lambda 1$	29.5 nm	22.5 nm
$\lambda 2$	746.1 nm	752.2 nm
$\Delta\lambda 2$	52.9 nm	81.1 nm
R	0.94	0.93

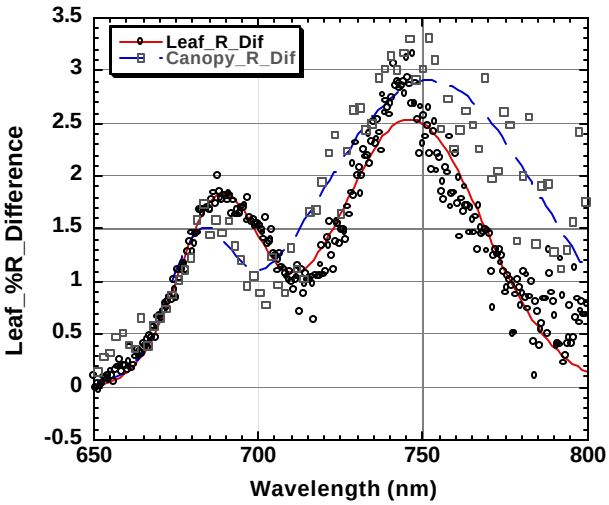

Figure 4.20. The measured difference reflectance spectra corresponding to Figures 4.2 and 4.18 have been fitted with a double-gaussian function. The fit parameters are presented in Table 4.4.

4.2.3.3.- Diurnal variation of apparent reflectance and fluorescence

Results in this diurnal study show that optical indices in the 680-690 nm region track changes in Fv/Fm; R_{680}/R_{630}, R_{685}/R_{630}, R_{687}/R_{630} and R_{690}/R_{630}, to achieve correlation coefficients r^2=0.93, r^2=0.94, r^2=0.92, and r^2=0.91, respectively. Indices sensitive to changes in the reflectance curvature in the 675-690 nm region, that were observed

previously (Zarco-Tejada *et al.*, 2000a), also show correlation with diurnal changes in Fv/Fm, i.e. $R_{685}^2/(R_{675} \cdot R_{690})$ (Figure 4.21) yields $r^2=0.95$.

The diurnal variation range of each one of the indices was also studied. Figure 4.22 shows the four indices normalized to the first image so that their ranges of variation can be compared. The plot shows that R_{685}/R_{630} varies up to 17% during the day, while the percentage variation of $(R_{685}^2)/(R_{675} \cdot R_{690})$ is 10%. All the indices tested in the 680-690 nm region vary similarly, with comparable behaviour. The behaviour of the indices is consistent with the theoretically expected variation: in the morning we get high values of Fv/Fm, therefore high values of F685-F690. R_{690}/R_{630} should therefore decrease during the day and then recover at night. A direct relationship is found between these indices and Fv/Fm, as expected.

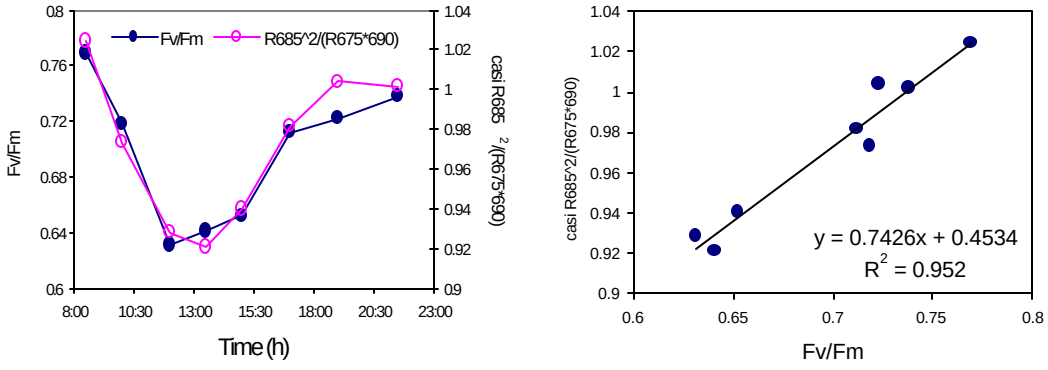

Figure 4.21. Diurnal variations of Fv/Fm and the optical index $R_{685}^2/(R_{675} \cdot R_{690})$ calculated from CASI canopy reflectance in laboratory using *Acer sacharum* M. seedlings. The behaviour of CF during the day is tracked by the optical index derived from CASI reflectance achieving $r^2=0.95$. Maple seedlings were moved inside the laboratory to make measurements of Fv/Fm and CASI reflectance, keeping the seedlings outside between measurements. Eight measurements were carried out from 8.30am to 9.30pm with plants dark-adapted for 15 minutes prior to readings of Fv/Fm.

Potential variations in these optical indices due to changes in the NIR or inconsistencies between the collected CASI images were examined relative to the behaviour of normalized Fv/Fm (Figure 4.23). It is shown that variations in the R680-R690 nm region (R_{690}/R_{630}) are independent of changes in the NIR (R_{850}) and R_{650}/R_{500}, where no response to chlorophyll fluorescence is expected.

A study of the optical index R_{690}/R_{630} using the FRT model shows that R_{690}/R_{630} behaves as expected by theory. Figure 4.24 shows the predicted R_{690}/R_{630} by the FRT model and the index calculated from CASI data, yielding high correlation (r^2=0.93) in the relationship between the predicted and calculated index. No relationship was found between fluorescence and the CASI optical index R_{750}/R_{710}, also in agreement with simulation based on the leaf FRT model that will be discussed in next section.

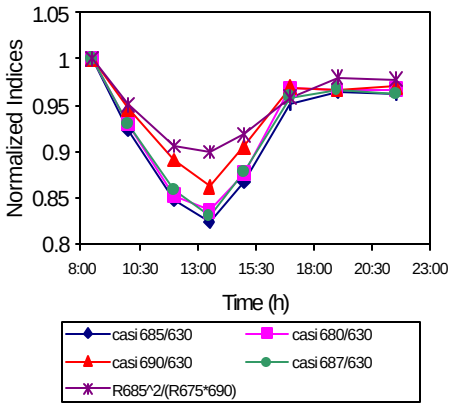

Figure 4.22. Comparison of R_{685}/R_{630}, R_{690}/R_{630}, R_{680}/R_{630}, R_{687}/R_{630} and $R_{685}^2/(R_{675}\cdot R_{690})$ normalized to the first measurement for comparison purposes. R_{685}/R_{630} varies up to 17% during the day, while the percentage variation of $R_{685}^2/(R_{675}\cdot R_{690})$ is 10%. All indices show similar behaviour as expected, for changes in the 680-690 nm region due to fluorescence.

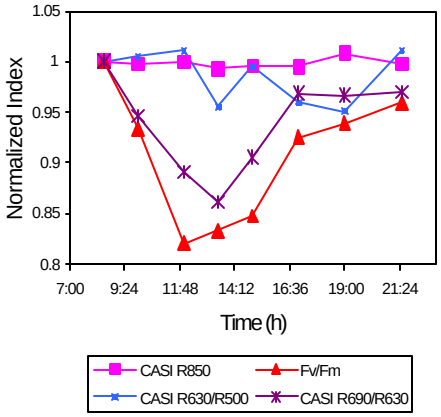

Figure 4.23. Variations in R680-R690 nm region (R_{690}/R_{630}) are independent of changes in the NIR (R_{850}) and R_{650}/R_{500}, where no response to chlorophyll fluorescence is expected. Variations in these optical indices are not due to changes in the NIR or inconsistencies between the collected CASI images. The diurnal behaviour of R_{690}/R_{630} is similar to Fv/Fm.

4.2.3.4.- Reflectance measurements of steady-state fluorescence in healthy and stressed plant material

CASI reflectance measurements over healthy and stressed plant material were collected in laboratory (Figure 4.25), where PAM-2000 measurements derived ΔF/Fm', Ft and Fm' to which optical indices can be compared. Direct relationship between steady-state fluorescence and dark-adapted Fv/Fm should be found, as reported previously, where diurnal variations of Fv/Fm were directly related to ΔF/Fm', Ft and Fm'. Optical indices $R_{683}^2/(R_{675} \cdot R_{691})$ and R_{685}/R_{655}, sensitive to changes in chlorophyll fluorescence, were studied at this intermediate level at the laboratory between leaf and field canopy.

Results show that the two trays with maple seedlings with different stress status show differences in ΔF/Fm', Fm' and Ft steady-state features. The indices behave consistently with the model and with previous experiments: indices calculated from the 680-690 nm region, such as R_{685}/R_{655} and $R_{683}^2/R_{675} \cdot R_{691}$ show consistent behaviour with the other two experiments carried out. Indices show lower values in the stressed than in the healthy plant material. This is also consistent with results predicted by the FRT model (Table 4.5).

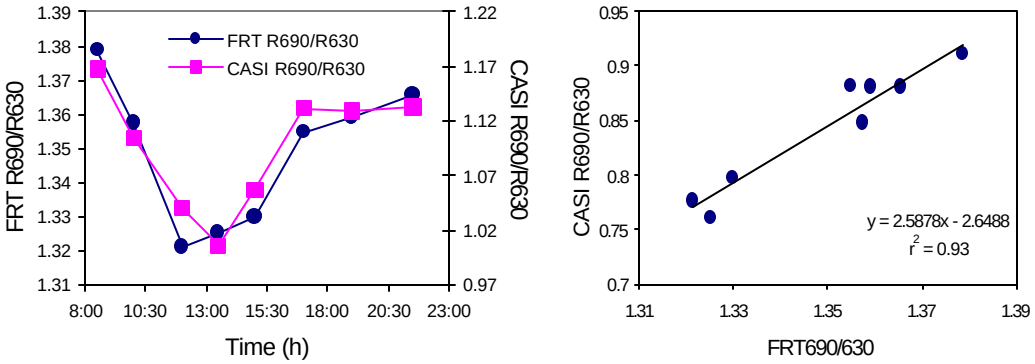

Figure 4.24. Study of the optical index R_{690}/R_{630} modelled by the FRT model (companion paper) and calculated from CASI canopy reflectance. Plot shows that predicted R_{690}/R_{630} by the FRT model and the index calculated from CASI data behave consistently. The linear relationship between the predicted and calculated index is shown, achieving r^2=0.93.

Table 4.5 shows four different stress situations, two of them at the extremes: stressed (low photochemical efficiency Fv/Fm, low chl_{a+b}), healthy (high photosynthetic efficiency Fv/Fm, high chl_{a+b}). The other two are intermediate stress. This simulation helps us to understand the experimental results obtained and demonstrate that they are consistent with theory. When the plant is stressed (photochemical efficiency, Fv/Fm=0.5, chl_{a+b}=15) we expect lower R_{685}/R_{655} values than when the plant is healthy (Fv/Fm=0.8, chl_{a+b}=50). This is confirmed in the experimental results. R_{750}/R_{710} is shown in the FRT simulation as insensitive to changes in photochemical efficiency. Model simulation of R_{750}/R_{710} predicts a change from 1.6 (chl_{a+b}=15, Fv/Fm=0.5, Fv/Fm=0.8) to 1.9 (chl_{a+b}=50, Fv/Fm=0.5, Fv/Fm=0.8). That is, R_{750}/R_{710} is affected by changes in chl_{a+b}, not by changes in CF. This is also consistent with previous experiments which show that R_{750}/R_{710} is not tracking changes in fluorescence. Results in this experiment show that

R_{750}/R_{710} is able to differentiate between the two stress conditions, due to their different values of chl_{a+b} (SPAD=20 → ~15 chl_{a+b} µg/cm^2; SPAD=35 → ~35 chl_{a+b} µg/cm^2). Accordingly to the FRT model simulation, the CASI R_{750}/R_{710} from the stressed plants shows lower values than the healthy plants, with the effect due to changes in chl_{a+b}, not to changes in CF.

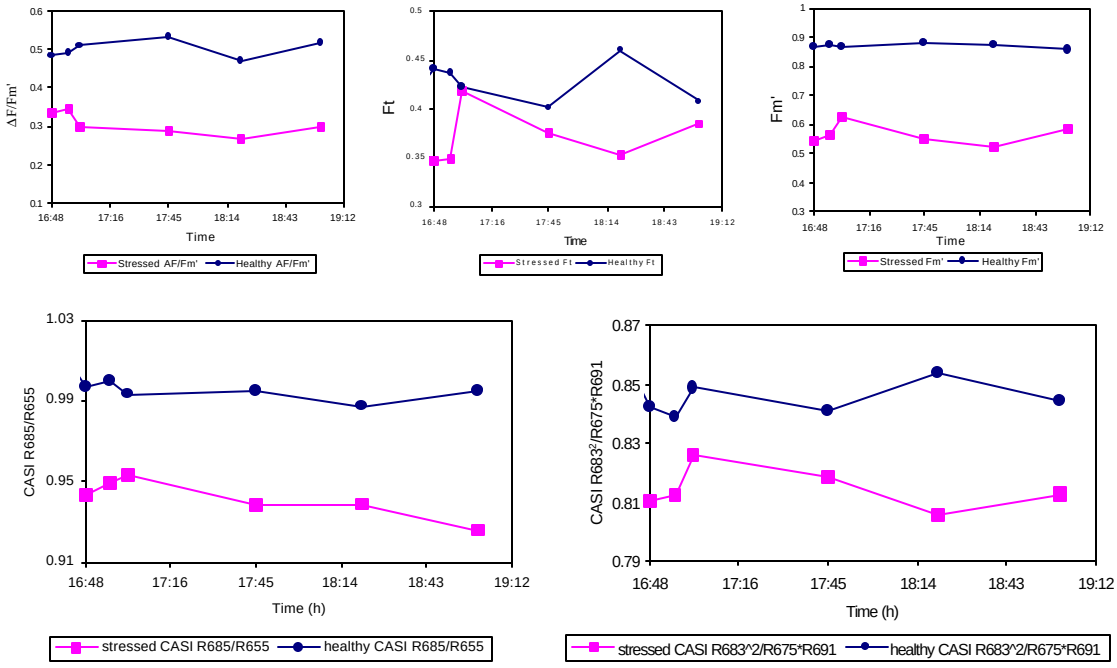

Figure 4.25. CASI canopy reflectance measurement over healthy and stressed seedlings of *Acer saccharum* M. in laboratory, where PAM-2000 fluorescence measures ΔF/Fm', Ft and Fm' (top) and reflectance optical indices (below) are compared. The two trays with maple seedlings with different stress status show differences in ΔF/Fm', Fm' and Ft steady-state features. The indices behave consistently with the model and with previous experiments: indices calculated in the 680-690 nm region, R_{685}/R_{655} (bottom-left) and $R_{683}^2/R_{675}\cdot R_{691}$ (bottom-right) show consistency with the other two experiments in this paper. The two indices show lower values in the stressed than in the healthy plant material.

Table 4.5. FRT model simulation of R_{750}/R_{710} and R_{685}/R_{655} for four different chlorophyll and fluorescence values, with two considered the stress extremes: (i) stressed (low photochemical efficiency Fv/Fm, low chl_{a+b}); (ii) healthy (high photochemical efficiency Fv/Fm, high chl_{a+b}). In stressed conditions (photochemical efficiency=0.5, chl_{a+b}=15) results show lower R_{685}/R_{655} values than when the plant is healthy (photochemical efficiency Fv/Fm=0.8, chl_{a+b}=50). In the FRT simulation R_{750}/R_{710} is not sensitive to changes in photochemical efficiency: when efficiency changes, R_{750}/R_{710} varies from 1.6 (chl_{a+b}=15, Fv/Fm=0.5, Fv/Fm=0.08) to 1.9 (chl_{a+b}=50, Fv/Fm=0.5, Fv/Fm=0.8). This shows that R_{685}/R_{655} is affected by both changes in chl_{a+b} and CF, and it is sensitive to variations in CF when chl_{a+b} is constant.

FRT Simulation	Efficiency Fv/Fm	chl_{a+b}	R_{750}/R_{710}	R_{685}/R_{655}
Stressed	0.5	15	1.64	1.19
–	0.8	15	1.63	1.24
	0.5	50	1.91	1.24
Healthy	0.8	50	1.90	1.35

4.2.4.- Diurnal Above-Canopy Data Collection Experimental Results Under Natural Illumination Conditions

Consistent results were found in the diurnal experiments over a canopy of *Acer saccharum* M. seedlings (Figure 4.26, upper plot), and from one of the healthy forest sites (Figure 4.26, lower plot) where reflectance and CF measurements were collected at different times to investigate the effects of CF in canopy apparent reflectance. Effects of CF on apparent reflectance were found in canopy reflectance measurements with a fibre spectrometer, where results of the diurnal experiments over a canopy of *Acer saccharum* M. seedlings (Figure 4.26, upper plot) showed that reflectance difference between 8.20h and 13.30h was higher than reflectance difference between 8.20h and 9.00am. The maximum in the 690-700nm region due to the effects of CF is higher in the early morning than in mid-day, when light saturation reduces the CF, and therefore its effects on the apparent reflectance. Dark-adapted CF measurements from the maple

seedlings showed a variation in Fv/Fm and Ft during the day, decreasing in the afternoon: Fv/Fm=0.574, Ft=0.495 at 9:09h; Fv/Fm=0.524, Ft=0.418 at 11:22h; and Fv/Fm=0.516, Ft=0.396 at 13:23h. These results demonstrate consistency with artificial light and laboratory experiments, showing that CF changes can be tracked under natural illumination conditions using a fibre spectrometer over small canopies.

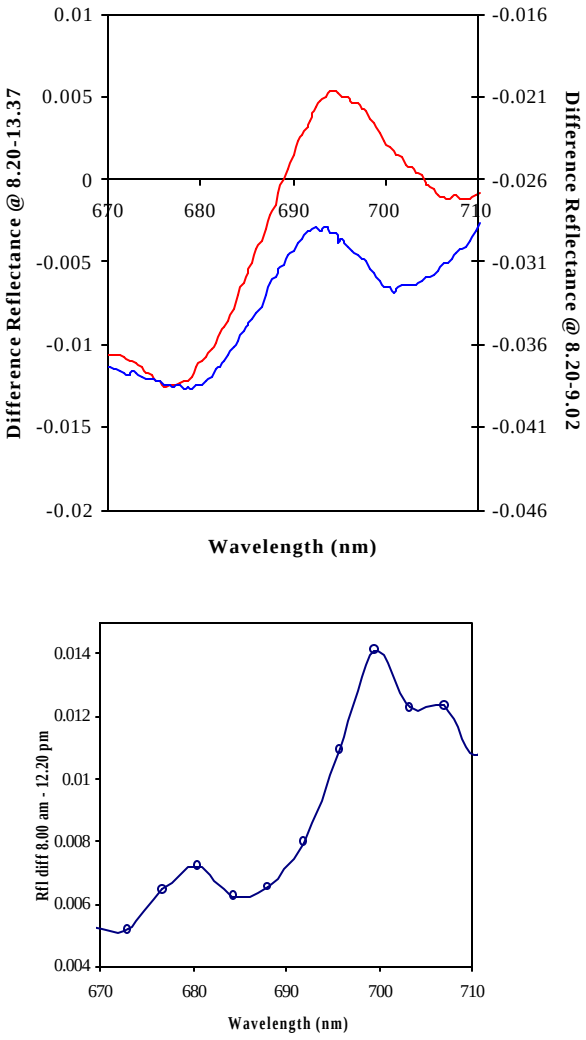

Figure 4.26. Reflectance difference obtained in the diurnal experiments over a canopy of *Acer Saccharum* M. seedlings (upper plot, $r_{8.20}$-$r_{13.30}$) using a fibre spectrometer, and from one of the healthy forest sites (lower plot, $r_{8.00}$-$r_{12.20}$) collected with CASI sensor.

Subsequent experiments with the airborne CASI hyperspectral sensor over forest sites in diurnal acquisitions in 1999 and 2000 revealed promising but less convincing results (Zarco-Tejada, *et al.*, in press). Analysis results from one of the healthy forest sites are shown in Figure 4.26 (lower plot) where reflectance in the 72-channel CASI mode and CF measurements were collected at different times of the day. Reflectance difference between CASI measurements at 8.00h and 12.20h shows a maximum at 700nm,

consistent with higher value of reflectance at 700nm due to the higher CF effects in the early morning before photosystem saturation. Ground truth CF measurements showed a decrease in the non-dark-adapted Ft: Ft=0.74 at 8.00h, Ft=0.72 at 9.30h, Ft=0.46 at 12.30h, and dark-adapted Fv/Fm: Fv/Fm=0.83 at 8.00h, Fv/Fm=0.82 at 9.30h, Fv/Fm=0.79 at 12.30h. Results from the experiments in June 2000 using higher spatial resolution of 0.56x1.08m and a CASI bandset of 9 bands centered in the 695 nm spectral region did not show clear and definitive results. The effect of the atmosphere with the water vapour and O_2 bands in the 690-700 nm region was an issue investigated for both cases in which different sensors and data correction was carried out. For the measurements with the fibre spectrometer, a Spectalon panel measurement collected every time facilitated the elimination of atmospheric features in the reflectance data. For the CASI data collected at different times, a post-processing refinement after atmospheric correction was performed in order to remove residual correction errors in the 670-710 nm region by selecting road spectra from the images. Correction factors were applied to the data using a *flat field* approach, removing residual atmospheric effects in the difference spectra.

4.3.- AIRBORNE FIELD-CANOPY STUDY RESULTS

In this section the results are shown that were obtained with CASI reflectance data from the study sites for the estimation of chl_{a+b} and CF by the scaling-up and model inversion approaches, as described in Sections 2.4.1 and 2.4.2, respectively. The first section deals with the selection of input canopy simulation parameters needed for the SAILH and *Kuusk* CR models, in order to show the effect of structural parameters in optical indices calculated for the scaling-up and the numerical inversion methods for pigment estimation.

4.3.1.- Model Parameter Sensitivity Study using SAILH CR model

The methodologies studied here for chl_{a+b} estimation using CR models require input parameters for the canopy structure and viewing geometry at the time of data collection. They have an effect, which magnitude depends upon the method used for estimation: using either optical indices or single reflectance channels in the merit function adopted for minimization. In this section the effect of such structural and viewing geometry parameters on the optical indices that may be used for prediction is examined.

For monitoring of bioindicators by remote sensing, changes are expected in the solar zenith angle θ_s during data acquisition in diurnal and seasonal cycles. LAI variations occur with changes in the canopy conditions, in addition to changes in LADF between species. A modelling study was carried out in order to determine the influence of changes in these CR parameters on the calculated optical indices and therefore in the final bioindicator prediction. Input parameters for the SAILH model were changed to study

their sensitivity on the indices derived from the simulated canopy spectra. LAI was stepped from LAI=1 to LAI=8; LADF was changed to simulate 4 different canopy types: planophile (q=0º, e=0.985), erectophile (q=90º, e=0.985), plagiophile (q=45º, e=0.95), and spherical (e=0). Solar zenith angle q_s was stepped from q_s=20º to q_s=60º. Two single leaf measurements of reflectance and transmittance, collected as part of the experiment, were used for the modelling study. The two leaves used in the study were chosen from the two study sites that showed highest and lowest Fv/Fm and chl_{a+b} values in the field: Fv/Fm=0.69 and chl_{a+b}=17.31 µg/cm^2 for the high stressed leaf, and Fv/Fm=0.83 and chl_{a+b}=32.2 µg/cm^2 for the low stressed or healthy leaf. The modelling study consisted of the

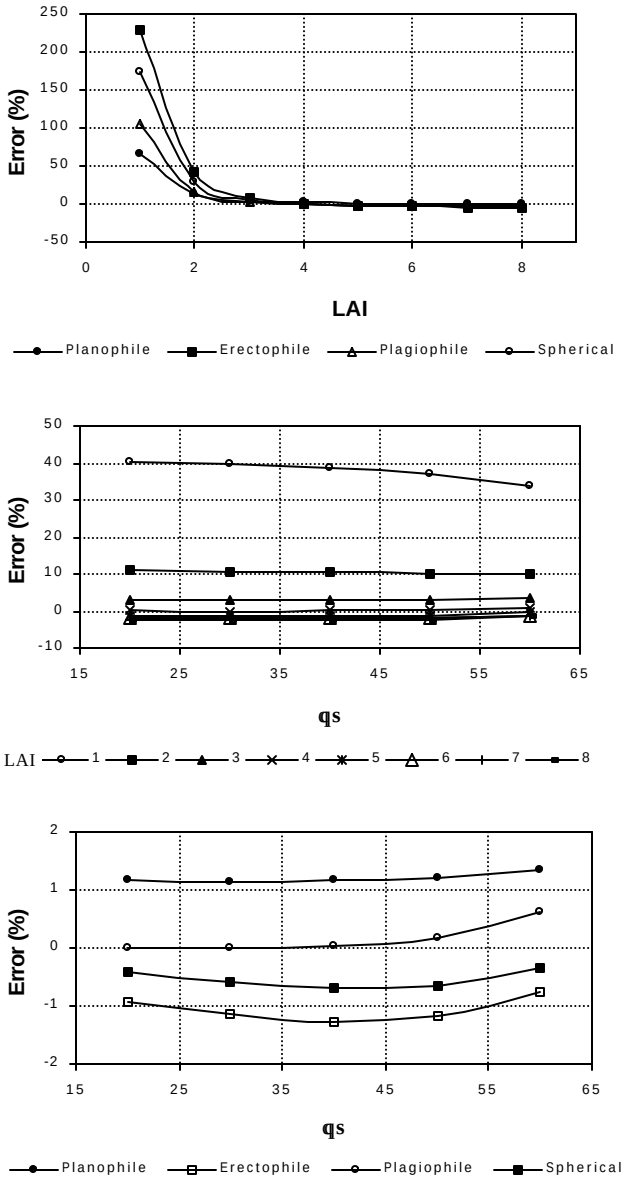

Figure 4.27. Model parameter sensitivity study shows that low LAI affects bioindicator estimation regardless the type of canopy (top plot, Gitelson & Merzylak index (R_{750}/R_{700}), $qs = 30°$) and qs angle (middle plot, Vogelmann index (R_{740}/R_{720}), plagiophile canopy). When $qs = 30°$ and LAI > 3 the canopy type is irrelevant (top plot). qs has no effect in the bioindicator estimation as can be seen in the middle plot (LAI ranging from 1 to 8) and bottom plot (DP21 index ($D_{\lambda o}/D_{703}$), LAI = 4) for any type of canopy. The % Error is the relative error to nominal SAILH CR parameters (plagiophile canopy, LAI = 4, $qs = 30°$) for *Acer saccharum* M.

comparison of the predicted bioindicator from optical indices through the SAILH CR model with nominal CR parameters relative to the prediction when other CR parameters are used.

Representative optical indices were selected from the 4 categories used in the modelling study: PRI $(R_{531}-R_{570})/(R_{531}+R_{570})$ and Lichtenthaler (R_{440}/R_{690}) from the Visible Ratios optical indices; Gitelson & Merzylak (R_{750}/R_{550}) and NDVI $(R_{774}-R_{677})/(R_{774}+R_{677})$ from the Visible/NIR ratios; Carter (R_{695}/R_{760}), Vogelmann (R_{740}/R_{720}), Vogelmann $(R_{734}-R_{747})/(R_{715}+R_{726})$ and Gitelson & Merzylak (R_{750}/R_{700}) from the Red Edge Reflectance-Ratio Indices; and DP21 $(D_{\lambda o}/D_{703})$, λ_p and Vogelmann (D_{715}/D_{705}) from the Spectral and Derivative Red Edge Indices. At low LAI (<2) the errors in the predicted bioindicator become large regardless of the type of canopy considered. Figure 4.27 (top) shows this result using the R_{750}/R_{700} optical index (Gitelson and Merzylak, 1997) for θ_s=30° as a function of canopy type and LAI. For values of LAI higher than 3 the differences between the predicted bioindicator using nominal canopy parameters and the prediction with varying θ_s and LADF canopy parameters is insignificant. Moreover, when the LAI is higher than 3 and the θ_s is a nominal 30° the type of canopy is irrelevant for the bioindicator prediction (Figure 4.27, top).

For a given plagiophile canopy type (Figure 4.27, middle) errors of less than 5% are found in the predicted bioindicator when LAI is higher than 3 and the optical indices used are the Red Edge Reflectance-Ratio Indices and Spectral and Derivative Red Edge

Indices (R_{740}/R_{720} optical index, Vogelmann *et al.*, 1993 is shown in the figure). These results indicate that bioindicator prediction in closed canopies with LAI>3 are not affected by LAI variability. This further suggests that LAI variations between the 12 *Acer saccharum* M. study sites (2.85 to 5.17) in a plagiophile canopy have an insignificant effect on the optical indices and on the bioindicator prediction; less than 5% differences are expected relative to predictions made with a nominal LAI=4.

Results also demonstrate the small effect of the solar zenith angle θ_s especially in red edge spectral and derivative indices (Figure 4.27, middle and bottom). It shows the insignificant variation of the predicted bioindicator when θ_s changes from 20° to 60° where the optical indices used are Vogelmann (R_{740}/R_{720}) and DP21 ($D_{\lambda o}/D_{703}$), respectively. Therefore changes in θ_s from 29° to 41° in the 12 CASI images obtained from the study sites are not expected to affect the bioindicator prediction when θ_s=30° was chosen as nominal input parameter in the CR model when scaling from leaf-level to canopy-level. This study shows that derivative indices are less sensitive to low LAI values than other optical indices. Vogelmann (D_{715}/D_{705}), λ_p and DP21 ($D_{\lambda o}/D_{703}$) predict the bioindicator with only 15-20% error when LAI=1 relative to the prediction with nominal LAI=4. Non-derivative optical indices show higher errors: for example, Gitelson & Merzylak (R_{750}/R_{550}) 140%, Carter (R_{695}/R_{760}) 150%, Vogelmann (R_{740}/R_{720}) 65%, Gitelson & Merzylak (R_{750}/R_{700}) 200% for LAI=1. This demonstrates that red edge and derivative indices are more suitable for bioindicator prediction and mapping with high

spatial resolution hyperspectral remote sensing, where the effects of shadows and canopy openings can be selectively discriminated against in data analysis.

The effect of the hotspot was also considered in order to determine if hotspot effects in canopy reflectance would affect the measured reflectance by the CASI sensor under the viewing geometry used for the data acquisition. The SAILH model canopy reflectance was compared to the SAILH model with no hotspot implementation, calculating the % change in the VIS and NIR reflectance as a function of the hotspot (0.007 to 0.1), viewing angle (-20° to 20°) and solar zenith angle (25° to 45°). A critical parameter of the hotspot function by Kuusk (1985) is defined as the leaf element length divided by the canopy height, with a value of 0.007 (7 cm over 10 m) applicable to maple canopies in this study. Results showed that, for data CASI collection in this research, the % variation in reflectance due to the hotspot is less than 3% in the visible and less than 2% in the NIR, even for low solar zenith angle. For normal data CASI collection, with 35-40° solar zenith angle, hotspot=0.007 and viewing angle ±17°, the percentage variation in the retrieved reflectance due to the hotspot is less than 2% in both VIS and NIR regions.

4.3.2.- Application of scaled-up optical indices to CASI hyperspectral data

The leaf-level relationships calculated from single leaf reflectance and transmittance data collected from the ground-truth deployments in June and July 1998 and 1999, and scaled-up to above-canopy level through infinite reflectance models, and SAILH and *Kuusk* canopy reflectance models were applied to CASI hyperspectral data for chl_{a+b} and Fv/Fm

estimation. For the application of the SAILH and *Kuusk* canopy reflectance models nominal input parameters derived from the study areas were: LAI=3.5, plagiophile leaf angle distribution function (LADF), soil reflectance data derived from CASI imagery and model-estimated skylight irradiance fraction based on conditions during airborne acquisitions. Additional parameters needed in the *Kuusk* model were n=1.4, s/l=0.007 & θ^*=40°, and ε=0.95 & θ_m=45° for the LADF for the assumed plagiophile LADF. Tables 4.6 and 4.7 show the correlation coefficients and RMSE obtained in chlorophyll a&*b* and Fv/Fm estimations applying relationships from r, $R_{\infty 1}$, $R_{\infty 2}$, and $R_{\infty 3}$ optically-thick leaf simulation models and SAILH and *Kuusk* CR models to *CASI* data collected over the *Acer saccharum* M. study sites in 1998 (n=12) and 1999 (n=12). The best estimations through optical indices are organized by the best relationships that were obtained at leaf level between indices and chl_{a+b} in 1999 to allow for comparison between leaf-level relationships and CASI-canopy-level estimations. These results show consistency between CASI-level and leaf-level relationships obtained between optical indices and chl_{a+b} concentration. The best indices for chl_{a+b} estimation that were found at leaf level are the ones achieving better estimations when applied to CASI canopy reflectance. It is also demonstrated that a cross-seasonal consistency exists in the performance of the best indices for 1998 and 1999, showing that the good estimation performed by the best indices is maintained from 1998 to 1999.

Red-edge indices, specially λ_p and DP21, and spectral and derivative indices, such as R_{750}/R_{710}, Vog1 (R_{740}/R_{720}), G_M2 (R_{750}/R_{700}), Vog3 (R_{734}-R_{747})/(R_{715}+R_{720}), Vog2 (R_{734}-

R_{747})/(R_{715}+R_{726}), Vog4 (D_{715}/D_{705}), G_M1 (R_{750}/R_{550}), Ctr2 (R_{695}/R_{760}) are the best optical indices for chl_{a+b} estimation at canopy level. Other optical indices show significance when used as estimators of chl_{a+b}, but inconsistency within deployments, such as Lic4 (area under 450-680 region) (r=0.26, 1998; r=0.7, 1999), PRI2 (R_{550}-R_{531}) / (R_{550}+R_{531}) (r=0.57, 1998; r=0.37, 1999), and R_o (r=-0.005, 1998; r=0.58, 1999). Traditional and well accepted optical indices for pigment estimation and indicators of vegetation status, such as NDVI and SR, performed poorly in the two consecutive years: r=0.1, 1998; r=0.24, 1999 (NDVI), and r=0.05, 1998; r=0.22, 1999 (SR). These traditional indices, calculated as ratios of NIR/VIS, are primarily tracking canopy structural changes but are not able to track subtle changes due to pigment content variation between study sites. Therefore, canopies with homogeneous structure but different chlorophyll content need the use of red edge and spectral indices to estimate changes in pigment content.

For CF estimation at canopy level, a similar methodology to that for chl_{a+b} estimation was followed, applying leaf-level relationships derived between optical indices and Fv/Fm to CASI hyperspectral data. Table 4.7 shows that the indices obtaining best results were the red edge and derivative, and PRI3 (R_{570}-R_{539}) / (R_{570}+R_{539}), Lic2 (R_{440}/R_{690}) and Lic3 (R_{440}/R_{740}). In all cases except for Lic2 and Lic3, correlation coefficients decreased from 1998 to 1999 campaigns, consistent with leaf-level results showing similar pattern, and in large measure likely due to the decreased range of variation in 1999.

Table 4.6. Determination coefficients and RMSE (µg/cm^2) obtained in chlorophyll a&*b* estimations applying relationships from $R_{\infty 1}$, $R_{\infty 2}$, and $R_{\infty 3}$ optically-thick leaf simulation models and SAILH and *Kuusk* CR models to *CASI* data collected over *Acer saccharum* M. study sites in 1998 (*n*=12) and 1999 (*n*=12). Indices organized by the best relationships that were obtained at leaf level between indices and chl_{a+b} (1999) to allow for comparison between leaf-level relationships and CASI-canopy-level estimations. Colour codes: visible ratios (green), VIS/NIR ratios (yellow), red-edge indices (red), and spectral and derivative indices (blue). Light blue shows relationships with r>0.6, and grey shows RMSE<10.

	Correlation Coefficient		**RMSE (µg/cm^2) 1998**						**RMSE (µg/cm^2) 1999**					
	r 1998	**r 1999**	***r***	**$R_{\infty 1}$**	**$R_{\infty 2}$**	**$R_{\infty 3}$**	**R_{SAIL}**	**R_{Kuusk}**	***r***	**$R_{\infty 1}$**	**$R_{\infty 2}$**	**$R_{\infty 3}$**	**R_{SAIL}**	**R_{Kuusk}**
750/710	0.69	0.75	21.67	9.95	5.38	8.11	10.78	12.09	24.68	8.53	4.25	8.27	11.39	10.41
Vog1	0.75	0.68	27.36	14.2	7.94	5.76	8.03	9.75	37.49	17.24	4.35	5.32	7.66	9.26
G_M2	0.61	0.75	22.84	10.86	6.44	8.03	11.91	12.32	18.08	4.85	5.62	9.91	13.82	11.46
Vog3	0.74	0.75	34.62	15.5	5.29	7.95	8.83	10.48	41.72	14.72	4.75	7.84	9.99	7.56
lpr	0.73	0.72	10.18	5.75	7.46	21.12	25.73	31.71	11.17	4.78	6.1	14.23	4.9	5.43
Vog2	0.75	0.75	34.82	16.07	5.37	7.83	8.57	10.29	39.98	14.2	4.93	8.02	10.33	7.52
Vog4	0.6	0.81	8.57	5.36	5.74	9.81	13.47	15.78	14.92	6.79	3.85	3.39	7.96	10.19
G_M1	0.54	0.71	-	-	-	-	-	-	54.56	28.81	13.14	4.16	6.46	6.12
Ctr2	0.62	0.72	17.97	11.51	7.52	8.9	15.01	14.38	16.3	6.65	5.65	13.11	22.74	16.55
DP21	0.76	0.69	32.19	12.74	7.48	4.92	7.02	8.55	46.92	18.84	4.76	3.95	5.61	6.25
Ctr1	0.4	0.54	-	-	-	-	-	-	-	-	-	-	-	-
DP22	0.65	0.4	8.23	13.45	9.98	8.13	11.24	6.59	-	-	-	-	-	-
Lic4	0.26	0.7	-	-	-	-	-	-	27.24	27.07	27.06	6.83	10.61	11.03
G	0.51	0.66	-	-	-	-	-	-	5.58	4.99	4.97	15.67	4.81	4.86
Cur	-0.65	-0.67	31.52	31.23	31.22	46.22	31.56	36.86	40.37	39.91	39.9	57.22	39.81	47.13
DPR1	0.26	0.11	-	-	-	-	-	-	-	-	-	-	-	-
Lic2	0.52	0.45	-	-	-	-	-	-	-	-	-	-	-	-
SIPI	0.09	0.34	-	-	-	-	-	-	-	-	-	-	-	-
PRI1	0.45	0.21	-	-	-	-	-	-	-	-	-	-	-	-
DPR2	0.39	-0.22	-	-	-	-	-	-	-	-	-	-	-	-
PRI2	0.57	0.37	-	-	-	-	-	-	-	-	-	-	-	-
PRI3	0.19	0.006	-	-	-	-	-	-	-	-	-	-	-	-
ADR	0.1	0.42	-	-	-	-	-	-	-	-	-	-	-	-
NDVI	0.1	0.24	-	-	-	-	-	-	-	-	-	-	-	-
SR	0.05	0.22	-	-	-	-	-	-	-	-	-	-	-	-
Lic1	0.12	0.27	-	-	-	-	-	-	-	-	-	-	-	-
Rs	0.12	0.42	-	-	-	-	-	-	-	-	-	-	-	-
R0	-0.005	0.58	-	-	-	-	-	-	-	-	-	-	-	-
NPCI	-0.39	-0.085	-	-	-	-	-	-	-	-	-	-	-	-
SRPI	-0.4	-0.07	-	-	-	-	-	-	-	-	-	-	-	-
Lic3	0.18	0.09	-	-	-	-	-	-	-	-	-	-	-	-
NPQI	-0.04	0.063	-	-	-	-	-	-	-	-	-	-	-	-

*See Table 4.1 for the definition of the indices in this Table.

Table 4.7. Determination coefficients and RMSE obtained in CF (Fv/Fm) estimations applying relationships from $R_{\infty 1}$, $R_{\infty 2}$, and $R_{\infty 3}$ optically-thick leaf simulation models and SAILH and *Kuusk* CR models to *CASI* data collected over *Acer saccharum* M. study sites in 1998 (n=12) and 1999 (n=12). Indices organized by the best relationships that were obtained at leaf level between indices and Fv/Fm (1998) to allow for comparison between leaf-level relationships and CASI-canopy-level estimations. Colour codes: visible ratios (green), VIS/NIR ratios (yellow), red-edge indices (red), and spectral and derivative indices (blue).

	Correlation Coefficient		**RMSE 1998**						**RMSE 1999**					
	r 1998	**r 1999**	***r***	**$R_{¥1}$**	**$R_{¥2}$**	**$R_{¥3}$**	**R_{SAIL}**	**R_{Kuusk}**	***r***	**$R_{¥1}$**	**$R_{¥2}$**	**$R_{¥3}$**	**R_{SAIL}**	**R_{Kuusk}**
Cur	-0.34	-0.26	0.081	0.079	0.079	0.104	0.078	0.087	0.084	0.083	0.083	0.091	0.079	0.091
DP22	-0.37	-0.12	0.024	0.038	0.025	0.025	0.033	0.021	0.013	0.015	0.012	0.015	0.015	0.015
DPR1	0.54	0.48	0.086	0.073	0.11	0.054	0.053	0.044	0.098	0.017	0.01	0.038	0.069	0.027
PRI3	0.6	0.36	0.051	0.051	0.051	0.046	0.05	0.045	0.009	0.009	0.009	0.01	0.009	0.01
DPR2	0.53	0.39	0.027	0.041	0.045	0.018	0.019	0.022	0.11	0.037	0.013	0.009	0.028	0.01
Lic2	0.35	0.44	0.021	0.021	0.021	0.021	0.021	0.022	0.055	0.054	0.054	0.016	0.047	0.053
DP21	0.54	0.24	0.071	0.033	0.022	0.019	0.025	0.029	0.037	0.022	0.01	0.011	0.014	0.018
Lic3	-0.22	0.46	0.078	0.061	0.045	0.078	0.025	0.025	0.063	0.033	0.011	0.01	0.011	0.011

*See Table 4.1 for the definition of the indices in this Table.

The estimation of chl_{a+b} over the study sites using the different methods described for deriving prediction algorithms can be compared through: i) simple relationships between leaf reflectance and chl_{a+b}; ii) scaling up the relationships using infinite reflectance models; and iii) scaling up the relationships using canopy reflectance models. The objective is to examine if viewing geometry and canopy structure information required for the scaling up of optical indices through CR models improves the estimation of chl_{a+b} relative to the other methods. Figure 4.28 shows the estimation of chl_{a+b} from a Vog1 (R_{740}/R_{720}), DP21 ($D_{\lambda p}/D_{703}$) and G_M2 (R_{750}/R_{700}) optical indices using *r*, $R_{\infty 1}$, $R_{\infty 2}$ and $R_{\infty 3}$, and the SAILH and *Kuusk* CR models. It can be seen that the estimation improves when SAILH and *Kuusk* CR models are used. For all indices used the estimations improve (linear regression slope progressively approaches unity) and RMSE significantly decreases when the optical indices are calculated using first R_{∞} and then canopy reflectance (CR) models, although RMSE does not improve significantly when CR

models are used. In addition, generally lower RMSE is found with $R_{\infty 2}$ and $R_{\infty 3}$ than with R_{SAILH} and R_{Kuusk}. From the three infinite reflectance models used, $R_{\infty 3}$ (Hapke) and $R_{\infty 2}$ (Yamada and Fujimura) are the ones achieving best estimations, approaching the predictive ability of SAILH and *Kuusk* CR models.

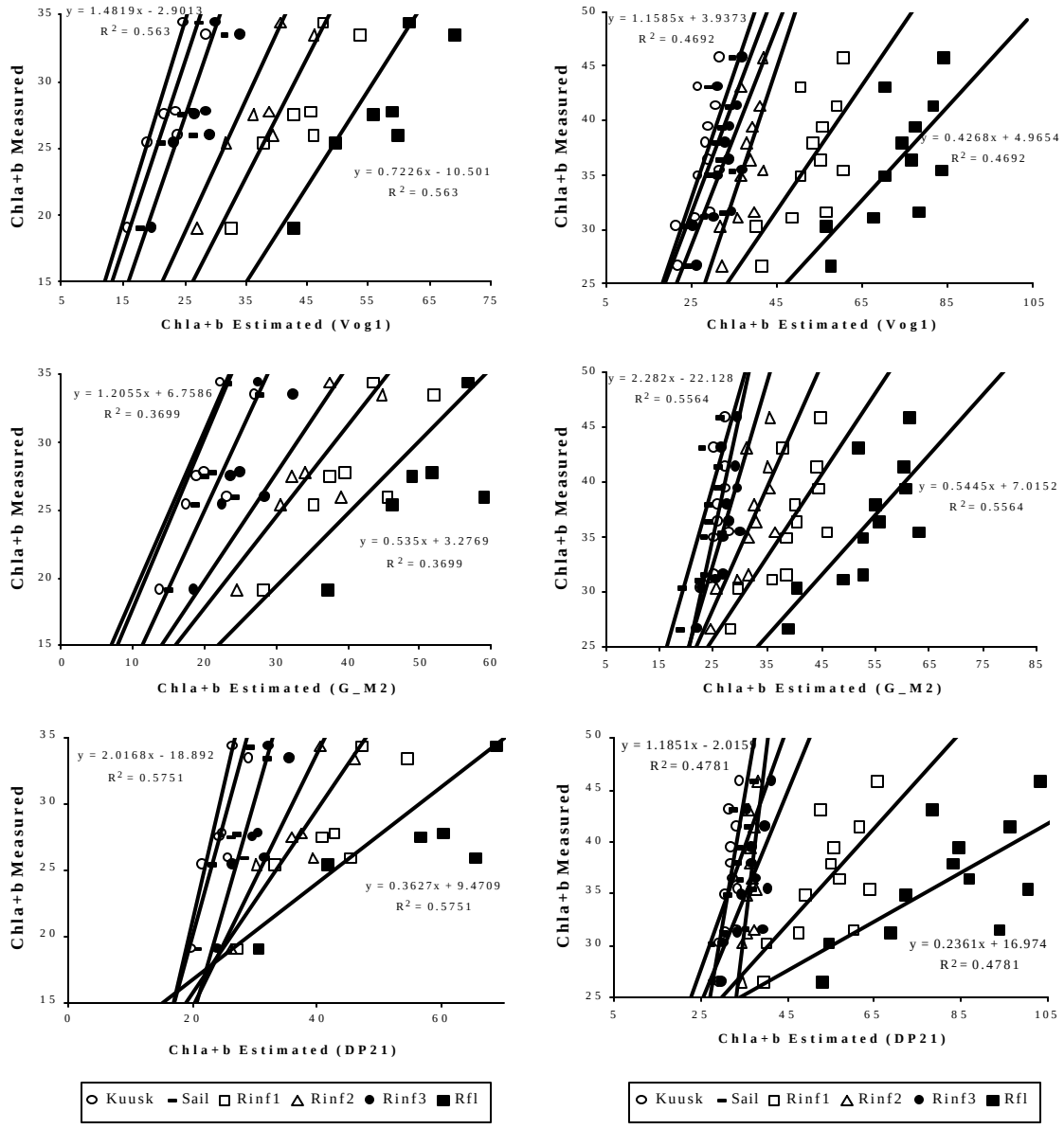

Figure 4.28. Estimation of chl_{a+b} from *CASI* data using Vog1 (R_{740}/R_{720}), G_M2 (R_{750}/R_{700}) and DP21 ($D_{\lambda p}/D_{703}$) indices developed at leaf level through *r*, R_∞ and CR models in 12 *Acer saccharum* M. study sites for 1998 (left) and 1999 (right).

4.3.2.1.- Seasonal variation of relationships

Determination coefficients of the relationships developed at leaf level were found to be consistent through the season, with similar significance level in consecutive deployments. Nevertheless, changes in the slopes of the relationships between pigments and indices were found. These results are consistent with Demarez (1999), and Blackburn (1999) in which stacks of leaves at different senescence stages showed a quadratic relationship between red edge optical indices (R_{750}/R_{700}, R_{750}/R_{550}) and chl_{a+b}, which further suggests that relationships are variable through the season. Therefore, leaf data collected in June and July deployments of 1998 and 1999 are function of the senescence stage, and relationships between indices and chl_{a+b} are variable due to changes in leaf thickness and transmittance during the season.

Statistical significance of the variation of relationships was studied using the *F* test (Chow, 1960) that performs a test of equality between sets of coefficients in two linear regressions. One of the more common applications of the *F* test (derived for testing linear hypotheses) is the test of structural change. In specifying a regression model, we assume that its assumptions of linearity of the Regression Model apply to all the observations in our sample. It is, however, straightforward to test the hypothesis that some or all the regression coefficients are different in subsets of the data. The *F* statistic [Equation 4.2] for testing the restriction that the coefficients in the two equations (for 1998 and 1999) are the same is,

$$F\,[J, n_1+n_2-2K] = \frac{[e'_r e_r - (e'_1 e_1 + e'_2 e_2)]/J}{(e'_1 e_1 + e'_2 e_2)/(n_1+n_2-2K)} \quad [4.2]$$

where,

$e'_r e_r$	residual sum of squares from the restricted regression, assuming the coefficient vectors are the same for the two periods;
$e'_1 e_1$	residual sum of squares for period 1998;
$e'_2 e_2$	residual sum of squares for period 1999;
J	number of restrictions (number of coefficients);
(n_1+n_2-2K)	degrees of freedom, with K the number of parameters in the regression model;

Table 4.8. Chow test F values (rejects hypothesis of equality between the two relationships if F>~3.00). Relationships tested are for June vs July 1999 when calculated from *r* (reflectance), $R_{\infty 3}$ (infinite reflectance model from Hapke), and CR_{SAILH} (SAILH canopy reflectance model).

	F (*r*)	**F($R_{\infty 3}$)**	**F(CR_{SAILH})**
Vog1	3.48	13.11	10.52
G_M2	1.47	19.45	11.42
Vog3	2.80	23.19	19.56
lpr	7.33	15.48	17.93
Vog2	2.96	22.59	19.70
Vog4	12.34	28.76	25.09
G_M1	6.39	25.09	12.84
Ctr2	8.21	7.50	6.63
DP21	1.50	26.56	23.15
Ctr1	8.04	10.53	10.56
DP22	11.89	8.14	5.06
Cur	5.06	23.34	27.62

Figure 4.29 shows the relationships obtained between Vog3 $(R_{734}-R_{747})/(R_{715}+R_{720})$ optical index calculated from leaf reflectance and through SAILH canopy reflectance model from June and July senescence stages. The Chow test, that performs a test of equality between sets of coefficients in two linear regressions, for example for Vog3, accepts the hypothesis of equality for an index from reflectance with F=2.8, and rejects the test from CR with the corresponding F=19.56 (Table 4.8). Relationships show a

larger change between development stages (June to July) when the index is calculated from CR model likely because it takes into account leaf transmittance in the calculation of simulated CR. Leaf transmittance varies with leaf thickness and therefore affects relationships calculated from reflectance and transmittance at different stages. Similar results were found between the earlier (June) and later (July) seasons in 1998 which shows consistency across the temporal study.

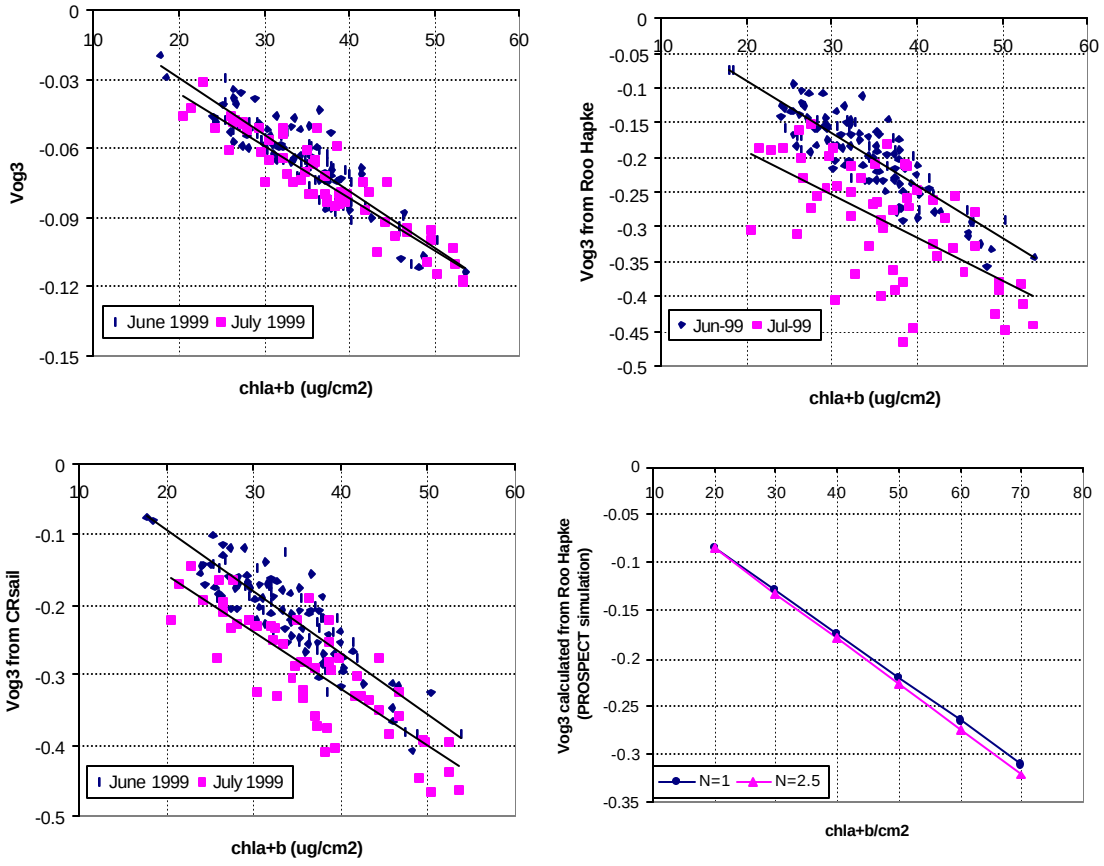

Figure 4.29. Relationship obtained between Vog3 $(R_{734}-R_{747})/(R_{715}+R_{720})$ optical index calculated from leaf reflectance (upper left), $R_{\infty 3}$ (upper right) and through SAILH canopy reflectance model (lower left) from June (blue) and July (pink) 1999 senescence stages. Chow test, that performs a test of equality between sets of coefficients in two linear regressions, accepted the hypothesis of equality for the index from reflectance with F=2.8, and rejected the tests from R_{∞} Hapke with F=23.2, and CR with F=19.5. Lower right plot shows the index from $R_{\infty 3}$ simulated from PROSPECT for N=1 and N=1.6.

To prove that the variation of relationships between optical indices and chl_{a+b} is due to leaf structural changes through the season, a simulation approach was chosen. Single leaf reflectance and transmittance from June and July in the two consecutive years were used to calculate the N structural parameter by PROSPECT model inversion. Results show that the averaged N parameter estimated at earlier stages is lower than at later senescence stages (N=1.51, *s*=0.08 June-1998 (*n*=234); N=1.54, *s*=0.05, July-1998 (*n*=193); N=1.37, s=0.08, June-1999 (*n*=118); N=1.41, s=0.09, July-1999 (*n*=66).

Differences in N parameter between 1998 and 1999 show that higher values were found in 1998, probably related to a different development stage at the time of data collection in July of each of the two years. Moreover, a simulation was performed with the PROSPECT model in order to study if variations in the relationship between the Vog3 optical index and chl_{a+b} followed the same pattern between measured and model-simulated index. Vog3 $(R_{734}-R_{747})/(R_{715}+R_{720})$ optical index calculated through $R_{\infty 3}$ and SAILH from leaf samples shows a displacement of the relationship to lower values in later stages (Figure 4.29). Simulation from PROSPECT demonstrated consistency with the hypothesis, showing that higher values of N expected through the season, and confirmed by model inversion, affect the optical index obtaining lower values. Nevertheless, the change in the modelled relationship by PROSPECT for different values of N does not change as much as in the real data. It suggests that the PROSPECT N parameter does not adequately model the structural changes expected through the season due to variations in transmittance as a function of leaf thickness. Therefore leaf-level

relationships more accurately represent variation in structural changes through the season than the PROSPECT model-based approach.

4.3.3.- Estimation of chl_{a+b} by model inversion

SAILH (Verhoeff, 1984) and MCRM (Kuusk, 1995a; 1995b; 1996) CR models and PROSPECT leaf model were used for chl_{a+b} estimation by inversion, using 1998 and 1999 CASI data. The inversion of the coupled MCRM and PROSPECT model was performed as indicated in Kuusk (1998) by minimizing a Merit function *F* (Kuusk, 1991). Two different ways were used: i) setting LAI to a nominal value LAI=4 so that the results are comparable to the scaling-up methodology, in which LAI was set to a nominal value of 4; and ii) allowing LAI and chl_{a+b} to vary. Other model parameters (Table 4.9) were set to nominal values derived from the study areas, such as plagiophile LADF, 35° solar zenith angle, and a hotspot parameter s/l=0.008. Inversion of PROSPECT from

Table 4.9. Input parameters for the inversion of MCRM canopy reflectance model in the estimation of chl_{a+b} over 12 *Acer saccharum* M. study sites for 1998 and 1999.

LAI	4	Leaf Area Index
q_m, e	45°, 0.95	Parameters for LADF
sl	0.008	Leaf size/H
N (PROSPECT)	1.54, 1.41	Structural Parameter N
l_z	1.1	Markov parameter
q_s	35°	Solar zenith angle
q	0°	Viewing angle
y	0°	Azimuth relative to the sun
b	0.18	Angstrom turbidity factor
chl_{a+b}	Variable	Chlorophyll content (µg/cm^2)
C_w	0.03	Water content (cm)
C_p	0.001	Protein content (g/cm^2)
C_c	0.001	Cellulose + lignin content (g/cm^2)

reflectance and transmittance leaf data demonstrated that there was a change in the N structural parameter for the same period in the two consecutive years: N=1.54 in July 1998, N=1.41 in July 1999. N was therefore set to those values to account for changes in leaf internal structure from 1998 to 1999.

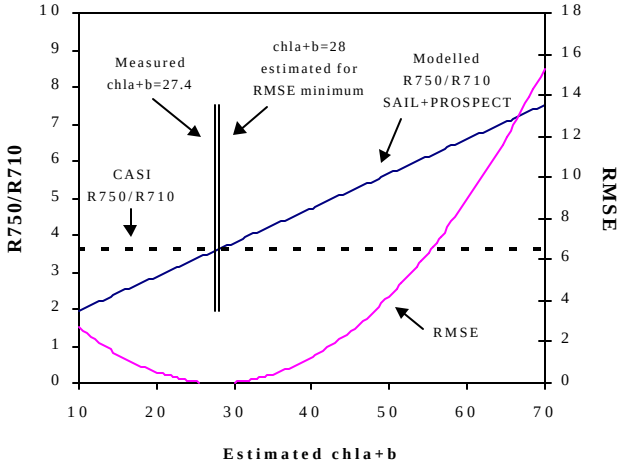

Figure 4.30. Estimation of chl_{a+b} by SAILH+PROSPECT model inversion using R_{750}/R_{710} in the merit function. Estimated chl_{a+b} is found when RMSE is minimum, calculated between R_{750}/R_{710} from CASI reflectance and modelled R_{750}/R_{710}. CASI data collected in 1998 from the GY01 *Acer Saccharum* M. study site, was used for this inversion.

The inversion of SAILH + PROSPECT models was performed by iteration and minimizing a function as indicated in Jacquemoud (1993; 1995) for all the CASI channels in the visible and NIR, as described in Section 2.4. A methodology consisting of minimizing a function based on a red edge optical index (Figure 4.30) was also carried out, were both chl_{a+b} and LAI were allowed to vary in the range, 4-7 for LAI, and 10-70 $\mu g/cm^2$ for chl_{a+b}, with the merit function,

$$F(LAI, chl_{a+b}) = \left[\left(\frac{R_{750}}{R_{710}} \right)_{CASI} - \left(\frac{R_{750}}{R_{710}} \right)_{SAILH+PROSPECT} \right]^2 \qquad [4.3]$$

A comparative result of the estimation methodologies is shown in Table 4.10, with r^2=0.33 and RMSE=12.0 μg/cm^2 (1998), r^2=0.49 and RMSE=5.91 μg/cm^2 (1999) when all CASI channels were used as a minimizing function with no weighting w_i coefficients and LAI=4. When coefficients w_i are specified as the inverse of the measured reflectance, results are r^2=0.32 and RMSE=16.8 μg/cm^2 (1998), r^2=0.47 and RMSE=11.43 μg/cm^2 (1999), showing that the RMSE increases when weighting coefficients are used.

Results using the coupled MCRM and PROSPECT model inversion show r^2=0.33 and RMSE=8.22 μg/cm^2 (one outlier) in 1998; and r^2=0.34 and RMSE=5.89 μg/cm^2 in 1999, therefore with similar RMSE but lower r^2 as in SAILH and PROSPECT inversion.

Table 4.10. Estimation of chl_{a+b} over 12 *Acer saccharum* M. 30x30 m study sites in 1998 and 1999 by model inversion and scaling-up methods, with leaf structural parameter N estimated by inversion (N=1.54, 1998; N=1.43, 1999). For SAILH and PROSPECT model inversion 3 methods were used: minimizing a function with all spectral channels without weighting coefficients ($\cancel{w_i}$), with weighting coefficients calculated as the inverse of the reflectance (w_i) and by a function based on the optical index R_{750}/R_{710}.

	SAILH + PROSPECT (r^2, RMSE in μg/cm^2)		**MCRM + PROSPECT** (r^2, RMSE in μg/cm^2)	**SCALING-UP R_{750}/R_{710}** (r^2, RMSE in μg/cm^2)	
1998	$\cancel{w_i}$ w_i R_{750}/R_{710}	0.33 , 12.0 0.32 , 16.8 0.43 , 5.57	0.33 , 8.22 (one outlier)	CR_{SAILH} $R_{\infty 3}$	0.47 , 10.7 0.47 , 8.11
1999	$\cancel{w_i}$ w_i R_{750}/R_{710}	0.49 , 5.91 0.47 , 11.43 0.57 , 12.48	0.34 , 5.89	CR_{SAILH} $R_{\infty 3}$	0.57 , 11.4 0.57 , 8.3

The effect of the Markov parameter λ in the MCRM model was studied using one study site. Markov parameter for 1998 and 1999 chl_{a+b} estimation was set to 1.1 as indicated in Kuusk (1998) where mixed vegetation was used for model inversion. The effect of λ in

the estimation of chl_{a+b} was practically imperceptible while λ ranged from λ=0.4 (chl_{a+b} estimated = 40.63) to λ=1.1 (chl_{a+b} estimated = 40.13), with chl_{a+b} measured in GY41-99 = 39.4. In a study site with larger estimation error the effect was also small: chl_{a+b} estimated = 49.45 (λ=0.4), and chl_{a+b} estimated = 50.69 (λ=1.1), with chl_{a+b} measured in MD39-99 = 37.99.

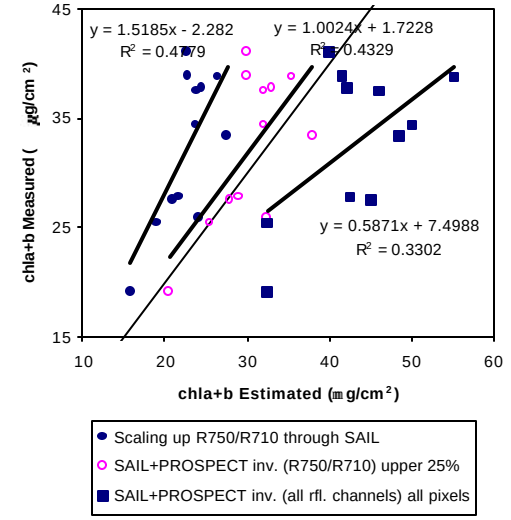

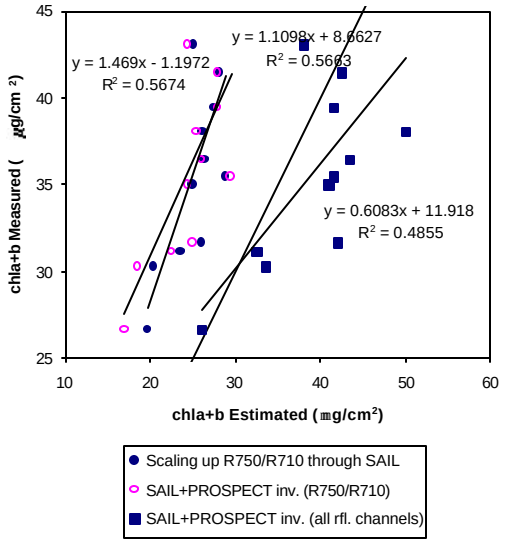

Figure 4.31. Estimation of chl_{a+b} over 12 *Acer saccharum* M. 30x30 m study sites in 1998 (top) and 1999 (bottom) by i) SAILH and PROSPECT model inversion using all reflectance channels in the merit function; ii) SAILH and PROSPECT model inversion using R_{750}/R_{710} in the merit function; and iii) scaling-up R_{750}/R_{710} through SAILH canopy reflectance model. LAI was set to 4, and N=1.54 (1998), N=1.41 (1999), estimated from leaf samples by PROSPECT model inversion. The 1:1 line is shown in both plots to compare it with the prediction methods.

Results of SAILH and PROSPECT model inversion using the red edge index R_{750}/R_{710} as a minimizing function by iteration indicates comparable results to the scaling-up methodology, with r^2=0.43 and RMSE=5.57 µg/cm^2 (LAI=4) in 1998; and r^2=0.57 and RMSE=12.48 µg/cm^2 (LAI=4) in 1999. These results show similar estimation as the scaling-up method for 1998 and 1999 using the same index: r^2=0.47 with $RMSE_{SAILH}$=10.7 µg/cm^2; $RMSE_{R\infty 3}$=8.11 µg/cm^2 in

1998; and r^2=0.57, $RMSE_{SAILH}$=11.4 μg/cm^2; $RMSE_{R\infty 3}$= 8.3 μg/cm^2 in 1999, Table 4.10. Figure 4.31 shows the comparison of estimation made in 1998 and 1999 by i) scaling up R_{750}/R_{710} index through SAILH; ii) by SAILH and PROSPECT inversion using all CASI reflectance channels; and iii) by SAILH+PROSPECT inversion using the red edge R_{750}/R_{710} index.

Both scaling-up and SAILH+PROSPECT model inversion methods obtained comparable results when the same minimizing function based on a red edge index was used, and poorer estimation when all CASI reflectance channels are used. Figure 4.32 shows the small effect of LAI in the estimation of chl_{a+b} by SAILH+PROSPECT model inversion with all reflectance channels as merit function with $w_i=1/r_i$: r^2=0.32, RMSE=16.8 μg/cm^2 for LAI=4; r^2=0.32, RMSE=16.6 μg/cm^2 for LAI variable (1998); r^2=0.47, RMSE=11.43 μg/cm^2 for LAI=4; r^2=0.41, RMSE=12.16 μg/cm^2 for LAI variable (1999).

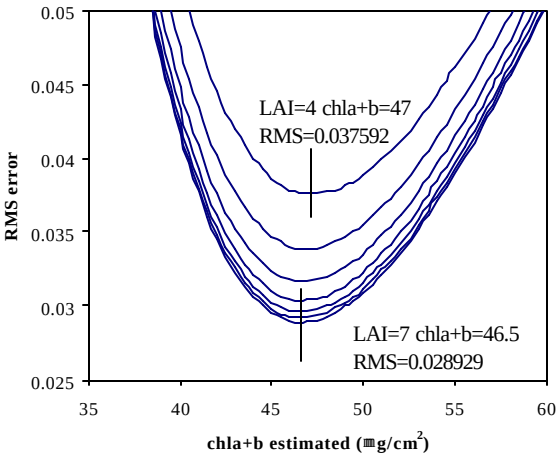

Figure 4.32. Estimation of chl_{a+b} varying LAI=4 to 7 by SAILH+PROSPECT model inversion with all reflectance channels in merit function with $w_i=1/r_i$. It can be seen that LAI has a very small effect in chl_{a+b} estimation: 47 μg/cm^2 (LAI=4) and 46.5 μg/cm^2 (LAI=7).

These results clearly demonstrate that minimizing functions based on spectral channels, weighted or not as a function of wavelength, obtain poorer determination

coefficients and RMSE than a single optical index calculated in the red edge spectral region, such as R_{750}/R_{710}.

SAILH, *Kuusk* CR models and infinite reflectance models, used for model inversion or in the scaling-up method, have an improvement in the prediction capabilities compared to statistical leaf-level linear relationships. Nevertheless, both SAILH and *Kuusk* models are useful for infinite plane-parallel turbid-medium canopies, and the infinite reflectance models consider a thick layer depending upon the assumptions made for the multiple scattering. Canopy openings, shadows, and changes in the geometry of the canopy elements are not considered as part of the canopy structural set of input values, therefore their use may be in cases such as non-dense vegetation. In order to simulate a plane-parallel canopy from our CASI data, all the results discussed were obtained by a pre-selection of the upper pixels in the NIR, therefore selecting the brightest pixels minimizing shadows and canopy openings in all study areas. The different methodologies used here for pigment estimation were tested for both i) calculating the average reflectance from all 20x20 m study sites by selection of the upper 25% pixels in the NIR, as done before, and ii) averaging all pixels from the 20x20 m sites, therefore affecting the averaged reflectance by shadows. Since we are dealing with a dense canopy, the effects of the shadows in the spatial resolution can be studied, and especially its effect in the different methodologies used for pigment estimation. Tables 4.11 and 4.12 show the results obtained for 1998 and 1999 CASI data, for eight methods of pigment estimation: i, ii and iii) scaling up the R_{750}/R_{710} optical index through $R_{\infty 1}$, $R_{\infty 2}$ and $R_{\infty 3}$ infinite

reflectance models; iv) scaling up the R_{750}/R_{710} optical index through SAILH canopy reflectance model; v and vi) numerical inversion of SAILH and PROSPECT using all reflectance channels in the merit function, and using R_{750}/R_{710} in the merit function; and vii and viii) numerical inversion of $R_{\infty 2}$ and $R_{\infty 3}$ coupled with PROSPECT using R_{750}/R_{710} in the merit function.

Results show that little effect is caused by shadows in the estimation of the chl_{a+b} when the red edge optical index R_{750}/R_{710} is used in the merit function with any of the methods used: RMSE=5.57 $\mu g/cm^2$ (brightest 25%), RMSE=5.48 $\mu g/cm^2$ (all pixels) in 1998 with SAILH and PROSPECT inversion using R_{750}/R_{710} in the merit function; but a large effect is found when all reflectance channels are used in the minimizing function: RMSE=12 $\mu g/cm^2$ (brightest 25%), RMSE=23.1 $\mu g/cm^2$ (all pixels) in 1998 with SAILH and PROSPECT inversion. This finding is consistent in all cases (Tables 4.11 and 4.12) demonstrating that optical indices in the red edge are less affected to structural changes and shadows (Figure 4.33) than single reflectance channels (Figure 4.34), where it can be seen that red edge R_{750}/R_{710} optical index used for model inversion through canopy modelling is not perceptibly affected when all pixels are included in the averaged reflectance from the 20x20 m study sites (2x2 m pixel size), thereby including canopy shadows and openings.

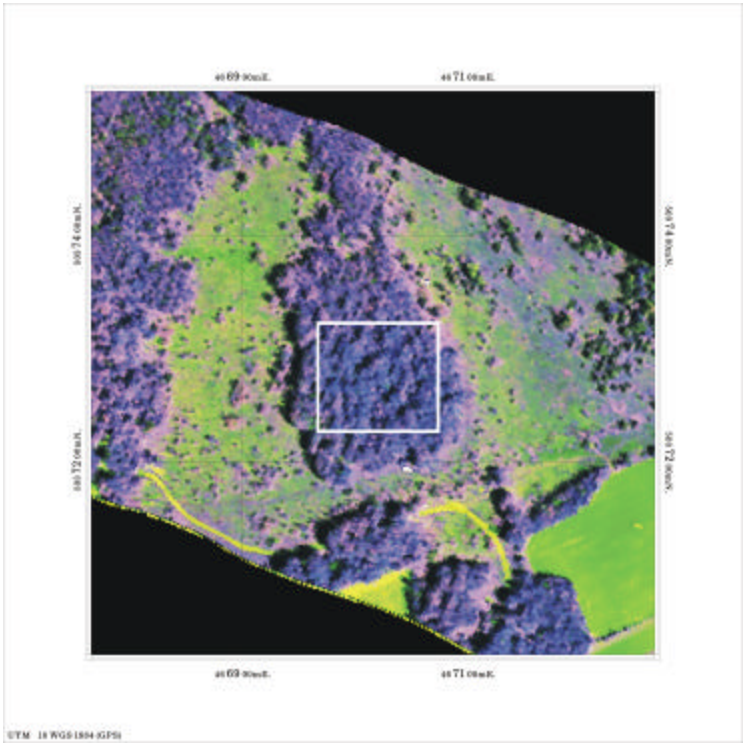

(a)

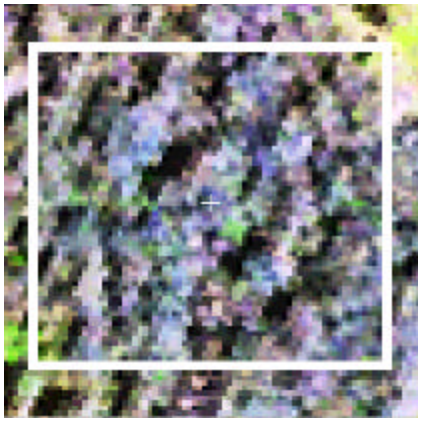

(b)

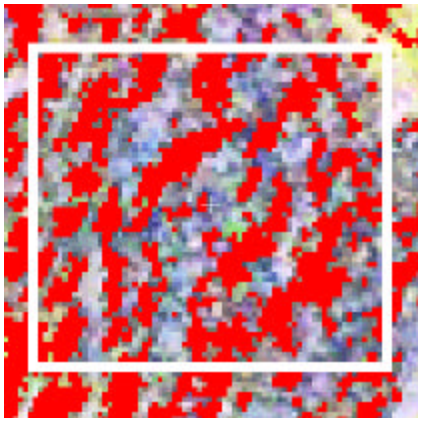

(c)

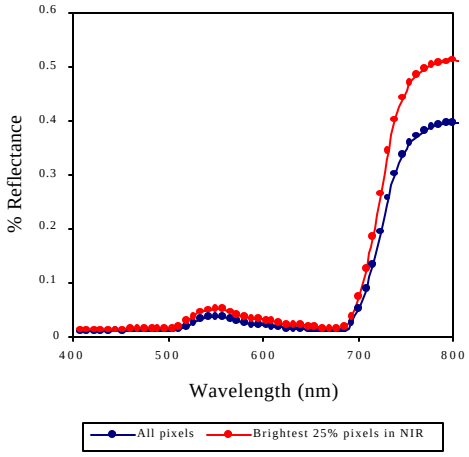

(d)

Figure 4.33. Reflectance spectra obtained from one *Acer saccharum* M. study site by selection of all pixels (d, in blue) and targeting the brightest 25% in the NIR (d, in red). The plot (b,c) from the study area (a) is subset and a channel in the NIR (800nm) used to select the brightest pixels. Red pixels in (c) are those ones that are not selected when the spectrum is calculated targeting only the crowns, therefore not including shadows and canopy openings.

Results also demonstrate that chl_{a+b} estimation by scaling up through $R_{\infty 2}$ infinite reflectance model is the methodology generating smaller RMSE, although higher errors are found when the same infinite reflectance model is used coupled with PROSPECT. This suggests that leaf-level derived relationships are more accurate for scaling up through $R_{\infty 2}$ than reflectance and transmittance modelled by PROSPECT. If no leaf-level relationships are derived, model inversion using $R_{\infty 3}$+PROSPECT showed lower RMSE than SAILH+PROSPECT, each with R_{750}/R_{710} in the merit function.

Table 4.11. Comparison of RMSE ($\mu g/cm^2$) and r^2 for chl_{a+b} estimation by scaling-up leaf level optical indices in 1998 and 1999 deployments considering all pixels in the 20x20 m area averaged reflectance with 2m spatial resolution and 72-channel CASI data (100 pixels), and selecting the upper 25% pixels in the NIR to minimize shadows and openings in a dense canopy of *Acer saccharum* M.

	Scaling up $D^2=f(R_{750}/R_{710}, R_{¥1})$				**Scaling up $D^2=f(R_{750}/R_{710}, R_{¥2})$**				**Scaling up $D^2=f(R_{750}/R_{710}, R_{¥3})$**				**Scaling up $D^2=f(R_{750}/R_{710}, R_{SAILH})$**			
	1998		*1999*		*1998*		*1999*		*1998*		*1999*		*1998*		*1999*	
	up	*all*	*up*	*all*	*up*	*all*	*up*	*all*	*up*	*all*	*up*	*all*	*up*	*all*	*up*	*all*
R^2	0.48	0.46	0.57	0.44	0.47	0.46	0.57	0.44	0.47	0.46	0.57	0.44	0.47	0.46	0.57	0.44
RMSE	9.95	11.12	8.53	11.1	5.38	6.00	4.25	4.13	8.11	7.5	8.3	7.4	10.7	10.2	11.4	10.3

Table 4.12. Comparison of RMSE ($\mu g/cm^2$) and r^2 for chl_{a+b} estimation in 1998 and 1999 deployments considering all pixels in the 20x20 m area averaged reflectance with 2m spatial resolution and 72-channel CASI data (100 pixels), and selecting the upper 25% pixels in the NIR to minimize shadows and openings in a dense canopy of *Acer saccharum* M. LAI=4 was considered in all cases, and no weighting coefficients were used in the model inversion when all channels are used in the merit function.

	SAILH+PROSPECT $D^2=f(S\,R_l)$				**SAILH+PROSPECT $D^2=f(R_{750}/R_{710})$**				**$R_{¥2}$ + PROSPECT $D^2=f(R_{750}/R_{710})$**				**$R_{¥3}$ + PROSPECT $D^2=f(R_{750}/R_{710})$**			
	1998		*1999*		*1998*		*1999*		*1998*		*1999*		*1998*		*1999*	
	up	*all*	*up*	*all*	*up*	*all*	*up*	*all*	*up*	*all*	*up*	*all*	*up*	*all*	*up*	*all*
R^2	0.33	0.34	0.48	0.11	0.43	0.41	0.57	0.47	0.47	0.45	0.57	0.44	0.47	0.44	0.56	0.45
RMSE	12	23.1	5.9	16.7	5.57	5.48	12.48	11.01	22.5	24.2	8.9	11.9	5.36	6.03	5.13	4.35

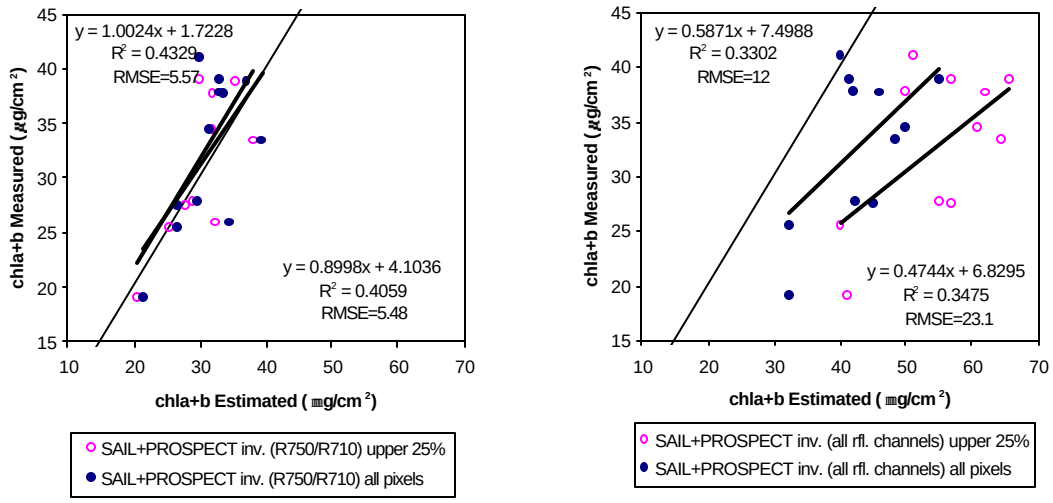

Figure 4.34. Effect of shadows and canopy structure in the estimation of chl_{a+b} by SAILH+PROSPECT model inversion using R_{750}/R_{710} (left) and all CASI spectral channels (right) in the merit function. The red edge R_{750}/R_{710} optical index used for model inversion through canopy modelling does not get affected when all pixels are included in the averaged reflectance from the 20x20 m study sites (2x2 m pixel size), therefore including canopy shadows (data from the 1998 campaign).

4.4.- IMPLICATIONS FOR FOREST MONITORING BY OPTICAL REMOTE SENSING

A validation of the methodologies developed with 1997, 1998 and 1999 data over 12 study sites was carried out in June 2000 selecting a different set of 14 plots of the same species of *Acer saccharum* M. The objectives of the campaign carried out were i) to validate methodologies for closed canopies developed in previous campaigns, using a different set of sites; and ii) to propose an operational methodology for chl_{a+b} estimation in closed canopies using a satellite sensor with red edge spectral bands, such as MERIS, to be launched in 2001 by ESA. The new study sites belong partially to the *Maple Decline* network used previously, and to the *Ice Storm Damage* sites located in Ontario that suffered from 1998 ice storm in eastern Canada. Five maple trees from each site were sampled, collecting 4 leaves per branch for measurements of reflectance, chlorophyll fluorescence and pigment content. Biochemical analysis of samples showed a narrower range of chl_{a+b} content from the new set of 14 sites compared to the 1998 and 1999 sites, with values falling into the 29.8-42.7 $\mu g/cm^2$ interval (while in previous years ranges were 19.1-41.1 $\mu g/cm^2$ in 1998, and 26.6-45.8 $\mu g/cm^2$ in 1999). Similar procedures as reported in Chapter 3 were followed in order to collect CASI data from the new study sites, while 3x3 feet white panels were placed on the study area to allow for accurate plot location on the airborne data. Two missions were flown over the sites, i) a Mapping Mission at 0.88x0.86m spatial resolution and 7 bands, resampled to 0.8x0.8m; and ii) and a Hyperspectral Mission at 0.86x3.4m spatial resolution and 72 bands, resampled to 1.5x1.5m (see Appendix for spectral band configurations). Similarly, the Mapping

Mission allowed for site location due to the higher spatial resolution, and the Hyperspectral Mission allowed for extraction of reflectance spectra selecting all pixels from the 80x80m plots and targeting crowns, therefore minimizing shadows and understorey. Three numerical model inversion methods that obtained best results in 1998 and 1999 for chl_{a+b} estimation were used for validation: i) SAILH coupled with PROSPECT with all 72 CASI channels in the minimizing merit function, with no weighting function; ii) SAILH coupled with PROSPECT (N=1.4) with R_{750}/R_{710} optical index as merit function; and iii) $R_{\infty 3}$ coupled with PROSPECT (N=1.4) with R_{750}/R_{710} optical index as merit function. Table 4.13 shows the results obtained for the three methods when all pixels and only the brightest 25% pixels in the NIR are targeted in the 80x80 m plots. Results confirm and validate 1998 and 1999 conclusions, demonstrating that better estimations are achieved when the merit function is based on a red edge optical index such as R_{750}/R_{710}: r^2=0.18, RMSE=14.8 µg/cm^2 (SAILH+PROSPECT inversion using all reflectance channels, all pixels); r^2=0.43, RMSE=5.2 µg/cm^2 (SAILH+PROSPECT inversion using R_{750}/R_{710} red edge index, all pixels).

Table 4.13. Comparison of RMSE and r^2 for chl_{a+b} estimation in 2000 deployment considering all pixels in the 80x80m area averaged reflectance of 0.86x3.4m resampled to 1.5x1.5m spatial resolution and 72-channel CASI data (2809 pixels), and selecting the upper 25% pixels in the NIR to minimize shadows and openings in a dense canopy of *Acer saccharum* M. LAI=4 was considered in all cases, and no weighting coefficients were used in the model inversion. MERIS-equivalent spectra were obtained from CASI 72-channel data, and R_{750}/R_{705} used for model inversion with SAILH and $R_{\infty 3}$ coupled with PROSPECT.

	CASI 72-channel data						**MERIS Simulation from CASI 72-channel data**			
	SAILH+ PROSPECT $D^2=f(SR_1)$		**SAILH+ PROSPECT $D^2=f(R_{750}/R_{710})$**		**$R_{\infty 3}$ + PROSPECT $D^2=f(R_{750}/R_{710})$**		**SAILH+ PROSPECT $D^2=f(R_{750}/R_{705})$**		**$R_{\infty 3}$ + PROSPECT $D^2=f(R_{750}/R_{705})$**	
	up	*all*	*up*	*all*	*up*	*all*	*up*	*all*	*up*	*all*
R^2	0.2	0.18	0.42	0.43	0.43	0.44	0.44	0.44	0.43	0.43
RMSE	4.8	14.8	3.0	5.2	5.0	8.9	3.0	3.97	3.9	6.98

The small effect of shadows on pigment estimation when R_{750}/R_{710} index is used with SAILH+PROSPECT model inversion was also confirmed: RMSE=3.0 µg/cm^2 (brightest 25%), RMSE=5.2 µg/cm^2 (all pixels), showing a larger variation in RMSE when all reflectance channels are used: RMSE=4.8 µg/cm^2 (brightest 25%), RMSE=14.8 µg/cm^2 (all pixels), Figure 4.35. Results obtained with $R_{\infty 3}$ infinite reflectance model coupled with PROSPECT also demonstrate its applicability in closed canopies with high LAI. PROSPECT coupled with SAILH and $R_{\infty 3}$ with R_{750}/R_{710} in the merit function obtained similar results (r^2=0.4), although RMSEs are slightly smaller with SAILH: RMSE=3.0 µg/cm^2 (SAILH+PROSPECT, brightest 25%), RMSE=5.0 µg/cm^2 ($R_{\infty 3}$+PROSPECT, brightest 25%); RMSE=5.2 µg/cm^2 (SAILH+PROSPECT, all pixels), RMSE=8.9 µg/cm^2 ($R_{\infty 3}$+PROSPECT, all pixels).

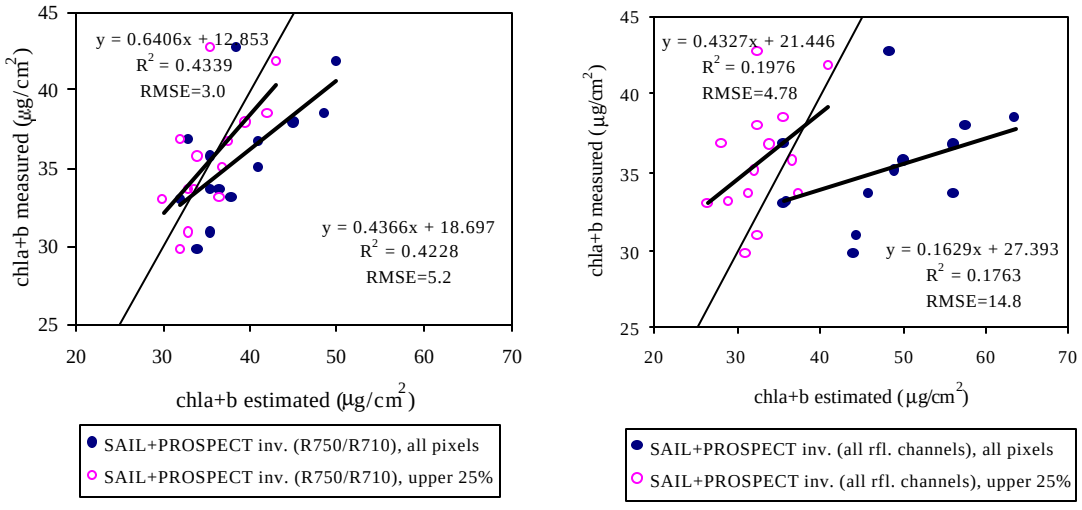

Figure 4.35. The effect of shadows in the estimation of chl_{a+b} by SAILH+PROSPECT model inversion using R_{750}/R_{710} (left) and all CASI reflectance channels (right) in the merit function is confirmed with the CASI 2000 data. The red edge R_{750}/R_{710} optical index used for model inversion through canopy modelling does not get as much as affected when all pixels are included in the averaged reflectance from the 80x80 m study sites (0.86x3.4m resampled to 1.5x1.5m pixel size), therefore including canopy shadows.

MERIS equivalent spectra were calculated from the CASI-72-channel data in order to perform a simulation to study the applicability of MERIS red edge bands for pigment estimation by model inversion. Although careful atmospheric correction must be performed, two MERIS spectral bands located along the red edge, at 705 nm (10nm bandwidth) and 753.75 nm (7.5 nm bandwidth), can be proposed for calculating the index R_{750}/R_{705} to be used in the merit function. The similar spectral bandwidth of the CASI sensor in the 72-channel mode of operation of 7.5 nm, wavelength dependent (Czapla-Myers, 2000), allowed for simulation by interpolation of the MERIS centre wavelengths from CASI data (see Appendix). MERIS-equivalent images were built from CASI data, and reflectance data extracted from the plots (Figure 4.36). Same methodologies were then carried out for chl_{a+b} estimation by model inversion using SAILH and $R_{\infty 3}$ coupled with PROSPECT, using MERIS R_{750}/R_{705} red edge index for the merit function. Results in Table 4.13 show that R_{750}/R_{705} used for MERIS performs similarly as R_{750}/R_{710} used for estimations with CASI, obtaining r^2=0.44, and RMSE=3.0 µg/cm^2 (SAILH + PROSPECT, brightest 25%

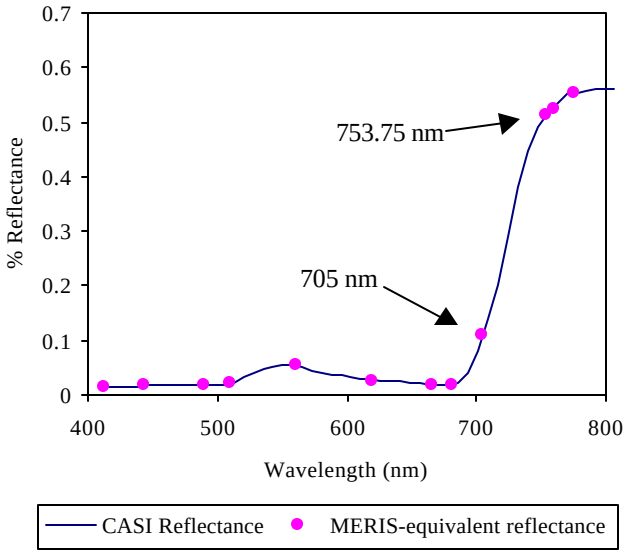

Figure 4.36. MERIS-equivalent spectra obtained from CASI 72-channel data from one of the *Acer saccharum* M. study sites collected in June 2000, with 25% brightest pixels targeted. The channels proposed for model inversion through the red edge optical index R_{750}/R_{705} are shown.

pixels), RMSE=3.97 µg/cm^2 (SAILH+PROSPECT, all pixels). These results suggest that methodologies investigated here based on pigment estimation by model inversion using red edge indices can be transferred to MERIS sensor to be launched in 2001 by ESA.

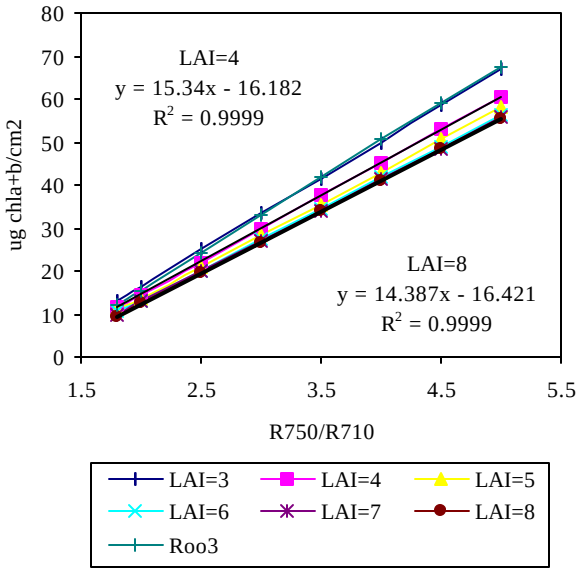

Figure 4.37. Relationships obtained between chl_{a+b} and R_{750}/R_{710} optical index by model inversion of SAILH and $R_{\infty 3}$ coupled with PROSPECT (N=1.4). Nominal structural and viewing geometric parameters were used for SAILH, with LAI variable.

This methodology of numerical model inversion using SAILH and $R_{\infty 3}$ coupled with PROSPECT allows the spatial mapping of chl_{a+b} in closed canopies of *Acer saccharum* M. Model inversion by SAILH and PROSPECT, using N=1.4 and nominal viewing geometry and canopy structure parameters (LAI=3.5; plagiophile LADF; soil reflectance derived from CASI imagery; model-estimated skylight irradiance fraction; hotspot parameter s/l=0.007; θs=35°; and θv=0°), and by $R_{\infty 3}$ coupled with PROSPECT was performed. Numerical model inversion for a range of chl_{a+b} and LAI, with constant structural and geometrical parameters was performed in order to obtain relationships between chl_{a+b} and sensor-derived R_{750}/R_{710} optical index. This approach to look-up table (LUT) generation allows for faster estimations in a pixel by pixel approach over large areas. Figure 4.37 shows the relationships obtained between chl_{a+b} and

R_{750}/R_{710} for SAILH+PROSPECT with variable LAI, and for $R_{\infty 3}$+PROSPECT, considering N=1.4 and the mentioned structural and geometry parameters. It shows that relationships from $R_{\infty 3}$ + PROSPECT and SAILH+PROSECT are the same when LAI=4. Consistency is found with previous results (Figure 4.27) which demonstrated that red edge indices become insensitive to LAI variation when LAI>4. Relationships found by model inversion for LUT generation show that there is no variation when LAI>5 (Figure 4.37). The effect of N structural parameter from PROSPECT was also studied (Figure 4.38) showing that differences are found in chl_{a+b} estimation for high R_{750}/R_{710} values when N changes from 1.2 to 1.8, producing up to 15 µg/cm^2 variation. LUT from SAILH+PROSPECT with LAI=4 and N=1.4 was used for mapping chl_{a+b} over large areas of *Acer saccharum* M. from 2000 campaign CASI data (Figures 4.39, 4.40 and 4.41), considering 6 classes of chl_{a+b} (µg/cm^2): i) < 20 (very low chlorophyll, trees in poor condition or fall senescence); ii) 20-25 (low chlorophyll, trees probably stressed); iii) 25-30 (below average, may be a mix of stressed and healthy trees); iv) 30-35 (average chlorophyll, trees usually healthy); v) 35-40 (average to above average chlorophyll, trees healthy); and vi) > 40 (above average chlorophyll, trees

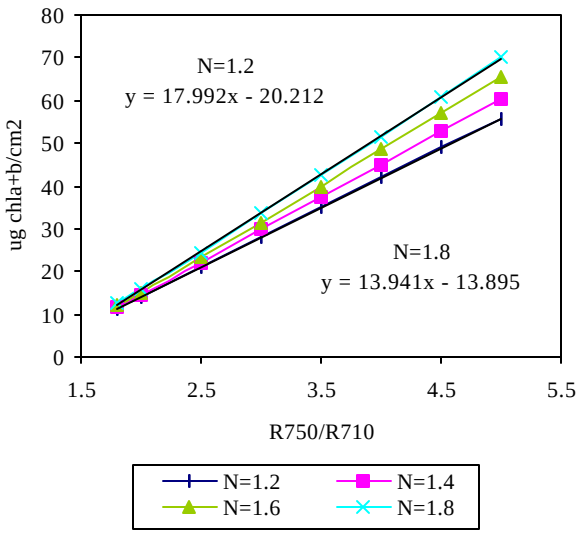

Figure 4.38. Relationships obtained between chl_{a+b} and R_{750}/R_{710} optical index by model inversion of SAILH coupled with PROSPECT (LAI=4). Nominal structural and viewing geometric parameters were used for SAILH, with N (PROSPECT) variable.

healthy, but could be a sign of other factors such as a high lime/high nutrient soil or fertilizer application). The same methodology for pigment mapping was used for CASI data obtained from the 12 study sites collected in 1998 and 1999, using N=1.54 (1998) and N=1.41 (1999) with LAI=4 with nominal parameters for model inversion. Figure 4.42. shows chl_{a+b} estimation over the study areas (500x500m) that presented extreme values of chl_{a+b} measured in the field in 1998 and 1999 campaigns, with the highest values measured in leaf samples of 38.8 $\mu g/cm^2$ (GY41, 1998, Figure 4.42, higher left) and 45.8 $\mu g/cm^2$ (GY15, 1999, Figure 4.42, lower left). The lowest values of chl_{a+b} measured were 19.08 $\mu g/cm^2$ (MD35, 1998, Figure 4.42, higher right) and 26.58 $\mu g/cm^2$ (MD33, 1999, Figure 4.42, lower right).

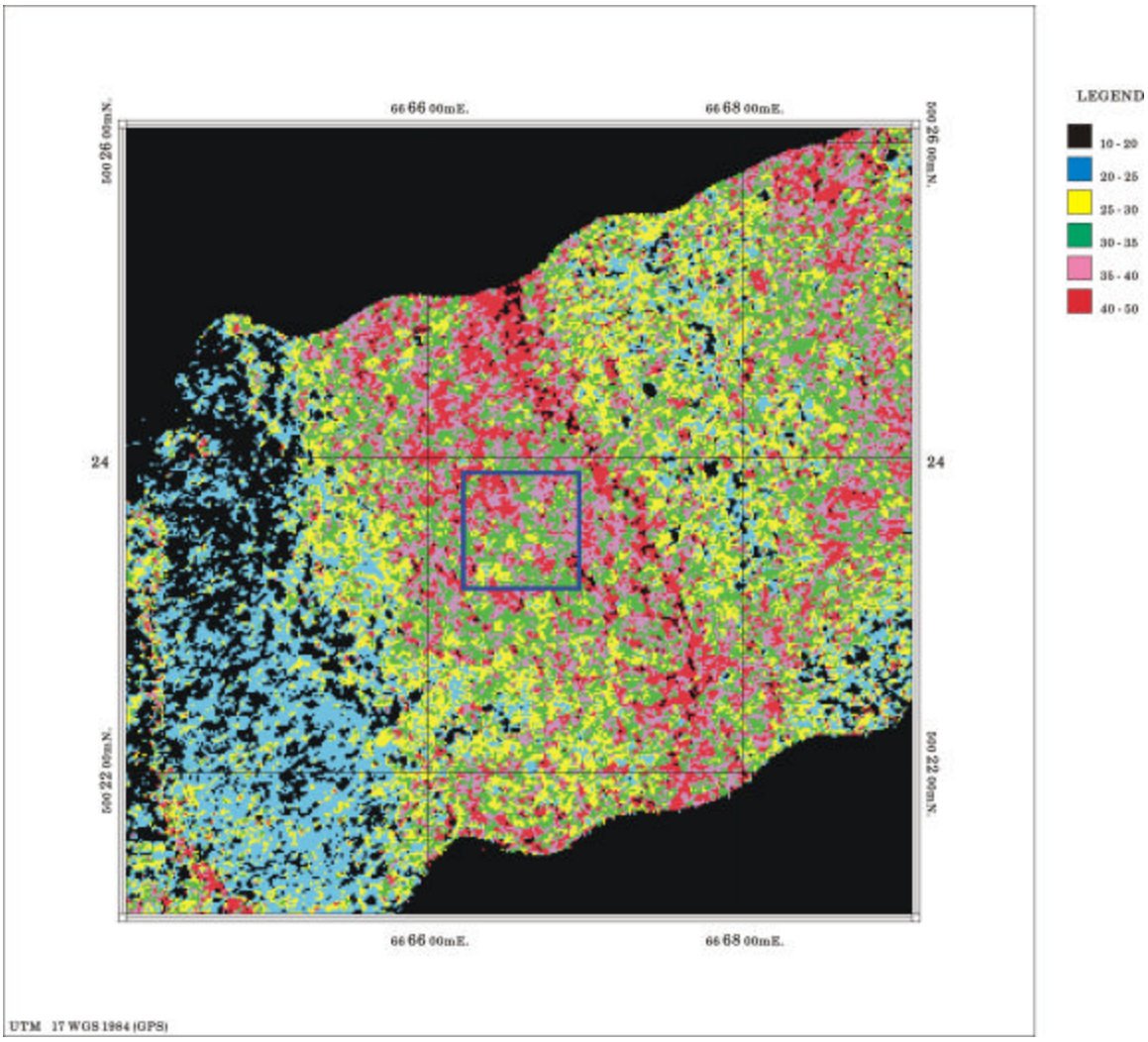

Figure 4.39. Estimation of chl_{a+b} from 72-channel CASI data of 0.86x3.4m resampled to 1.5x1.5m spatial-resolution over one of the study sites of *Acer saccharum* M. (MD67) that presented an average of 35.7 µg/cm^2 of chl_{a+b} measured on leaf samples collected from the plot (blue box). SAILH model (with input nominal structural and viewing geometry parameters calculated at the time of data collection) coupled with PROSPECT (N=1.4) were used to perform the estimations with R_{750}/R_{710} for the merit function. Six classes of chl_{a+b} (µg/cm^2) were considered: i) <20 (very low chlorophyll); ii) 20-25 (low chlorophyll); iii) 25-30 (below average); iv) 30-35 (average chlorophyll, usually healthy); v) 35-40 (average to above average chlorophyll, trees healthy); and vi) >40 (above average chlorophyll, trees healthy, but could be a sign of other factors).

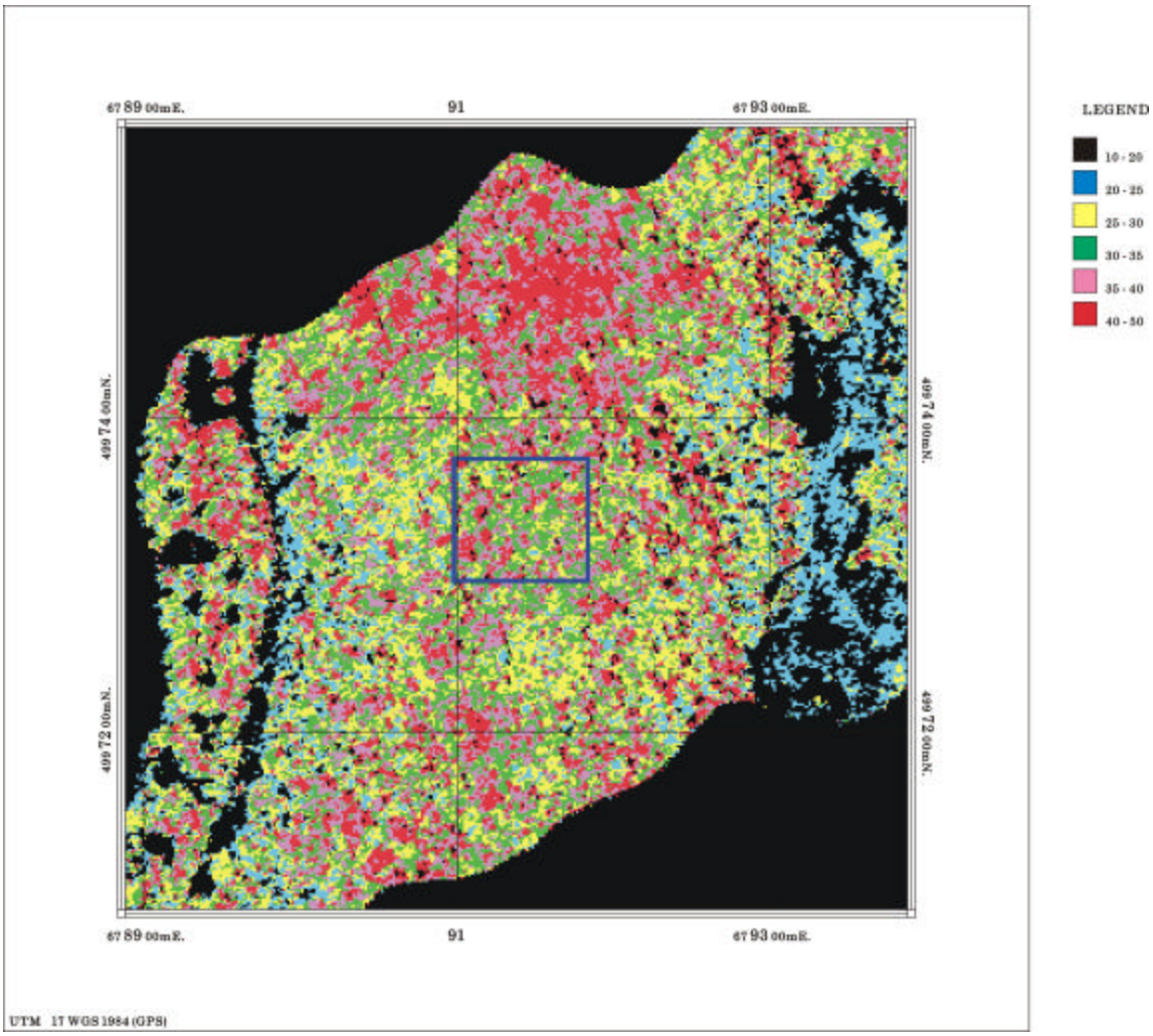

Figure 4.40. Estimation of chl_{a+b} from 72-channel CASI data of 0.86x3.4m resampled to 1.5x1.5m spatial-resolution over one of the study sites of *Acer saccharum* M. (MD65) that presented an average of 29.8 $\mu g/cm^2$ of chl_{a+b} measured on leaf samples collected from the plot (blue box). SAILH model (with input nominal structural and viewing geometry parameters calculated at the time of data collection) coupled with PROSPECT (N=1.4) were used to perform the estimations with R_{750}/R_{710} for the merit function. Six classes of chl_{a+b} ($\mu g/cm^2$) were considered: i) <20 (very low chlorophyll); ii) 20-25 (low chlorophyll); iii) 25-30 (below average); iv) 30-35 (average chlorophyll, usually healthy); v) 35-40 (average to above average chlorophyll, trees healthy); and vi) >40 (above average chlorophyll, trees healthy, but could be a sign of other factors).

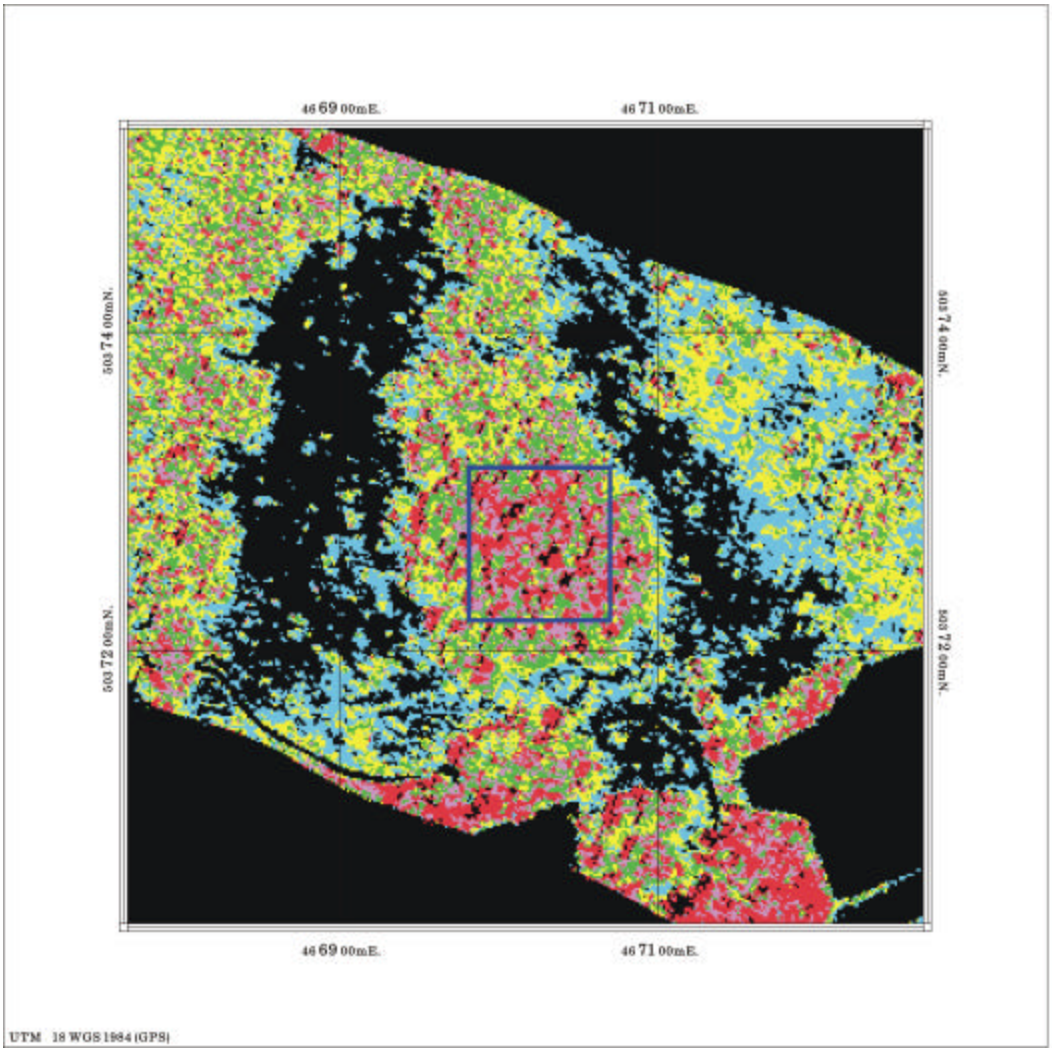

Figure 4.41. Estimation of chl_{a+b} from 72-channel CASI data of 0.86x3.4m resampled to 1.5x1.5m spatial-resolution over one of the study sites of *Acer saccharum* M. (ID40) that presented an average of 42.7 $\mu g/cm^2$ of chl_{a+b} measured on leaf samples collected from the plot (blue box). SAILH model (with input nominal structural and viewing geometry parameters calculated at the time of data collection) coupled with PROSPECT (N=1.4) were used to perform the estimations with R_{750}/R_{710} for the merit function. Six classes of chl_{a+b} ($\mu g/cm^2$) were considered: i) <20 (very low chlorophyll); ii) 20-25 (low chlorophyll); iii) 25-30 (below average); iv) 30-35 (average chlorophyll, usually healthy); v) 35-40 (average to above average chlorophyll, trees healthy); and vi) >40 (above average chlorophyll, trees healthy, but could be a sign of other factors).

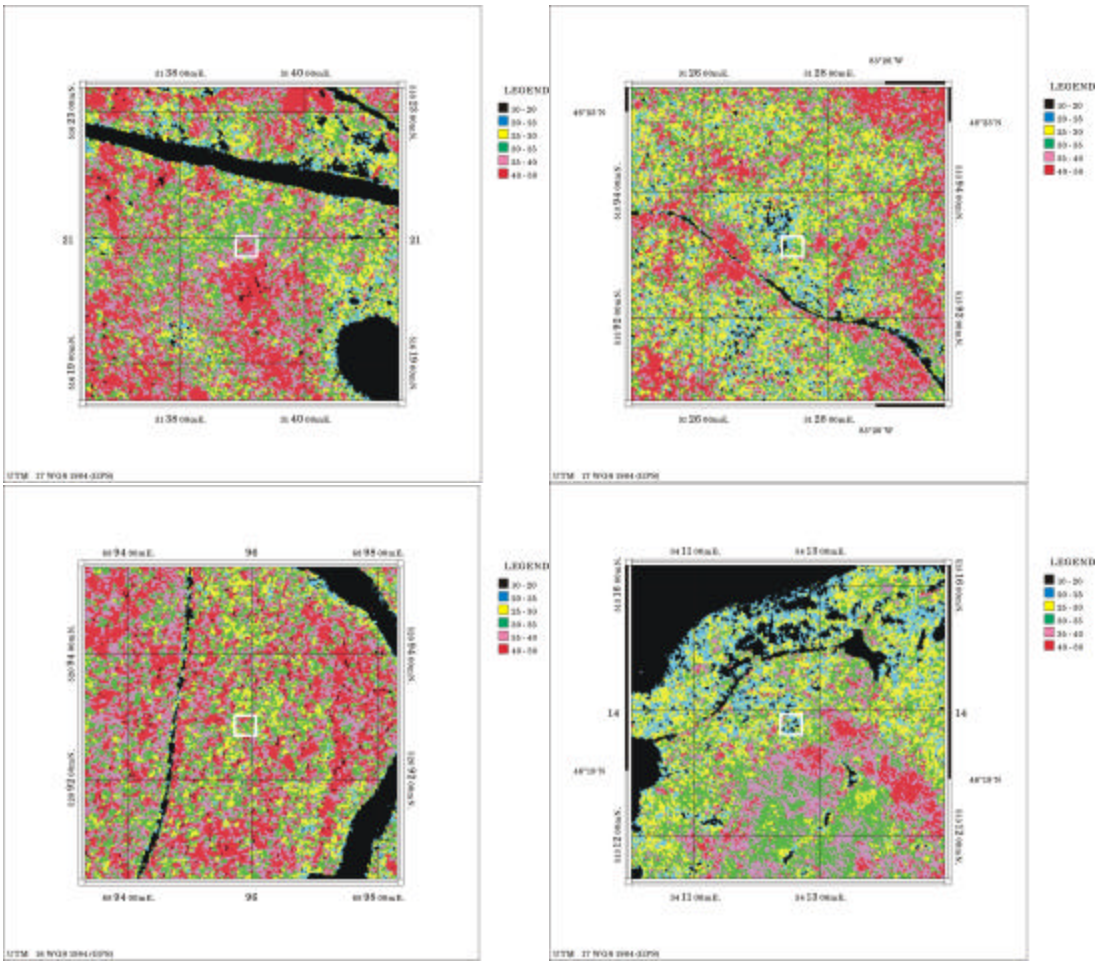

Figure 4.42. Chl_{a+b} estimation over the study areas (500x500m) that presented extreme values of chl_{a+b} measured in the field in 1998 (up) and 1999 (bottom) campaigns. The highest values of chl_{a+b} (left) were measured in leaf samples from GY41 (upper left, chl_{a+b} measured=38.8 μg/cm^2 in 1998) and GY15 (lower left, chl_{a+b} measured=45.8 μg/cm^2 in 1999). The lowest values of chl_{a+b} (right) were measured in leaf samples from MD35 (upper right, chl_{a+b} measured=19.08 μg/cm^2 in 1998) and MD33 (lower left, chl_{a+b} measured=26.58 μg/cm^2 in 1999). White box shows the study area of 20x20m where leaf sampling was carried out.

CHAPTER 5. CONCLUSIONS

The primary objective of this research was to study whether two indicators of stress in vegetation at the leaf level, chlorophyll fluorescence and chlorophyll content, can be predicted using airborne hyperspectral reflectance data. Radiative transfer theory and modelling assumptions were applied at leaf, laboratory and field scales in order to study the link between leaf reflectance and transmittance and canopy airborne hyperspectral data acquired with different spectral and spatial characteristics.

This dissertation demonstrates quantitatively, using both experimental and model simulation approaches, that leaf apparent reflectance is affected by chlorophyll fluorescence at leaf, laboratory and canopy levels. A set of laboratory experiments with *Acer saccharaum* M. leaves permitted the collection of leaf reflectance and transmittance using a Li-Cor integrating sphere attached to a fibre spectrometer, as well as CF measurements using a PAM-2000 Fluorometer. A measurement scheme was developed, consisting on a long-pass optical filter $\lambda > 695$ nm placed between the light source and the leaf sample to enable the separation of reflectance and transmittance measurements without fluorescence and including the effect of fluorescence.

A diurnal experiment was carried out, keeping chlorophyll content constant while CF was variable due to diurnal patterns. It showed that the reflectance difference at 740 nm followed the same pattern and correlated with Fv/Fm and steady-state fluorescence (r^2=0.66, Fv/Fm; r^2=0.54, Ft). A time-decay study using broad leaves illuminated for 5 minutes from a dark-adapted state showed differences in reflectance in the 690 and 750 nm regions, corresponding to CF bands. The variation of apparent reflectance at 690 and 755 nm with time after exposure showed behaviour similar to the Kautsky curve measured by the PAM-2000 Fluorometer.

The FRT (Fluorescence-Reflectance-Transmittance) model, based on Kubelka Munk theory, modified to include the addition of fluorescence flux, was presented here. It demonstrates that experimental results are theoretically consistent with CF expected as a superimposed signal on the leaf reflectance and transmittance spectral signatures. Model assessment shows that a theoretical basis exists for the relationships reported between CF and apparent reflectance at 690 and 750 nm. Reflectance differences at 750 nm calculated from leaves with constant chl_{a+b} and variable CF showed good correlation with modeled spectra using Fv/Fm as fluorescence efficiency (r^2=0.58).

The FRT model and the experiments with leaf samples with constant chl_{a+b} permitted a validation of optical indices that can track changes of CF through reflectance. Indices associated to changes at 690 and 750 nm were tested, such as R_{750}/R_{800} (r^2=0.75, Fv/Fm), for which correlation degrades with leaf-measured CF when leaf reflectance without

fluorescence is used (r^2=0.23, Fv/Fm). Indices in the 690 nm region showed good relationships with both dark-adapted Fv/Fm and steady-state fluorescence: R_{685}/R_{655} (r^2=0.85, Fv/Fm; r^2=0.75, Ft); R_{690}/R_{655} (r^2=0.86; Fv/Fm; r^2=0.76, Ft); and a curvature index using the hyperspectral CASI sensor bandset in the 72-channel mode $R_{683}^2/[R_{675}\cdot R_{691}]$ (r^2=0.77, Fv/Fm; r^2=0.65, Ft).

Canopy-reflectance optical indices from hyperspectral data related to chlorophyll fluorescence were studied at three different levels for diurnal trials: i) with canopies of seedlings in the laboratory under artificial light with the CASI hyperspectral sensor; ii) with the same small canopies under natural illumination with fibre spectrometer; and iii) with forest canopies and the airborne CASI sensor in diurnal experiments. Laboratory hyperspectral reflectance measurements from a canopy of maple seedlings verified a quantitative link between canopy reflectance and chlorophyll fluorescence when optical indices in the 680-690 nm region are used. Laboratory experiments using alternately a Schott blocking filter that cuts off the red light and a halogen lamp demonstrated that canopy reflectance is affected by photosystem II excitation. Diurnal variation of Fv/Fm in maple plant material was shown to be strongly correlated with indices in the 680-690 nm region, such as R_{685}/R_{655} and the curvature index $R_{683}^2/(R_{675}\cdot R_{691})$, among others. A time-decay experiment also showed at a laboratory level that canopy reflectance is affected by changes in chlorophyll fluorescence when dark-adapted plant material is illuminated with light over a 3-minute period. Consistency with previous experiments at leaf level and with theory using the FRT model is found when canopy optical indices are

calculated from stressed and healthy plant material at the laboratory level. It shows that indices from the 680-690 nm region are directly related to steady-state fluorescence Ft, Fm' and ΔF/Fm' measured with a PAM-2000 Fluorometer.

Diurnal trials under natural illumination using a fibre spectrometer over a canopy of seedlings produced positive results, showing that canopy reflectance is affected by diurnal variation of CF, and that such reflectance changes are measurable under natural illumination conditions. However, airborne experiments with the CASI hyperspectral sensor produced promising but inconclusive results in the diurnal experiments carried out in 1999 and 2000, in which small variations of reflectance due to the effect of CF were observed. Results from the 12 study sites in the two-year study showed that red edge and spectral and derivative indices show also the best relationships with CF, and other indices such as DP22 ($D_{\lambda p}/D_{720}$), DPR1 ($D_{\lambda p}/D_{\lambda p+12}$) (derivative indices), curvature index ($(R_{675} \cdot R_{690})/R_{683}^2$) (red edge), and PRI indices, in which changes at 530-550 nm region are consistent with photosynthetic radiation use efficiency changes described by other authors. The real applicability of these results in vegetation canopies depends on difficulties associated with the small changes in reflectance due to CF and the spectral regions where they occur, requiring a very accurate atmospheric correction. Measurements under natural illumination conditions were conclusive to whether CF effects in canopy apparent reflectance are measurable in diurnal trials, showing consistency of results at all levels of experimental study and modelling.

Work carried out to study chl_{a+b} estimation in closed forest canopies of *Acer saccharum* M. focussed on scaling-up and numerical model inversion approaches. In both cases, red edge and spectral and derivative indices consistently showed the best relationships in the three consecutive years, especially R_{750}/R_{710}, Vog1 (R_{740}/R_{720}), Vog2 (R_{734}-R_{747})/(R_{715}+R_{726}), Vog3 (R_{734}-R_{747})/(R_{715}+R_{720}), Vog4 (D_{715}/D_{705}), GM1 (R_{750}/R_{550}), GM2 (R_{750}/R_{700}) and Ctr2 (R_{695}/R_{760}) (red-edge indices), and λp, DP21 ($D_{\lambda p}/D_{703}$), and DP22 ($D_{\lambda p}/D_{720}$) (spectral and derivative indices). These results obtained at leaf level from leaf samples confirmed the strong link existing between leaf chlorophyll-*a*&*b*, and red edge and derivative indices calculated from leaf reflectance spectra. A methodology for linking leaf-level relationships between optical indices and pigment content to canopy-level reflectance was presented. It is demonstrated that leaf-level relationships calculated from single leaf reflectance and transmittance data collected from the ground can be scaled-up to above-canopy level through infinite reflectance and canopy reflectance models using nominal input parameters derived from the study areas. The three scales of study used in this research, through statistical relationships, infinite reflectance models, and through canopy reflectance models, progressively more closely represent the observed above-canopy reflectance spectra from the sites, showing improvements in the estimation of leaf-based physiological indicators. The high spatial resolution of the airborne hyperspectral CASI data permitted the selection of crowns, eliminating shadows and understorey, therefore allowing the use of SAILH and *Kuusk* turbid-medium canopy models.

Canopy structure was shown to play an important role in this link from leaf-level measurements to canopy-level hyperspectral data, affecting optical indices in different ways. A sensitivity study showed that low LAI values are very critical to the accuracy of predicted bioindicator regardless of the considered type of canopy. Differences between the predicted bioindicator using nominal canopy parameters and the prediction with variable θ_s and LADF is insignificant when LAI is higher than 3. Furthermore, the canopy type is irrelevant for the estimations when LAI is higher than 3 and the θ_s is a nominal 30°. It is shown that derivative indices are less sensitive to low LAI values than other optical indices, demonstrating that red edge and derivative indices are more suitable for bioindicator prediction and mapping with high spatial hyperspectral remote sensing data.

Relationships between canopy-modelled indices and chl_{a+b} were shown to be variable due to changes in leaf thickness and transmittance during the season. Relationships showed a larger change during the season when the index is calculated from a CR model, which is a function of both reflectance and transmittance. Model inversion of PROSPECT from reflectance and transmittance leaf data demonstrated changes in the N structural parameter during the season from leaf samples obtained from the study sites in the two consecutive years.

The results obtained in the scaling-up approach through canopy reflectance models and hyperspectral canopy reflectance from *Acer saccharum* M. study sites showed that

red-edge indices, specially λ_p and DP21, and spectral and derivative indices, such as R_{750}/R_{710}, Vog1 (R_{740}/R_{720}), G_M2 (R_{750}/R_{700}), Vog3 (R_{734}-R_{747})/(R_{715}+R_{720}), Vog2 (R_{734}-R_{747})/(R_{715}+R_{726}), Vog4 (D_{715}/D_{705}), G_M1 (R_{750}/R_{550}), Ctr2 (R_{695}/R_{760}) are the best optical indices for chl_{a+b} estimation at canopy level. Furthermore, traditional and widely used optical indices for pigment estimation and indicators of vegetation status, such as NDVI and SR, performed poorly in the two consecutive years: r=0.1, 1998; r=0.24, 1999 (NDVI), and r=0.05, 1998; r=0.22, 1999 (SR). These traditional indices primarily track canopy structural changes but are not able to track subtle changes due to pigment content variation between study sites. This demonstrates that canopies with homogeneous structure but different chlorophyll content need the use of red edge and spectral indices to estimate changes in pigment content.

The results obtained for chl_{a+b} estimation in closed *Acer saccharum* M. canopies used in this research with optically thick models, which don't need structural and viewing geometry as input parameters, therefore of much faster and easier applicability, demonstrated a predictive potential that was close, and for some indices, superior to canopy models. For all indices used, the RMSE significantly decreased when the optical indices were calculated using first R_∞ and then canopy reflectance models, showing that RMSE does not significantly improve when CR models are used. Furthermore, generally lower RMSE is found with $R_{\infty 2}$ and $R_{\infty 3}$ than with R_{SAILH} and R_{Kuusk}. From the three infinite reflectance models used, $R_{\infty 3}$ (Hapke) and $R_{\infty 2}$ (Yamada and Fujimura) are the ones achieving best estimations, suggesting that infinite reflectance models can be used

for canopy reflectance modelling in closed forest canopies of high LAI, performing as well as canopy reflectance models when crowns are targeted.

The scaling-up approach of optical indices through canopy models was compared to the numerical model inversion of coupled PROSPECT leaf radiative transfer model with SAILH, MCRM and infinite reflectance models, in which no leaf sampling is required to develop the statistical relationships. Results of the numerical model inversion by iteration showed that superior results were found when a methodology consisting of minimizing a function based in a red edge optical index was used, rather than by matching all the CASI channels in the visible and NIR. Results of SAILH and PROSPECT coupled model inversion using the red edge index R_{750}/R_{710} as a minimizing function by iteration shows comparable results to the scaling-up methodology, obtaining an order of r^2=0.57 and RMSE=12.48 $\mu g/cm^2$ (LAI=4) in 1999 campaign. It is demonstrated that minimizing functions based on single spectral channels obtain higher RMSE than a single optical index calculated in the red edge spectral region, such as R_{750}/R_{710}. Furthermore, results show that small effect is caused by shadows in the estimation of the chl_{a+b} when the red edge optical index R_{750}/R_{710} is used in the merit function: RMSE=5.57 $\mu g/cm^2$ (targeting crowns), RMSE=5.48 $\mu g/cm^2$ (all pixels including shadows) with SAILH and PROSPECT inversion using R_{750}/R_{710} in the merit function. A large effect is found when all reflectance channels are used in the minimizing function and shadows are included: RMSE=12 $\mu g/cm^2$ (targeting crowns), RMSE=23.1 $\mu g/cm^2$ (all pixels including shadows) with SAILH and PROSPECT inversion. This result might have important

implications, showing the value of red edge indices for both scaling-up and model inversion approaches in pigment estimation of closed canopies.

Results obtained in this research for three consecutive years, two of them with extensive leaf sampling campaigns, using a set of 12 *Acer saccharum* M. sites, were validated with a new set of 14 sites in order to test the conclusions. The successful validation campaign carried out in the summer of 2000 confirmed the hypothesis developed in previous years, obtaining comparable RMSE for chl_{a+b} estimation by numerical model inversion of coupled SAILH and PROSPECT models with nominal input parameters and R_{750}/R_{710} in the merit function. A special study was carried to simulate MERIS bands from the CASI 72-channel mode, and proposing R_{750}/R_{705} MERIS channels to be used for red edge index in the numerical model inversion. Successful and promising results were obtained, showing that R_{750}/R_{705} calculated from MERIS-equivalent spectra performs similarly to R_{750}/R_{710} used for estimations with CASI, obtaining r^2=0.44, and RMSE=3.0 $\mu g/cm^2$ (SAILH+PROSPECT, brightest 25% pixels), RMSE=3.97 $\mu g/cm^2$ (SAILH+PROSPECT, all pixels). These results suggest that methodologies investigated here based on pigment estimation by model inversion using red edge indices can be transferred to MERIS sensor to be launched by ESA, although the implication of the spatial heterogeneity of the forest landscape compared to the 300m sensor spatial resolution will need to be evaluated.

Results presented in this dissertation demonstrate the capability of hyperspectral sensors to map pigment content over closed canopies through radiative transfer models. The

assumptions made for the selection of turbid medium models in forest canopies are demonstrated to be valid with hyperspectral reflectance data of high spatial resolution, where the selection of crowns can be performed. Moreover, even when the spatial resolution does not allow for selection of the crown reflectance, therefore including increased contribution by openings and shadows, the use of spectral transforms from the red edge region in the merit function shows validity in forest canopies, minimizing such effects. Methodologies shown in this dissertation for closed canopies might be transferred to open canopies with the use of specific canopy reflectance models for simulation of the architecture in the canopy reflectance. In addition, for general applicability, the potential improvements through inversions of LAI merit study. On the other hand, turbid medium models could be valid when off-nadir viewing geometry is used for reflectance measurements to decrease openings, allowing this simpler approach to be used.

Furthermore, evidence is shown that hyperspectral sensors may offer a means to track changes in solar-induced fluorescence in vegetation canopies, as demonstrated at all levels of study carried out along the present research work described in this manuscript.

References

Abuelgasim, A.A., Gopal, S. and Strahler, A.H. (1998), Forward and inverse modelling of canopy directional reflectance using a neural network, *International Journal of Remote Sensing.* 19: 453-471.

Ahern, F.J. (1988), The effects of bark beetle stress on the foliar spectral reflectance of lodgepole pine, *Int. J. Remote Sens.* 9:1451-1468.

Allen, W. A. and Richardson, A. J. (1968), Interaction of light with a plant canopy, *Journal of the Optical Society of America.* 58**:**1023-1028.

Allen, W.A., Gausman, H.W., Richarson, A.J., and Thomas, J.R. (1969), Interaction of isotropic light with compact plan leaf, *J. Optic. Soc. Amer.* 59 (10): 1376-1379.

Allen, W.A., Gayle and Richarson A.J. (1970), Plant canopy irradiance specified by the Duntley equations, *J. Opt. Soc. Am.* 60(3):372-376.

Anon. (1993), A master plan to examine forest growth and dynamics in Ontario. Ont. Min. Nat. Resour., Ont. For. Res. Inst., Sault Ste. Marie, Ont. 68 p.

Barnes, J.D. (1992), A reappraisal of the use of DMSO for the extraction and determination of chlorophylls *a* and *b* in lichens and higher plants, *Environmental Experimental Botany.* 2,85-100.

Bicheron, P., Leroy, M., and Hautecoeur, O. (1998),LAI and fAPAR mapping at global scale by model inversion against spaceborne POLDER data, in *IGARSS'98 Seattle (Washington).*

Blackburn, G.A., and Steele, C.M., (1999), Towards the Remote Sensing of Matorral Vegetation Physiology: Relationships between Spectral Reflectance, Pigment, and Biophysical Characteristics of Semiarid Bushland Canopies, *Remote Sensing of Environment*. 70:278-292.

Braswell, B.H., Schimel, D.S., Privette, J.L., Moore, III, B.M., Emery, W.J., Sulzman, E.W., and Hudak, A.T., (1996),Extracting ecological and biophysical information from AVHRR optical data: An integrated algorithm based on inverse modeling, *Journal of Geophysical Research.* 101(D18):23335-23348.

Breece, H.T., Holmes, R.A., (1971), Bidirectional Scattering Characteristics of Healthy Green Soybean and Corn Leaves *Vivo, Appl. Opt.* 10:119-127.

Butler, W. L. and Kitajima, M. (1975), Fluorescence quenching in photosystem II of chloroplasts, *Biochim. Biophys. Acta.* 376**:**116-125.

Canadian Council of Forest Ministers. (1995), Defining sustainable forest management: A Canadian approach to criteria and indicators. Can. For. Serv., Nat. Resour. Can., Ottawa, ON.

Carter, G.A. (1991), Primary and secondary effects of water content of the spectral reflectance of leaves, *Am. J. Bot.* 78:916-924.

Carter, G.A. (1993), Responses of leaf spectral reflectance to plant stress, *Am. J. Bot. 80:*239-243.

Carter, G. A. (1994), Ratios of leaf reflectances in narrow wavebands as indicators of plant stress, *International Journal of Remote Sensing.* 15**:**697-704.

Chandrasekhar, S., (1950), *Radiative Transfer.* Oxford: Clarendon Press.

Chang, S. and Collins, W. (1983), Confirmation of the airborne biogeophysical mineral exploration technique using laboratory methods, *Economic Geology*. 1983**:**723-736.

Chappelle, E. W., Kim, M. S. and McMurtrey, J. E. I. (1992), Ratio analysis of reflectance spectra (RARS): an algorithm for the remote estimation of the concentrations of chlorophyll *a*, chlorophyll *b*, and carotenoids in soybean leaves, *Remote Sensing of Environment*. 39**:**239-247.

Chen, J.M. (1996), Evaluation of Vegetation Indices and a Modified Simple Ratio for Boreal Application, *Canadian Journal of Remote Sensing*. 22:229-242.

Chow, G.C. (1960), Tests of equality between sets of coefficients in two linear regressions, *Econometrica*, Vol. 28 (3), pp.591-605.

Curran, P.J. (1983), Estimating Green LAI from Multispectral Aerial Photography, *Photogrammetric Engineering and Remote Sensing*. 49:1709-1720.

Curran, P.J., Dungan, J.L., Macler, B.A., Plummer, S.E., and Peterson, D.L. (1992), Reflectance Spectroscopy of French Whole Leaves for the Estimation of Chemical Concentration, Elsevier Science Publishing Co Inc. New York.

Czapla-Myers, J. (2000), Spectral Bandwidth Characterization Methodologies for Imaging Spectrometers, February 2000 *M.Sc. Thesis, Graduate Program in Earth and Space Science, York University, Toronto.*

Dawson, T. P., Curran, P. J. and Plummer, S. E. (1998), LIBERTY-Modeling the effects of leaf biochemical concentration on reflectance spectra, *Remote Sensing of Environment.* 65**:**50-60.

Demarez, V., Gastellu-Etchegorry, J.P. Mougin, E., Marty, G., Proisy, C., Dufrene, E., and Le Dantee, V. (1999), Seasonal variation of leaf chlorophyll concentration through PROSPECT inversion, *International Journal of Remote Sensing,* 20(5):879-894.

Demarez, V., and Gastellu-Etchegorry, J.P., (2000), A Modeling Approach for Studying Forest Chlorophyll Content, *Remote Sensing of Environment*, 71:226-238.

Demetriades-Shah, T. H., Steven, M. D. and Clark, J. A. (1990), High resolution derivative spectra in remote sensing, *Remote Sensing of Environment.* 33**:**55-64.

Duntley, S.Q., (1942), The optical properties of diffusing materials, *J. Opt. Soc. Am.* 32(2): 61-70.

Enke, C. G. and Nieman, T. A. (1976), Signal-to-noise ratio enhancement by least-squares polynomial smoothing, *Analytical Chemistry.* 48**:**705A-712A.

Farabee, M.J., (1997), Photosynthesis, http://gened.emc.maricopa.edu/bio/bio181/BIOBK/BiobookPS.html

Filella, I. and J. Peñuelas, (1994), The red edge position and shape as indicators of plant chlorophyll content, biomass and hydric status, *Int. J. Remote Sensing*. 15-7:1459-1470.

Filella, I., Amaro, T., Araus, J.L., and Peñuelas, J. (1996), Relationship between photosynthetic radiation-use efficiency of barley canopies and the photochemical reflectance index (PRI), *Physiologia Plantarum.* 96: 211-216.

Fourty, T., Baret, F., Jacquemoud, S., Schmuck, G. and Verdebout, J. (1996), Leaf optical properties with explicit description of its biochemical composition: direct and inverse problems, *Remote Sensing of the Environment.* 56**:**104-117.

Fukshansky, L. and Kararinova, N. (1980), Extension of the Kubelka-Munk theory of light propogation in the intensely scattering materials to fluorescent materials, *Journal of the Optical Society of America.* 70**:**1101-1111.

Fukshansky, L., Fukshansky-Kazarinova, N. and Remisowsky, A. M. V. (1991), Estimation of optical parameters in a living tissue by solving the inverse problem of the multiflux radiative transfer, *Applied Optics.* 30**:**3145-3153.

Gamon, J.A., Field, C.B., Bilger, W., Björkman, O., Fredeen, A.L., and Peñuelas, J., (1990), Remote sensing of the xanthophyll cycle and chlorophyll fluorescence in sunflower leaves and canopies, *Oecologia.* 85:1-7.

Gamon, J.A., Peñuelas, J., and Field, C.B., (1992), A narrow-waveband spectral index that tracks diurnal changes in Photosynthetic Efficiency, *Remote Sens. Environ*. 41:35-44.

Gamon, J. A., Serrano, L. and Surfus, J. S. (1997), The photochemical reflectance index: An optical indicator of photosynthetic radiation-use efficiency across species, functional types, and nutrient levels, *Oecologia.* 112:492-501.

Gamon, J. A. and Surfus, J. S. (1999), Assessing leaf pigment content and activity with a reflectometer, *New. Phytol.* 143**:**105-117.

Ganapol, B.D., Johnson, L.F., Hammer, P.D., Hlavka, C.A. and Peterson, D.L. (1998), LEAFMOD: a new within-leaf radiative transfer model, *Remote Sens. Environ.* 63:182-193.

Ganapol, B.D., Johnson, L.F., Hlavka, C.A., Peterson, D.L., and Bond, B. (1999), LCM2: A coupled Leaf/Canopy radiative transfer model, *Remote Sens. Environ.* 70:153-166.

Gausman, H.W., Allen, W.A., Cardenas, R. and Richarson, A.J. (1970), Relation of light reflectance to histological and physical evaluations of cotton leaf maturity, *Appl. Optic.* 9:545-552.

Genty, B., Briantais, J. M. and Baker, N. R. (1989), The relationship between the quantum yield of photosynthetic electron transport and quenching of chlorophyll fluorescence, *Biochim. Biophys. Acta*. 990**:**87-92.

Gitelson, A. A. and Merzlyak, M. N. (1996), Signature Analysis of Leaf Reflectance Spectra: Algorithm Development for Remote Sensing of Chlorophyll, *Journal of Plant Physiology.* 148**:**494-500.

Gitelson, A. A. and Merzlyak, M. N. (1997), Remote estimation of chlorophyll content in higher plant leaves, *International Journal of Remote Sensing.* 18**:**2691-2697.

Gitelson, A. A., Buschman, C., and Lichtenthaler, H. K., (1999), The chlorophyll fluorescence ratio F735/F700 as an accurate measure of chlorophyll content in plants, *Remote Sensing of Environment.* 69:296-302.

Goel, N.S., (1988), Models of Vegetation Canopy Reflectance and their Use in Estimation of Biophysical Parameters from Reflectance Data, *Remote Sensing Reviews*, 4:1-212.

Goel, N. S. and Thompson, R. L. (2000), A sanpshot of canopy reflectance models and a universal model for the radiation regime, *Remote Sensing Reviews*, in Press.

Govindjee (1995), Sixty-three years since Kautsky: Chlorophyll a fluorescence, *Aust. J. Plant Physiol.* 22**:**131-160.

Goward, S.N., Tucker,C.J., and Dye,D.G., (1985), North American vegetation patterns observed with the NOAA-7 advanced very high resolution radiometer, *Vegetation.* 64:3-14.

Gray, L., Freemantle, J., Shepherd, P., Miller, J., Harron, J. and Hersom, C. (1997), Characterization and calibration of the CASI airborne imaging spectrometer for BOREAS, *Canadian Journal of Remote Sensing.* 23**:**188-195.

Guenther, A., (1993), Natural volatile organic compound emission rate estimates for U.S. woodland landscapes, *Am. J. Bot.* 80:239-243.

Guyot, G. (1990), Optical properties of vegetation canopies. In Applications of Remote Sensing in Agriculture, edited by M.D. Steven and J.A. Clark (London: Butterworths) pp.19-44.

Hapke, B. (1993), *Theory of Reflectance and Emittance Spectroscopy*, Cambridge University Press.

Harron, J. W. and Miller, J. R. (1995), An alternate methodology for reflectance and transmittance measurements of conifer needles, In *17th Canadian Symposium on Remote Sensing*, Saskatoon, Saskatchewan, Vol. II, pp. 654-661.

Hayden, J., Kerley, J., Carr, D., Kenedi, T. and J. Hallarn. (1995), Field manual for establishing and measuring permanent sample plots. Ont. Min. Nat. Resour., Ont. For. Res. Inst., Sault Ste. Marie, Ont. 161 p.

Heinz-Walz-GmbH, (1993), Portable *Fluorometer* PAM-2000 and data acquisition software DA-2000, *Effeltrich, Germany.*

Horler, D. N. H., Barber, J. and Barringer, A. R. (1980), Effects of heavy metals on the absorbance and reflectance spectra of plants. *International Journal of Remote Sensing.* 1**:**121-136.

Horler, D.N.H., Dockray M., and Barber J., (1983), The red edge of plant leaf reflectance, *Int. J. Remote Sens.* 4(2):273-288.

Huete, A., and Justice, C., (1999), MODIS Vegetation Index (MOD 13) Algorithm Theoretical Basis Document, Greenbelt: NASA Goddard Space Flight Centre, http://modarch.gsfc.nasa.gov/MODIS/LAND/#vegetation-indices, 129pp.

Hunt E.R. and Rock, B.N., (1987), Measurement of leaf relative water content by infrared reflectance, Remote Sens. Environ., 22:429-435.

Ishimaru, A., (1978), Wave Propagation and Scattering in Random Media *Vol. 2. Multiple Scattering, Turbulence, Rough Surfaces, and Remote Sensing.* New York: Academic Press.

Jackson, R.D., Reginato, R.T., Printer, P.J., and Idso, S.B., (1979), Plant Canopy Information Extraction from Composite Scene Reflectance of Row Crops, *Appl. Opt.* 18:3775-3782.

Jacquemoud, S. (1993), Inversion of the PROSPECT+SAIL canopy reflectance model from AVIRIS equivalent spectra: theoretical study, *Remote Sensing of Environment.* 44**:**281-292.

Jacquemoud, S. and Baret, F. (1990), Prospect: A model of leaf optical properties spectra, *Remote Sensing of Environment*. 34**:**75-91.

Jacquemoud, S., Baret, F., Andrieu, B., Danson, F. M. and Jaggard, K. (1995), Extraction of vegetation biophysical parameters by inversion of the PROSPECT+SAIL models on sugar beet canopy reflectance data. Application to TM and AVIRIS sensors, *Remote Sensing of Environment.* 52**:**163-172.

Jacquemoud, S., Ustin, S. L., Verdebout, J., Schmuck, G., Andreoli, G. and Hosgood, B. (1996), Estimating leaf biochemistry using the PROSPECT leaf optical properties model, *Remote Sens. Environ.* 56**:**194-202.

Jacquemoud, S., Bacour, C., Poilve, H. and Frangi, J.P., (2000), Comparison of four radiative transfer models to simulate plant canopies reflectance–Direct and inverse mode, *Remote Sensing of Environment*, in Press.

Jahnke, L.S. and Lawrence, D.B. (1965), Influence of Photosynthetic Crown Structure on Potential Productivity of Vegetation, Based Primarily on Mathematical Models, *Ecology*, 46:319-326.

Jensen, J.R. (2000), Remote Sensing of the Environment, an earth resource perspective. Toronto: Prentice-Hall Canada, Inc.

Johnson, L. F., Hlavka, C. A. and Peterson, D. L. (1994), Multivariate analysis of AVIRIS data for canopy biochemical estimation along the Oregon transect, *Remote Sensing of Environment.* 47**:**216-230.

Kawata, S. and Minami, S. (1984), Adaptive smoothing of spectroscopic data by a linear mean-square estimation, *Applied Spectroscopy.* 38**:**49-58.

Knipling E.B. (1969), Leaf reflectance and image formation on colour infrared film, in Remote Sensing in Ecology (P.O. Johnson, Ed), University of Georgia, Athens, pp. 17-29.

Krause, G. H. and Weis, E. (1984), Chlorophyll fluorescence as a tool in plant physiology. II. Interpretation of fluorescence signals, *Photosynthesis Res.* 5**:**139-157.

Kubelka, P. and Munk, F., (1931), Ein Beitrag zur Optik der Farbanstriche, *Ann. Techn. Phys.* 11: 593-610.

Kupiec, J. A. and Curran, P. J. (1995), Decoupling effects of the canopy and foliar biochemicals in AVIRIS spectra, *Int. Journal of Remote Sensing.* 16**:**1731-1739.

Kuusk, A., (1985), The hot spot effect of a uniform vegetative cover, *Sov. Journal of Remote Sensing.* 3:645-658.

Kuusk, A., (1991), Determination of vegetation canopy parameters from optical measurements, *Remote Sens. Environ.* 37: 207-218.

Kuusk, A. (1995a), A Markov chain model of canopy reflectance, *Agricultural and Forest Meteorology*. 76:221-236.

Kuusk, A. (1995b), A fast, invertible canopy reflectance model. *Remote Sensing of Environment*, 51:342-350.

Kuusk, A. (1996), A computer-efficient plant canopy reflectance model, *Computers & Geosciences.* 22**:**149-163.

Kuusk, A. (1998), Monitoring of vegetation parameters on large areas by the inversion of a canopy reflectance model, *International Journal of Remote Sensing.* 19**:**2893-2905.

Larcher, W. (1994), Photosynthesis as a tool for indicating temperature stress events, In *Ecophysiology of photosynthesis*, (Schulze, E. D. and Caldwell, M. M., Ed.), Springer, Berlin, pp. 261-277.

Li, X., and Strahler, A.H., (1986), Geometrical-Optical Bidirectional Reflectance Modeling of a Conifer Forest Canopy, *IEEE Trans. Geosci. Remote Sensing.* GE-24 906-919.

Li, X., and Strahler, A.H., (1992), Geometric-optical bidirectional Reflectance modeling of the Discrete-Crown Vegetation Canopy: Effect of Crown Shape and Mutual Shadowing, *IEEE Trans. Geosci. Remote Sensing.*, 30:276-292.

Li, X., Strahler, A.H., and Woodcock, C.E. (1995), A hybrid geometric optical-radiative transfer approach for modeling albedo and directional reflectance of discontinuous canopies, *IEEE Trans. Geosci. Remote Sens.* 33:466-480.

Lichtenthaler, H.K., (1988), Applications of Chlorophyll Fluorescence in Photosynthesis Research, Stress Physiology, Hydrobiology and Remote Sensing. The Netherlands: Kluwer Academic Publishers.

Lichtenthaler, H. K. and Rinderle, U. (1988), The role of chlorophyll fluorescence in the detection of stress conditions in plants, *CRC Crit. Rev. Anal. Chem.* 19 (Suppl. 1)**:**529-585.

Lichtenthaler, H. K. (1992), The Kautsky effect: 60 years of chlorophyll fluorescence induction kinetics, *Photosynthetica.* 27**:**45-55.

Li-Cor-Inc. (1983), 1800-12 Integrating Sphere Instruction Manual, Publication Number 8305-0034.

Lillestaeter, O. (1982), Spectral reflectance of partly transmitting leaves: Laboratory measurements and mathematical modelling, *Remote Sensing of the Environ.* 12**:**247-254.

Lorenzen, B., and Jensen, A. (1989), Changes in leaf spectral properties induced in barley by cereal powdery mildew, *Remote Sensing of Environ.* 27: 201-209.

Madden, H. H. (1978), Comments on the Savitzky-Golay convolution method for least-squares fit smoothing and differentiation of digital data, *Analytical Chem.* 50**:**1383-1386.

Marchand, P. and Marmet, L. (1983), Binomial smoothing filter: a way to avoid some pitfalls of least-squares polynomial smoothing, *Rev. Sci. Instrum.* 54**:**1034-1041.

Matson, P., Johnson, L., Billow, C., Miller, J. and Pu, R. (1994), Seasonal patterns and remote spectral estimation of canopy chemistry across the Oregon transect, *Ecological Applications.* 4**:**280-298.

McLaughlin D.L., Corrigan, D.E., and McIlveen, W.D. (1992), Etiology of sugar maple decline at selected sites in Ontario (1984-1990). Ontario Ministry of the Environment, Report No. ARB-052-92-PHYTO, ISBN 0-7729-9344-0.

McLaughlin, D.L., Kinch, J.C., Liljalehto, H., and Boysen, E. (1999), Hardwood forest health surveys in Ontario - the first 10 years. Ontario Ministry of Environment and Energy, Ontario Ministry of Natural Resources, in press.

Miller, J.R., Wu, J. Boyer, M.Y., Belanger, M., and Hare, E.W., (1991), Seasonal patterns in leaf reflectance red-edge characteristics, *Int. J. Remote Sensing.* 12(7) 1509-1523.

Miller, J. R., Steven, M. D. and Demetriades-Shah, T. H. (1992), Reflection of layered bean leaves over different soil backgrounds: measured and simulated spectra, *International Journal of Remote Sensing.* 13**:**3273-3286.

Miller, J., Freemantle, J., Shepherd, P., Gray, L., O'Neill, N., Royer, A. and Senese, E. (1995), Deployment of CASI to meet the needs of BOREAS science, *Proceedings of 17th Canadian Symposium on Remote Sensing*, Saskatoon, Saskatchewan, pp. 169-175.

Mohammed, G. H., Binder, W. D., and Gillies, S. L., (1995), Chlorophyll fluorescence: A review of its practical forestry applications and instrumentation, *Scand. J. For. Res.* 10**:**383-410.

Mohammed, G.H. (1997), The status and future of stock quality testing, *New For.* 13:491-514.

Mohammed, G.H., Noland, T. L., Parker, W. C., and Wagner, R. G. (1997a), Pre-planting physiological stress assessment to forecast field growth performance of jack pine and black spruce, *For. Ecol. Manage.* 92:107-117.

Mohammed, G. H., Sampson, P. H., Colombo, S. J., Noland, T. L., and Miller, J. R., (1997b), Bioindicators of forest sustainability: Development of a forest condition rating system for Ontario project strategy, Report 137, Ontario Forest Research Institute, Sault Ste. Marie, ON.

Ni, W., Li, X., Curtis, E., Caetano, M., and Strahler, A.H., (1999), An Analytical Hybrid GORT Model for Bidirectional Reflectance Over Discontinuous Plant Canopies, *IEEE Transactions on Geoscience and Remote Sensing*. 37(2): 987-999.

O'Neill, N. T., Zagolski, F., Bergeron, M., Royer, A., Miller, J. R. and Freemantle, J. (1997), Atmospheric correction validation of casi images acquired over the BOREAS Southern Study Area, *Canadian Journal of Remote Sensing.* 23**:**143-162.

Ontario Ministry of Natural Resources (1994), Class environmental assessment for timber management on crown land in Ontario: Terms and conditions. Toronto, ON.

Papageorgiou, G. (1975), Chlorophyll fluorescence: An intrinsic probe of photosynthesis, In *Bioenergetics of Photosynthesis*, Govindjee, ed., Academic Press, New York, pp. 319-371.

Park, J.K., and Deering, D.W., (1982), Simple Radiative Transfer Model for Relationships between Canopy Biomass and Reflectance, *Appl. Opt.* 21: 301-309.

Peñuelas, J., Filella, I., Lloret, P., Muñoz, F., Vilajeliu, M., (1992), Remotely measured canopy temperature of greenhouse strawberries as indicator of water status and yield

under mild and very mild water stress conditions, *Agricultural and Forest Meteorology*, 58:63-77.

Peñuelas, J., Gamon, J.A., Fredeen, A.L., Merino, J., and Field, C.B., (1994), Reflectance indices associated with physiological changes in nitrogen- and water-limited sunflower leaves, *Remote Sensing of Environ*. 48:135-146.

Peñuelas, J., Filella, I., Lloret, P., Muñoz, F., and Vilajeliu, M., (1995), Reflectance assessment of mite effects on apple trees, *Int. J. Remote Sensing.* Vol. 16-14: 2727-2733.

Peñuelas, J., Llusia, J., Piñol, J. and Filella, I. (1997), Photochemical reflectance index and leaf photosynthetic radiation-use-efficiency assessment in Mediterranean trees, *International Journal of Remote Sensing.* 18**:**2863-2868.

Peñuelas, J., Filella, I., Llusia, J., Siscart, D. and Pinol, J. (1998), Comparative field study of spring and summer leaf gas exchange and photobiology of the mediterranean trees *Quercus ilex* and *Phillyrea latifolia*, *J. Exp. Bot.* 49**:**229-238.

Peterson, D. L., Aber, J. D., Matson, P. A., Card, D. H., Swanberg, N., Wessman, C. and Spanner, M. (1988), Remote sensing of forest canopy and leaf biochemical contents, *Remote Sensing of Environment.* 24**:**85-108.

Pragnère, A., Baret, F., Weiss, M., Myneni, R.B., Knyazikhin, Y., Wang, L.B., (1999), Comparison of three radiative transfer model inversion techniques to estimate canopy biophysical variables from remote sensing data, in: *Proceeding of the International Geoscience and Remote Sensing Symposium (IGARSS'99),* Hamburg, Germany.

Rock, B. N., Hoshizaki, T., and Miller, J. R. (1988), Comparison of In Situ and airborne spectral measurements of the blue shift associated with forest decline, *Remote Sens. of Environment*. 24**:**109-127.

Rosema, A., Verhoef, W., Schroote, J. and Snel, J. F. H. (1991), Simulating fluorescence light-canopy interaction in support of laser-induced fluorescence measurements, *Remote Sensing of Environment.* 37**:**117-130.

Rouse, J.W., (1974), Monitoring the vernal advancement of retrogradation of natural vegetation, NASA/GSFC, Type III, Final Report Greenbelt, MD, 371 pp.

Running, S.R., and Nemani, R.R. (1988), Relating seasonal patterns of the AVHRR vegetation index to simulate photosynthesis and transpiration of forests in different climates, *Remote Sens. Environ.* 24: 347-367.

Running, S.W., Justice C.O., Solomonson, V., Hall, D., Barker, J., Kanfmann, Y.J., Strahler, A.H., Huete, A.R., Muller, J.P., Vanderbilt, V., Wan, Z.M., Teilletland, P. and

Carneggie, D., (1994), Terrestrial Remote Sensing and Algorithms Planned for EOS/MODIS, *International Journal of Remote Sensing*, 15(17):3587-3620.

Sampson, P.H., Templeton, C.W.G., and Colombo, S.J., (1997), An overview of Ontario's Stock Quality Assessment Program, *New. For.* 13: 469-487.

Sampson, P. H., Mohammed, G. H., Colombo, S. J., Noland, T. L., Miller, J. R., Zarco-Tejada, P. J. (1998), Bioindicators of forest sustainability progress report, Report 142, Ontario Forest Research Institute, Sault Ste. Marie, ON.

Savitzky, A. and Golay, M. J. E. (1964), Smoothing and differentiation of data by simplified least squares procedures, *Analytical Chem.* 36**:**1627-1639.

Schreiber, U. and Bilger, W. (1987), Rapid assessment of stress effects on plant leaves by chlorophyll fluorescence measurements, In *Plant response to stress*, (Tenhunen, J. D. and Catarino, E. M., Ed.), Springer-Verlag, Berlin, Germany, pp. 27-53.

Schreiber, U. and Bilger, W. (1993), Progress in chlorophyll fluorescence research: Major development during the past years in retrospect, *Progress in Botany*. 54**:**151-173.

Schreiber, U., Bilger, W. and Neubauer, C. (1994), Chlorophyll fluorescence as a non-destructive indicator for rapid assessment of in vivo photosynthesis, *Ecol. Stud.* 100**:**49-70.

Sellers, P.J., (1987), Canopy reflectance, photosynthesis, and transpiration. II. The role of biophysics in the linearity of their interdependence, *Remote Sensing of Environ*. 21:143-183.

Sellers, P.J., (1989), Vegetation-canopy spectral reflectance and biophysical processes. *Theory and applications of optical remote sensing*, 8:297-333. Wiley, United States.

Smith, J.A. (1993), LAI inversion using back propagation neural network trained with multiple scattering model, *IEEE Transactions on Geoscience and Remote Sensing.* 31:1102-1106.

Soffer, R. (1996), Bidirectional reflectance factors of an open tree canopy by laboratory simulation. *M.Sc. Thesis, Graduate Program in Earth and Space Science, York University, Toronto,* 204pp.

Stokes, G.G., (1862), On the intensity of the light reflected from or transmitted through a pile of plates, Proc. Roy. Soc. (London) 11, 545.

Strahler, A.H., and Jupp, D.L.B., (1990), Modeling bidirectional reflectance of forest and woodlands using Boolean models and geometric optics, *Remote Sens. Environ.* 34: 153-160.

Subhash, N. and Mohanan, C. N. (1997), Curve-fit analysis of chlorophyll fluorescence spectra: Application to nutrient stress detection in sunflower, *Remote Sens. Environ.* 60**:**347-356.

Suits, G.H., (1972a), Azimuthal Variation in Directional Reflectance of Vegetative Canopies, *Remote Sens. Environ.* 2:175-182.

Suits, G.H., (1972b), Prediction of Directional Reflectance of a Corn Under Stress. 4th Annual ER. Program Review, Jan. 17-21, 11 pp.

Suits, G.H., (1972c), The calculation of the Directional Reflectance of Vegetative Canopy, *Remote Sens. Environ.* 2:117-125.

Suits, G.H. and Safir, G. (1972), Verification of a Reflectance Model for Mature Corn with Application to Corn Blight Detection, *Remote Sens. Environ.* 2:183-192.

Taiz, L. and Zeiger, E. (1998), *Plant Physiology*, 2nd Edition, Sinauer Associates Ltd., Sunderland, Massachusetts.

Templeton, C.W.G. and Colombo S.J., (1995), A portable system to quantify seedling damage using stress-induced volatile emissions, *Can. J. For. Res.* 25:682-686.

Terjung, W.H. and Louie, S.S.F., (1972), Potential Solar Radiation on Plant Shapes, *Int. J. Biometeor.* 16:25-43.

Tsai, F. and Philpot, W. (1998), Derivative analysis of hyperspectral data, *Remote Sensing of Environment.* 66**:**41-51.

Van Kooten, O. and Snel, J. F. H. (1990), The use of chlorophyll fluorescence nomenclature in plant stress physiology, *Photos. Res.* 25**:**147-150.

Verhoef, W., (1984), Light scattering by leaf layers with application to canopy reflectance modelling: the SAIL model, *Remote Sensing of Environment*. 16:125-141.

Verhoef, W. (1998), Theory of radiative transfer models applied in optical remote sensing of vegetation canopies. Wageningen: Grafisch Service Centrum Van Gils.

Verhoef, W. and Bunnik, N.J.J. (1981), Influence of crop geometry on multispectral reflectance determined by the use of canopy reflectance models, *Proc. Int. Colloquium on Spectral Signatures of Objects in Remote Sensing*, Avignon, France, Sept. 1981.

Vidaver, W.E., Lister, G.R., Brooke, R.C. and Binder, W.D. (1991), A manual for the use of variable chlorophyll fluorescence in the assessment of the ecophysiology of conifer seedlings. *B.C. Ministry of Forests*, Victoria, B.C. FRDA Report 163. 60 pp.

Vogelmann, J. E., Rock, B. N. and Moss, D. M. (1993), Red edge spectral measurements from sugar maple leaves, *International Journal of Remote Sensing.* 14**:**1563-1575.

Walker, D. A. (1985), Measurement of oxygen and chlorophyll fluorescence, In *Techniques in bioproductivity and photosynthesis*, (Coombs, J., D.O. Hall, S.P. Long, and J.M.O. Scurlock, Ed.), Pergamon Press., Toronto, pp. 95-106.

Weiss, M., and Baret, F., (1999), Evaluation of canopy biophysical variable retrieval performances from the accumulation of large swath satellite data, *Remote Sensing of Environment*. 70: 293-306.

Weiss, M., Baret, F., Myneni, R.B., Pragnere, A. and Knyazikhin, Y., (2000), Investigation of a model inversion technique to estimate canopy biophysical variables from spectral and directional reflectance data, *Agronomie.* 20:3-22.

Wellburn, A. R. (1994), The spectral determination of chlorophylls a and b, as well as total carotenoids using various solvents with spectrophotometers of different resolutions, *J. Plant Physiol.* 144**:**307-313.

Wessman, C. A., Aber, J. D., and Peterson, D. L. (1989), An evaluation of imaging spectrometry for estimating forest canopy chemistry, *Int. J. Remote Sensing.* 8**:**1293-1316.

Willstatter, R., and Stoll, A., (1913), Untershuchunger uber die Assimilation der Kolhensaure (Springer, Berlin).

Woolley, J.T., (1971), Reflectance and transmittance of light leaves, *Plant Physiol.* 47:656-662.

Yamada, N. and Fujimura, S. (1988), A mathematical model of reflectance and transmittance of plant leaves as a function of chlorophyll pigment content, *in Proceedings of the International Geoscience and Remote Sensign Symposium*, T.D. Guyenne and J.J. Hunt eds. (European Space Agency, Noodwijk, The Netherlads, 1988), pp.833-8334.

Yamada, N. and Fujimura, S. (1991), Nondestructive measurement of chlorophyll pigment content in plant leaves from three-color reflectance and transmittance, *Applied Optics.* 30**:**3964-3973.

Yoder, B. J. and Pettigrew-Crosby, R. E. (1995), Predicting nitrogen and chlorophyll content and concentrations from reflectance spectra (400-2500 nm) at leaf and canopy scales, *Remote Sensing of Environment.* 53**:**199-211.

Youkhana, S.K. (1983), Canopy Modeling Studies. Ph.D. Thesis, Colorado State University, Fort Collin, Co.

Zagolski, F., Pinel, V., Romier, J., Alcayde, D., Fotanari, J., Gastellu-Etchegorry, J. P., Giordano, G., Marty, G., and Joffre, R. (1996), Forest canopy chemistry with high spectral resolution remote sensing, *Int. J. Remote Sensing.* 17**:**1107-1128.

Zarco-Tejada, P. J. and Miller, J. R. (1999), Land cover mapping at BOREAS using red edge spectral parameters from CASI imagery, *Journal of Geophysical Research.* 104**:**27921-27933.

Zarco-Tejada, P. J., Miller, J. R., Mohammed, G. H., Noland, T. L. and Sampson, P. H. (1999a), Canopy Optical Indices from Infinite Reflectance and Canopy Reflectance Models for Forest Condition Monitoring: Application to Hyperspectral CASI data, In *IEEE 1999 International Geoscience and Remote Sensing Symposium, IGARSS'99*, Hamburg (Germany).

Zarco-Tejada, P. J., Miller, J. R., Mohammed, G. H., Noland, T. L. and Sampson, P. H. (1999b), Optical Indices as Bioindicators of Forest Condition from Hyperspectral CASI data, In Proceedings 19th Symposium of the European Association of Remote Sensing Laboratories (EARSeL), Valladolid (Spain).

Zarco-Tejada, P. J., Miller, J. R., Mohammed, G. H., Noland, T. L. (2000a), Chlorophyll Fluorescence Effects on Vegetation Apparent Reflectance: I. Leaf-Level Measurements and Model Simulation, *Remote Sensing of Environment*. In press.

Zarco-Tejada, P. J., Miller, J. R., Mohammed, G. H., Noland, T. L and Sampson, P.H. (2000b), Chlorophyll Fluorescence Effects on Vegetation Apparent Reflectance: II. Laboratory and Airborne Canopy-Level Measurements with Hyperspectral data, *Remote Sensing of Environment*. In Press.

Zarco-Tejada, P.J., J.R. Miller, G.H. Mohammed, T.L. Noland, and P.H. Sampson, (2000c), Estimation of Chlorophyll Fluorescence under Natural Illumination from Hyperspectral Data. Second EARSeL Workshop on Imaging Spectroscopy, Enschede (Holland), 11th-13th July 2000.

Appendix.

Spectral bandwidth and centre location for different modes of operation

Appendix. Spectral bandwidth and centre location for different modes of operation

Channel	405 CASI Mode (1998)		Mapping CASI Mode		FLUOR CASI Mode		MERIS	
	Wavelength	Half-Bandwidth	Wavelength	Half-Bandwidth	Wavelength	Half-Bandwidth	Wavelength	Half-Bandwidth
1	405.3650	4.2481	489.5074	5.2292	680.47	2.45	412.5	2.5
2	412.8720	4.2523	554.9756	5.2528	684.27	2.45	442.5	2.5
3	420.3790	4.2565	624.6262	5.2769	688.06	2.45	490.0	2.5
4	427.8860	4.2605	681.4203	3.3978	691.86	2.45	510.0	2.5
5	435.3935	4.2645	706.1180	3.4018	695.66	2.45	560.0	2.5
6	442.9015	4.2685	742.3069	3.4075	699.46	2.45	620.0	2.5
7	450.4095	4.2723	776.6904	5.3256	703.27	2.45	665.0	2.5
8	457.9180	4.2761			707.07	2.45	681.25	1.87
9	465.4275	4.2798			710.87	2.45	705.0	2.5
10	472.9375	4.2834					753.75	1.87
11	480.4490	4.2869					760.0	0.67
12	487.9610	4.2904					775.0	3.7
13	495.4740	4.2938					865.0	5.
14	502.9890	4.2971					890.0	2.5
15	510.5050	4.3003					900.0	2.5
16	518.0225	4.3034						
17	525.5420	4.3065						
18	533.0625	4.3094						
19	540.5855	4.3123						
20	548.1100	4.3152						
21	555.6370	4.3180						
22	563.1660	4.3206						
23	570.6975	4.3232						
24	578.2315	4.3257						
25	585.7680	4.3282						
26	593.3075	4.3305						
27	600.8500	4.3328						
28	608.3950	4.3350						
29	615.9430	4.3371						
30	623.4945	4.3392						
31	631.0485	4.3411						
32	638.6071	4.3430						
33	646.1685	4.3448						
34	653.7335	4.3466						
35	661.3030	4.3482						
36	668.8754	4.3498						
37	676.4530	4.3513						
38	684.0340	4.3527						
39	691.6195	4.3541						
40	699.2090	4.3553						
41	706.8035	4.3565						
42	714.4025	4.3576						
43	722.0060	4.3586						
44	729.6140	4.3596						
45	737.2280	4.3605						
46	744.8460	4.3613						
47	752.4700	4.3620						
48	760.0990	4.3626						
49	767.7340	4.3632						
50	775.3740	4.3636						
51	783.0195	4.3640						
52	790.6714	4.3644						
53	798.3290	4.3646						
54	805.9920	4.3648						
55	813.6620	4.3649						
56	821.3380	4.3649						
57	829.0205	4.3648						
58	836.7095	4.3647						
59	844.4050	4.3644						
60	852.1075	4.3641						
61	859.8165	4.3638						
62	867.5330	4.3633						
63	875.2565	4.3628						
64	882.9865	4.3621						
65	890.7250	4.3614						
66	898.4700	4.3607						
67	906.2230	4.3598						
68	913.9840	4.3589						
69	921.7525	4.3579						
70	929.5289	4.3568						
71	937.3135	4.3556						
72	945.1060	4.3544						